Mid- to Late-Quaternary evolution of the Wilderness barrier dunes, South Africa

Adam Christopher Dunajko

Submitted for the degree of Doctor of Philosophy

University of Sheffield

Department of Geography

July 2011

For my mother, Barbara, who always

encouraged me to do interesting things

Abstract

Barrier dunes represent potentially long-term, but complex, archives of coastal evolution. The examples occupying the Wilderness embayment, on the southern Cape coast of South Africa, form a regionally unique system of three shore-parallel barriers reaching up to 200 m in height and extending up to ~32 km alongshore. This research combines chronological and sediment provenance analyses to reconstruct the emplacement and evolution of the Wilderness barrier dunes through the Mid- to Late-Quaternary.

Thirty-six new luminescence ages collected from ten sites across the three Wilderness barriers are presented, and are combined with a compilation of dates from the literature to produce a high-resolution chronology of barrier accumulation. The record spans at least the last two glacial-interglacial cycles, with notable phases between 245-217 ka, 155-143 ka, 128-121 ka, 91-86 ka and post-6 ka. Analysis of trace element geochemistry, heavy minerals, particle size, carbonate content and offshore topographic evidence all combine to indicate the provenance of the barrier sands has remained constant throughout their formation, and must involve marine transport pathways. The hypothesis that barrier accumulation at Wilderness during periods of low sea level was sustained by terrestrial aeolian activity is thus disproven, and evidence for a regional pre-MIS 5 marine transgression is provided.

The terrestrially derived fraction of the barrier sands predominantly comprises quartzitic material derived from Table Mountain Group (TMG) rocks, most likely sourced from the Gouritz River ~75 km west of Wilderness. In addition to sediment from the TMG, the barrier sands also contain contributions of material derived from local geology, of material recycled from previous generations of aeolianite, and of authigenic marine sediment. The extensive coversand deposits inland of the Wilderness embayment, dated to >1.6 Ma using isothermal thermoluminescence, are demonstrated not to have made any significant input of sediment to the barriers.

The Wilderness barriers record a complex history of erosion, as well as deposition through the Mid- to Late-Quaternary, and the preserved record clearly reflects the influence of local nearshore bathymetry on the rate of sea-level regression. The importance of previous generations of aeolianite in both fixing the position of subsequent depositional episodes, and protecting them from erosion, is also evident. The barriers exhibit similar behaviour to deposits on tectonically stable coastlines elsewhere, and contrast with the more complete and widely spaced barrier records present on uplifting coasts.

Acknowledgements

First and foremost, I owe special thanks to my supervisor Professor Mark Bateman. It was Mark's lectures on Quaternary environments that encouraged me to begin this Ph.D., and his continually excellent support and guidance that enabled me to finish it.

Thanks to Dr Darrel Swift, my second supervisor, for his help and advice throughout my research, and particularly during the writing up process. Without his input this thesis would be a much lesser piece of work.

Academic assistance from numerous others has been invaluable. I'm very grateful to Dr Andy Carr, Dr Robert Bryant, Professor Peter Holmes, Dr Claire Boulter, Dr Dan Muhs, Dr Stefano Andreucci, Professor Charles Pattie, and Professor Margret Marker for their various inputs. Professor Curtis Marean is also thanked for his generosity in South Africa.

If I gave everyone in the University of Sheffield Geography Department the thanks they deserve, these acknowledgements would form an entire chapter of this thesis. In particular, Rob Ashurst has been incredibly generous with his time and expertise throughout. I'm less grateful to Rob for running a faster mile than I ever will. I must also mention Paul Coles for his help with the cartography.

My Ph.D. was funded by a University of Sheffield scholarship, and I gratefully acknowledge their support. Thanks are also due to the Sheffield Centre for International Drylands Research, who provided funding for my fieldwork and various analyses. South African National Parks, and especially Ian Russell, are thanked for their assistance and for permission to work in the Garden Route National Park.

Finally, I would like to thank my sister Sophie and my father George for rapidly gathering that it is most impolite to ask a Ph.D. student how their work is going.

Contents

1 Introduction and rationale

The primary aim of this research is to reconstruct the emplacement and geomorphological evolution of a coastal barrier dune system at Wilderness, on the southern Cape coast of South Africa. Coastal barrier dunes are a common element of sandy coastlines globally, and numerous examples are known to have persisted for multiple glacial-interglacial cycles. The palaeoenvironmental records they represent are thus complex, particularly on tectonically stable coastlines such as the southern Cape. In combining dating and provenance data to produce a model of barrier evolution at Wilderness, this research also aims to provide a framework for interpreting similar deposits elsewhere.

The intention of this short first chapter is to provide a broad explanation of the rationale behind palaeoenvironmental reconstruction, introduce the study area, and describe in detail the aims and objectives of the research. It also outlines the structure of the remainder of the thesis, and notes the publications that have arisen from it.

1.1 Studying past environments: why and how

Fundamental to all forms of palaeoenvironmental reconstruction is the principle of uniformitarianism and the famous maxim "*the present is the key to the past*", attributed to James Hutton (1788) and Charles Lyell (1830). Uniformitarianism states that the physical, chemical and biological processes occurring today have operated throughout the history of the Earth, and by relating evidence of contemporary and previous occurrences of these processes, it is possible to reconstruct and interpret past environments. Suitable evidence can be obtained from a broad range of proxy sources. These range from geological and sedimentological records, upon which early applications of uniformitarian principles first permitted the recognition that continental-scale glaciation had taken place on multiple occasions (Flint, 1957 and references therein), through to an increasingly diverse array of biotic and abiotic components of the Earth system.

Up until the 1960s, research into past environments was driven largely through academic curiosity. Any inferences about climate made from the various proxies under consideration were largely qualitative (Oldfield, 2004), and little crossover between disciplines occurred (Flenley, 1981). In more recent decades, increasing concern over anthropogenic modifications of climate has focussed various fields on this agenda, and palaeoenvironmental research is now commonly justified by placing it in the context of investigating the effects of

contemporary and future climate change. Particularly relevant are studies concerning the Quaternary period (c. 2.6 million years ago (Ma) to present), as it is the beginning of the Quaternary that marks the major onset of the most recent cycle of glacial and interglacial activity within which the Earth remains today (Gradstein et al., 2004). By extending the climate record beyond the diminutive volume of instrumental data available, contemporary changes can be placed within a longer perspective and the underlying forcing factors and feedback mechanisms in the climate system can be identified (Bradley, 2000). Complimentary to this, palaeoenvironmental data is fundamental in improving understanding of how changes in climate are expressed in terms of landform and biosphere response.

1.2 The significance of coastal areas

Coastal areas provide some of the most dynamic geomorphological responses to climate change. They can erode, accrete and alter in shape and location as a consequence of shifts in a wide variety of environmental processes, including changes in relative sea level, wind direction and strength, aridity, storm frequency, vegetation type and cover, and sediment supply. With the likelihood of significant modifications to many of these controlling factors now measured on a decadal scale (IPCC, 2007), and the increasing concentration of human populations in coastal areas (50 % of the world's population is predicted to live within 100 km of the coast by 2030: Adger et al., 2005), understanding the likely nature of coastal landscape response to climate change is particularly important. Reconstructing changes in coastal sites that have occurred in response to previous shifts in environmental conditions is one way in which this can be achieved.

Information derived from past changes in coastal sites is important at regional as well as local scales. In locations far removed from former ice-sheet locations where glacio-isostatic crustal rebound is not a concern (known as far-field sites), chronologically controlled coastal deposits can be used to construct or refine regional sea-level records (e.g. Chen et al., 1991; Murray-Wallace, 2002; Ramsay and Cooper, 2002). Applications of coastal palaeoenvironmental reconstruction are also not solely related to sea-level and climate-change issues. Evidence suggests modern *Homo sapiens* has relied on marine resources since its biological emergence during the Middle Stone Age some 200 thousand years ago (ka) (Erlandson, 2001; Marean et al., 2007), and many important archaeological sites are located in the coastal zone (e.g. Butzer, 2004; Rick et al., 2005; Finlayson et al., 2006). Reconstructing the environments around these sites during the period they were occupied can provide additional insights into the archaeological record.

Despite the utility of palaeoenvironmental reconstruction in the coastal zone, the driving mechanisms behind coastal evolution, particularly on millennial time scales, remain by no means comprehensively understood. In 2004 the International Geoscience Programme (IGCP) Project 495 "*Quaternary Land-Ocean Interactions: Driving Mechanisms and Coastal Responses*" identified a number of areas requiring further investigation, including:

- The role of sediment influx as a driving mechanism behind shoreline evolution; and
- How terrestrial and marine processes interact to control lateral changes in shoreline position.

The research arising from IGCP 495 has demonstrated several sites at which the interaction between terrestrial and marine sediment supply has proven significant in coastal evolution during the Holocene (Heyvaert and Baeteman, 2007; Patterson et al., 2007). The Wilderness barrier dunes, located on the southern Cape coast of South Africa between the towns of George and Knysna, provide an ideal opportunity to further investigate the controls on coastal landscape evolution, over multiple glacial-interglacial cycles.

1.3 Study area: the Wilderness barrier dunes, South Africa

At Wilderness, incision of an extensive, low-relief coastal embayment has permitted the preservation of multiple generations of calcareous coastal aeolianites as discrete barrier dunes, interspersed by a series of back-barrier lagoons (Figure 1.1). Reaching up to 200 m in height, the Wilderness barriers form some of the most spectacular fossil dune topography in South Africa, with one section described by Rust (1991: p. 400) as an "*aeolian Everest*". The separation of the barriers across the embayment contrasts with the stacked aeolianite deposits more typical elsewhere on the tectonically stable southern Cape coast (Illenberger, 1996 and references therein).

1.1 (A) Looking eastward from the western edge of the Wilderness embayment towards the barriers and their associated lagoons; (B) The barrier adjacent to the contemporary coastline (known as the "seaward" barrier) photographed from behind. Note houses on both photos for scale.

A detailed description of the morphology of the Wilderness barrier dunes, and a review of previous research conducted upon them, is provided in chapters 3 and 4. In brief, three morphologically distinct barriers are present within the embayment, separated by a series of back-barrier lagoons (Figure 1.2). The three barriers are termed the seaward, middle and landward barriers based on their proximity to the modern coastline (after Illenberger, 1996). The seaward and middle barriers possess clearly defined seaward and landward slopes but the landward barrier is less distinct, and appears to comprise sand banked up against the hard-rock geology at the edge of the embayment. The remnants of several presently submerged barriers are also identifiable offshore (Birch et al., 1978; Martin and Flemming, 1986), and the area immediately inland of the embayment is characterised by a deep layer of

unconsolidated and decalcified medium- to fine-grained coversand (Figure 1.2), also understood to be of aeolian origin (Marker and Holmes, 2002; Holmes et al., 2007).

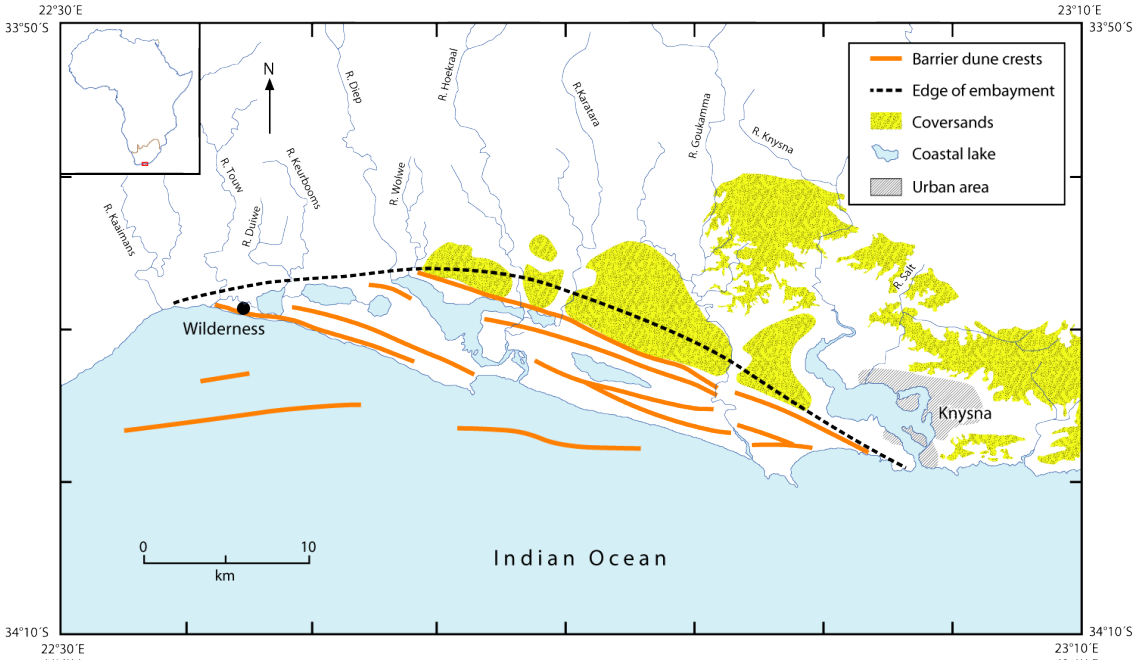

1.2 The southern Cape coastal area between the towns of Wilderness and Knysna, showing the extent of the Wilderness embayment and the barrier crests and associated back-barrier lakes within it. The location of the offshore barriers is based on a seismic survey conducted by Birch et al. (1978). The coversand deposits inland of the embayment are also shown, based on mapping by Illenberger (1996) and Marker and Holmes (2002). River courses are based on mapping by Toerien and Roby (1979).

Although the Wilderness barriers were widely assumed to have formed primarily in response to sediment delivery via marine transport pathways during sea-level highstands (Birch, 1980; Illenberger, 1996), recent optically stimulated luminescence (OSL) dating of the seaward barrier has indicated multiple phases of accumulation through the Late Quaternary, including some ages from periods when sea levels were much lower than present (Carr et al., 2007). The relatively humid southern Cape climate would have resulted in rapid revegetation and immobilisation of shelf sediments exposed during marine regressions (Barwis and Tankard, 1983; Illenberger, 1996), suggesting increased input of local, terrestrial sediment may have been more important for dune building at these times. Bateman et al. (2004) cite evidence of highly variable carbonate content within the seaward barrier as potentially supporting this hypothesis. However, the provenance of the vast quantity of sediment from which the Wilderness barriers are formed has received scant attention in the form of quantitative research, and remains undetermined. The nature of the relationship between the coversands and the barrier dunes has also yet to be firmly established. OSL dating of the coversands has demonstrated they are significantly older than the seaward Wilderness barrier, but the

limitations of the technique mean that only minimum ages have been obtained for them (Holmes et al., 2007).

1.4 Research aims and objectives

The overarching aim of this research is to reconstruct the emplacement and geomorphological evolution of the Wilderness barrier dunes and, in a broader context, improve understanding of how sandy coastlines evolve across multiple glacial-interglacial cycles. With this in mind, a number of objectives were constructed:

1. Increase substantially the number of OSL-dated sites in the seaward barrier to provide a high-resolution chronological framework for its formation along the full length of the embayment. This chronology should be detailed enough to reveal any lateral or vertical trends in the age of the barrier. As far as possible, produce a similarly detailed OSL chronology of the (presumably) older and previously undated middle and landward barriers.
2. Use these data to firmly constrain the relationship between sea level and the timing of barrier formation at Wilderness.
3. Clarify the relationship between the barriers and the inland coversand deposits, by obtaining a more detailed chronology of the timing of coversand deposition. Test the applicability of a new luminescence dating protocol (isothermal thermoluminescence, or ITL) (e.g. Jain et al., 2005; Choi et al., 2006) for dating the coversands, and potentially revise the minimum OSL ages obtained for them by Holmes et al. (2007).
4. Establish whether the relative importance of terrestrial vs. marine sediment input to the Wilderness barriers has changed with time, and whether or not sediment from local terrestrial sources has been significant in their formation.
5. Combine the dating and provenance data to inform a detailed reconstruction of the emplacement and geomorphological evolution of the Wilderness barrier dunes.
6. Compare this research to studies of Quaternary coastal barrier dune systems elsewhere, in order to develop a generalised model of barrier accumulation across glacial-interglacial cycles.

1.5 Thesis structure

This chapter has considered the broad rationale for reconstructing past environments, briefly introduced the study area for this research, and outlined its aims and objectives. Chapter 2 discusses in greater detail the controls on the formation of coastal-dune systems and how they come to be preserved in the palaeorecord. The first part of chapter 3 collates the information required for reconstructing the evolution of the Wilderness barriers, and the second part presents a detailed review of the existing literature concerning them. Chapter 4 explains the study design and how it enables the objectives of this research to be met; it also details the field sampling procedures and describes the sample sites. Chapter 5 describes the laboratory methods employed and the rationale for their use. Results are presented in chapter 6, which is divided into dating and provenancing sections. All results are then interpreted in combination in chapter 7, and the emplacement and evolution of the Wilderness barriers is reconstructed. A generalised model of barrier accumulation is also presented. Finally, conclusions are drawn in chapter 8 along with suggestions for future research.

1.6 Publications arising from this thesis

The research presented here has formed the basis for/contributed to four journal articles (listed below), all of which have been published. The relationship between these articles and the chapters of this thesis is briefly detailed in the following paragraphs.

Andreucci, S., Bateman, M.D., Zucca, C., Kapur, S., Akşit, İ., Dunajko, A.C. and Pascucci, V. (2011). Evidence of Saharan dust in upper Pleistocene reworked palaeosols of North-west Sardinia, Italy: palaeoenvironmental implications. *Sedimentology,* doi: 10.1111/j.1365-3091.2011.01285.x.

Bateman, M. D., Carr, A. S., Dunajko, A. C., Holmes, P. J., Roberts, D. L., McClaren, S. J., Bryant, R. G., Marker, M. E., and Murray-Wallace, C. V. (2011). The evolution of coastal barrier systems: a case study of the Middle-Late Pleistocene Wilderness barriers, South Africa. *Quaternary Science Reviews* **30,** 63-81.

Carr, A.S., Boom, A., Dunajko, A.C., Bateman, M.D., Holmes, P.J., and Berrio, J.-C. (2010). New evidence for the age and palaeoecology of the Knysna Formation, South Africa. *South African Journal of Geology* **113,** 241-256.

Dunajko, A. C., and Bateman, M. D. (2010). Sediment provenance of the Wilderness barrier dunes, southern Cape coast, South Africa. *Terra Nova* **22,** 417-423.

Dunajko and Bateman (2010) arose from a talk delivered at the IAS Meeting of Sedimentology 2009, and represents the initial stage of the provenancing results. The material in chapters 6 and 7 is a development of this work. Carr et al. (2010) contains the methodological development and results of ITL dating as applied to the coversand deposits. This work appears largely unaltered in chapter 5. Andreucci et al. (2011) is not directly related to the content of this thesis, but employs a trace element provenancing methodology similar to the one used at Wilderness in order to identify atmospheric dust inputs to Sardinian palaeosols. Bateman et al. (2011) presents the barrier chronology and palaeoenvironmental reconstruction aspects of this thesis. It reports the 36 OSL ages from samples of the Wilderness barrier dunes collected and dated here along with their site descriptions. This material forms parts of chapters 4 and 6. The research, results and discussion included in chapters 2, 3, 6 and 7 of this thesis also contributed significantly to the model of the geomorphological evolution of the Wilderness embayment presented in Bateman et al. (2011), and the more general discussion of barrier system evolution therein.

2 Coastal dunes: formation, preservation and reconstruction

2.1 Introduction

The first part of this chapter considers the variables that influence coastal-dune formation and morphology. The discussion centres on barrier dunes of the type that occupy the Wilderness embayment, but first introduced are two other classes of coastal dune (foredunes and transgressive dunes), as many of the processes that influence them are shared. The second part of the chapter discusses how coastal dunes come to be preserved in the palaeorecord as aeolianite, and what can be interpreted from examples of such deposits. The importance of determining sediment provenance in order to understand coastal-dune evolution is also discussed.

2.2 Coastal-dune formation

The diversity of climatic zones in which large coastal aeolian deposits are found, including arid (e.g. Namibia: Lancaster, 1982), semi-arid (the Mediterranean: Tsoar and Blumberg, 2002), temperate (Denmark: Clemmensen et al., 1996) and high rainfall (America's Pacific northwest: Cooper, 1958), is testament to their greater degree of independence from climate relative to inland dune systems. In fact, Hesp (2002) identified climate as only one of five major controlling variables on coastal-dune evolution, with its influence exerted predominantly through modulation of vegetation type and cover. The other four variables identified by Hesp (2002) are: (i) sediment budget; (ii) sea-level state; (iii) wave energy/surfzone type; and (iv) wind energy. In addition to these factors, the area of land available for dune accumulation at a given site (its “accommodation space”) is also understood as being of central importance in the evolution of coastal-dune systems (e.g. Wilson et al., 2001; Aagaard et al., 2007; Psuty and Silveira, 2010). At coastal locations accommodation space is often directly controlled by sea-level state, though in Hesp’s (2002) discussion the influence of sea level is primarily considered via its additional important functions in eroding previous dune accumulation and modulating sediment budget.

Determining the relative importance of the various possible controls on coastal-dune activity within a particular system is fundamental to producing a coherent palaeoenvironmental reconstruction of it. In order to inform the reconstruction of the Wilderness barriers this research aims to produce, the following sections discuss three primary

coastal-dune morphologies (foredunes, transgressive coastal dunefields and barrier dunes). The current process-based understanding of their occurrence and evolution is reviewed, with respect to the potential controlling variables outlined in the previous paragraph.

2.2.1 Foredunes

Foredunes are defined by Hesp (2002: p. 245) as "*shore-parallel dune ridges formed on the top of the backshore by aeolian sand deposition within vegetation*". They tend to be less than 5 m high and 20 m wide and are the most ephemeral and dynamic of coastal-dune types, frequently releasing or acquiring sediment from the beach (Olivier and Garland, 2003). Psuty (1988) presented a conceptual model explaining the nature of foredune–beach coupling, shown in Figure 2.1. Given a positive beach sediment budget, the development of individual foredunes is limited as they are periodically stranded by beach progradation to form beach ridges or strand plains (the beach-ridge quadrant of the model). As sediment supply to the beach reduces, the period of aeolian accumulation at a given site is extended and the foredune has a greater sediment budget. A point will be reached at which beach progradation does not occur and maximum foredune development is permitted (foredune development quadrant). With a negative beach sediment budget and associated shoreline retreat, foredunes diminish in size and move inland as they increasingly suffer from overwash and scarping (foredune attenuation quadrant).

Foredune sediment budget is closely linked to beach characteristics. A distinction can be drawn between "dissipative" and "reflective" beaches (Wright et al., 1979). Reflective beaches form under low to moderate energy conditions typical of sheltered situations, have a virtually absent surf zone, coarse sand, small waves and steep profiles which reflect most wave energy back to sea. At the other end of the spectrum, dissipative beaches develop under high wave energy conditions when there is an abundant supply of medium to fine sand, and are characterised by a broad surf zone with a fairly uniform and gentle slope where waves dissipate most of their energy as breakers before reaching the beach face (Short, 1984). Foredunes (and other dune types) associated with reflective beaches are typically small, whereas those to the rear of dissipative beaches are larger. Sea-level state also exerts an important influence on sediment budget, with regressing sea levels resulting in wider beaches and a consequent increase in sediment supply (Hesp, 2002).

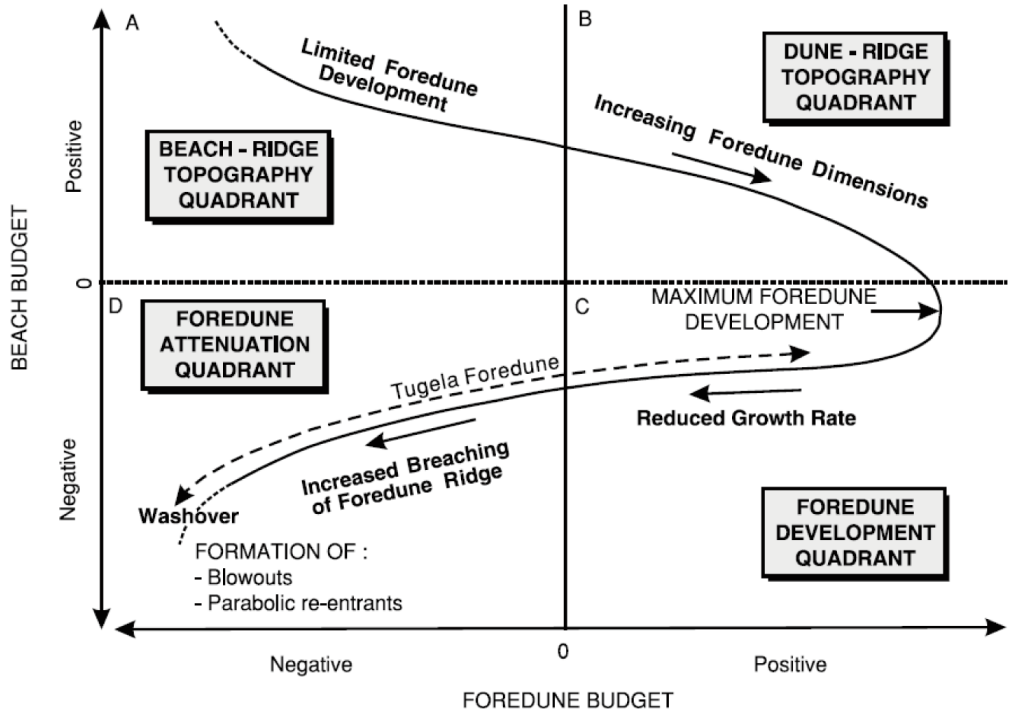

2.1 Conceptual relationship between sediment budget in the beach and foredune. Adapted from Psuty (1988) by Olivier and Garland (2003).

As well as beach type and sea-level state, the possibility for deflation of beach sediment, and thus foredune size, also depends on the strength of the wind and its angle incident to the beach. As wind direction shifts from onshore (shore perpendicular) to shore parallel (oblique), total sediment transport from the beach to the foredune at any given point alongshore reflects a trade-off between transport reduction (as at increasingly oblique angles larger volumes of sand are transported downwind of the dune boundary), and transport enhancement, because of larger fetch distances traversed by the wind prior to encountering the dune line (Bauer and Davidson-Arnott, 2003). Foredunes thus typically vary in size along the length of a beach.

2.2.2 Transgressive dunes

Whereas foredunes are integrally coupled to the littoral zone, dunes further back from the beach are subject to controls on their behaviour akin to those acting on dunes in any other environment. It follows that a distinction is made between primary coastal dunes (foredunes) and secondary coastal dunes (Bauer and Sherman, 1999). Foredunes may become secondary dunes if they are stranded by shoreline progradation (e.g. Compton and Franceschini, 2005; Brooke et al., 2008), but large-scale secondary coastal dunes typically take the form of transgressive coastal dunefields. Not to be confused or automatically associated with marine

transgression, “transgressive dunes” is a term coined by Gardner (1955) to describe coastal dunes whose migratory behaviour results in their advancing over, or transgressing, prior terrain. Requisite environmental conditions for the formation of transgressive dunes are simply large quantities of sediment available for deflation and strong onshore winds (Pye, 1983), and they are consequently associated with dissipative beaches. Although transgressive dunes still depend on sediment supply from the beach (and/or erosion of foredunes), they are only indirectly linked to the littoral zone and can possess morphologies also present in entirely inland settings (Bauer and Sherman, 1999).

Vegetation cover, wind regime, and sediment supply control the type of dunes which populate transgressive coastal dunefields. Parabolic dunes, which are U- or V-shaped mounds of sand with elongate arms that follow behind the central part of the dune, are probably the most widely occurring type of transgressive dune (Pye, 1983). They form under unidirectional wind regimes, and are most common in humid coastal areas where the vegetation required to stabilise the dune arms is easily established (Tsoar and Blumberg, 2002). In more sparsely vegetated systems, or under stronger wind regimes and/or high sediment supply conditions, transverse dunes tend to dominate (Nishimori and Tanaka, 2001; Nield and Baas, 2008). Transverse dune ridges are characterised by a lack of stabilising vegetation, migrate in a direction perpendicular to the prevailing wind direction, and stand as single large distinct features (Goldsmith, 1978). On coastlines with little or no effective sand-binding vegetation, transgressive dunefields can extend kilometres to tens of kilometres inland (e.g. Illenberger and Rust, 1988; Chase and Thomas, 2006).

2.2.3 Barrier dunes

Whilst barrier dunes (also known as coastal barriers, barrier islands, cordon dunes or simply barriers) do not feature in the coastal-dune classification schemes of Pye (1983), Bauer and Sherman (1999), Carter (1990) and others, they are a common element of numerous coastlines in Australia, Brazil, South Africa and elsewhere. Barriers comprise large, shore-parallel sand bodies, of greater size and width than foredunes (up to several hundred metres high and three kilometres wide), composed of multiple sandy lithofacies which may include beach, dune, shoreface, tidal delta, inlet and washover sediments (Roy et al., 1994; Illenberger, 1996). They sometimes, though not always, separate back-barrier lagoons from the sea. The following sections discuss: (i) how sea level, sediment supply and coastal geometry control barrier morphology and evolution; (ii) the occurrence of barriers vs. transgressive dunes, with reference to the southern African coast; and (iii) methods of barrier genesis.

2.2.3.1 Barrier morphology and evolution

The occurrence of coastal barrier dunes is restricted mainly to gently sloping coastal plains located on the trailing edges of continents, and they are best developed in regions with tidal ranges of less than approximately 2 m and high wave energy (Hayes, 1979). Within these confines, barriers exhibit a considerable range of morphologies and behaviours, with their emplacement and evolution representing a complex response to sea-level position, sediment supply and substrate gradient (Roy et al., 1994). Similar to foredune behaviour in Psuty's (1988) model of foredune–beach coupling (discussed in section 2.2.1), barriers may be progradational, transgressive, or aggradational. Each of these barrier types is discussed in turn below.

Barrier progradation typically occurs under regimes of abundant sediment supply and stable or slowly rising sea levels, and results in the formation of multiple, shore-parallel dune ridges of relatively low relief (in the order of 3-10 m above sea level), with absent or insubstantial water bodies inland (Figure 2.2a) (Roy et al., 1994). Mid- to Late-Holocene examples of progradational barrier systems can be observed in various locations, including the USA (Stapor et al., 1991; Dougherty et al., 2004), Northern Europe (Beets et al., 1992; Madsen et al., 2010) and West Africa (Anthony et al., 2002). Barrier progradation can also occur under falling sea levels. The present sea-level highstand means extant examples of barriers formed under low or falling sea levels are limited, but in Australia submerged barrier complexes are associated with low-gradient, relatively sediment-rich shelves, and exhibit similar dimensions to their onland counterparts (Roy et al., 1994). Compton and Franceschini (2005) interpret the coastal barrier sequence at Sixteen Mile Beach near Cape Town, South Africa, as reflecting sea-level regression following the Mid-Holocene maxima.

Barrier transgression occurs when sediment supply is unable to keep pace with sea-level rise. In such cases the process of overwash, whereby sediment is transported across the barrier by waves and deposited on its landward margin, causes retreat of the barrier inland (Davis and FitzGerald, 2004). Transgressive barriers are typically 15-25 m deep and rise 2-4 m above mean sea level (Thom, 1984), and an illustration of a typical transgressive barrier is provided in Figure 2.2b. This scenario has been more common in the Holocene than barrier progradation, and examples can be found on the east coast of the USA (Kraft et al., 1987), southeastern Australia (Roy et al., 1980), northern Europe (Rieu et al., 2005) and elsewhere. The morphology of transgressive barriers is controlled by coastal geometry. For a constant relative sea-level rise, modelling suggests that as substrate steepens the rate of retreat, the amount of sand recycled and the cross-sectional area of the barrier all decrease, and the back-barrier lagoon narrows and deepens (Roy et al., 1994).

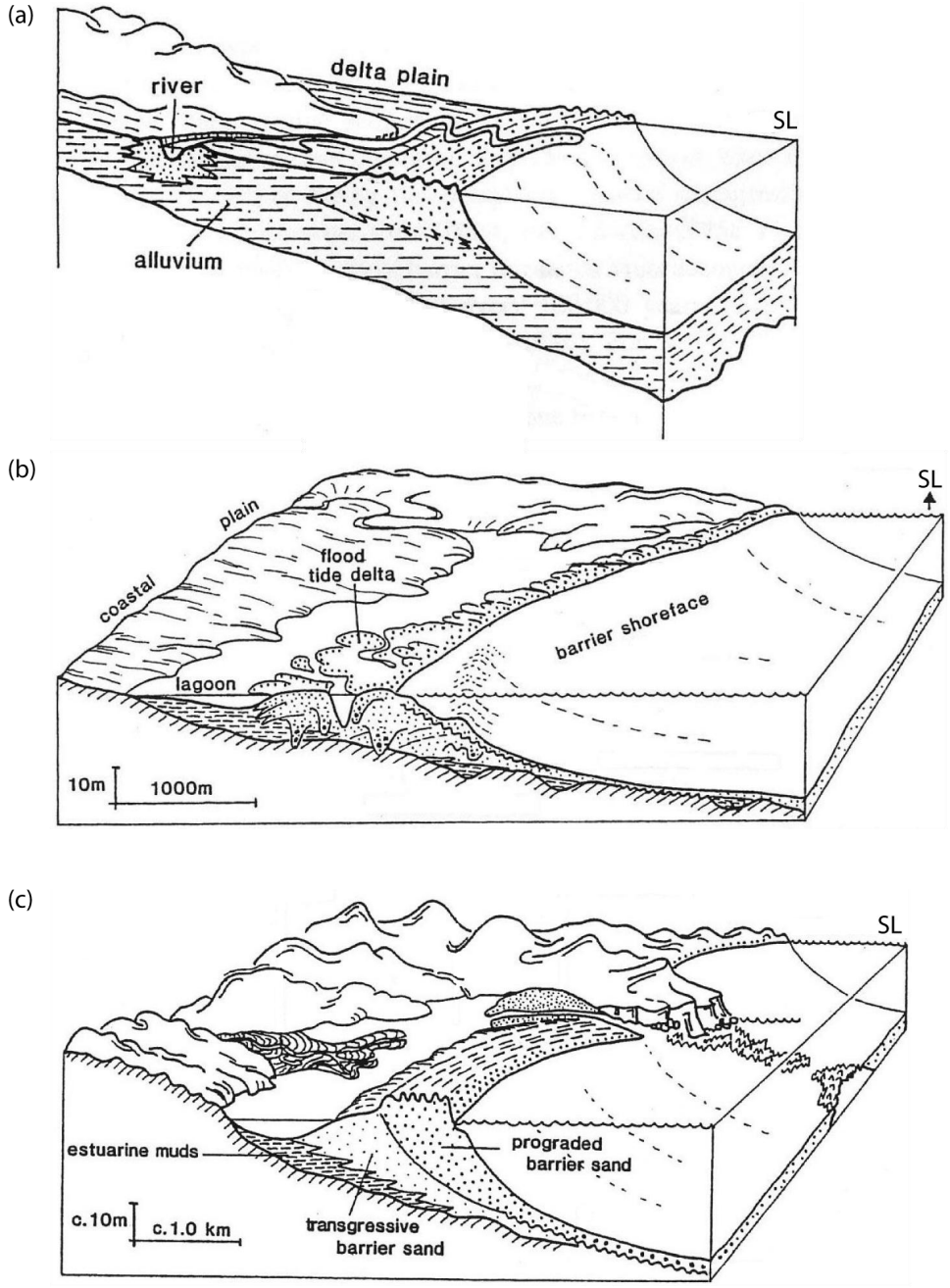

2.2 Various modes of barrier evolution: (a) prograding barrier; (b) transgressive barrier; (c) combined transgressive and progradational barrier giving the impression of stability. SL = sea level. Adapted from Roy et al. (1994).

Barriers that have accumulated vertically through time and occupy approximately the same footprint as they did when first formed or stabilised are termed aggradational barriers (Davis and FitzGerald, 2004). Roy et al. (1994) suggest aggradational barriers may fluctuate between prograding and transgressing conditions to give the impression of relative stability over long periods (illustrated in Figure 2.2c). Observations and stratigraphic analyses reveal aggradation of stationary barriers can also take place via the coalescence of various smaller dune types, such as parabolic and transverse dunes (e.g. Illenberger, 1996; Armitage et al.,

2006; Roberts et al., 2009; Murray-Wallace et al., 2010), allowing them to reach much greater heights (up to several hundred metres) than prograding or transgressive barriers. Barriers in several locations are observed to rest directly on remnants of similar deposits from previous interglacials (e.g. Armitage et al., 2006; Tomazelli and Dillenburg, 2007; Murray-Wallace et al., 2010), indicating aggradation can span multiple glacial-interglacial cycles given a broad concordance in successive sea-level highstand positions (Murray-Wallace et al., 2010). The barriers occupying the Wilderness embayment that are the focus of this research are interpreted as being of this type (Illenberger, 1996).

2.2.3.2 Barrier dunes vs. transgressive dunes

On the South African coast, Roberts et al. (2009) propose that the tendency for coastal dunes either to migrate onshore and form transgressive dunefields or to accrete vertically to form barriers is strongly influenced by whether local environmental conditions are conducive to dune stabilisation. There, barrier dune systems are located exclusively on the southern and eastern coasts (Illenberger, 1996; Porat and Botha, 2008; Roberts et al., 2008), whereas transgressive dunefields are dominant on the west coast (Butzer, 2004; Chase and Thomas, 2006). The prevailing wind direction is sub-parallel to the shoreline on both coasts (southerly on the west coast and westerly on the south coast: Figure 2.3), and coastal topography is similar (low-relief coastal plains with alternating rocky headlands and sandy bays). Wave energy is also consistently high around the South African coast (Cooper, 2001). Given the similarity of all these factors, Roberts et al. (2009) propose the reason for the contrast in dune morphology between the western and southern/eastern coasts lies in the timing of maximum wind velocity and vegetation cover, as modulated by seasonal rainfall patterns.

On the west coast of South Africa, the timing of maximum annual wind velocity coincides with summer aridity, causing vegetation to be overwhelmed by sand and dunefields to extend inland rather than aggregate vertically. In contrast, the annual maximum in wind velocity on the southern coast occurs in winter, coincident with significant rainfall. The resulting more hospitable conditions for vegetation prevent significant onshore transgression, and encourage vertical accumulation of dunes to form barriers instead (Roberts et al., 2009). The situation is summarised in Figure 2.3 (note: the climate of southern Africa is discussed in detail in chapter 3 section 3.5). In the few instances where transgressive dunefields do occur on the southern coast they are located on coastal promontories, e.g. the Alexandria coastal dunefield (Illenberger and Rust, 1988) and Cape Agulhas (Carr et al., 2006a), where winds are at their strongest (Roberts et al., 2009).

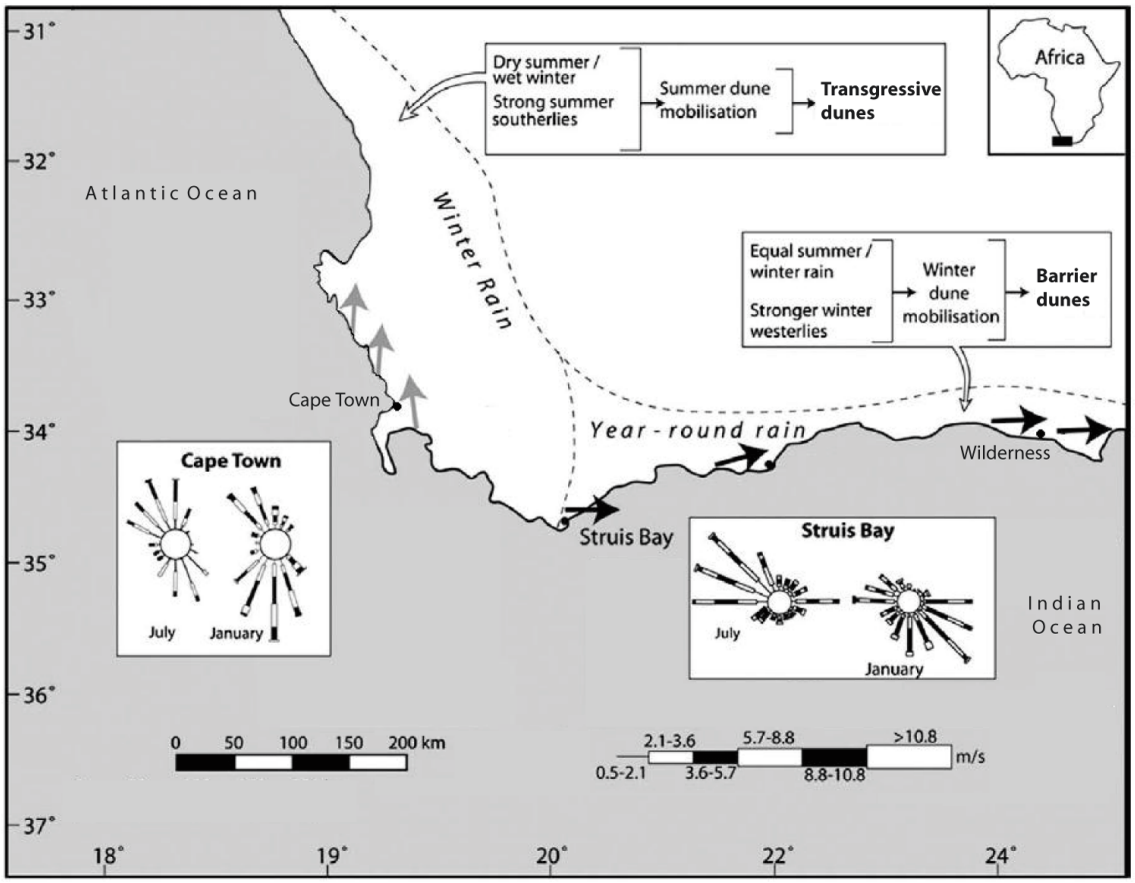

2.3 Map illustrating the reasons for contrasts in coastal dune morphology on the southern African coast. Wind roses are shown for the west (Cape Town) and south (Struis Bay) coasts. Heavy black arrows show the orientation of barrier dunes on the south coast, and grey arrows show the orientation of major transgressive dunefields on the west coast. Flow diagrams illustrating the controls on dunefield morphogenesis on the west and south coasts are also included. Modified from Roberts et al. (2009).

2.2.3.3 Barrier genesis

Whilst the controls on barrier dune formation proposed by Roberts et al. (2009) for the southern African coast explain their regional distribution and their considerable vertical accretion, they do not incorporate a mechanism to explain the common presence of back-barrier lagoons inland of barriers, such as at Wilderness. Several generalised theories have been proposed for the genesis of barrier dunes with associated back-barrier lagoons, namely: (i) spit extension from headlands; (ii) up-building of offshore bars; and (iii) submergence of coastal ridge features (Hoyt, 1973 and references therein). Schwartz (1971) argued that barrier formation can arise from any of the above mechanisms, acting individually or in combination. However, whilst examples of barriers attributed to spit growth (e.g. Hoffmann et al., 2005; Murray and Mohanti, 2006; Tribe and Kennedy, 2010) and offshore bar development (e.g. Davis et al., 2003; Bennett et al., 2009) are common, no examples of ridge submergence have been documented in recent literature (Davis et al., 2003). Determining how a barrier

originated is often complicated by substantial modification of its original form and stratigraphy as it transgresses, progrades or aggrades in response to changes in sea level or sediment budget (Davis and FitzGerald, 2004; Tribe and Kennedy, 2010). Literature pertaining to the Wilderness barrier dunes is reviewed in chapter 3, but briefly, the presence of marine facies visible at the base of the middle barrier suggests they originally formed offshore as barrier islands (Illenberger, 1996).

2.3 Preservation of coastal dunes and the palaeorecord

In order to obtain a broader and longer-term perspective on the evolution of coastal barrier dunes, it is necessary to consider examples from the palaeorecord. However, aeolian deposits are intrinsically vulnerable to reworking and erosion. Entire sand seas can leave no geological record, and events of varying magnitudes can leave no impression, or be removed subsequent to their cessation (Kocurek, 1999). Kocurek (1999) considered the three phases necessary for the creation of what he terms an "*aeolian rock record*":

1. Formation of sand dunes;
2. Accumulation of strata, such that deposited sediment passes from above to below the accumulation surface and a body of deposited sediment accumulates over time;
3. Preservation, in which accumulated strata are incorporated into the rock record.

The formation of sand dunes (phase one of creating an aeolian rock record) requires a positive sand supply, wind energy sufficient to transport the sand, and space to accommodate it (Kocurek, 1991). With regard to the second and third phases, accumulation and preservation, the potential for these processes to occur is often significantly greater for coastal dunes than their inland counterparts. The position of the water table can be an important factor in controlling aeolian accumulation, with sand below it protected from the potential erosional influence of the wind (Kocurek and Havholm, 1993). Water tables are commonly high in coastal-dune settings, due to the shallow slope of the groundwater table on gently dipping coastal plains and the high water retention and poor rainfall runoff of unconsolidated, porous aeolian sands (Fryberger et al., 1988). Water, either phreatic or vadose, also permits calcium carbonate-rich sands, as are common in many coastal locations, to undergo lithification and be preserved as aeolianite. The controls on aeolianite formation, and its resulting distribution, are considered in the following section.

2.3.1 Aeolianite formation

Where sands are rich in calcium carbonate (also referred to as $CaCO_3$ or simply carbonate), dune bedding structures may subsequently be preserved by early diagenetic cementation. Water residing in carbonate sediments, present due to either percolation of precipitation or the position of the water table, can become supersaturated with respect to $CaCO_3$. This $CaCO_3$ may subsequently be reprecipitated at points of grain contact and in intergranular pore spaces between the carbonate, quartz or other detrital grains which form the deposit, causing it to lithify (McKee and Ward, 1983). The resulting material is most commonly known as aeolianite, though dune rock, dune calcarenite, calcareous coastal aeolianite, aeolian limestone or various combinations of these terms are also used (e.g. Xitao and Goldsmith, 1989; Pye and Tsoar, 1990). The lithification process is understood to occur quickly, certainly in ten years or less (Dravis, 1996), and a testament to its rapidity is provided by the numerous spectacularly preserved faunal and hominid trackways observed in coastal aeolianites in South Africa dating to the last interglacial (e.g. Figure 2.4, also Roberts, 2008; Roberts et al., 2008).

2.4 Faunal trackway (bok) preserved in finely bedded aeolianite, observed on the southern Cape coast of South Africa.

Where coastal-dune depositional morphologies are preserved as aeolianite, Brooke (2001: p. 136) states they are most commonly in the form of "*elongate, shore-parallel bodies*", often comprising "*a complex of coalesced and at places stacked smaller dunes*", i.e. barrier dunes. This is unsurprising: whilst aeolianites are by no means invulnerable to erosion, the larger size of aggradational barriers relative to other types of coastal dunes affords them a greater degree of persistence in the environment. Where depositional morphologies are not preserved, distinguishing aeolianites from carbonate-cemented shallow-marine or beach deposits (which can also lithify rapidly: Friedman, 1998) can prove problematic, but an effective diagnostic criteria is the presence of cross-stratified, high-angle (typically between 30-34°) bedding (McKee and Ward, 1983).

Since the lithification of coastal dunes into aeolianite depends on the presence of carbonate-rich sands, the global distribution of such deposits is governed by zones of marine carbonate production. Marine "carbonate factories", in which conditions are favourable for the growth of carbonate-precipitating marine organisms, fall into three categories: *tropical shallow-water* factories, *cool-water* (or temperate) factories, and *mud-mound* factories (Schlager, 2003). As indicated in Figure 2.5, tracts of coastal aeolianite are most commonly associated with heterozoan* carbonate production in cool-water and tropical shallow-water locations (Brooke, 2001), and are common enough to be described as "*omnipresent*" along many coastlines between 50° N and 45° S (Frébourg et al., 2008: p. 177). These latitudes also coincide with the trade wind belts, the permanence and intensity of which is favourable to continued aeolian activity (Frébourg et al., 2008).

The accumulation of carbonate in temperate shallow-water locations (defined by mean sea-surface winter isotherm values of 10-20 °C: James, 1997), such as the southern Cape coast of South Africa, is strongly influenced by nutrient availability. Though warm water carbonate-producing biota are significantly more productive than cool-water species, deep-ocean upwelling zones encourage carbonate productivity through the provision of nutrient-rich waters (Rao, 1996 c.f. Brooke, 2001). Carbonate production rates are also controlled by terrigenous sediment flux, with significant carbonate deposits occurring only in regions with

*Heterotrophic organisms feed on other organisms, whereas phototrophs rely on light-based photosynthesis. Photozoan carbonate systems tend to dominate tropical and subtropical waters, whereas heterozoan carbonates occur in cooler waters (temperate to polar latitudes) and in lower latitude settings influenced by nutrient-rich waters resulting from ocean-current upwelling (James, 1997).

low or absent clastic input (Flügel, 2004). Carbonate production off the southern Cape coast of South Africa is considered in greater detail in chapter 3 section 3.5.2.

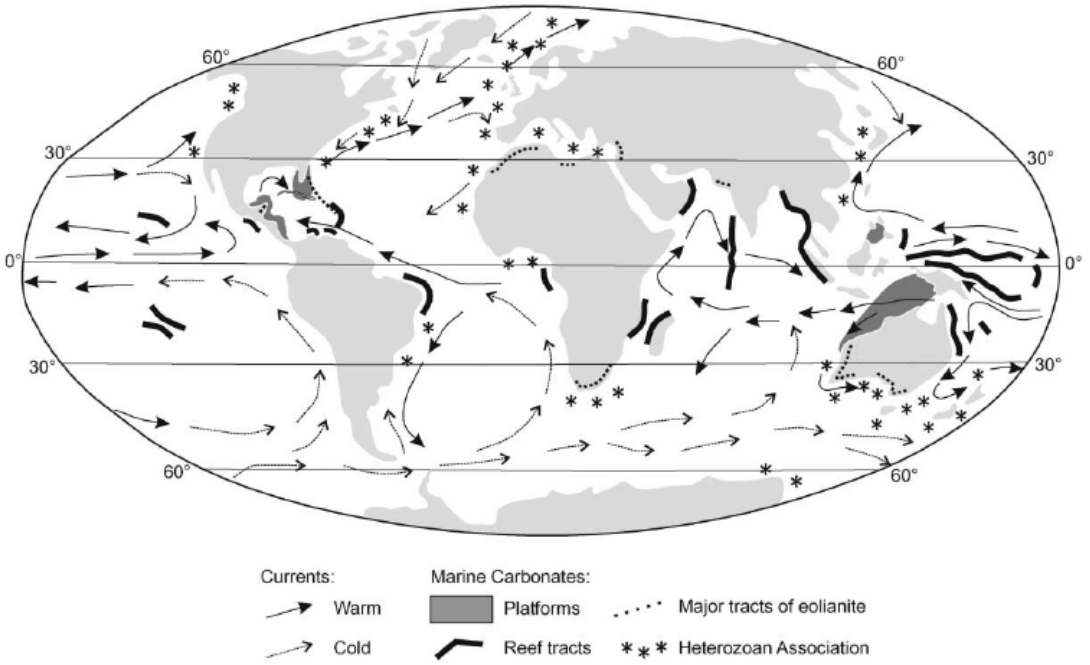

2.5 Ocean currents and the coincidence of Heterozoan carbonate provinces and major tracts of coastal aeolianite. From Brooke (2001).

2.3.2 Palaeoenvironmental significance of aeolianites

The environmental significance of coastal aeolianites was considered as long ago as the 19th century, when on the voyage of the *Beagle* Darwin noted the "*vast extent*" of aeolianite along the coastline of Australia and pondered whether similar deposits on coastlines in South America and elsewhere, lacking the well preserved fragments of marine organisms in the Australian examples, were formed in the same manner (Darwin, 1851: p. 147). It is only relatively recently, however, that the development and refinement of luminescence dating (detailed in chapter 5) has made possible accurate and efficient determinations of the burial age of aeolianite deposits, allowing their relationships with various environmental factors to be explored. These are discussed below with reference to examples from the palaeorecord.

2.3.2.1 Sea-level state

Brooke (2001) categorised coastal aeolianite deposits as relating to either: (i) glacial sea-level lowstands, during which carbonate sediments that accumulated offshore during the previous interglacial are exposed for deflation by the wind; or (ii) interglacial sea-level

highstands, when transgressing seas move large volumes of sediment shorewards for incorporation into dunes. Coastal barriers preserved as aeolianite and dating to sea-level highstands are globally widespread, occurring in Brazil (Tomazelli and Dillenburg, 2007), Bermuda and the Bahamas (Hearty and Kindler, 1995), southern Australia (Murray-Wallace et al., 2001), eastern Africa (Armitage et al., 2006) and elsewhere.

Coastal aeolianites dating predominantly to sea-level lowstands are less common. Where they do occur it is in arid regions such as Mallorca (Clemmensen et al., 2001; Fornos et al., 2009) and parts of SE Australia (Zhou et al., 1994), where vegetation is unable to colonise exposed continental shelves and sediment is free to be deflated by the wind. The presence of submerged aeolianite ridges in several locations, e.g. off the southern and eastern Africa coast (Birch et al., 1978; Cooper and Pilkey, 2002; Schleyer et al., 2006), northern Israel (Belknap and Mart, 1999), and southeast Australia (Sprigg, 1979) suggests the relative paucity of examples of coastal aeolianites dating to glacial periods may reflect their erosion and/or current submergence, rather than a lack of coastal-dune building activity during marine regressions in the first instance. Finally, coastal aeolianites containing units dating to both interglacial and glacial periods can be observed in some locations, e.g. Western Australia (Price et al., 2001) and Israel (Frechen et al., 2004). Brooke (2001) attributed diachronous deposits such as these to aeolian reworking of material deposited in previous interglacials during subsequent arid glacial periods, though another potential explanation is the geometry of the coastlines upon which they were deposited. This possibility is discussed in the following section.

2.3.2.2 Coastal geometry

The geometry of the continental shelves upon which coastal aeolianites are present is an important influence on both the timing and manner of their formation, through its modulation of sea-level change and the availability of accommodation space. Regarding its influence on the timing of aeolianite formation, on steep-rimmed ocean platform locations (such as Bermuda and the Bahamas) accumulation is focussed around sea-level highstands, as in such locations once sea level falls below the platform edge sediment supply is withdrawn (Abegg et al., 2001; Carew and Mylroie, 2001). Conversely, coastlines on low-angle shelves can host aeolianites deposited during a much wider range of sea levels due to a more continuous supply of marine sediment. Aeolianite formation typically tracks coastline position, though in arid locations where meteoric cementation and stabilisation by vegetation of sediments exposed in sea-level regressions is inhibited, sediment is free to be transported long distances inland (e.g. Williams and Walkden, 2001).

The influence exerted by continental shelf geometry on the timing of coastal aeolianite formation was demonstrated by Price et al. (2001), who compared the depositional ages of aeolianites on Lord Howe Island, a composite basalt and aeolianite oceanic island situated 600 km east of Australia and rising from water depths of >1800 m, to Rottnest Island, a limestone island situated on the shallow continental shelf about 18 km off the western Australian shoreline. The Lord Howe Island aeolianites were found to date only to during or shortly after sea-level highstands, with deposition ceasing when sea level reached -50 m or more below the island platform. In contrast, those from Rottnest Island and the adjacent shoreline were found to have been deposited during both the Last Glacial Maximum (LGM) and the last interglacial, which Price et al. (2001) attributed to continued sediment supply from the adjacent shallow continental shelf during periods of low sea level.

Coastal geometry is also significant with respect to the morphology of coastal aeolianite deposits. Barriers formed on relatively steep substrates will generally develop a narrower and higher shape, as successive deposits stack on top of one another (e.g. Illenberger, 1996 and references therein; Carew and Mylroie, 2001). Erosion of previous generations of deposition in such locations is also likely, due to limited accommodation space. Conversely, barrier formation on gentle substrates (and consequently with more accommodation space) will result in spatially separated deposits. This is especially pronounced in tectonically uplifting areas, such as the Coorong coastal plain in southern Australia. There, gentle epeirogenetic uplift has permitted the preservation of thirteen separate coastal barriers formed during successive Quaternary interglacial and interstadial sea-level highstands and now reaching ~100 km inland (Murray-Wallace, 2002).

2.3.2.3 Climatic factors

Although chronologies derived from coastal aeolianites are often interpreted with respect to sea-level state, in some instances such deposits can also function as sensitive archives of various climatic variables, as recorded in their orientation, geometry and/or palaeontology. As discussed in section 2.2.3.2, the distribution of barrier dune and transgressive dune systems on the southern African coast is governed by the relative degree of aridity during the period in which maximum annual wind velocities occur (Roberts et al., 2009). In the same article, Roberts et al. (2009) also interpret the attenuated dimensions of transgressive coastal dunefields from the last interglacial relative to those formed in the Middle Pleistocene and Holocene as a possible indicator of a weakened South Atlantic Anticyclone at that time. On smaller scales, pulses of Late Holocene coastal-dune activity

record episodes of increased storminess in numerous locations (e.g. Rink and Forrest, 2005; Aagaard et al., 2007; Clemmensen et al., 2009), palaeosols interspersed between aeolian sediments indicate periods of increased humidity (e.g. Havholm et al., 2004), and climatic inferences can even be made from faunal footprints preserved in aeolianite bedding. Roberts et al. (2008) used elephant trackways dating to the last interglacial preserved in coastal aeolianite at Still Bay, South Africa to infer the presence of more woodland, and thus a higher rainfall regime then than at present.

2.3.3 Terrestrial sediment input

Thus far, discussion of coastal dunes in this chapter has centred largely on their marine component, as a significant volume of carbonate is required for their preservation as aeolianite. However, coastal dunes also often include a minor to moderate fraction of quartz or other detrital grains originally of terrestrial origin. In some locations, the association of coastal dunes with terrestrial sediments delivered by rivers to the littoral zone is clear, e.g. the barrier islands on the Mozambique coast (Armitage et al., 2006) and the prograded Encounter Bay barriers in the Murray Lakes region of western Australia (Murray-Wallace et al., 2010). Both of these deposits date to sea-level highstands. In other situations, interruption of fluvial sediment supply by rising sea levels can cause erosion. For example, at the Rio Grande do Sol coastal barrier dunes in Brazil, present high sea levels are currently preventing sediment carried by streams and rivers reaching the coast by trapping it in back-barrier lagoons, causing net erosion of the barriers (Tomazelli et al., 1998; Dillenburg et al., 2004).

The importance of establishing sediment provenance relationships is well recognised in reconstructions of inland aeolian system evolution (e.g. Muhs et al., 2003; Pease and Tchakerian, 2003; Yang et al., 2007). However, the geochemical and mineralogical techniques commonly used for sediment provenancing purposes (see chapter 5) prove most successful where potential sources display strongly contrasting geology and/or where sediment transport pathways are relatively simple. Thus, whilst several studies have successfully identified atmospheric dust inputs from distal sources to coastal carbonate substrates (e.g. Muhs et al., 2007a; Muhs et al., 2007b), attempts to relate possible local terrestrial sediment sources to coastal-dune sands (which are inevitably well mixed by marine and aeolian transport) are much rarer. In the limited number of studies where provenance relationships have been established for coastal-dune sands, they have proven useful in interpreting their evolution. For example, by considering the textural and geochemical properties of coastal cliff-top dune sands at Rubjerg Knude, Denmark, Saye et al. (2006) were able to ascertain that although they

contained a marine component, the main source of sand was provided by underlying glaciofluvial and glaciolacustrine deposits released by a recent acceleration in the rate of coastal cliff retreat. Similar techniques were used by Saye and Pye (2000) to determine that the large and currently eroding Aquitaine coastal-dune system, in southwest France, formed predominantly from reworking of underlying coversands with very limited input from external sediment sources, highlighting the threat of further erosion in the future.

2.4 Chapter summary

This chapter has discussed the major morphological types of coastal dune, and the factors that determine which of these dune types occurs in a given location. The manner in which coastal dunes are preserved as aeolianite has been described, as have the controls on where and when aeolianite occurs. Finally, the palaeoenvironmental significance of preserved coastal aeolianite deposits was discussed, with reference to various examples from the palaeorecord. The information presented here is utilised in describing the Wilderness barriers in chapter 3, and in interpreting the dating and provenance results to reconstruct their emplacement and evolution in chapter 7.

3 Geology and palaeoenvironmental history of Wilderness and the southern Cape

3.1 Introduction

The purpose of this chapter is to collate data necessary for producing a coherent reconstruction of the Mid- to Late-Quaternary evolution of the Wilderness barrier dunes. The first part of the chapter outlines the geological, geomorphological and tectonic evolution of the southern Cape. This information informs a detailed description of the mineralogy of the geology local to Wilderness, as is required for heavy mineral sediment provenance analyses of the Wilderness barrier sands. Possible offshore sources of sediment are also described. The modern and Quaternary climate of the Wilderness region is discussed, as is the local oceanography, as these are potentially fundamental controls on barrier activity. Quaternary coastal-dune activity elsewhere on the southern Cape is also considered. The latter part of the chapter (section 3.7) presents a detailed review of existing literature concerning the Wilderness barriers, highlighting the gaps in knowledge this research aims to address.

3.2 Evolution of the southern Cape

3.2.1 Geology

The southern Cape of South Africa emerged as a coastal region with the break-up of the supercontinent Gondwana and the opening of the Southern Ocean and South Atlantic, which initiated during the Early Jurassic (190-180 million years ago (Ma)) and was largely completed by the Mid-Cretaceous around 100 Ma (Veevers, 2004). The geology of the southern Cape, as shown in Figure 3.1, has its origins long before this division took place. The basement rocks of the southern Cape belong to the "pre-Cape" Saldania Belt, which was deposited as basin infill during the Neoproterozoic (800-545 Ma), and folded and sheared in the Saldania orogenic episode towards the end of this period (Frimmel et al., 2001). The largest surface exposure of Saldania Belt rocks is found in the Cape Town area (the Malmesbury Group), and smaller east-west orientated inliers are located further east at Outdshoorn (Kango Group), Wilderness (Kaaimans Group) and Nature's Valley (Gamtoos Group) (Rozendaal et al., 1999). During the Mid- to Late-Precambrian and Cambrian (560-510 Ma) intrusive granite plutons formed in the Saldania Belt in three locations: two on the western coast and a third

eastern group (the “George granites”) close to Wilderness (Harris et al., 1997). The granites are mapped together with the Saldania Belt in Figure 3.1 and located in greater detail in Figure 3.2, which shows the geology in the immediate vicinity of the Wilderness embayment.

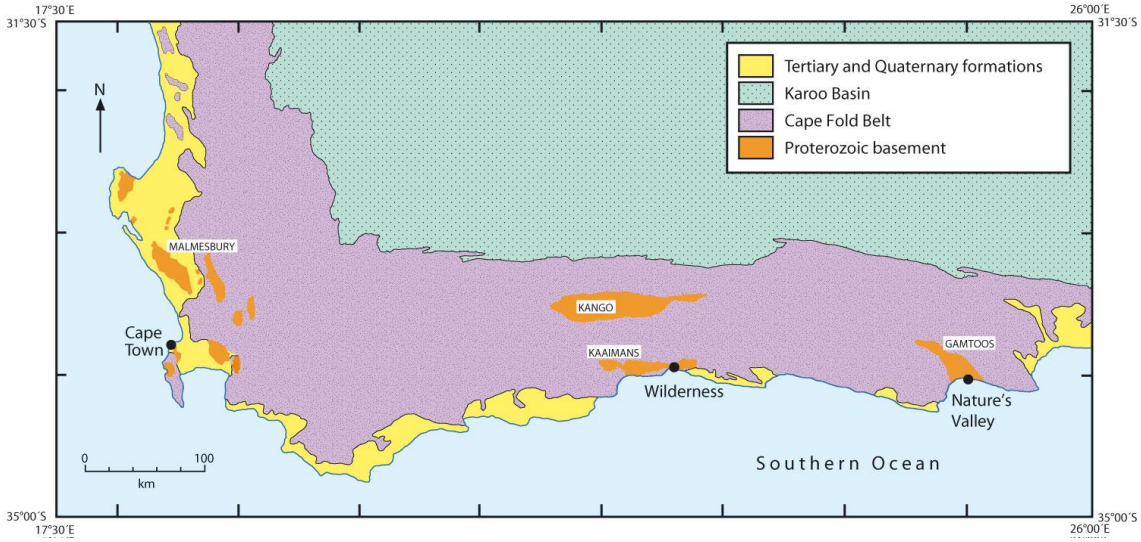

3.1 Major geological formations of the southern Cape. The area mapped as Proterozoic Basement includes both Saldania Belt metasediments (names labelled) and the granites intruded into them. Based on Goldblatt and Manning (2002).

Overlying the Neoproterozoic Saldania Belt basement rocks, the Cape Fold Belt (CFB) stretches ~1300 km along the southern Cape and comprises rocks originally laid down as shallow marine and coastal delta sediments during the Ordovician and Early Carboniferous (490-354 Ma) (Frimmel et al., 2001). The CFB rocks can be divided into three groups, which named from youngest to oldest (and also from north to south) are the Witteberg, Bokkeveld and Table Mountain Groups (Rust, 1977). Of interest to this research are the Table Mountain Group (TMG) rocks, which form a ~30-60- km-wide belt along the current southern Cape coastline and contain only a few narrow infolds of Bokkeveld Group shales (Figure 3.2). Dating of detrital zircon grains in the sedimentary TMG reveals it contains material derived from both the Saldania Belt rocks and the intrusive granites (Fourie et al., 2011).

An episode of orogeny took place prior to rifting of Gondwana in the Permian and Triassic (280-220 Ma) (Ferré and Améglio, 2000) and uplifted the CFB to form the Cape Fold Mountains. As elevation took place, the mountains became a southerly source of sediment for the inland Karoo Basin that formed coeval with the Cape orogeny (Deacon et al., 1992). During the separation of Gondwana and the Cape orogeny the CFB rocks of the newly emerging coastline were subject to tensional stresses, producing a series of half-graben structures (Shone and Booth, 2005). Conglomerates and fanglomerates comprising well rounded

quartzite boulders with interbedded red and white silty marls, collectively known as the Keurbooms Formation, were deposited within these in the Late Jurassic and Cretaceous periods (140-65 Ma) (Helgren and Butzer, 1977; Marker and Holmes, 2005). Preserved beds of Keurbooms Formation deposit are absent from the Wilderness embayment, but are present at the edges of Knysna lagoon to the east (Figure. 3.2).

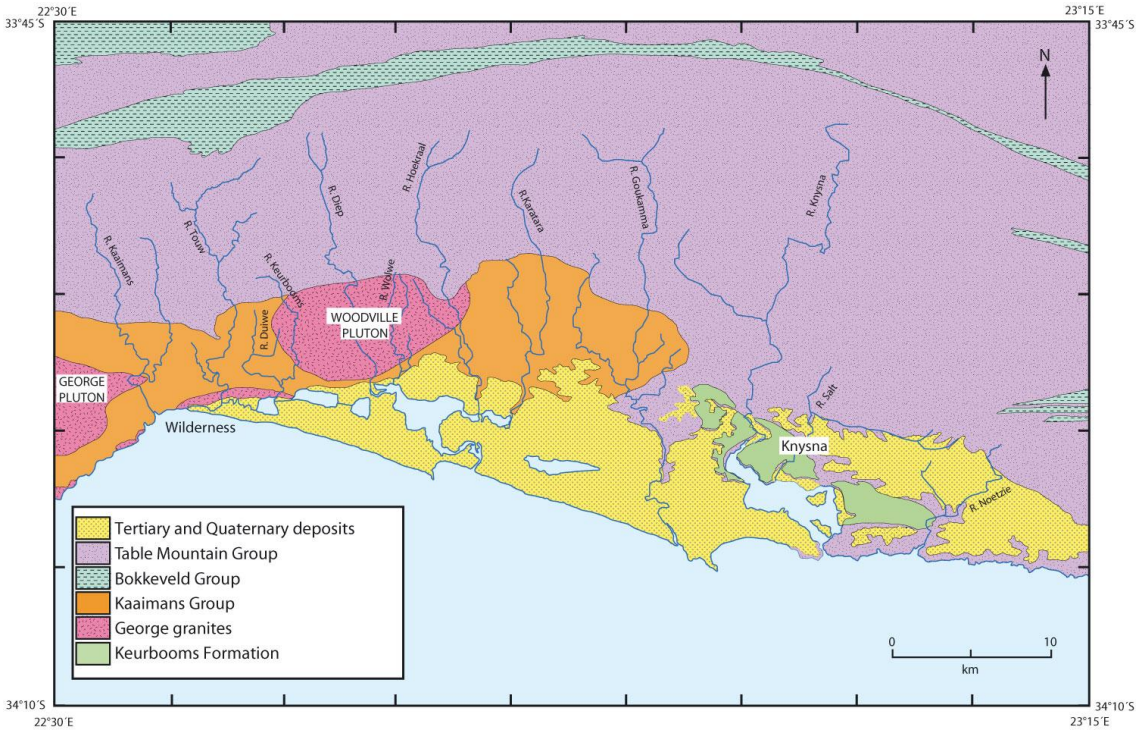

3.2 Geology in the immediate vicinity of the Wilderness embayment. The Woodville and George plutons of the George granites are labelled individually, as are the towns of Wilderness and Knysna. Coversands are included with the Tertiary and Quaternary deposits. Map also shows river courses. Based on Toerien and Roby (1979).

The youngest geological units on the southern Cape are the Late Tertiary and Quaternary successions of calcareous and quartzitic beach rock, shallow marine and aeolianite sediments. These deposits reflect relative sea-level movements during these periods, and occur intermittently along the southern Cape coastline in a belt between ~10-56 km wide and up to ~200 m thick (Figure 3.1) (Siesser, 1972; Malan, 1990). Around Cape Town they are referred to as the Alexandria Formation, on the east coast the Algoa Group, and on the southern Cape coast the Bredasdorp Group (Siesser, 1972; Maud and Botha, 2000). The Wilderness barriers are incorporated within the Bredasdorp Group (Malan, 1990).

The area immediately inland of the Wilderness embayment is characterised by a deep layer of unconsolidated and carbonate-poor quartzitic medium- to fine-grained coversands

(mapped in chapter 1 Figure 1.3). As it is extremely localised in distribution this deposit, known as the Knysna coversands, is not formally recognised as a geological component of the landscape. However, Marker and Holmes (2002) presented an extensive discussion of its distribution and properties. The coversands reach a maximum thickness of ~6 m in the vicinity of Knysna estuary, and thin inland and westward over a distance of 6-8 km to a depth of less than 0.5 m. The coversands have no distinct topography and display no aeolian bedding structures, though based on their position in the landscape and their well sorted, fine- to medium-grained particle size distributions they are assumed to be of aeolian origin (Marker and Holmes, 2002; Holmes et al., 2007). Holmes et al. (2007) attempted to date the coversands at two locations east of Knysna Lagoon using OSL. Whilst problems with saturation prevented the calculation of absolute ages for their samples, minimum ages of c. 300 and 500 ka were obtained (Holmes et al., 2007).

3.2.2 Geomorphology

The present-day morphology of the southern Cape is strongly influenced by its geology. Prior to the break-up of Gondwana the elevation of southern Africa was uniformly high (around 2-2.5 km: Partridge and Maud, 1987), producing a substantial marginal escarpment at the time of rifting (Partridge and Maud, 2000). This feature is thought to have been driven rapidly inland by erosion in the humid climate of the Cretaceous (Tinker et al., 2008b; Tinker et al., 2008a), and where preserved the “Great Escarpment” now lies about 200 km inland from the southern coast of South Africa and 50 km from the western coast (Ollier, 1985). As the escarpment receded, erosion to absolute base level cut a gently sloping bench across the coastal hinterland (Partridge and Maud, 2000) and the east-west orientated CFB was exposed, creating a series of mountain ranges (Marker and Holmes, 2005). Inland of the Wilderness embayment TMG rocks form the Outeniqua Mountain range, whose relative proximity to the coast (20-30 km) results in a series of narrow, sub-parallel river catchments (Figure 3.2) (Marker and Holmes, 2005).

Whereas the southern Cape coastline displays a broadly convex curve, the half-graben faults formed during the separation of Gondwana trend NW-SE. This results in an alternating sequence of straight, hard-rock cliffs of TMG quartzites and sandy bays incised into the relatively less resistant Keurbooms sediments that were deposited in the half grabens during the Cretaceous (Marker and Holmes, 2005). The embayments at Wilderness and Nature’s Valley (located in Figure 3.1) are exceptions to this. At these locations there are no half-grabens filled with Keurbooms Formation conglomerates; rather, marine erosion has incised

directly into the easily erodible Proterozoic shales and phyllites of the Kaaimans and Gamtoos Groups respectively. At Wilderness this has resulted in the presence of a crescent-shaped embayment ~40 km long and 6 km deep (from the modern shoreline) at its centre. The embayment at Nature's Valley is much smaller at only ~3 km wide, and does not contain any barriers or aeolianites similar to those at Wilderness.

3.2.3 Tectonic setting

The current seismo-tectonic model determined for South Africa is a tectonically stable, passive intraplate-type environment (Goedhart and Booth, 2009). The occurrence of any tectonic movement post-Gondwana rifting is debated. Based on geomorphological evidence, Partridge (1997) and Partridge and Maud (1987) suggest two episodes of uplift have occurred on the southern Cape, one in the Early Miocene (c. 20 Ma) and one in the Late Pliocene (between 5.3-2.6 Ma). However, the evidence in support of these episodes has been subject to some criticism: Brown et al. (2000) suggest there may have been no significant uplift since the break-up of Gondwana, and Gurnis et al. (2000), whilst supportive of fission-track and offshore sedimentation evidence for post-rifting uplift, are sceptical of the evidence for the Pliocene episode. There is no evidence that the southern Cape coast has undergone vertical uplift or subsidence during the Quaternary. The assumption of tectonic stability underlies all recent interpretations of southern Cape palaeoenvironments and their relation to sea level through the Quaternary (e.g. Bateman et al., 2004; Roberts et al., 2009; Carr et al., 2010a; Fisher et al., 2010; Compton, 2011), and is similarly adopted in this research.

3.2.4 Summary

A summary of the major geological, geomorphic and tectonic events discussed in section 3.1 is provided in Table 3.1 overleaf.

Table 3.1 Geological time scale covering major geological and geomorphic events discussed in section 3.1

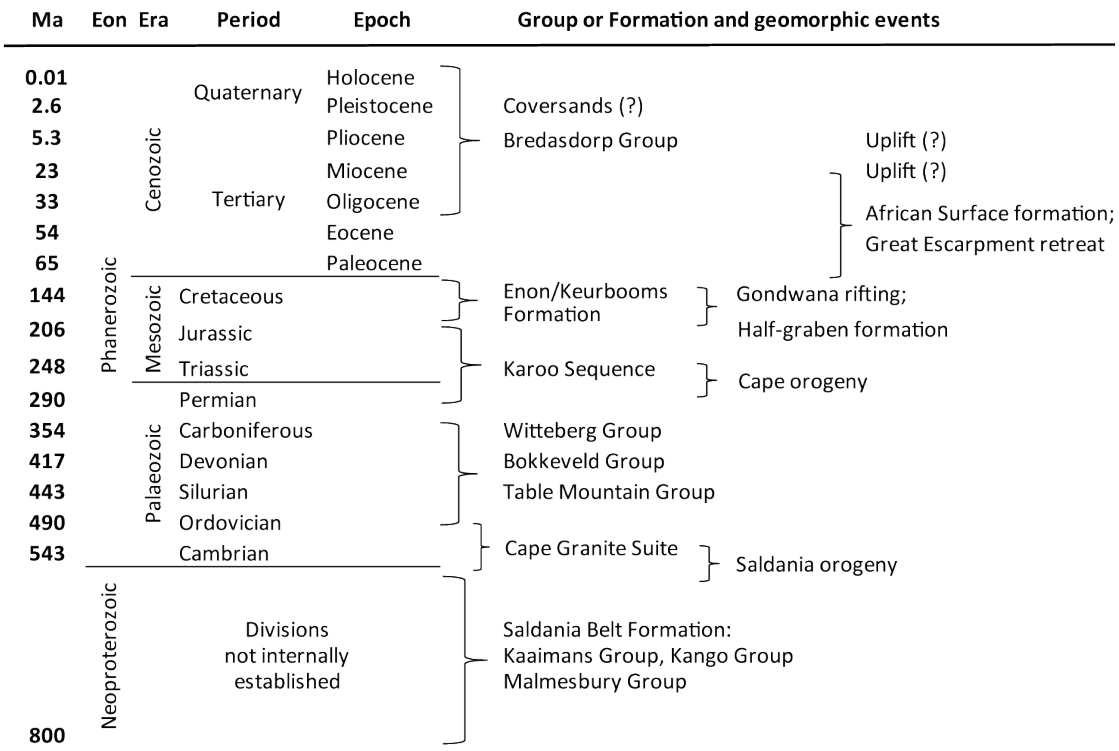

3.3 Mineralogy of the geological formations local to Wilderness

Figure 3.2 maps the extent of the geological formations local to the Wilderness embayment. This section describes the mineralogy of these rock types, one or more of which may potentially form the parent material of the barrier sands, as mineralogical data are required for the heavy mineral analysis conducted as part of this research. Formations are considered in order of age, beginning with the oldest (Kaaimans Group), then the intrusive George granites, and finally the TMG. Literature concerning the mineralogy of the Bredasdorp Group, within which the Wilderness barriers are included, is also discussed in this section. There are no published studies of the mineralogy of the coversand mineralogy, however it has been investigated as part of this research and findings are presented in chapter 6.

3.3.1 Kaaimans Group

The Kaaimans inlier measures ~100 km east to west and 15 km north to south, and has a total thickness of ~6 km (Gresse, 1983). It comprises feldspathic quartzites, phyllites and schists of low- to medium-metamorphic grade, reaching the middle greenschist-biotite zone[†] (Frimmel and Vanachterbergh, 1995). The Kaaimans Group is divided into six formations, which strike roughly east-west and dip southwards. The formations are divided primarily on the basis of lithology, and are exposed at the surface unit by unit from north to south as if this were the younging direction (Gresse, 1983). In stratigraphic order they are the Silver River; Saasveld; Sandkraal; Skaapkops; Soetkraal; and Victoria Bay formations. A systematic increase in metamorphic grade also exists from north to south (Frimmel and Vanachterbergh, 1995). Primary minerals are quartz, feldspar, biotite, chlorite, muscovite and albite. The suite of accessory heavy mineral species increases in diversity towards the south, and includes amphibole, andalusite, apatite, zircon, tourmaline, apatite, zoisite/clinozoisite, epidote, hematite, zoisite/clinozoisite, and sphene. Garnet is also present close to the granite intrusions (Gresse, 1983; Frimmel and Vanachterbergh, 1995).

3.3.2 George granites

Four plutons of S-type granites (i.e. formed from the melting of buried sedimentary and metamorphic rocks), collectively referred to as the George granites and named the Great Brak River, Rooiklip, George, and Woodville plutons, occur in the Kaaimans inlier (Ferré and Améglio, 2000). The locations of the two plutons closest to Wilderness (George and Woodville) are shown in Figure 3.2. Krynauw (1983) broadly summarised the petrography of the George granites: they are rich in feldspar, plagioclase and quartz, with biotite the primary heavy mineral, in places altered to chlorite, muscovite and/or clinozoisite. Accessory minerals are identified as garnet, zoisite, calcite, epidote, rutile, zircon, apatite, tourmaline, ilmenite, sphene, magnetite and fluorite.

[†] Metamorphic grade depends on the temperature/pressure conditions the rock is subjected to during the metamorphic event, and can be inferred from rock type and mineral assemblage. For example, chlorite beings to crystallize under relatively low temperatures of ~200 °C, indicating low-grade metamorphism. Chlorite, muscovite, biotite, garnet, staurolite, kyanite and sillimanite respectively indicate increasingly high temperatures (and corresponding metamorphic grades) up to 800 °C + (Monroe and Wicander, 2009).

3.3.3 Table Mountain Group

Metamorphism associated with the Cape orogeny (and thus the TMG strata) was less intense than the Saldania orogenic episode responsible for metamorphosing the Kaamains Group rocks, and for the most part only reached lower greenschist facies conditions (chlorite zone) (Frimmel and Vanachterbergh, 1995). The majority of the TMG rocks consist of quartzitic sandstones, with subordinate amounts of feldspar (usually less than 5 %), mica and rock fragments (Visser, 1974).

Young et al. (2004: p. 326) noted that "*there is little published geochemical information from rocks of the Table Mountain Group*", and this also extends to its mineralogy, especially away from the western Cape. Potgieter (1950) provides a qualitative, but reasonably detailed, description of TMG mineralogy in the immediate vicinity of Wilderness, noting that apart from the metamorphosed phyllite and schist horizons, the series is composed mainly of quartzitic sandstones, with zircon the most common accessory mineral. Rutile, tourmaline, hematite and magnetite are fairly abundant, and hornblende, garnet and titanite are sparingly present. Muscovite is more important to the west around George, but becomes less significant eastward where microcline increases in abundance. Where metamorphism has been significant chlorite is abundantly developed, and muscovite and ottrelite are also common (Potgieter, 1950).

3.3.4 Bredasdorp Group

The mineralogy of the Bredasdorp Formations is reported as being uniform, consisting mostly of sand-sized terrigenous material (predominantly quartz and feldspar, presumably derived from the older geological formations discussed previously in this chapter) and comminuted biogenic shelly material set in a calcitic cement (Siesser, 1972). Malan (1990) reports that carbonate content varies from 23-92 % depending on the amount of shell material present, though Bateman et al. (2004) found parts of the Wilderness barriers to be devoid of carbonate. Heavy minerals were noted to comprise a very minor component of the Bredasdorp Group by Siesser (1972) (species not described), along with the presence of small but significant quantities of glauconite grains (usually 1-2 %). Glauconite is an authigenic marine mineral indicative of diagenesis of terrigenous material during periods of low sediment accumulation in water depths of 50-500 m (Wigley and Compton, 2007), and it is abundant on the southern Cape continental shelf (Birch, 1979; Bailey and Rogers, 1997).

3.4 Terrigenous offshore sediments

As discussed in chapter 2, marine carbonates are typically the dominant source of material for large coastal-dune systems, and carbonate production off the southern Cape is discussed in section 3.5.2. However, sediments of terrestrial origin also form a significant component of the material residing on the southern African continental shelf. The majority of modern terrigenous sediment input occurs on the east coast (Figure 3.3 area 4), but the continental margin there is narrow, shallow and extremely high energy. The Agulhas current that flows along it reaches velocities of 2.5 m s^{-1}, and terrigenous sediment input is thus transported rapidly southwards in the form of large underwater dunes before leaving the shelf and entering the Natal Valley via submarine canyons (Flemming, 1978; Flemming, 1980). Further south and west, on the southern Cape coast (Figure 3.3 area 3), the continental shelf broadens to form the wide Agulhas Bank, and the Agulhas current retroflects southward and eastward, ceasing to dominate the shelf (Bailey and Rogers, 1997). Accumulation of terrigenous sediment is thus more significant on the Agulhas Bank than the east coast.

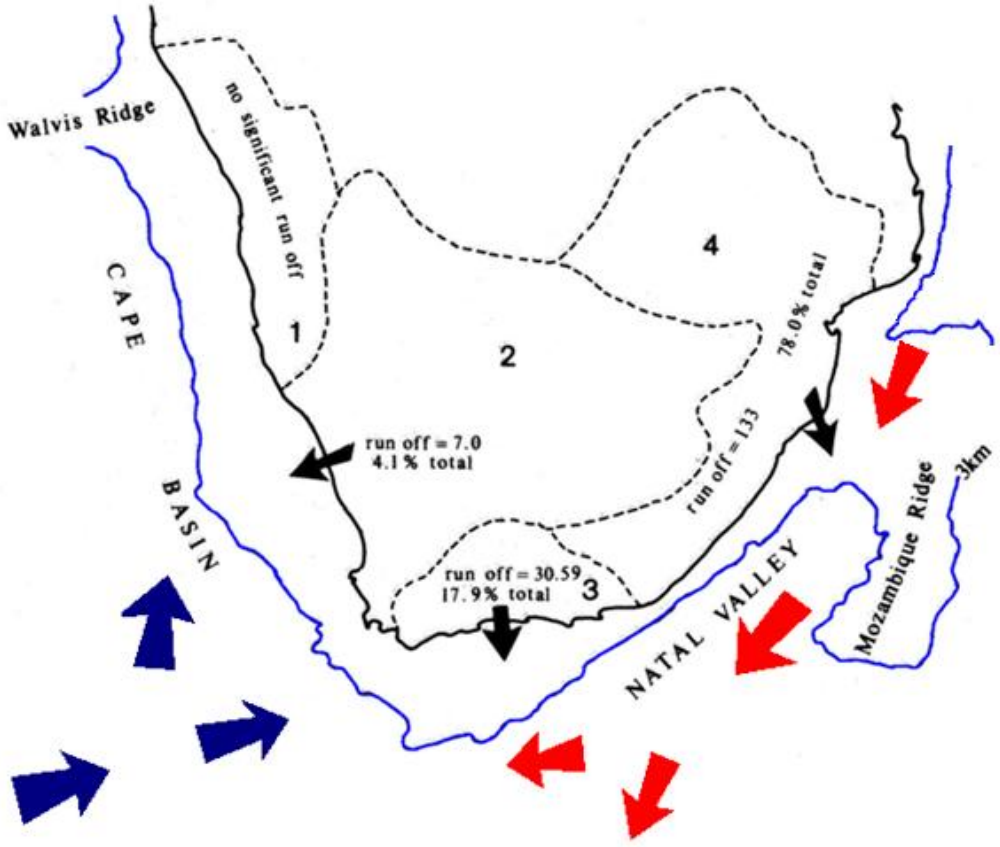

3.3 Drainage areas and fluvial sediment yields (as a percentage of total input and in X 10^6 m^3 a^{-1}) in southern Africa. Offshore, the blue line represents the 3 km isobath. The general pathways of the cold Benguela current (blue arrows) and warm Agulhas current (red arrows) are also shown. The oceanography of the region is discussed further in section 3.5.1 and displayed in greater detail in Figure 3.6. Modified from Dingle et al. (1987).

At its broadest the Agulhas Bank extends 270 km south, with the shelf break lying at 200 m water depth south of Cape Agulhas and shoaling to 140 m off Port Elizabeth (Martin and Flemming, 1986). The extent of the Bank is shown in Figure 3.4. The outer and middle shelf regions are dominated by biogenic shelly sands relict from earlier marine lowstand high energy depositional environments, which contain an increasing terrigenous quartz component landward (Bailey and Rogers, 1997). Abundant glauconite deposits are also present (Parker and Siesser, 1972; Birch, 1979). The inner shelf predominantly hosts quartzitic material of terrigenous origin deposited since sea levels rose following the last glacial maximum, referred to as the "Holocene sediment wedge" (Martin and Flemming, 1986).

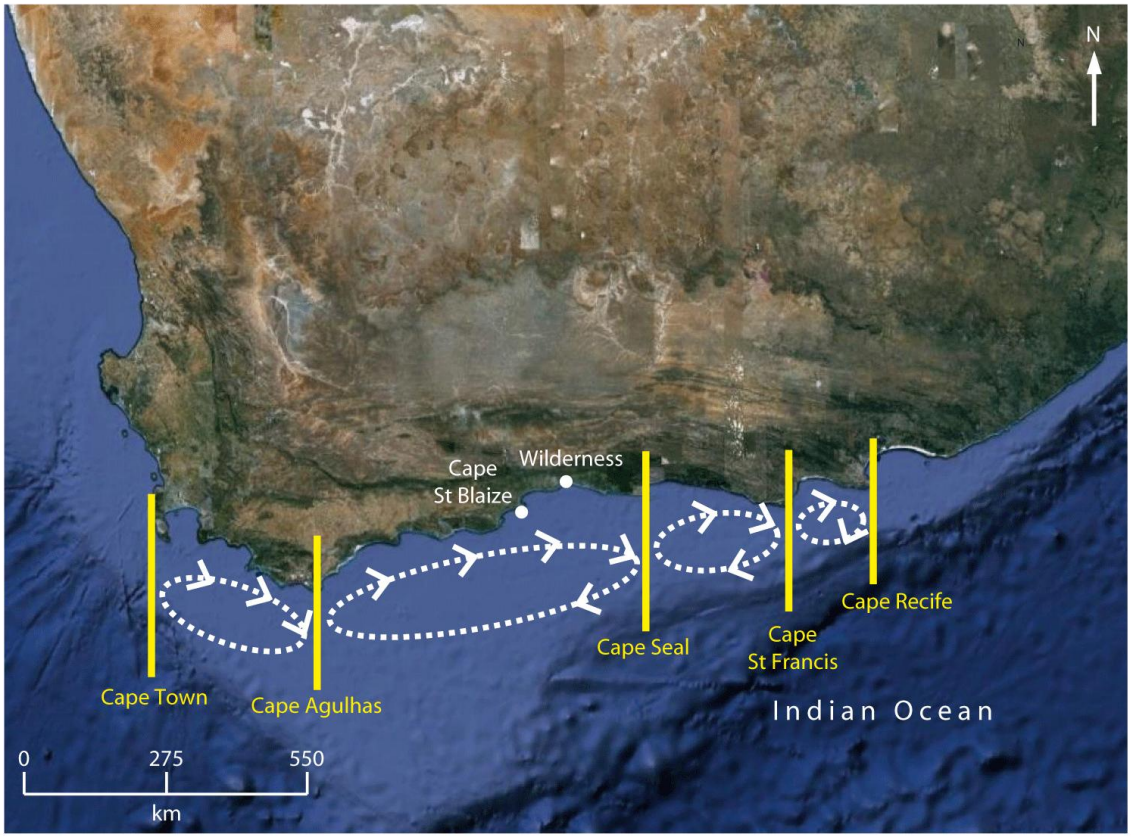

3.4 Sediment compartments on the southern Cape coast, as defined by Birch (1980). From left to right the yellow lines mark Cape Town, Cape Agulhas, Cape Seal, Cape St Francis and Cape Recife, which act as barriers to eastward sediment movement via longshore drift. At these headlands sediment forms offshore spits and is subsequently entrained by the Agulhas current to be transported south and west. The extent of the Agulhas Bank (light blue) is also clear.

Along the southern Cape coast wind-driven forcing is significant, and littoral drift occurs in an eastward direction. However, the numerous prominent headlands and bays mean the potential for sediment movement along the coast via this mechanism is limited, and the Holocene sediment wedge can thus be divided into a number of relatively discrete units. Eastward-moving sand is deposited in large spits east of headlands and subsequently moved

offshore by the Agulhas current, rather than rounding the headland and entering the next bay (Martin and Flemming, 1986; Illenberger, 1993). Using seismic profiling to map these spits, Birch (1980) identified four “sediment compartments” in the nearshore zone between Cape Town in the west and Cape Recife in the east: (i) Cape Town - Cape Agulhas; (ii) Cape Agulhas - Cape Seal; (iii) Cape Seal - Cape St Francis, and (iv) Cape St Francis - Cape Recife (Figure 3.4).

The Holocene sediment wedge in the Cape Town to Cape Agulhas compartment is poorly developed due to minimal terrigenous input and siltation within estuaries, and the Cape Seal to Cape St Francis compartment likewise also only contains minor amounts of unconsolidated sediment (Birch, 1980). Based on detailed seismic and side-scan sonar surveys conducted by the Geological Survey of South Africa, Birch (1980) estimates the majority of nearshore sediment accumulation on the southern Cape (approximately 43 %) is located between Cape St Blaize and Cape Seal in the Cape Agulhas -Cape Seal compartment (Figure 3.4), much of which is further concentrated in the vicinity of the Wilderness embayment. As shown in Figure 3.5, the sediment wedge broadens eastward from Cape St Blaize to the Wilderness embayment, extending 26 km seaward from the present shoreline at its western edge and narrowing to 5.5 km by the eastern edge of the embayment (Birch, 1980). The sediment wedge thickens east of Knysna, and forms a spit-like feature off Cape Seal. Between Mossel Bay and Nature’s Valley, the Holocene wedge is estimated to total 20 X 10^9 m^3 of sediment (Martin and Flemming, 1986).

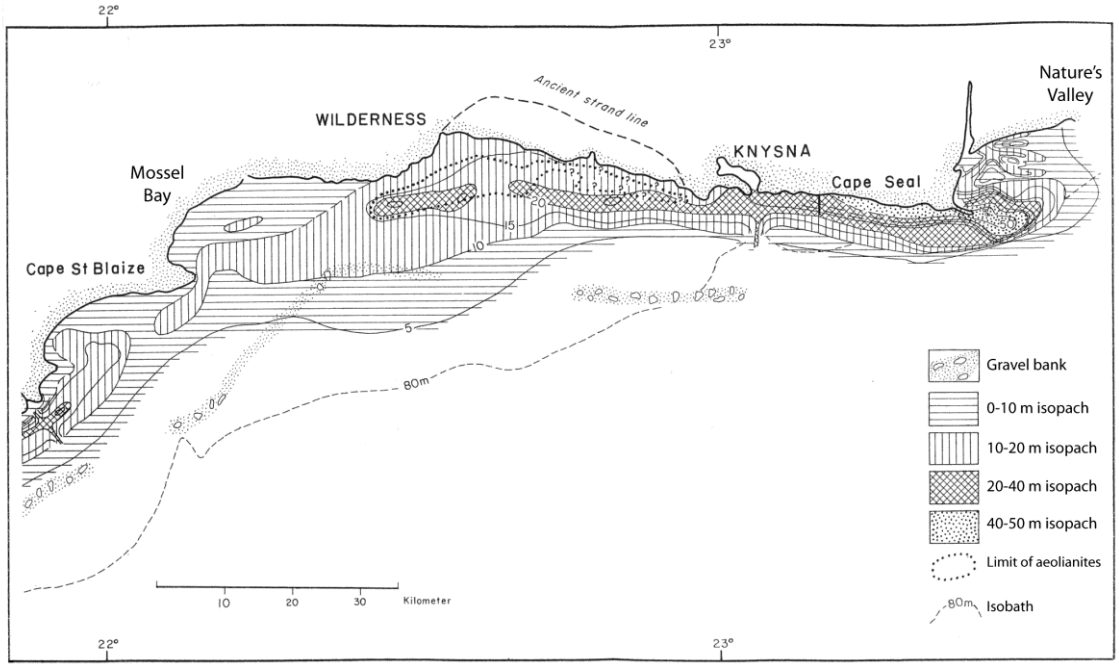

3.5 Thickness of unconsolidated sediment offshore of the Wilderness embayment. Also shows presumed extent of aeolianite offshore. Modified from Birch (1980).

3.4.1 Source of the Holocene sediment wedge

The river catchments between Mossel Bay and Nature's Valley are small, with their headwaters rising in the Outeniqua Mountains only 20-30 km from the coast (Figure 3.2). They currently deliver 0.57 X 10^6 m^3 a^{-1} of sediment to the ocean (Martin and Flemming, 1986). Southern Cape sediment yields may have increased due to human activity in historic times (Martin, 1987; Illenberger, 1993; Marker and Holmes, 2005), but assuming this rate has remained the same for the past 10 ka, it can still only account for 5.7 X 10^9 m^3 of sediment (i.e. just under 30 % of the volume of the Holocene sediment wedge). However, the volume of local fluvial sediment input is more than sufficient to account for the maximum accumulation rate of the Wilderness barriers inferred from Illenberger's (1996) estimations (~0.438 X 10^6 m^3 a^{-1}) (see Table 3.2 in section 3.7.1).

Birch (1980) suggests the large volume of the nearshore sediment wedge around Wilderness may be at least partly explained by the geometry of the coastline. The north-easterly trend of the coast from Cape Agulhas refracts sharply at the western edge of the embayment to one slightly south of east (evident in Figure 3.4), with the now-filled embayment presumably once forming a major re-entrant on an otherwise relatively smooth coastline and acting as a trap for material being moved eastward (Birch, 1980). Martin and Flemming (1986) suggest the Gouritz River, ~75 km west of Wilderness, as a possible source for this material. The Gouritz possesses the third largest catchment in South Africa at 45,702 km^2 (Heydorn, 1989b). Its course predominantly traverses the sandstones and shales of the Cape Fold Belt (Heydorn, 1989b), as described in sections 3.2 and 3.3. The other main source of the nearshore sediment at Wilderness suggested by Martin and Flemming (1986) is erosion of the barriers themselves and the presently submerged aeolianite ridges offshore, evident in Figure 3.5 as the 20-40 m isopachs. These offshore ridges are discussed further in section 3.7.2.

3.5 Oceanography, climate and vegetation

3.5.1 Oceans and ocean currents

The South African coast is a high-energy environment dominated by swell waves, which peak at a modal height of 2.1 m and a period of 11 s along the southern Cape and decrease slightly northward in both directions (Cooper, 2001). The tidal range of the South African coast is consistently small (upper microtidal), with most areas experiencing a spring tidal range of between 1.8-2 m and neap tides between 0.6-0.8 m (Cooper, 2001).

At a hemispheric scale, South Africa lies at the interface of three ocean masses: the South Atlantic to the west, the Southern Ocean to the south and the Indian Ocean to the south east and east. Its coastline also marks the meeting point of several major elements of the global ocean circulation system, illustrated in Figure 3.6. Bordering the eastern and south-eastern coasts is the warm Agulhas current, which, directed by the topography of the continental shelf, transports equatorial waters westward and poleward to the tip of the Agulhas Bank. There it meets the Antarctic circumpolar current and retroflects eastward, returning to the Indian Ocean as the Agulhas Return current. In the South Atlantic to the west of the continent is the Benguela current, one of the largest coastal, wind-driven upwelling systems on Earth (Lutjeharms et al., 2001). The large expanse of cold water that is created by the Benguela upwelling is evident in the asymmetric pattern of sea surface temperatures (SSTs) around the country; at 33° S on the west coast SSTs vary seasonally from 8-16 °C and at the same latitude on the east coast between 20-28 °C (Heydorn and Tinley, 1980 c.f. Tinley, 1985).

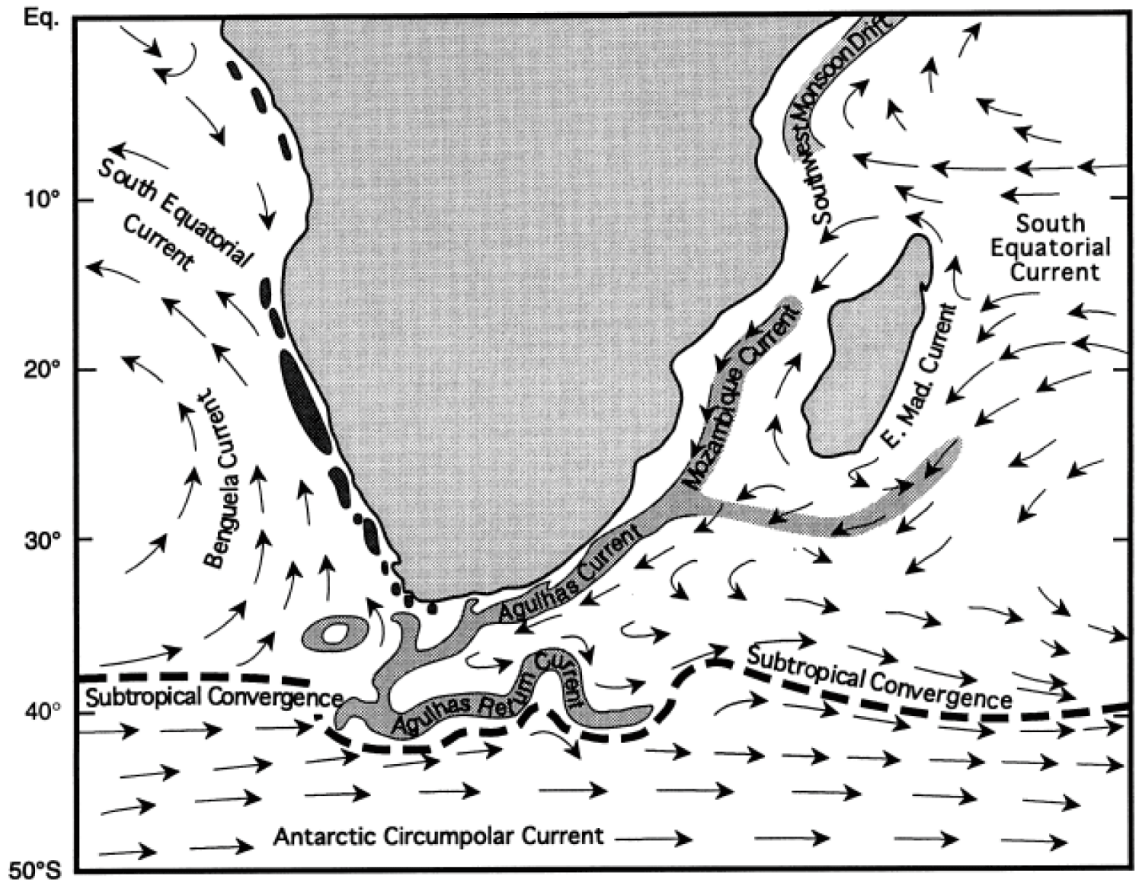

3.6 Ocean currents around southern Africa. The shaded areas off the west coast represent cells of cold water produced by the Benguela upwelling system. From Lutjeharms et al. (2001).

3.5.2 Marine carbonate production

The temperature and nutrient content of ocean waters act as major controls on rates of marine carbonate production (James, 1997). Interaction between the warm Agulhas current and the cold upwelling Benguela current is known to have undergone significant variations across glacial-interglacial cycles (Rau et al., 2002; Peeters et al., 2004), and Bateman et al. (2004) speculated that this variation could be responsible for carbonate-poor sediments found in the Wilderness barrier dating to the MIS 1-2 and MIS 4-5 transitions.

Upwelling of cool, nutrient-rich Indian Ocean water along the eastern edge of the Agulhas Bank, which occurs as a result of interactions with the Agulhas Current, varies seasonally and is known to reduce in response to winter westerlies (Probyn et al., 1994). Thus, it probably also lessened in association with increased windiness during glacial periods (see section 3.6.1 below). However, the position of the Agulhas current is strongly guided by the bathymetry of the Agulhas Bank, and sedimentary records indicate it continued to flow through the last glacial with little change in its lateral position (Winter and Martin, 1990). The middle and outer Agulhas Bank is dominated by relict carbonate sand (Bailey and Rogers, 1997), suggesting carbonate accumulation upon it has never been significantly curtailed. Additionally, Rau et al. (2002) reported the total carbonate content present in an ocean core obtained due south of Cape Town (36°19'S, 19°28'E), representing 450 ka of accumulation. It revealed no clear glacial-interglacial trend and, importantly, consistently high rates of carbonate production, with the $CaC0_3$ content varying from 62-85 % throughout (Figure 3.7).

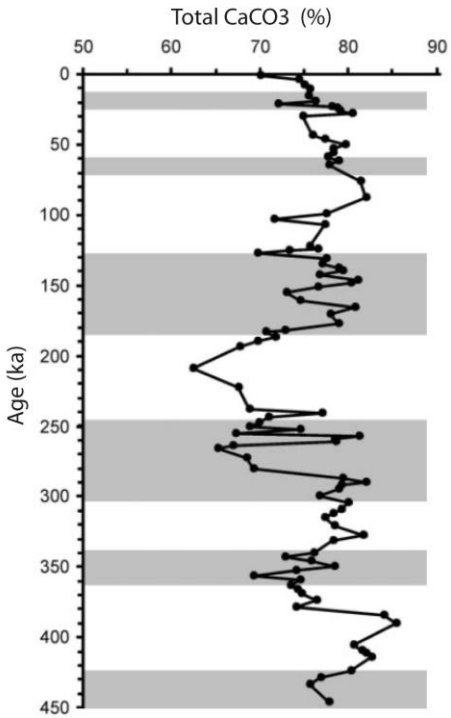

3.7 Calcium carbonate content of an ocean core taken from the Agulhas Bank due south of Cape Town (36°19'S, 19°28'E). Horizontal grey shaded periods represent glacial MIS. From Rau et al. (2002).

3.5.3 Atmospheric circulation and climate

Much of southern African lies astride the southern hemisphere sub-tropical high-pressure ridge, which is centred at around 30° S and arises from the descending portion of the Hadley Cell. Semi-permanent high-pressure cells are located in the South Atlantic and Indian Ocean, both of which undergo a 3-6° seasonal latitudinal oscillation, moving further north in winter. This shift in position allows the mid-latitude belt of westerlies to penetrate further northwards, bringing with them cyclonic depressions and northwesterly winds. In summer the high-pressure cells lie further south and as the mid-latitude westerlies weaken so the tropical easterlies tend to strengthen, resulting in a bimodal annual wind regime blowing quasi-parallel to the southern Cape coastline (Tyson, 1986; Stone et al., 1998). Seasonal wind roses for the southern Cape averaged from offshore measurements are shown in Figure 3.8.

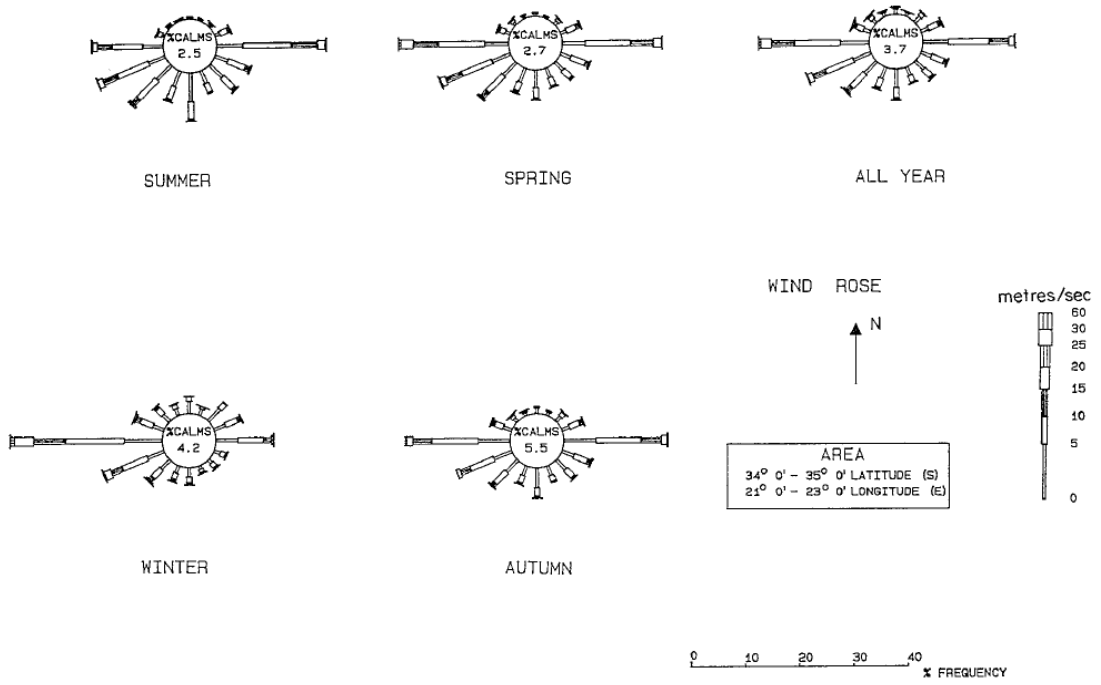

3.8 Wind roses for the southern Cape. Data collected from voluntary boat service in the area indicated. From Heydorn (1989b).

The competing pressure systems, combined with contrasting SSTs, result in a strongly asymmetric climate gradient across southern Africa. The region encompasses subtropical, semi-arid, arid, and to the extreme south-west, temperate climate systems. Wilderness falls in a transitional “year-round rainfall zone” (YRZ), between the winter rainfall zone (WRZ) of the south and west and the summer rainfall zone (SRZ) of the east and interior (Carr et al., 2006b). The YRZ receives precipitation in association with both the cyclonic winter depressions delivered by the mid-latitude westerlies to the WRZ, and the monsoon rainfall in the SRZ

arising as easterly winds associated with the intertropical convergence zone become dominant (Lindesay, 1998). The region local to Wilderness typically receives in excess of 700 mm of rainfall annually spread throughout the year (rising to >1000 mm inland in the Outeniqua Mountains), and has an annual average temperature of 16.9 °C (Grindley, 1985).

3.5.4 Vegetation

The considerably complexity of climate along the southern Cape is reflected in its ecology. The flora of the Cape region is so unusual that South Africa was recognised by Good (1947) as one of only six distinct floristic kingdoms globally. Good's scheme was refined by Takhtajan and Cronquist (1986), and it is now common to refer to the "Cape Floristic Province" (CFP). The CFP covers an area of roughly 90,000 km^2, encompassing the WRZ and extending east into the YRZ. It is one of the most botanically diverse regions on Earth and contains some 9000 plant species, separable into five vegetation biomes (Goldblatt and Manning, 2002). Within the Wilderness embayment, the barrier aeolianites support fine-leaved, sclerophyllous heathland vegetation known as fynbos. Fynbos also forms the typical ground cover inland and around the embayment, though the rugged terrain of the numerous local river valleys has also preserved indigenous Afromontane evergreen forest on cooler south-facing slopes (Marker, 2003). The generally low volume of precipitation on the southern Cape limits the contemporary occurrence of forest to coastal regions east of Mossel Bay, ~75 km west of Wilderness (Goldblatt and Manning, 2002), and around Wilderness and other locations climatically suitable for its occurrence trees have been largely removed from more accessible areas by human agency following European arrival in the 18^{th} century (Marker, 2003).

3.6 Palaeoenvironmental record

3.6.1 Climate

As discussed in chapter 2, the climatic factors most significant for coastal-dune activity are rainfall (through its influence on vegetation cover and, consequently, sediment supply and dune stability) and wind regime. The tropical and temperate weather systems responsible for these climatic variables over southern Africa are theoretically strongly influenced by glacial-interglacial cycles. The monsoon system that delivers rainfall to the SRZ relies on high SSTs and strong summer warming of the continent to create robust convection cells, conditions that are more pronounced in warm interglacials (Chase and Meadows, 2007). The extent and position

of the WRZ is dependent on the latitudinal position of the westerlies, which are also potentially influenced by glacial-interglacial climate cycles (Cockcroft et al., 1987).

Unfortunately, long, continuous Quaternary records of continental sedimentation in southern Africa from which regionally specific palaeoclimatic signals can be extracted are scarce. Attempts to synthesise the palaeoenvironmental history of the region cite a paucity of research (particularly outside the SRZ) and conditions not conducive to the preservation of traditional palaeoecological proxy data sources (e.g. pollen, insects etc.) as significant obstacles to producing complete reconstructions (e.g. Meadows and Baxter, 1999; Carr et al., 2006b; Chase and Meadows, 2007). The main sites from which YRZ palaeoclimatic data has been obtained are Boomplass, Blombos and Crevice caves, and the Vankervelsvlei coastal wetland. Boomplaas Cave, located 80 km inland north west of Wilderness, contains 5 m of stratified deposits spanning the last ~80 ka and incorporating micro- and macro-faunal remains introduced by owls, carnivores and *Homo sapiens* (e.g. Klein, 1978; Avery, 1982). Vankervelsvlei occupies an interdunal depression within the Wilderness embayment, and cores provide palynological data spanning ~50-2.5 ka (Irving, 1998 c.f. Chase and Meadows, 2007). Blombos Cave lies on the coast 150 km west of Wilderness, and incorporates faunal remains mostly introduced by human agency, providing an intermittent record between ~140-70 ka (Henshilwood et al., 2001). Crevice Cave is also coastal, 60 km west of Wilderness, and isotopic analysis of speleothems formed within it provide a continuous record of the relative strength of summer and winter rainfall from 90-53 ka (Bar-Matthews et al., 2010). Reconstructions based on data from these sites are discussed in the following sections.

3.6.1.1 Rainfall

A palaeoenvironmental synthesis produced by Carr et al. (2006b) combined evidence from a variety of sources to infer Late Quaternary trends in aridity for southern Cape regions including the WRZ, SRZ and YRZ (Figure 3.9). Their results for the YRZ infer relatively dry and windy conditions from 60-45 ka, wetter conditions between 42-30 ka, a period of relative aridity closer to conditions in the SRZ than the WRZ from then until post-LGM, increasing moisture availability into the Holocene, and some evidence for an arid period around 5 ka (Carr et al., 2006b). The Crevice Cave speleothem record also indicates a reduction in winter rainfall in the YRZ during MIS 4 (Bar-Matthews et al., 2010). Similarly, Meadows and Baxter (1999) interpret multiple palaeoclimatic records as indicating that the YRZ experienced arid conditions "*in phase*" with the SRZ interior during glacial periods. The synthesis by Chase and Meadows (2007) extends further, to the penultimate interglacial (MIS 5), and infers warmer

and wetter conditions at this time. It alsocorroborates evidence for a drier and colder LGM in the YRZ and a relatively arid Mid-Holocene. A less effective monsoonal system, increased continentality from the extended coastal plain and limited penetration of temperate cyclonic depressions due to an expanded continental anticyclone are suggested as explanations for drier glacial periods in the YRZ (Chase and Meadows, 2007).

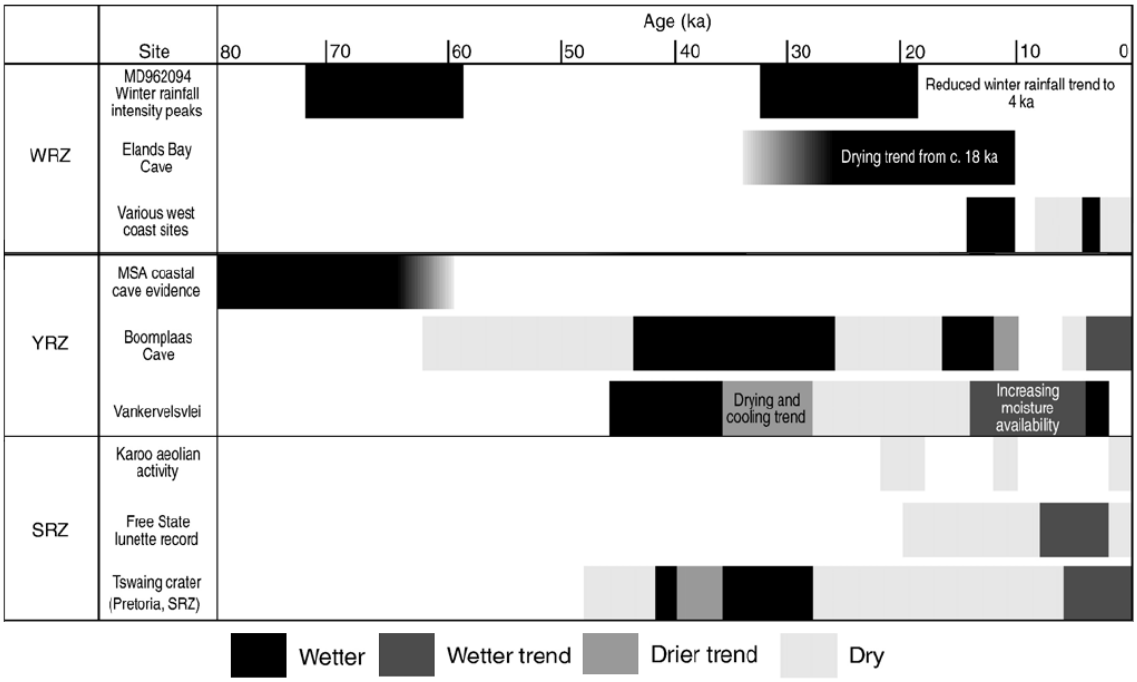

3.9 Palaeoclimatic synthesis for southern Cape regions (WRZ, YRZ, SRZ). Modified from Carr et al. (2006b).

3.6.1.2 Vegetation

Evidence demonstrates that the positions and extent of the vegetation biomes present on the southern Cape have shifted in response to changes in climate through the Late Quaternary (Carr et al., 2006b). The two major biomes present in the region around Wilderness are Afromontane evergreen forest and, in drier and/or more frequently disturbed locations, heath-like fynbos. Footprints of the forest dwelling African elephant (*Loxodonta Africana*) preserved in MIS 5 aeolianite bedding at Still Bay, ~130 km west of Wilderness, indicate the forest biome extended farther west during the last interglacial, providing additional evidence for a higher moisture regime then than at present. Importantly, whilst pollen and fossil evidence indicates the LGM was drier and cooler than at present in the YRZ, it also confirms the region remained vegetated (Irving and Meadows, 1997; Carr et al., 2006b and references therein). The vegetation likely to have colonised the Agulhas Bank when exposed by sea-level regression is described by Compton (2011) who, based on offshore

geology, hypothesises a mosaic of fynbos, grassland and strandveld (which includes more succulent species than fynbos and recovers less well from burning) would have covered the shelf.

3.6.1.3 Wind regime

Palaeowind regimes can be inferred from the orientation of preserved dune strata. Measurements from various southern Cape locations suggest that westerly winter wind directions similar to today have been dominant throughout the Late Quaternary (Roberts et al., 2008; Roberts et al., 2009). The attenuated dimensions of MIS 5 transgressive dunefields on the west coast of South Africa relative to their middle Pleistocene and Holocene counterparts are interpreted by Roberts et al. (2009) as indicating a reduction in wind strength during this period, attributed to reduced meridional pressure gradients. Marine sediment cores off the West African coast provide additional evidence for reduced wind strength during interglacials and stronger LGM winds, on the basis of variations in the particle size of aeolian sediments blown offshore (Stuut et al., 2002; Stuut et al., 2004),

3.6.2 Sea levels

The southern Cape is a far-field location distant from major glaciation centres, and is understood to have experienced no episodes of tectonic uplift or subsidence during the Quaternary. It is widely implied that far-field sites have a spatially homogenous response to relative sea-level (RSL) change (Woodroffe and Horton, 2005). Eustatic sea-level curves representing RSL changes in the "mean ocean" have thus been considered appropriate for use in palaeoenvironmental reconstructions of southern Cape coastal sites (e.g. Marean et al., 2007; Carr et al., 2010a), and are generally considered more accurate than curves based solely on geomorphological evidence. Ramsay and Cooper (2002) constructed a partial sea-level curve for South Africa covering the past 180 ka using terrestrial evidence, but both the accuracy and volume of the data points used has been criticised (Carr et al., 2010a).

One of the most widely cited, lengthy and complete eustatic sea-level curves is that of Waelbroeck et al. (2002), which combines isotopic records derived from benthic forams in sediment cores from the north Atlantic, southern Indian and equatorial Pacific oceans to span 430 ka in 1.5 ka increments. The curve is reproduced in Figure 3.10 and labelled with marine isotope stages (MIS). Oceanic oxygen isotope records were divided by Emiliani (1955) into stages numbered from the youngest sediments downwards: these MIS have been universally

adopted to provide a global stratigraphic framework for the alternating glacial-interglacial periods of the Quaternary, and are used throughout this thesis.

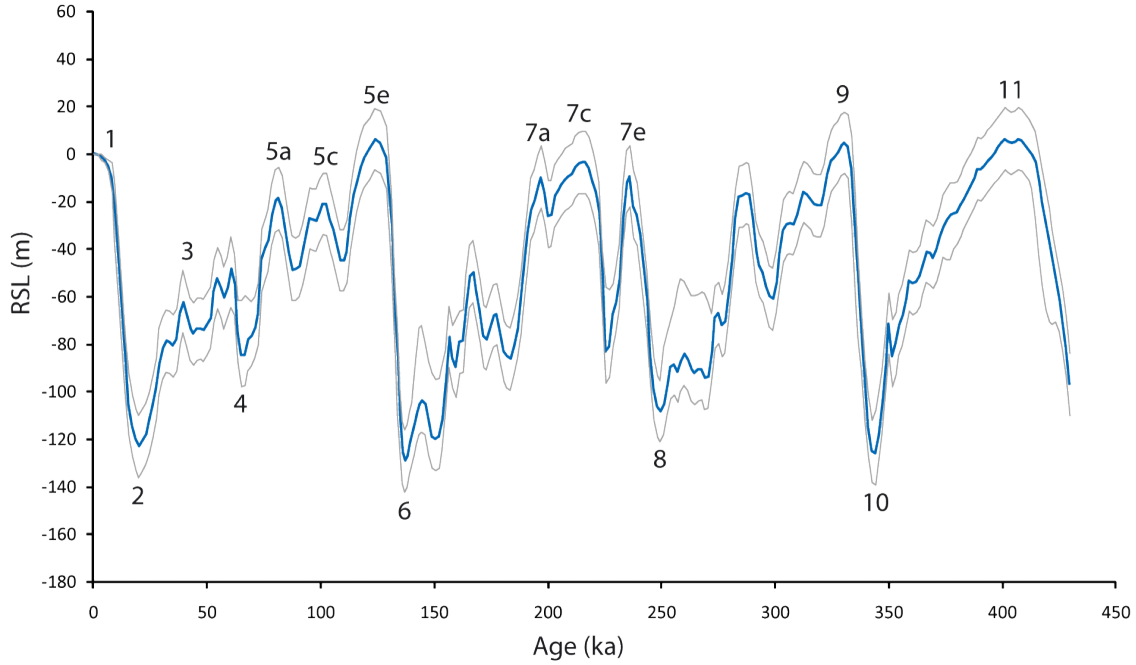

3.10 Global relative (eustatic) sea-level curve for the period 0-450 ka (bold blue line) and associated confidence interval (thin grey lines) redrawn from Waelbroeck et al. (2002). Numbers on peaks and troughs indicate MIS stages.

Dated terrestrial evidence suggests the Waelbroeck et al. (2002) curve is appropriate for the southern Cape. Carr et al. (2010a) used OSL and amino acid racemisation dating techniques to obtain MIS 5 sea-level index points from marginal marine and aeolian sediments at Sedgefield, within the Wilderness embayment, and from three other sites on the southern Cape coast. Tidal inlet facies at Sedgefield located 0.5 m above modern sea level (amsl) date to 138 ± 7 ka and 130 ± 8.2 ka at 4.5 m amsl, indicating a rising sea-level trend for this period, and a maximum sea level at 127 ± 6 ka of +5.6 m amsl, followed by sea-level regression as indicated by immediately overlying aeolian facies. Similar values were obtained from the other southern Cape sites, indicating an MIS 5e highstand of between 6-8.5 m amsl, and broad agreement throughout the last interglacial with the mean eustatic curve (Carr et al., 2010a). Fisher et al. (2010: p. 1386) also correlated the eustatic sea-level curve of Waelbroeck et al. (2002) with terrestrial sea-level indicators on the southern Cape from MIS 5e and MIS 11, noting them to be in good overall accordance with only "*some minor vertical disagreement*" [unspecified]. Additional detail for the MIS 5e highstand is provided by the sea-level curve of Hearty et al. (2007), who produced a high-resolution record for the period compiled from morphological, stratigraphic and sedimentological evidence from 15 far-field sites. Their

composite curve, shown in Figure 3.11, exhibits a double peak in sea level separated by a regression of at least several m at c. 125 ka that is not apparent in the global eustatic record.

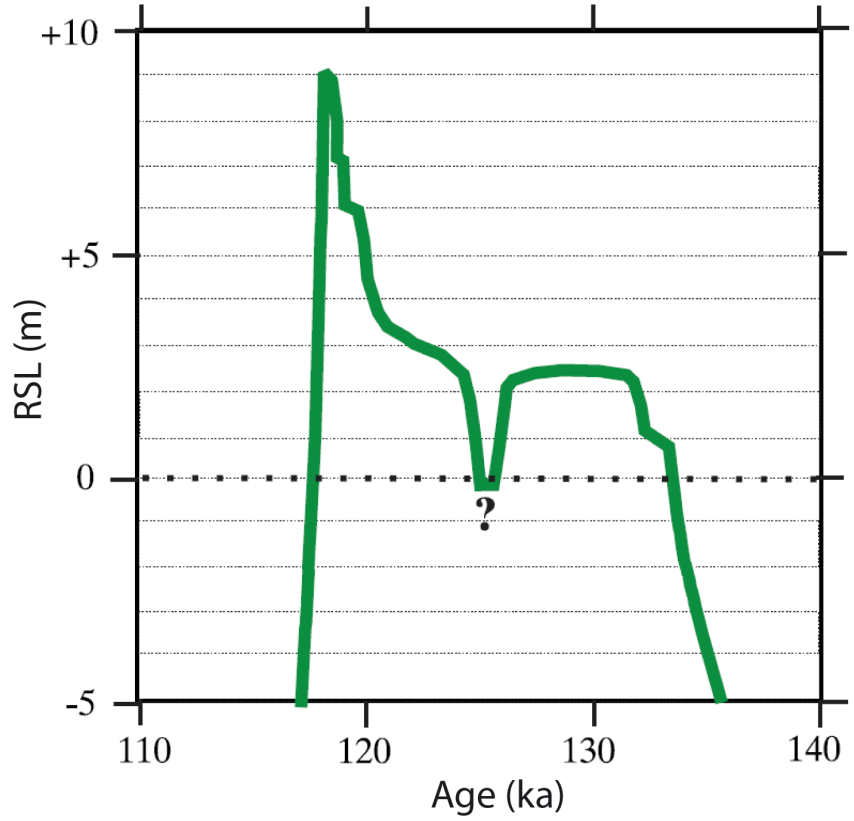

3.11 High-resolution MIS 5e sea-level curve compiled from gemorphological and morphostratigraphic evidence at 15 far-field localities. Modified from Hearty et al. (2007).

During the Holocene, sea-level records derived from terrestrial proxies on the south west and west coasts of South Africa indicate RSL approached modern sea level by 7-8 ka, a highstand of +3 m was attained between 7.3-6.5 ka, and sea level then rapidly regressed before returning to a level similar to present (Compton, 2001; Compton, 2006). A Holocene sea-level curve, constructed by Compton (2001) using estuarine cores from Langebaan Lagoon, ~100 km north of Cape Town, and constrained by data from other western and southern South African sites, is provided in Figure 3.12. Radiocarbon dating of lake sediments further south at Verlorenvlei, close to Cape Town, support the data, indicating a similarly rapid regression around 6.5 ka (Meadows and Baxter, 1999), and the curve has been considered appropriate for use elsewhere on the southern Cape (Carr et al., 2006a). Interestingly, the oscillations following the Mid-Holocene highstand are absent from the global eustatic record, and are tentatively attributed to hydro-isostatic loading effects (Compton, 2006).

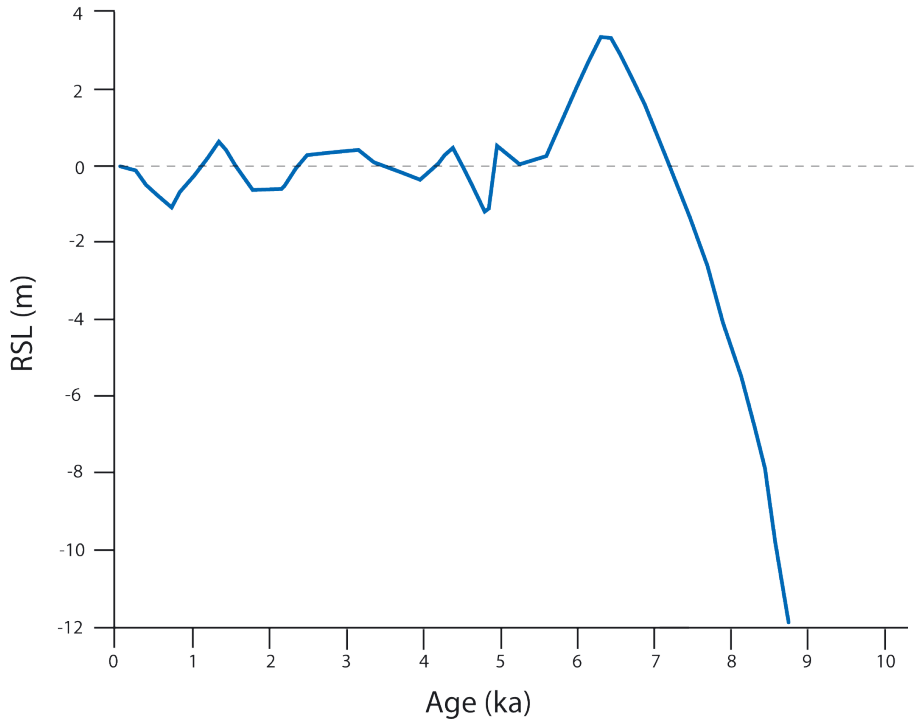

3.12 Holocene RSL curve for South Africa, redrawn from Compton (2001).

3.6.3 Coastline position

The importance of continental shelf geometry on the timing and nature of coastal-dune building activity, exerted via its control on the magnitude of shifts in coastline position caused by changes in sea level, was discussed in chapter 2. The gently sloping and broad Agulhas Bank off the southern Cape means even small shifts in vertical sea-level height can have a large and rapid effect on the position and shape of the coastline (Fisher et al., 2010; Compton, 2011), potentially making it a fundamental variable in reconstructing the evolution of the Wilderness barriers. A digital elevation model (DEM) of the nearshore shelf off the southern Cape was produced by Bateman et al. (2011) and used in conjunction with the relative sea-level curve of Waelbroeck et al. (2002) to determine the varying distance of the Wilderness embayment from the shore between MIS 7 and the present. An example image from the DEM, showing the coastline at the LGM (21 ka) is presented in Figure 3.13. At this time the southern Cape coastline was located over 100 km south of its present position. A topographic high adjacent to the new, lower coastline is visible in the DEM, interpreted by Bateman et al. (2011) as a lowstand barrier, and incised channels associated with the Touw and Swart Rivers can also be observed.

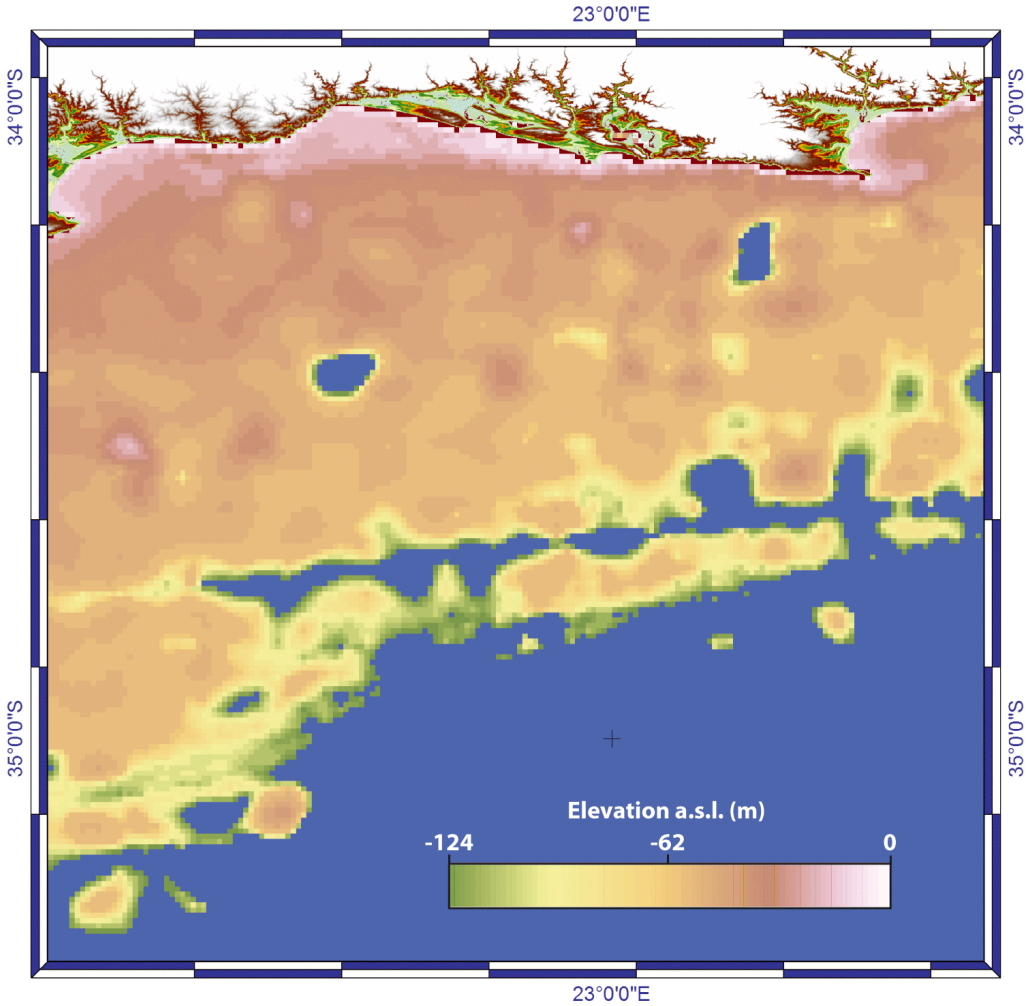

3.13 Nearshore bathymetric DEM showing southern Cape coastline during the LGM (21 ka), when sea level was -121 m below present. Extensions of the present Touw and Swart River channels onto the shelf are visible, as is a topgraphic high close to the LGM coastline intepreted to be a lowstand barrier. From Bateman et al. (2011).

3.6.4 Aeolian activity

Of South Africa's ~3000 km of shoreline, more than 80 % is presently composed of sandy beaches backed by dunes (Tinley, 1985). The high-energy, swell-dominated environment combined with the predominantly fine sediment of the region generally produces wide, gently sloping dissipative beaches (Cooper, 2001) that are conducive to the formation of substantial coastal dunes. Parabolic dunes are the dominant morphotype and, as discussed in chapter 2, are organised in two kinds of system: barrier dunes and transgressive dunefields. Transgressive dunefields predominate on the southwest and western coasts, whereas barriers are more common on the southern Cape. The distinction is largely driven by climate: the higher yearly total and more even annual distribution of precipitation in the YRZ inhibits landward dune transgression and instead encourages vertical accretion and the formation of barrier dunes (Roberts and Brink, 2002; Roberts et al., 2009). Transgressive dunes on the southern Cape are limited to promontories or headlands (where they are known as headland bypass dunes), e.g.

Cape Agulhas and Algoa Bay, where stronger wind regimes are able to overwhelm stabilisation by vegetation (Illenberger and Rust, 1988; Roberts et al., 2009).

Early researchers assumed that South African barrier systems formed from sediments deflated from the continental shelf when exposed during glacial marine regressions (e.g. Dingle and Rogers, 1972; Tankard and Schweitzer, 1974). Conversely, Barwis and Tankard (1983) argued that coastal aeolianites at Swartklip, ~120 km west of Wilderness, were deposited during a sea-level highstand, as vegetation would have rapidly colonised the continental shelf during glacial sea-level lowstands and prevented significant aeolian transportation of sediment inland. Illenberger (1996) also applied the same argument to the Wilderness barriers (see section 3.7 below). More recently, advances in dating techniques have permitted quantitative assessments of the timing of Quaternary dune accumulation on the southern African coast. The ages obtained generally support the highstand model, being clustered around Mid- to Late-Quaternary interglacial sea-level maxima (predominantly MIS 5 and MIS 1, with a small number of ages from MIS 7 and MIS 11) on the east coast (Armitage et al., 2006; Porat and Botha, 2008), southwestern Cape (Roberts et al., 2009) and the southern Cape (Carr et al., 2010a). Considered in detail, however, the pattern is more complex. The majority of studies yield a small number of ages from periods when sea levels were considerably lower than present, including MIS 6 (Armitage et al., 2006; Porat and Botha, 2008), the MIS 4-5 transition c. 70 ka (Jacobs et al., 2003a; Bateman et al., 2004; Porat and Botha, 2008) and MIS 3 c. 40 ka (Carr et al., 2007).

Obtaining complete chronologies from the majority of southern African barrier systems is problematic, as their stacked nature prevents sampling of the oldest deposits. Armitage et al. (2006) speculate that barrier islands on the Mozambique coast probably contain material deposited as early as MIS 7, though OSL sampling retrieved no ages older than 150 ka. Similarly, at Maputaland on the east coast, a composite aeolianite barrier peaking at 172 m in height contains material dating from >366 ka to the Holocene (Porat and Botha, 2008), making interpretation of its history particularly challenging. Illenberger (1996) cites several other examples of stacked aeolianite deposits on the southern African coast and identifies Wilderness as an exception, with its shallow coastal embayment permitting the formation of separate barriers.

3.7 Evolution of the Wilderness barriers

The morphology of the Wilderness barrier dunes and some of the previous palaeoenvironmental research conducted upon them was briefly discussed in chapters 1 and 2. This section reviews the existing literature in greater detail.

3.7.1 Timing and nature of barrier formation

Potgieter (1950) proposed that the Wilderness embayment was initially occupied by a single large lake, separated from the ocean by a sandbank laid down during a period of sea level considerably above that at present. As this highstand declined, the lake was filled with fluvial sediment delivered by local rivers, which was subsequently reworked by aeolian activity to form the present landscape of barriers and lagoons (Potgieter, 1950). Martin (1962) criticised the lack of geomorphological evidence in support of Potgieter's model and published a more thorough morphological description of the deposits within the Wilderness embayment, concluding that the barriers formed as a combination of offshore bars and dune sands during several Quaternary oscillations of sea level. Four separate shore-parallel barriers were identified and termed I, II, III and IV, with I being the oldest and IV the youngest. Martin (1962) also noted the presence of beach terraces and palaeo sea cliffs cut into the barriers in several locations at ~2.5 m and 6-8 m amsl, interpreting these as indicating at least one marine transgression to sea levels greater than present part-way through the evolution of the barriers. Their locations are shown in Figure 3.14a, along with Martin's numerical designation of the barriers. Birch et al. (1978) were the first to incorporate the currently submerged offshore aeolianite ridges (described in detail in the next section) into an evolutionary model of the Wilderness barriers, suggesting they were formed following deposition of the seaward barrier during marine stillstands around -35 and -45 m amsl at some point during MIS 2-4.

The morphological description of the Wilderness barriers was refined by Illenberger (1996), who, based on the overlap of Martin's barriers III and IV, proposed that three distinct barriers could be distinguished, which he termed the seaward, middle and landward barriers based on their proximity to the modern coastline. This terminology has been widely adopted and is used throughout this thesis. A geomorphological map of the three barriers is shown in Figure 3.14a. A DEM showing the actual spatial extent and height of the barriers is given in Figure 3.14b.

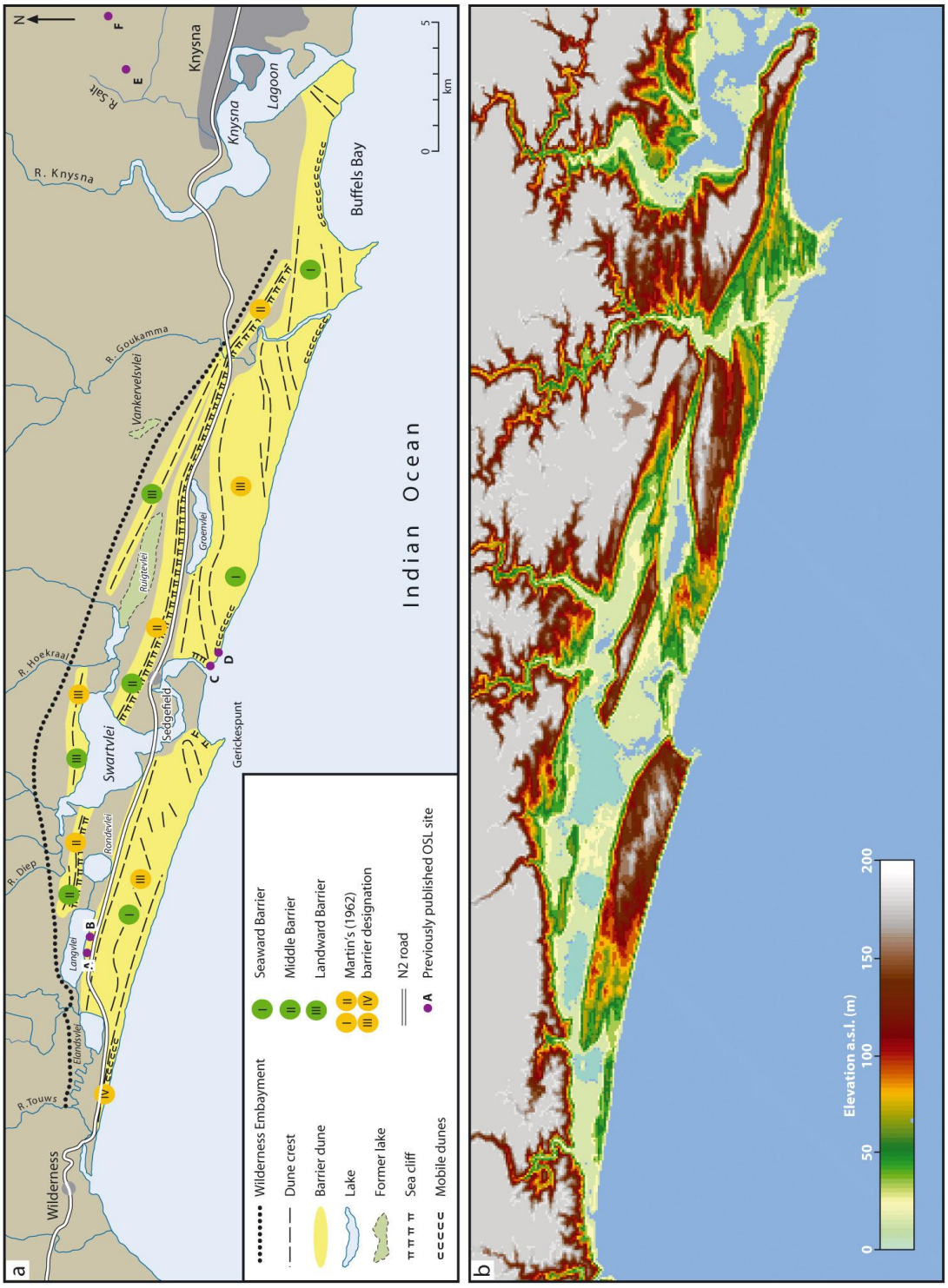

3.14 The Wilderness embayment. (a) Interpretative geomorphological map of the embayment, deliniating the seaward, middle and landward barriers and showing dune crest lines, marine terraces, mobile dunes atop the barriers and other major features. Published sample sites are also indicated: (A) Kirsten Tulleken Quarry from Carr et al. (2007); (B) Otto Sands Quarry from Bateman et al. (2004); (C) Carr et al. (2010a); (D) Bateman et al. (2008); (E) Blaricum Heights from Holmes et al. (2007); (F) Makhulu Quarry from Holmes et al. (2007). (b) DEM highlighting the extent and elevation of the barriers within the embayment. Modified from Bateman et al. (2011).

The evolutionary model of the Wilderness barriers by Illenberger (1996) proposed they initially formed as barrier islands, subsequently growing in height as parabolic dunes coalesced on top during successive interglacial sea-level highstands. To determine the age of the barriers, Illenberger estimated the volume of sand per m length of each of the three barriers when at their fullest, uneroded state, and related this to the presumed Holocene accumulation rate for the nearby radiocarbon-dated Alexandria coastal dunefield at Port Elizabeth. He calculated that 0.108 X 10^6 m^3 m^{-1} of sand has accumulated on the seaward Wilderness barrier over the past 6 ka, and extrapolated this to assume around 0.15 X 10^6 m^3 m^{-1} of barrier sand accumulates per interglacial. Based on these values, Illenberger (1996) concluded it would take approximately two interglacial periods (of ~10 ka each) for each barrier to form. Thus, the seaward barrier was assigned to the Holocene and last interglacial sea-level highstands (MIS 1 and 5; <10 ka and ~120 ka), the middle barrier to the second and third last interglacials (MIS 7 and 9; ~200 and ~320 ka), and the landward barrier to MIS 11 and 13 (~410 and ~500 ka) (Illenberger, 1996). Illenberger's estimations of sand volume per m length of barrier are given in Table 3.2. As an aside, Table 3.2 multiplies these values with measurements of total barrier length (obtained using Google Earth) to produce estimations of the total volume of sand contained in the barriers and total barrier accumulation rate.

Illenberger (1996) attributed the presence of the marine terrace cut into the seaward barrier either side of Swartvlei estuary mouth was attributed to the MIS 5 interglacial, and the terrace cut into the middle barrier to MIS 7, implying both accumulation and erosion occur during sea-level highstands. The current rate of erosion of the seaward barrier due to wave attack was suggested to be in the region of 0.3 m a^{-1} (Illenberger, 1996).

Table 3.2 Sand volume per m length of the Wilderness barriers in their uneroded state estimated by Illenberger (1996). Total sand volume and accumulation rate are new calculations based on Illenberger's (1996) volume estimations and assumption of barrier accumulation across two 10 ka interglacial periods, and measurements of barrier length made using Google Earth.

Barrier	Sand volume per m length (10^6 m^3 m^{-1})	Barrier length (m)	Total sand volume (10^6 m^3)	Accumulation rate (10^6 m^3 a^{-1})
Offshore	0.02	-	-	
Seaward barrier (Holocene component)	0.108	-	-	
Total seaward barrier	0.276	31,700	8749.2	0.438
Middle barrier	0.263	16,700	4392.1	0.22
Landward barrier	0.002	14,600	2920	0.146
Total sand volume in all barriers pre-erosion =			16.0613 X 10^9 m^3	

More recently, OSL dating techniques have been applied to the seaward Wilderness barrier, with Carr et al. (2007) and Bateman et al. (2004) obtaining series of ages from

exposures in quarries on the landward face of the dune (Otto Sands and Kirsten Tulleken quarries respectively: Figure 3.14a sites A and B). Their combined results indicate a scenario more complicated than Illenberger (1996) and other previous studies assumed, with clusters of seaward barrier accumulation identified at 157-154 ka and 140-125 ka, followed by a relatively constant rate of deposition through MIS 5 until c. 85 ka. Bateman et al. (2004) also obtained an age of 73 ka, though aeolian bedding structures were absent from the stratigraphic layer this sample was extracted from. Two ages of 40 and 21 ka were obtained by Carr et al. (2007), which they attributed to localised reworking at these times. Bateman et al. (2008) dated material from the unconsolidated dunes on top of the seaward barrier (Figure 3.14a site D), confirming these deposits are of Holocene age. Carr et al. (2010a) published the first OSL ages obtained from the sea cliffs cut into the seaward barrier adjacent to the current beach (Figure 3.14a site C). Despite being at considerably lower elevation than the quarry samples of Bateman et al. (2004) and Carr et al. (2007), the ages obtained were mostly younger (between 113-95 ka), further indicating Illenberger's (1996) model may be an oversimplification of the evolution of the barriers. Moreover, the minimum age estimates for the coversands inland of the barriers obtained by Holmes et al. (2007) of c. 300 ka at Blaricum Heights and 500 ka at Makhulu Quarry (Figure 3.14a sites E and F respectively) overlap with Illenberger's (1996) age estimates for the middle and landward barriers, leaving the relationship between the barriers and coversands unclear.

3.7.2 Submerged aeolianites

The existence of submerged offshore counterparts to the subaerially exposed Wilderness barrier dunes has long been known (Potgieter, 1950). Birch et al. (1978) conducted the first seismic reflection survey of the offshore deposits and located two main sections of aeolianite, approximately 20 m high and 1500 m wide, one on either side of the embayment (Figure 3.15). The gap in the central section of the embayment (also evident in the nearshore DEM shown in Figure 3.13) was assumed to be eroded, and a depression (partially infilled by sediment) was also identified between the coast and the ridge on the right-hand side of the embayment, inferred to be a drowned coastal lake similar to the adjacent onland occurrences (Birch et al., 1978). An assemblage of smaller ridges, 8-10 m high and 150-200 m apart, were also identified shoreward of the larger ridge on the western side of the embayment lying on an elevated ridge extending about 4 km out to sea (Birch et al., 1978). A more detailed survey, combining side-scan sonar, seismic profiling and observations by divers revealed that there are up to 14 of these ridges, and several more further seaward that are now completely buried by

Holocene sediments (Martin and Flemming, 1983 c.f. Martin and Flemming, 1986). Birch (1980) attributed the reduced height of the offshore barriers relative to those onland to a combination of erosion and infilling of interdune depressions following sea-level rise in the Holocene. The basal depths of the buried aeolianites were used to infer palaeo-shorelines at 40, 50-55, 65-70 and 80-90 m water depths (Martin and Flemming, 1986), though no estimation or measurement of their age beyond the MIS 2-4 period inferred by Birch et al. (1978) has been made.

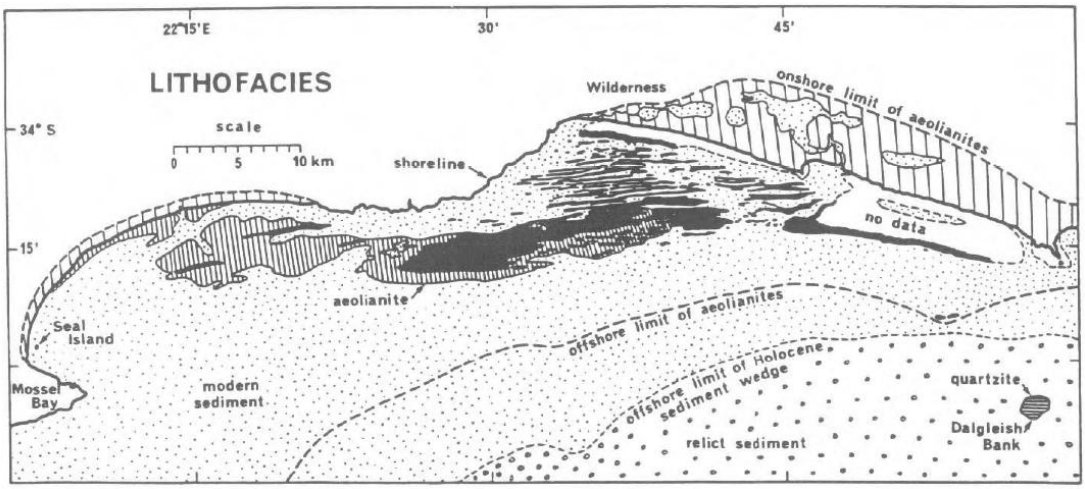

3.15 The distribution of aeolianite and unconsolidated sediment offshore of the Wilderness embayment, based on side-scan sonar and seismic reflection surveys. Symbology marked on figure. From Martin and Flemming (1986).

3.7.3 Provenance of the Wilderness barrier sands

The provenance of the vast quantity of sediment from which the Wilderness barriers are formed (over 16 million m^3 based on the uneroded volume of the barriers estimated by Illenberger (1996): Table 3.2) has received little attention relative to the efforts to date the dunes. This is surprising, given both the potential for sediment supply to modulate the timing of coastal-dune formation, and the relatively low carbonate contents of the Wilderness barrier sediments: reported values range between 0-35 % (Illenberger, 1996; Bateman et al., 2004; Carr et al., 2010a), significantly lower than the 50-90 % $CaC0_3$ of coastal aeolianite deposits in China, Australia, the Mediterranean and elsewhere (e.g. Xitao and Goldsmith, 1989; Murray-Wallace et al., 2001; Andreucci et al., 2009). Examining western Cape aeolianites, Roberts and Brink (2002) noted that aeolianites at False Bay, near Cape Town, had carbonate contents ranging up to "*only*" 57 %, due to their dilution by siliciclastic riverine sediments.

Bateman et al. (2004) noted significant down-profile variations in carbonate content in the Otto Sands Quarry sample site on the landward flank of the seaward barrier (Figure 3.14a

site B), identifying an upper unit containing <2 % carbonate and a lower unit ~23 % carbonate. Samples from the nearby Kirsten Tulleken Quarry site sampled by Carr et al. (2007) also possess relatively low carbonate contents compared to elsewhere in the barrier (3.9-16.9 %: A. Carr, *pers. comm.*). A lack of sedimentary evidence for leaching led Bateman et al. (2004) to discount weathering as an explanation for the paucity of carbonate within the Otto Sands upper unit, suggesting it may instead represent a predominance of terrestrial over marine sediment input during the period it was deposited (Bateman et al., 2004). However, geochemical and/or mineralogical evidence for whether the variation represents a change in provenance or weathering of the sands was not obtained.

Holmes et al. (2007) compared selected major and trace element concentrations of samples from the seaward barrier to those of the coversand deposits inland. Depletion of the mobile elements K, Mg and Sr and certain elements associated with heavy minerals (Ti, Y and Th), were interpreted as indicating the coversands are older and more weathered than the seaward barrier sands, but whether the coversands have contributed to the Wilderness barriers and/or whether they are from the same original source, was not speculated upon (Holmes et al., 2007).

3.8 Chapter summary

This chapter has collated information necessary for producing a coherent reconstruction of the Mid- to Late-Quaternary evolution of the Wilderness barriers and determining the provenance of the sediments from which they are formed. Possible local sources for the barrier sands have been identified both on- and offshore, and their mineralogy described. Late Quaternary records of climate and sea level appropriate for the Wilderness region have been detailed, and the geometry and morphological setting of the Wilderness embayment has been explained. Key points that are relevant to the reconstruction include:

- Drift direction along the southern Cape is eastward.
- Almost half of total nearshore sediment accumulation on the southern Cape is located between Cape St Blaize and Cape Seal, much of which is further concentrated in the vicinity of the Wilderness embayment.
- The volume of offshore sediment adjacent to Wilderness may be at least partly explained by the geometry of the coastline. The north-easterly trend of the coast from Cape Agulhas refracts sharply at the western edge of the embayment to one slightly south of east, with the now-filled embayment presumably once

forming a major re-entrant on an otherwise relatively smooth coastline and acting as a trap for material being moved eastward.

- The volume of sediment delivered to the ocean by rivers local to the Wilderness embayment is theoretically sufficient to account for the entire estimated annual accumulation rate of the barriers.
- Carbonate production on the Agulhas Bank exhibits no clear trend across glacial-interglacial cycles, and rates of production have been consistently high throughout the past 450 ka.
- Evidence suggests glacial periods will have been slightly drier in the region local to Wilderness, due to a less effective monsoonal system, increased continentality from the extended coastal plain and limited penetration of temperate cyclonic depressions. However, the region is understood to have maintained vegetative cover throughout the Late Quaternary.
- Westerly winter wind directions similar to today have been dominant throughout the Late Quaternary along the southern Cape. There may have been a reduction in wind strength during the MIS 5 interglacial, attributed to reduced meridional pressure gradients.
- The global eustatic sea-level curve compares favourably with terrestrial sea-level indicators on the southern Cape, making it appropriate for comparison to the timing of barrier formation at Wilderness. The region has been tectonically stable throughout the Quaternary.
- The gently sloping and broad Agulhas Bank off the southern Cape means even small shifts in vertical sea-level height will have a large and rapid effect on the position and shape of the coastline.

Section 3.7 reviewed existing literature pertaining to coastal dunes on the southern Cape and the evolution of the Wilderness barriers. Key issues that arise from this review are listed below. These issues form the basis for the objectives of this research as stated in chapter 1 section 1.4:

- The majority of aeolianite barriers on the southern Cape coast are stacked features representing multiple episodes of deposition, making interpretation of their evolution difficult. Erosion of a coastal embayment at Wilderness has permitted a regionally unique sequence of three separate barriers (seaward, middle and landward) to form.

- The current OSL chronology of barrier dune formation at Wilderness is dependent on a small number of sites, all of which are located in the seaward barrier. The age of the middle and landward barriers is consequently unknown.
- Several of the ages obtained for the seaward barrier fall within the MIS 4-5 and MIS 5-6 transitions, indicating Illenberger's (1996) assumption that barrier formation occurs only during interglacial sea-level highstands is erroneous. The limited number of dated samples prevents a thorough re-evaluation of the manner in which the Wilderness barrier dune system has evolved.
- Despite the relatively low proportion of marine carbonate in the Wilderness barriers compared to many other coastal aeolianites, the source of terrigenous sediment input to the dunes has not been quantitatively investigated.
- Variation in the carbonate content of the seaward barrier site sampled by Bateman et al. (2004) is suggested as indicating a change in sediment provenance, but this has not been investigated using geochemical or mineralogical methods of analysis.
- The relationship between the Wilderness barriers and the coversands inland of the embayment (that is, whether the coversands have contributed to the Wilderness barriers, and/or whether they are from the same original source) remains unknown.

4 Study design, sample sites and field methods

4.1 Introduction

The aims of this research, and the more detailed objectives constructed in order to achieve them, were originally stated in chapter 1 section 1.4. The first part of this chapter revisits the research objectives and explains how the study was designed in order to ensure they are met. The second part of the chapter describes: (i) the field sampling methods employed; and (ii) the morphology and morphological context of the sample sites. It is divided into separate sections for OSL samples and sediment provenance samples.

4.2 Study design

The overall, site-specific aim of this research is to produce a detailed reconstruction of the emplacement and geomorphological evolution of the barrier system within the Wilderness embayment. The research objectives constructed in order to meet this aim are:

1. Increase substantially the number of OSL-dated sites in the seaward barrier to provide a high-resolution chronological framework for its formation along the full length of the embayment. This chronology should be detailed enough to reveal any lateral or vertical trends in the age of the barrier. As far as possible, produce a similarly detailed OSL chronology of the (presumably) older and previously undated middle and landward barriers.
2. Use these data to firmly constrain the relationship between sea level and the timing of barrier formation at Wilderness.
3. Clarify the relationship between the barriers and the inland coversand deposits, by obtaining a more detailed chronology of the timing of coversand deposition. Test the applicability of the ITL protocol (e.g. Jain et al., 2005; Choi et al., 2006) for dating the coversands, and potentially revise the minimum OSL ages obtained for them by Holmes et al. (2007).
4. Establish whether the relative importance of terrestrial vs. marine sediment input to the Wilderness barriers has changed with time, and whether or not sediment from local terrestrial sources has been significant in their formation.
5. Combine the dating and provenance data to inform a detailed reconstruction of the emplacement and geomorphological evolution of the Wilderness barrier dunes.

In order to meet objectives 1-3, it was further decided that the suite of samples collected for luminescence dating should provide:

i. Full east-to-west coverage of the seaward barrier, to establish if any alongshore trend in barrier age can be identified.
ii. Samples from different elevations within the barriers, and from either side of erosive surfaces within the aeolianite bedding, to investigate the vertical rate of barrier accumulation.
iii. A range of locations within the middle and landward barriers, to extend the chronology of dune formation at Wilderness.
iv. Ages from additional coversand sites beyond the two locations close to Knysna sampled by Holmes et al. (2007), to provide greater spatial coverage of the deposit and identify any potential variability in age within it.

A fundamental concern with obtaining and using a suite of luminescence ages for palaeoenvironmental reconstruction is that the distribution of ages produced may reflect the employed sampling strategy, rather than an accurate portrayal of the age of the deposit(s) in question (Telfer and Thomas, 2007). A relatively common way in which this manifests is an inability to access the deepest, and therefore potentially the oldest, sediments within a dune, due to a lack of exposures. Fortunately at Wilderness the sea cliffs at the rear of the current beach provide ample access deep within the seaward barrier, and exposures around the back-barrier lagoons reveal the cores of the middle and landward barriers. In addition to these locations, sampling was conducted with the intention of obtaining dates from as wide a range of other elevations within the barriers as possible, in order to avoid introducing bias to the resulting chronology. The sites sampled for dating purposes are described individually in section 4.4.

The objectives of the research pertaining to the provenance of the Wilderness barrier sands are: (i) to establish whether the relative importance of terrestrial vs. marine sediment input to the barriers has changed with time; and (ii) to establish whether local terrestrial sediment sources have been significant in their formation. Underscoring both of these is a test of the suggestion made by Bateman et al. (2004), that barrier construction at Wilderness during periods of low sea level may have been sustained by a shift from marine sediment to material of local terrestrial origin. Variations present in the carbonate content of the seaward barrier, despite there being no visual evidence of post-depositional weathering or modification of the barrier sand were cited as evidence in support of this hypothesis (Bateman et al., 2004).

For logistical reasons (namely the strong offshore currents, high wave energy, water depth and presence of sharks), it was not considered possible to include samples of the offshore sediments within the sediment provenance sampling scheme. However, an assumption that the calcium carbonate fraction of coastal aeolianites is solely of marine origin is generally implicit in studies concerning carbonate coastal-dune provenance (e.g. Franceschini et al., 2003; Andreucci et al., 2009; Muhs and Budahn, 2009). As calcium carbonate is absent from southern Cape geological formations, beyond the narrow coastal belt of calcareous beach rock, shallow marine and aeolianite sediments within which the Wilderness barriers are included (the Bredasdorp Group: see chapter 3 section 3.2), this assumption is also considered valid here. Thin-section micromorphological analyses of samples from the Wilderness barriers further confirm that their carbonate content is marine, revealing it consists exclusively of sand-sized marine bioclasts and carbonate cements derived from them (Bateman et al., 2011).

Whilst a quartzitic component is present in the offshore sediments in addition to carbonate, this material is originally of terrestrial origin (Martin and Flemming, 1986; Bailey and Rogers, 1997: see also chapter 3 section 3.4). Given the sedimentary cells present on the Cape (Birch, 1980: chapter 3 Figure 3.4), it is also likely to be locally sourced. The sediment provenance sampling scheme thus focused on characterising local, terrestrial sources of sediment. Large coastal-dune systems are found immediately down-drift of river mouths elsewhere on the southern Cape (e.g. Illenberger and Rust, 1988; Armitage et al., 2006), so focussing on identifying a local, terrestrial component within the Wilderness barrier sands is logical.

In order to meet the provenancing objectives, it was decided that samples from the barriers and their possible local terrestrial sources would be compared using multiple analytical techniques: particle size, carbonate content, trace element geochemistry and heavy mineralogy. The rationale for selecting these techniques and the details of their use is provided in chapter 5. Comparisons between the following groups of samples were deemed necessary:

i. The seaward, middle and landward barriers, to investigate whether any differences in transport regime and/or provenance can be identified between them.
ii. Samples from different settings within the seaward barrier, to determine whether the variations in carbonate content within it indicate changes in sediment provenance or simply post-depositional modification of the sands.
iii. The barrier sands vs. the various possible local sediment sources, to identify whether a provenance relationship can be established between any of them.

The suite of sediment provenance samples collected in order to facilitate these comparisons is described in section 4.6.

4.3 OSL sampling methods

4.3.1 OSL sample collection

OSL samples were extracted from field sites by hammering opaque PVC tubes (50 mm diameter, 150 mm length) into cleaned exposures. Sample sites within the barrier dunes were preferentially selected based on clear visibility of bedding structures, in order to minimise the risk of accidentally sampling bioturbated or otherwise disturbed deposits. This was not possible in the coversand deposits where no bedding structures are apparent (Holmes et al., 2007), but at all sites stratigraphic boundaries, evidence of root casts and other indicators of potentially disturbed sediments were avoided. Where deposits were particularly well lithified, more robust stainless steel tubes of the same dimensions were used in place of PVC. Tube ends were capped and sealed with tape to prevent contamination by light, and tubes were stored in sealed black plastic bags for transportation back to the UK.

At two dune-crest sites in the middle barrier, a Dormer Engineering sand auger was used to obtain samples from depth (Figure 4.1). The auger head was a 100 mm diameter, 300 mm long sand-specific steel unit with 6 m of extension rods, powered by a manually turned T-handle. The intention of obtaining core samples was to avoid material potentially disturbed by bioturbation processes (most intensive in the uppermost 1-2 m: Bateman et al., 2007), whilst still sampling the crest of the dune, so this length was deemed sufficient. After drilling to a satisfactory depth, the auger head was swapped for a purpose-built luminescence sampling head which could be hammered into the base of the hole and retrieve a 30 cm long core of sediment. Once a core was in the sampling head, a PVC or stainless steel tube (depending on hardness) was pressed into it to capture the material and sealed as before.

4.1 The auger in use (a) and having reached a depth of 4.2 m (b). Both photos show sampling of the middle barrier dune crest at Rondevlei (site described in section 4.4.2.1).

4.3.2 Sample site logging

A GPS was used to record the location and elevation of all sample sites, sites were photographed and descriptions were written. At sites where reference to a point of known elevation was possible, such as sea level or a triangulation pillar, an Abney level and measuring tape were used to measure vertical displacement from that point to sub-metre precision. Sediment colour was described using a Munsell colour chart once samples were dried.

4.4 OSL sample sites

Samples were obtained from a total of 10 new sites within the three barriers, shown in Figure 4.2. The samples span the full width of the embayment, and represent various elevations within the barriers from dune crest to dune base. Sampling was most intense in the seaward barrier, with samples collected from its base at approximately regular intervals from west to east, in order to reveal any alongshore trend in the timing of its accumulation. Paired samples were also taken at three localities in the seaward barrier (Figure 4.2 sites 3b, 3c and

3e) bracketing bounding surfaces within the bedding, in order to assess the magnitude of erosional episodes such surfaces represent. Two samples from the coversands inland of the embayment were also obtained, with the intention of clarifying the relationship of these deposits to the barriers. The sample site locations and their geomorphological and sedimentological characteristics are described in the following sections. Figure 4.2 also shows the locations of previously published OSL sample sites (sites A, B, C, D, E and F), along with three additional sites (sites G, H and I) from Bateman et al. (2011). Ages from these sites are incorporated into the reconstruction of barrier evolution presented in this thesis.

4.4.1 Seaward barrier sites

The seaward barrier commences about 1.5 km east of the western edge of the Wilderness embayment, where it forms a relatively low (~30 m) and narrow belt seaward of Elandsvlei. This ridge becomes less distinct eastwards, until it eventually coalesces completely with the broader and higher barrier beginning at the eastern edge of Elandsvlei (Figure 4.2). The barrier increases in width and height eastwards, attaining a maximum altitude of 196 m amsl at Gerickes Point seaward of Swartvlei. The outlet of Swartvlei then dissects the barrier, and it recommences at a lower altitude (30-40 m) continuing for approximately 14 km along the shoreline until it is again dissected by the Goukamma River. Headland bypass dunes are present on top of the Buffels Bay headland, the very tip of which is formed from TMG sandstone (Kouga Formation). This is the only surface outcrop of hard-rock geology within the Wilderness embayment. The barrier continues eastward to the rock promontory at the edge of Knysna Lagoon, maintaining an elevation of ~40 m.

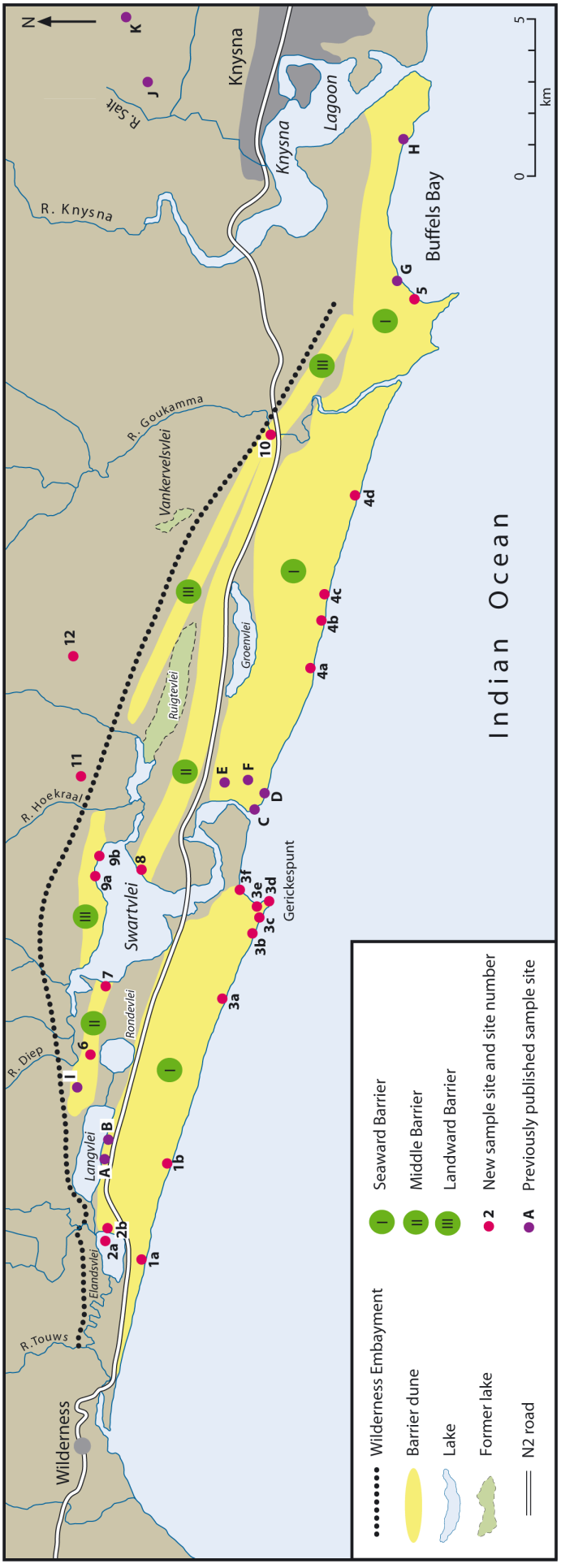

4.2 OSL sample site locations. Red circles denote sites sampled in this study and purple circles denote previously published sites: (A) Carr et al. (2007); (B) Bateman et al. (2004); (C) Carr et al. (2010a); (D) Bateman et al. (2008); (E, F, G, H, I) Bateman et al. (2011); (J) Holmes et al. (2007) Blaricum Heights; (K) Holmes et al. (2007) Makhulu Quarry.

The majority of the seaward barrier is overlain by vegetated, unconsolidated dune sands orientated between 15-30° to the shoreline, identified by Illenberger (1996) as parabolic dunes reflecting the dominant westerly wind direction. Along much of its length the seaward barrier is being eroded in response to contemporary sea levels, forming laterally and vertically extensive cliffs within which the steeply dipping cross-stratified aeolian bedding is clearly visible (e.g. Figure 4.3a). Sands are well sorted and uniform in colour (10YR 7/3 or 10YR 7/4: very pale brown). Samples were obtained from five sites, which from west to east are named Klein Krantz, Elandsvlei, Gerickespunt, Groenvlei and Buffels Bay. They are described in the following sections. Photos of selected seaward barrier sites are provided in Figure 4.3.

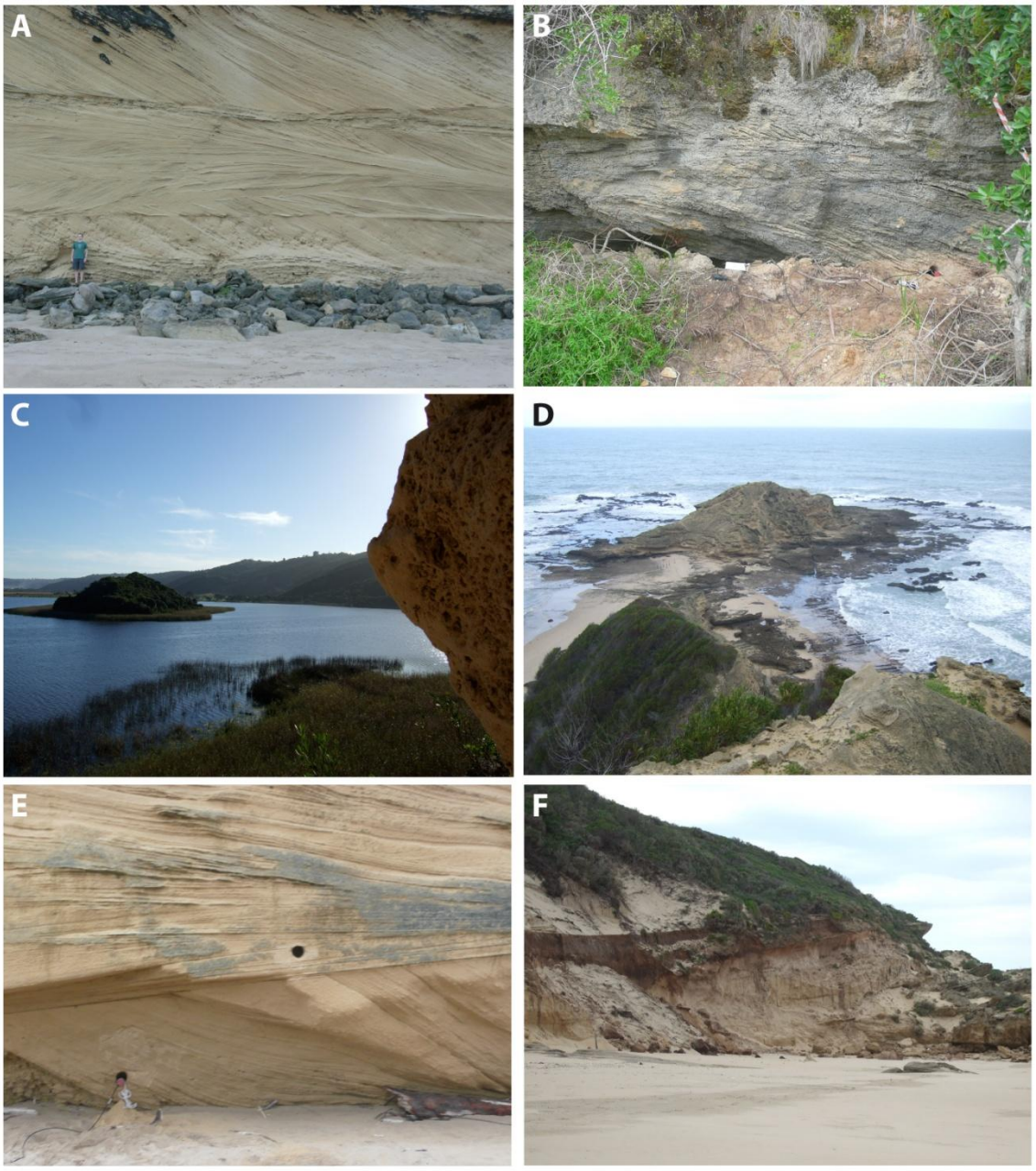

4.3 Seaward barrier sites: (a) sea cliff near Gerickes Point, displaying the well preserved, cross-stratified aeolianite bedding characteristic of the barrier; (b) marine herringbone bedding at the base of the East Elandsvlei exposure, also showing sample Shfd09076; (c) Elandsvlei Island; (d) Gerickes Point headland; (e) paired samples Shfd08176 and Shfd08177 either side of bounding surface (Gerickes Point site 3c); (f) palaeosol at Groenvlei.

4.4.1.1 Klein Krantz

Afrikaans for “little cliff”, Klein Krantz (34° 0’S 22° 39’E: Figure 4.2 site 1) marks the western-most point in the Wilderness embayment at which marine erosion has revealed the aeolianites of the seaward barrier. The currently eroding cliffs reveal ~30 m of carbonate-cemented aeolianite with well defined trough and cross-stratified bedding. Two samples were collected from aeolianite sections approximately 2.7 km apart, at 2.4 m amsl (Shfd09072) and 8 m amsl (Shfd09073). Sample site stratigraphy is shown in Figure 4.4 (sites 1a and 1b). The unconsolidated sand beneath sample Shfd09073 comprises a modern, partially vegetated foredune banked against the aeolianite sea cliff.

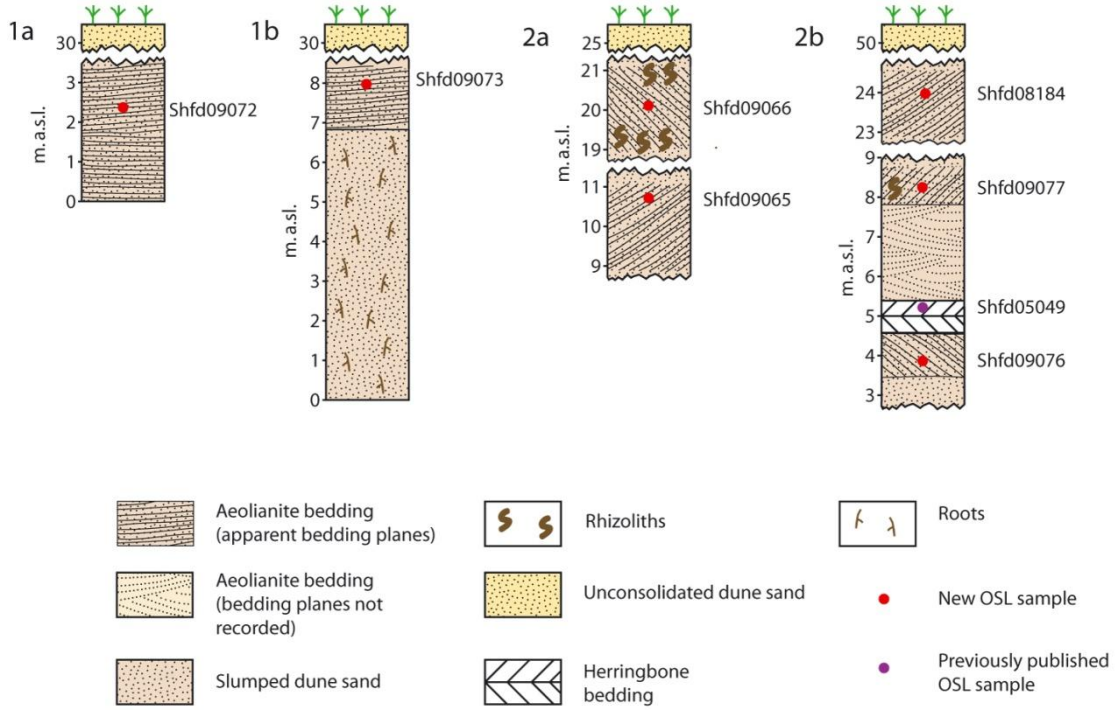

4.4 Sample site stratigraphy for Klein Krantz (1a and 1b), Elandsvlei Island (2a) and East Elandsvlei (2b) locations. Site numbers correspond with the position of the sample sites as shown in Figure 4.2.

4.4.1.2 East Elandsvlei and Elandsvlei Island

Directly inland of the narrow barrier at Klein Krantz is Elandsvlei. Erosion at the eastern shore of the lagoon has revealed an almost complete cross section of the core of the seaward barrier, from lake level (1.5 m amsl) to the barrier crest at 50 m amsl. This exposure is termed East Elandsvlei (33° 59’ S, 22° 38’ E; Figure 4.2 site 2b). Towards the base of the exposure, at 5 m amsl, Martin (1962) recognised clear evidence of a previous sea-level highstand in the form of calcareous beach/shoreface sediments characterised by small-scale (decimetre) packages of distinct “herringbone” bedding (Figure 4.3b). These marine facies can be traced horizontally

along the majority of the exposure. One OSL sample was obtained from high-angle aeolianite bedding beneath the herringbone bedding (Shfd09076, 3.9 m amsl) and two from aeolian deposits above it (Shfd09077 at 8.5 m amsl and Shfd08184 at 24 m amsl). The latter were carbonate-rich, partially cemented sands displaying high-angle foreset bedding, with occasional rhizoliths. These samples are supplemented by a date from the marine herringbone facies (sample Shfd05049) from Bateman et al. (2011). The stratigraphy of East Elandsvlei is illustrated in Figure 4.4 (site 2b).

In the centre of Elandsvlei is Elandsvlei Island (33^{o} 59' S, 22^{o} 38' E; Figure 4.2 site 2a). Composed entirely of aeolianite and aligned with the crest of the seaward barrier ridge (and Figure 4.3c), the island clearly represents an erosional remnant of the barrier. Martin (1962) speculated it became separated from the main body of the barrier either by marine erosion during the transgression responsible for depositing the marine sediments at East Elandsvlei, or by flow of the small Duiwe River. The island possesses a cliff line and associated wave-cut platform on its southern side. It is densely vegetated, but two samples were collected from small exposures of steeply bedded aeolianite (Shfd09065 and Shfd09066) (Figure 4.4 site 2a).

4.4.1.3 Gerickes Point

Gerickes Point is an aeolianite promontory formed by the seaward barrier just west of Swartvlei Estuary (34^{o} 02' S 22^{o} 45' E; Figure 4.2 sites 3a-f). The sea cliffs are at their highest on the west side of Gerickes Point, where they reach a maximum of 196 m altitude, and the tip of the promontory forms an island at high tide (Figure 4.3d). Aeolianites associated with this site have very distinct and well preserved bedding incorporating both high-angle foresets and low-angle beds. Rhizoliths are almost completely absent, indicative of rapid sediment accumulation. A total of 11 OSL samples were collected along a 5 km stretch of the coastline from a range of elevations: one from aeolianite exposed at low tide (Shfd09149); one from approximately one third of the way up the sea cliff at 49 m amsl (Shfd09067); and the remainder from between 1.3-4.5 m above the high-tide mark. Paired samples were taken at three localities (sites 3b, 3c and 3e) bracketing bounding surfaces within the bedding (e.g. Figure 4.3e), in order to assess the magnitude of erosional episodes such surfaces represent. The stratigraphy of the sample sites is illustrated in Figure 4.5.

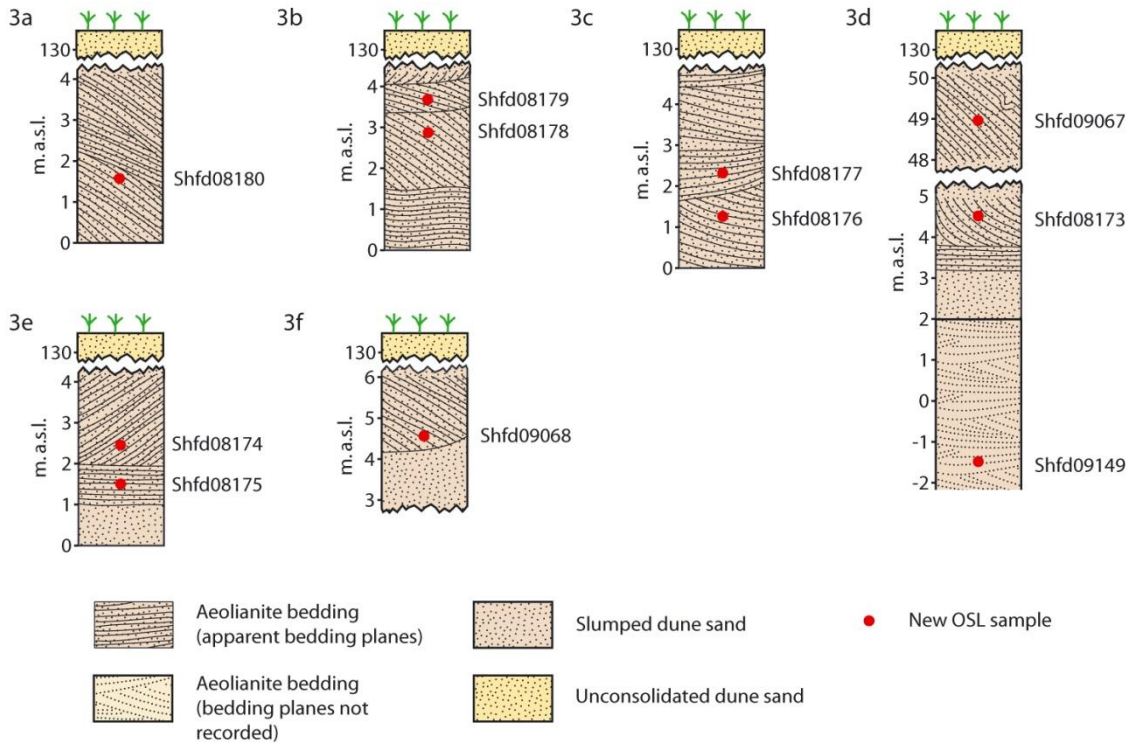

4.5 Gerickes Point sample site stratigraphy. Locations run west to east from 3a to 3f (located in Figure 4.2). Site numbers correspond with the position of the sample sites as shown in Figure 4.2.

4.4.1.4 Groenvlei

The Groenvlei site is located in cliffs eroded into the seaward barrier dune east of the Swartvlei Estuary (34° 03' S 22° 54' E; Figure 4.2 sites 4a-d). The site derives its name from the green-tinged back-barrier lagoon found immediately inland of the sampled locations. The aeolianites associated with this site are again well stratified, with a variety of both high-angle foresets and low-angle beds. Faunal trackways (bok) were observed in particularly finely bedded aeolianite (chapter 2 Figure 2.4), whilst elsewhere ripple preservation is excellent. Rhizoliths are more frequent than at Gerickes Point, and a well defined and laterally extensive palaeosol was observed between the aeolianite and the unconsolidated dunes on top of the barrier (Figure 4.3f). The palaeosol is characterised by rubification (5YR 4/3, reddish brown), de-calcification and presence of buried dune snails. It undulates significantly, strongly suggesting that it represents a palaeo-dune or interdune surface. Five OSL samples were collected from cliff exposures spread across a ~5 km stretch of the coastline. Sample site stratigraphy is illustrated in Figure 4.6 (Sites 4a to 4d).

4.4.1.5 Buffels Bay

At Buffels Bay an outcrop of sandstone (TMG Kouga Formation) has created a small headland within the wider Wilderness embayment (34° 4' S, 22° 58' E; Figure 4.2 site 5). To the north of the headland and inland of a densely vegetated and uncemented (presumably) Holocene headland bypass dune system, small exposures of well cemented aeolianite are exposed. Although unequivocally included within the seaward barrier by Illenberger (1996), Birch et al. (1978) correlated the seaward barrier at this point with the presently submerged offshore aeolianite ridge at ~35 m water depth (chapter 3 Figure 3.15), proposing they may have been separated by erosion caused by the Goukamma River. One sample (Shfd08185) was collected from aeolianite at 31 m amsl. Although frequent rhizoliths were present, fine high-angle bedding structures were also preserved. The stratigraphy of the sample site is shown in Figure 4.6 (site 5).

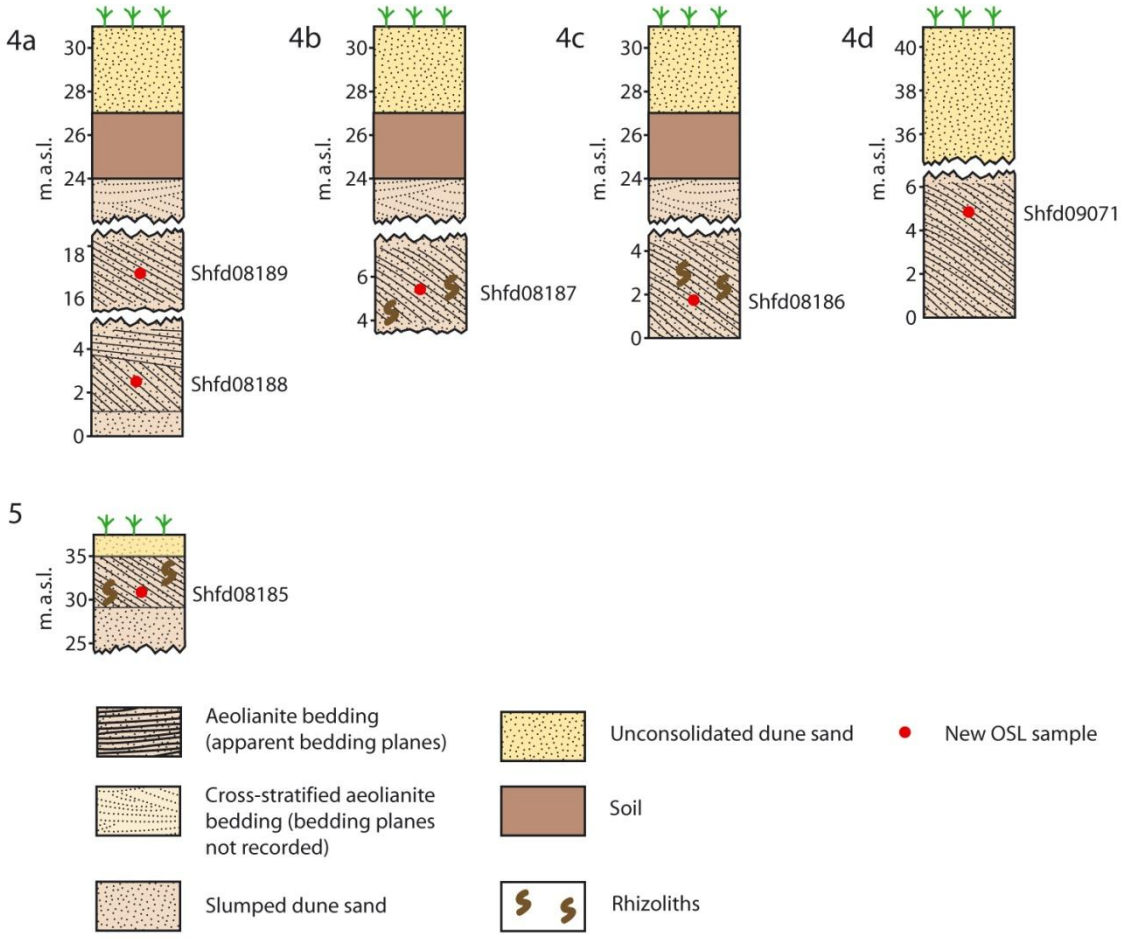

4.6 Groenvlei (4a to 4d) and Buffels Bay (5) sample site stratigraphy. Note: elevation and thickness of palaeosol at Groenvlei sites is approximate, as it was only possible to scale the cliff face and measure it at site 4a. It was not observed at site 4d. Site numbers correspond with the position of the sample sites as shown in Figure 4.2.

4.4.2 Middle barrier sites

The middle barrier runs from the northeast shore of Langvlei in the west of the embayment to the Goukamma River in the east (Figure 4.2). It forms two separate sections, separated by Swartvlei. On the eastern side of the embayment a continuous ridge can be traced for ~14 km, terminating by the Goukamma River floodplain. This part of the middle barrier attains a maximum altitude of 210 m amsl just east of Swartvlei (Figure 4.7a and 4.7b). Illenberger (1996) interpreted the southern flank of the barrier in this region as a palaeo-sea cliff relating to the MIS 5e highstand, though the relatively erodible nature of the aeolianite and consequent slumping made this hard to verify in the field. West of Swartvlei the middle barrier is more subdued, attaining a maximum altitude of 68 m amsl and extending 4 km west until its terminus north of Langvlei. This part of the barrier appears to be formed from two or three coalescing but offset ridges. Sands are identical in colour to the seaward barrier (10YR 7/3 or 10YR 7/4: very pale brown) and well sorted. Samples were obtained from three sites within the middle barrier (Rondevlei, West Swartvlei and East Swartvlei) and are described in the following sections. Photos of selected middle barrier sites are provided in Figure 4.7.

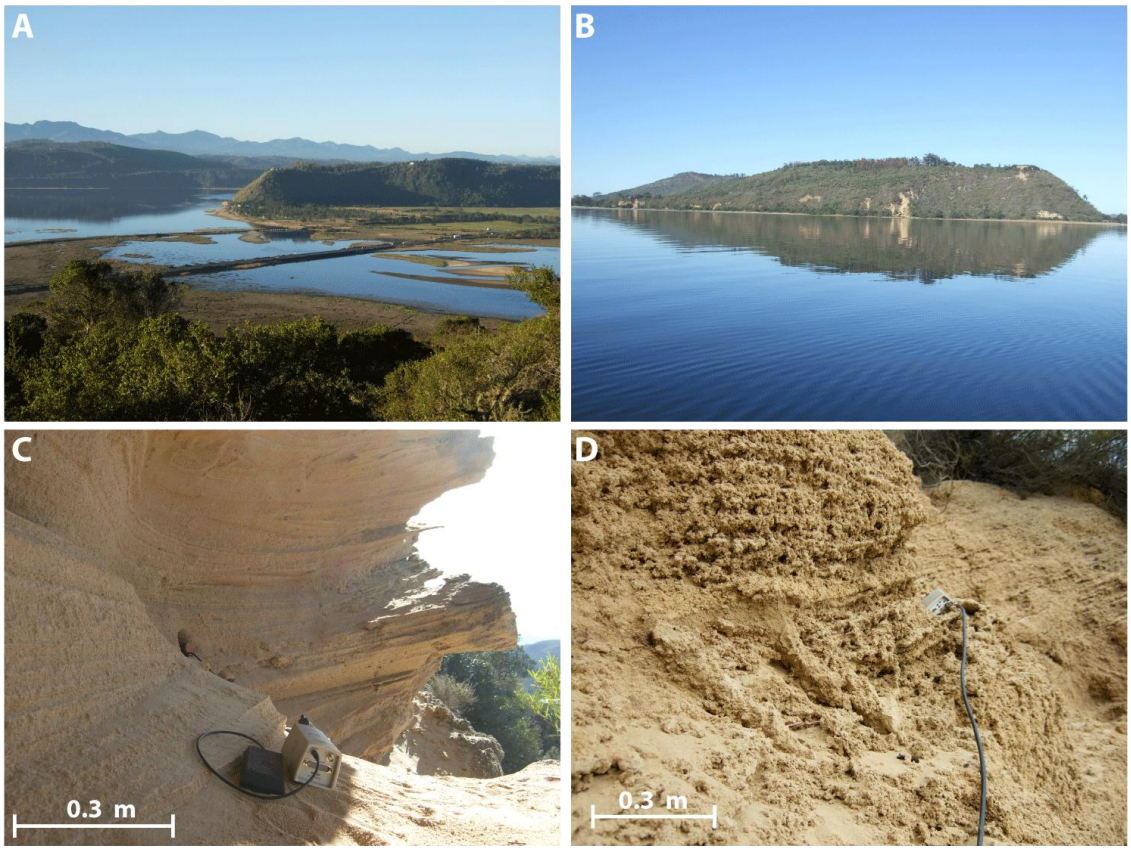

4.7 Middle barrier sites: (a) middle barrier extending east from Swartvlei; (b) cross-section of the middle barrier (East Swartvlei site), viewed facing east across Swartvlei; (c) finely bedded aeolianite at west Swartvlei site (sample Shfd09080); (d) aeolianite bedding with rhizoliths at east Swartvlei site (sample Shfd08182).

4.4.2.1 Rondevlei

The middle barrier dune was cored at a crestal location just north of Rondevlei (33° 59' S 22° 42' E; Figure 4.2 site 6). Coring revealed 4.2 m of unconsolidated, decalcified sand from which two samples were obtained. Coring ceased when aeolianite fragments started to be retrieved from the hole, indicating that this unconsolidated sand cover is a thin layer overlying an aeolianite core as exposed in the cliff at the terminus of the barrier. The stratigraphy of the sample site is shown in Figure 4.8 (site 6).

4.4.2.2 West Swartvlei

Swartvlei dissects the middle barrier, revealing cross-sectional exposures of aeolianite on both its western and eastern shores. Tinley (1985) suggested the location of southern Cape coastal barriers might be fixed by older cores of aeolianite at their centre, and these exposures provide an ideal opportunity to test this hypothesis. On the western side of Swartvlei (33° 59' S 22° 44' E; Figure 4.2 site 7) a network of footpaths permitted access to the exposure at all elevations, and three OSL samples were obtained: one from the dune crest via coring (Shfd09081); one from a natural aeolianite exposures at the cliff base (Shfd09082); and one from halfway up the exposure 25 m above the lake level of 1.2 m amsl (Shfd09080). At both cliff locations aeolianites comprised well sorted, lightly cemented sands, with well defined fine bedding and very few rhizoliths (Figure 4.7c). The core sample from the dune crest revealed 2.6 m of unconsolidated, decalcified sand lying above a core of aeolianite, similar to the Rondevlei site. The stratigraphy of the sample site is shown in Figure 4.8 (site 7).

4.4.2.3 East Swartvlei

Erosion at the eastern shore of Swartvlei (33° 59' S 22° 46' E; Figure 4.2 site 8) has revealed a cross section of the middle barrier dune from lake level (1.2 m amsl) upwards (Figure 4.7b). The site is morphologically similar to the seaward barrier exposure at East Elandsvlei, though here there is no evidence of marine bedding at the barrier base. Also, whilst high-angle aeolianite bedding is visible, it is less cemented than elsewhere and consequently obscured by slumping and vegetation in many areas. Rhizoliths are relatively common, indicating the presence of vegetation during dune accumulation (Figure 4.9d). Three OSL samples were collected: two from the head wall of a landslip towards the base of the dune (Shfd08181 at 36 m amsl and Shfd08182 at 43m amsl), and one from a small road cutting traversing the exposure higher up (Shfd08183, 73 m amsl). These samples are supplemented

by three further dates from Bateman et al. (2011): two from a road cutting running along the bottom of the exposure just above lake level (Shfd04284 and Shfd04285, both at 5 m amsl), and one from a road cutting at the dune crest (Shfd05048, 130 m amsl). Sample site stratigraphy is shown in Figure 4.8 (site 8).

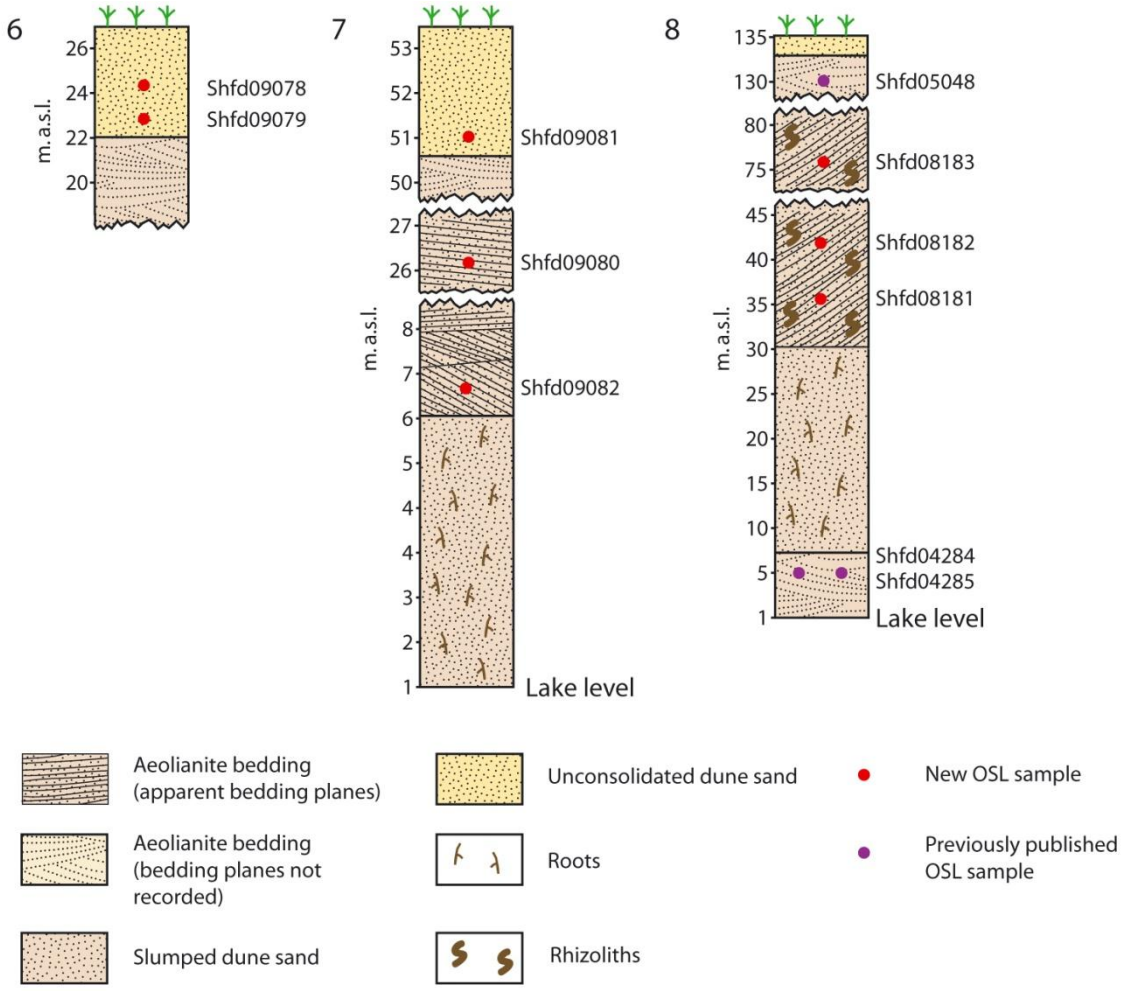

4.8 Stratigraphy of sample sites at Rondevlei (6), west Swartvlei (7) and east Swartvlei (8). Note: at east Swartvlei site, samples Shfd04284 and Shfd04285 are ~200 m apart horizontally. Site numbers correspond with the position of the sample sites as shown in Figure 4.2.

4.4.3 Landward barrier sites

The landward barrier dune is a less distinct geomorphological feature than the seaward and middle barriers, and is entirely absent from the western portion of the embayment (Figure 4.2). Behind Swartvlei the landward barrier is morphologically more of a sand ramp, with aeolianites backed up against the edge of the Wilderness embayment and no apparent lee side. Immediately to the east of Swartvlei the barrier is absent, presumably eroded by the Hoekraal and Karatara rivers. It recommences landward of the former lagoon

Ruigtevlei and displays a more obvious dune ridge along this section, almost coalescing with the middle barrier just west of the Goukamma River (Figure 4.9a). It attains a maximum altitude of 170 m amsl in this area, though it is unclear how much of this is accounted for by hard-rock geology underlying the aeolianites. A palaeo-sea cliff traceable along most of the length of the landward barrier was identified by Illenberger (1996), which he presumed formed concurrently with the middle barrier sea cliff. North of Swartvlei the situation is arguably slightly more complex, with two or three topographic "steps" apparently cut into the aeolianite as it rises towards the rim of the embayment. The landward barrier dune is currently under forest cultivation with limited access and very few natural exposures. As a consequence samples were obtained from only two sites (North Swartvlei and Goukamma), described in the following sections. Photos of the landward barrier sites are provided in Figure 4.9.

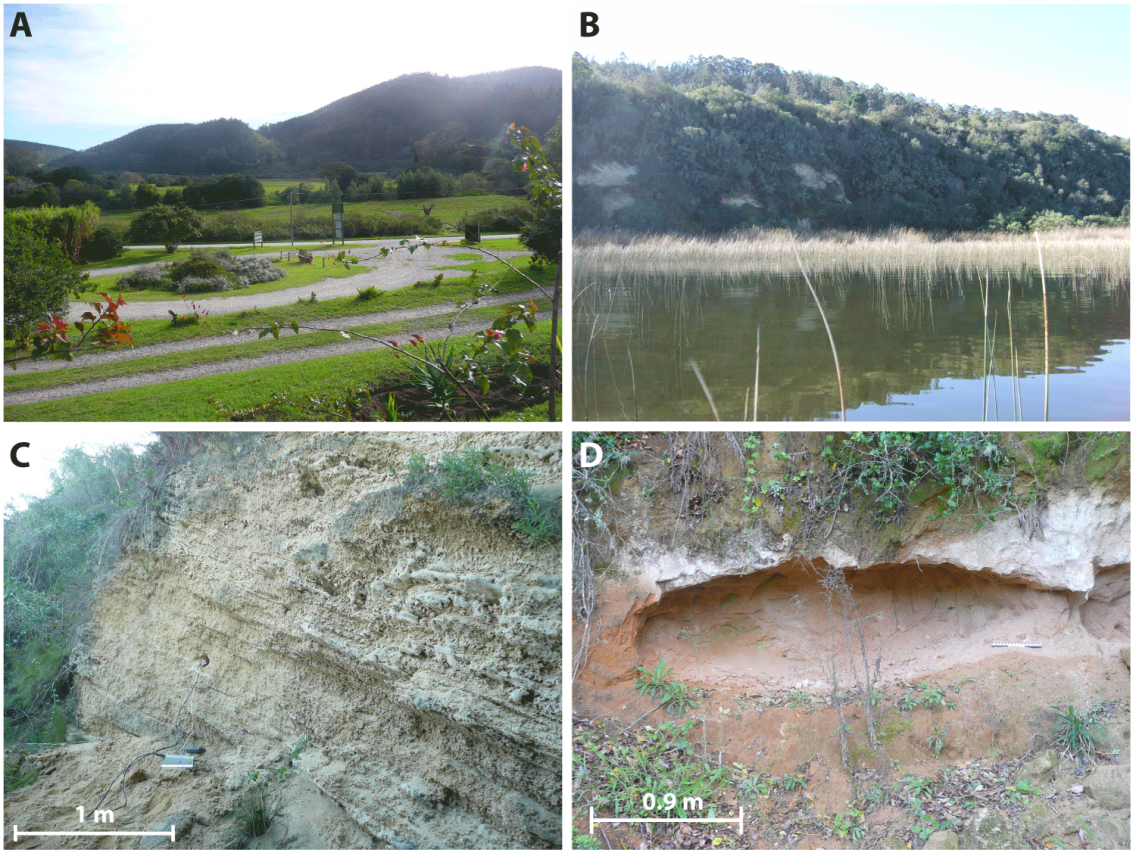

4.9 Landward barrier sample sites: (a) the terminus of the middle (centre of photo) and landward (right of photo) barriers at the Goukamma River floodplain. At this point their lower flanks overlap; (b) Exposures of landward barrier aeolianite on the north shore of Swartvlei lagoon; (c) close-up of bedding on north shore of Swartvlei (sample Shfd09074); (d) shallow burrow-like exposure at base of landward barrier, from which sample Shfd09069 was obtained.

4.4.3.1 North Swartvlei

Several aeolianite exposures are visible in the presumed palaeo sea cliff on the north shore of Swartvlei (33° 59' S 22° 46' E; Figure 4.2 sites 9a-b). Access could only be gained by boat, and two ~15 m high natural cliff exposures ~300 m apart horizontally were visited. Both exposures revealed well cemented carbonate-rich aeolianite with well defined high-angle bedding, and a sample was obtained from each (Shfd09074 and Shfd09075) (Figure 4.11b and 4.11c). Sands were well sorted and very pale brown in colour (10YR7/3). Their stratigraphy is shown in Figure 4.10 (sites 9a and 9b).

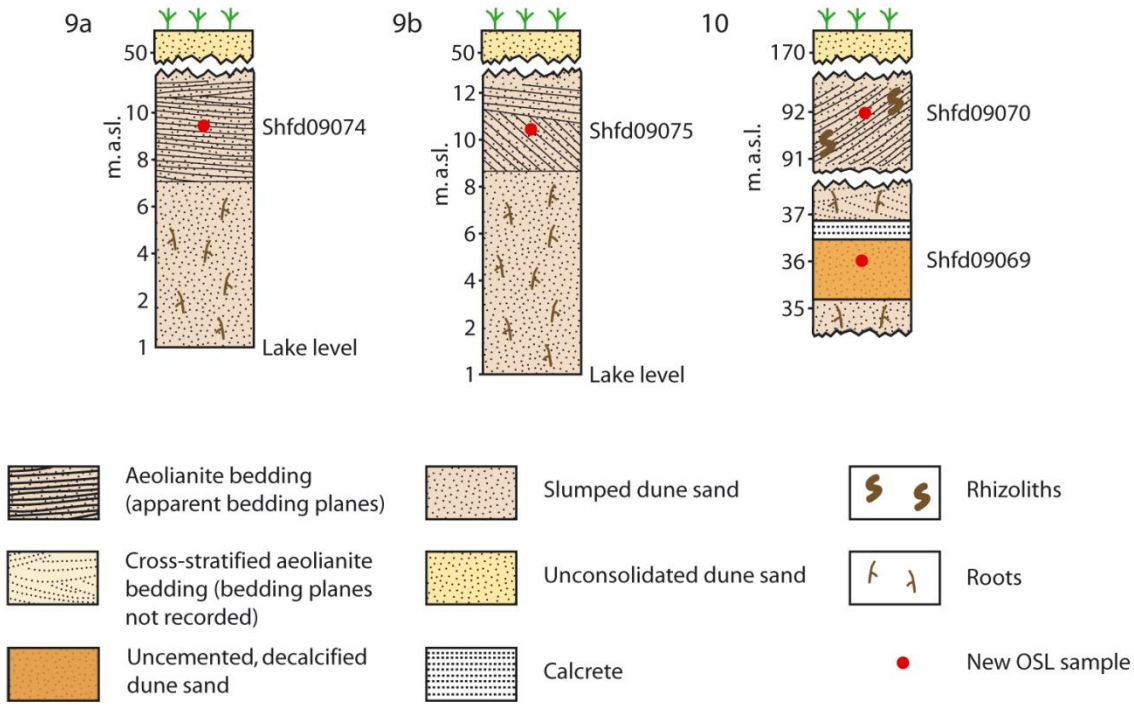

4.10 Stratigraphy of landward barrier OSL sample sites: north Swartvlei (9a and 9b) and Goukamma (10). Site numbers correspond with the position of the sample sites as shown in Figure 4.2.

4.4.3.2 Goukamma

The Goukamma site (34° 02' S 22° 56' E; Figure 4.2 site 10) is located on the eastern side of the Wilderness embayment where the lower flanks of the landward and middle barrier dunes overlap. Two samples were obtained, both from the seaward flank of the dune: one from a small burrow pit towards its base at 36 m amsl; and one from a road cutting two thirds up the dune at 92 m amsl. Stratigraphy at the basal site was atypical, with partially lithified aeolianite resting above a heavily indurated calcrete layer 0.5 m thick. Underneath this was a light brown (7.5 YR 6/3), uncemented, structureless decalcified sand unit from which a sample (Shfd09069) was obtained (Figure 4.11d). The small road cutting, from which the second OSL

sample (Shfd09070) was collected, revealed a partially lithified aeolianite identical in colour to the seaward and middle barrier sands (10 YR 7/3) in which indistinct high-angle bedding with some rhizoliths is present. Sample site stratigraphy is illustrated in Figure 4.10 (site 10).

4.4.4 Coversand sites

The coversands (mapped in chapter 1 Figure 1.3) reach their maximum thickness and extent in the vicinity of Knysna estuary, but the deposit also continues westward along the rear of the Wilderness embayment as far as Swartvlei. In the rolling, predominantly forested or cultivated landscape of this area it can be difficult to distinguish whether coversand is present in a specific location, but sedimentary exposures (present only in the form of road cuttings) make the distinction clear. The coversands are entirely decalcified, retain no bedding structures, are often laterised or underlain by laterised material, and are generally fine grained and prone to piping in places (Marker and Holmes, 2002; Marker and Holmes, 2005). Two coversand sites, further west than those from Holmes et al. (2007), were sampled and are described in the following sections. Photos of the coversand sites are provided in Figure 4.11.

4.4.4.1 Karatara Road

Close to the Swart River and the north-east corner of Swartvlei, the Karatara Road site (33^{o} 59' S 22^{o} 48' E; Figure 4.2 site 11) represents the point furthest west at which a coversand exposure suitable for OSL sampling could be located. One sample (Shfd08192) was obtained from a road cutting at 59 m amsl (Figure 4.11a and 4.11b) at the low end of a valley-side slope. The exposure revealed a very thin (0.1 m) organic layer with minimal soil development at the surface, overlying a 2- m-thick, pinkish (7.5YR 7/3), structureless, silty coversand unit with occasional modern rootlets, from which the sample was obtained. Underlying the coversand, and partially obscured by slumping, was a layer of strongly laterised reddish brown (2.5YR 5/4) extremely fine-grained material extending to the base of the exposure. Sample site stratigraphy is shown in Figure 4.12 (site 11).

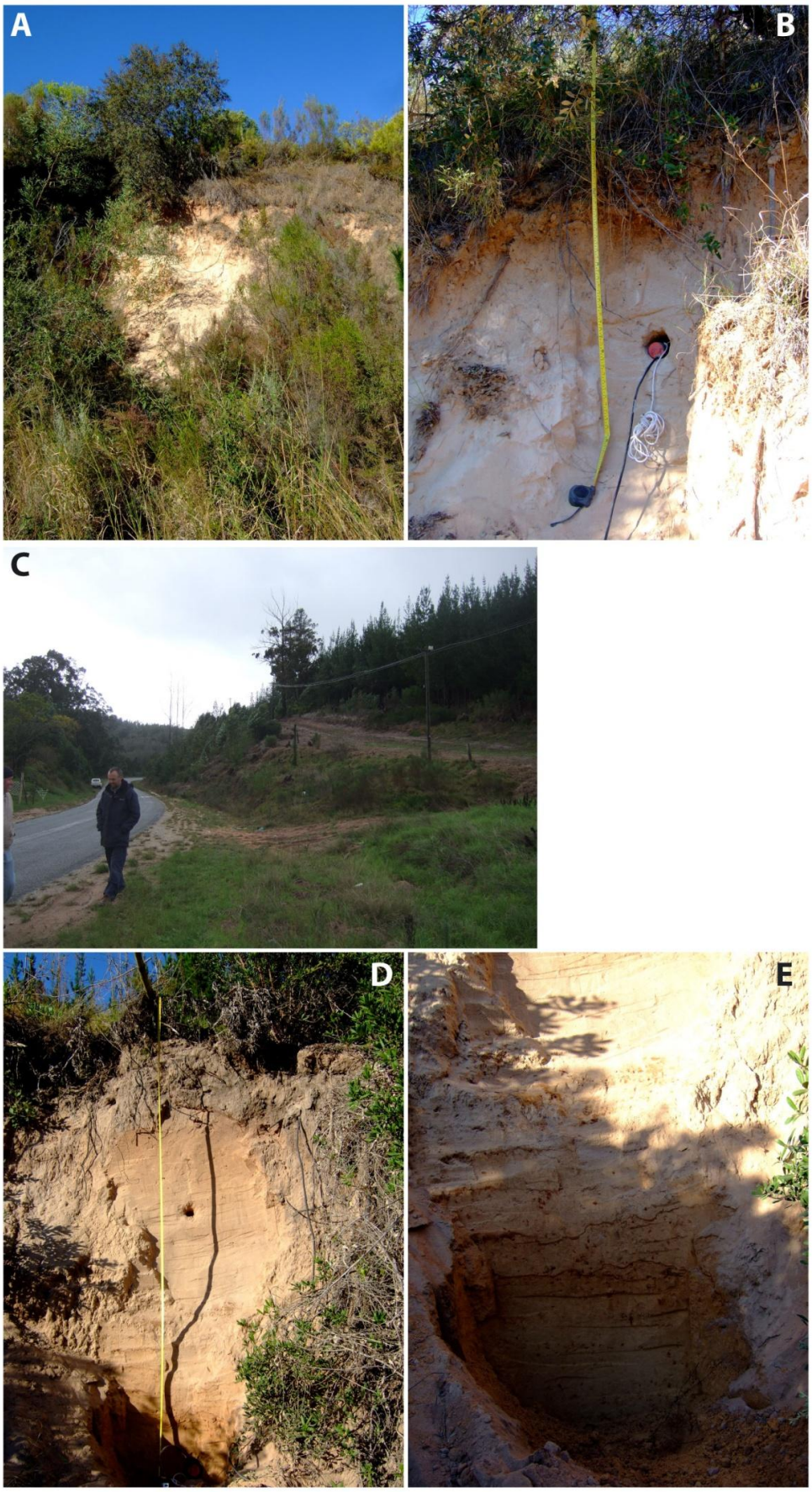

4.11 Coversand sample sites: (a) Karatara Road exposure (note: underlying laterite is obscured by slumping); (b) close up of Karatara Road exposure (sample Shfd08192) (1 m tape measure); (c) Barrington Road site; (d) Barrington road exposure (2 m tape measure); (e) iron pans visible in lower half of Barrington Road exposure, prior to extracting sample Shfd08191.

4.4.4.2 Barrington Road

The Barrington Road site (33° 59' S 22° 51' E; Figure 4.2 site 12) is located on the lower slope of a ridge-like feature (Figure 4.11c). It is further east than the Karatara Road site and possesses a deeper coversand unit. A reasonably well developed soil of 0.25 m thickness overlies a homogeneous and structureless fine sand/silt coversand unit of 2.5 m depth, light brown in colour (7.5YR 6/3) (Figure 4.11d). Sample Shfd08190 was obtained from this unit. Excavation of slumped material at the base of the exposure revealed a laterised and red-tinged (5YR) layer 0.6 m thick incorporating several iron pans and nodules (Figure 4.11e), underlain by further coversands. A second sample (Shfd08191) was obtained from the lower coversand unit beneath the iron pans. Sample site stratigraphy is shown in Figure 4.12 (site 12).

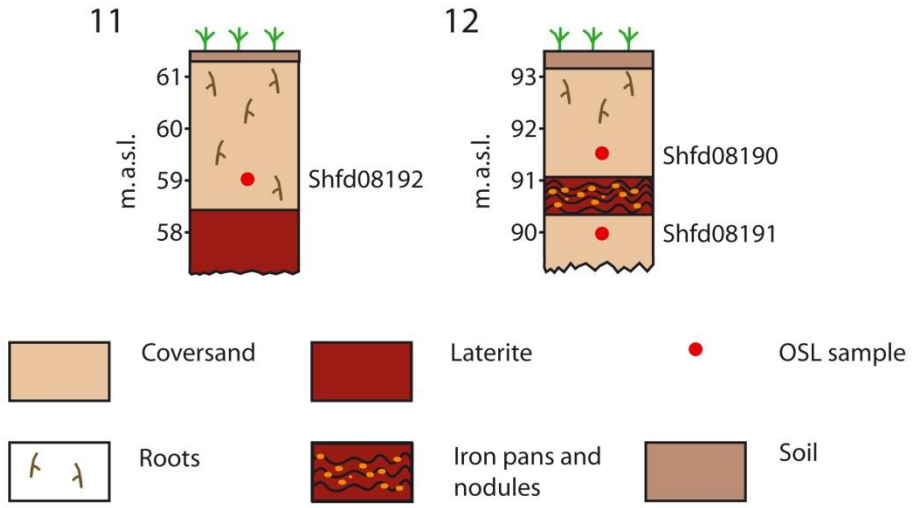

4.12 Coversand sample site stratigraphy: Karatara Road (site 11) and Barrington Road (site 12). Site numbers correspond with the position of the sample sites as shown in Figure 4.2.

4.5 Summary of OSL samples

In summary, ten new sites within the Wilderness barriers (five from the seaward barrier, three from the middle barrier and two from the landward barrier) and two coversand sites were sampled for OSL dating, yielding a total of 39 samples. The extensive spatial coverage and number of samples collected from the seaward barrier represent a significant increase in detail beyond the single-site studies of Bateman et al. (2004), Carr et al. (2007) and Carr et al. (2010a), and should be sufficient to provide a robust chronological framework for reconstructing the manner in which the barrier has evolved. Samples from the middle and landward barriers also cover a range of elevations and span the full width of the embayment, and will significantly extend the chronology of barrier formation at Wilderness. The two coversand sites represent exposures considerably farther west than have previously been

sampled for dating purposes, and will provide new information on the variability (or otherwise) in age of the deposit.

4.6 Sediment provenance sampling methods

4.6.1 Samples required for sediment provenancing

At the start of this chapter, it was explained that the suite of samples obtained for sediment provenancing purposes should facilitate comparisons between the following elements of the Wilderness barrier system:

i. The seaward, middle and landward barriers, in order to investigate what similarities and/or differences can be identified between them.
ii. Samples from different settings within the seaward barrier, to determine whether the variations in carbonate content within it indicate shifts from marine to terrestrial sediment provenance or simply post-depositional modification of the sands.
iii. The barrier sands vs. their various possible local sediment sources, to identify whether a provenance relationship can be established between any of them.

Regarding the first comparison above, the suite of samples collected for OSL dating purposes was considered adequate to describe the characteristics of the seaward, middle and landward barrier sands, without collecting additional material. Excess material from each of the 36 OSL samples from the barriers, in the form of sample tube ends, was thus subject to particle size analysis and carbonate-content determination (note: the laboratory techniques employed for sediment provenancing, and the rationale for their selection, is explained in chapter 5). The barrier sample sites and methods of sample collection were described in the previous section, and will not be elaborated on here.

Pre-existing samples were also employed for the second comparison on the above list, that is, samples from different settings within the seaward barrier. Trace element data relating to samples from various settings within the seaward Wilderness barrier has been generated in previous studies for OSL dosimetry purposes: from the relatively carbonate-poor KT section on the landward flank of the seaward barrier (Carr et al., 2007); from the Holocene dunes on its crest (Bateman et al., 2011); and from the carbonate-cemented aeolianites exposed in the sea cliffs at the rear of the current beach (Carr et al., 2010a; Bateman et al., 2011). Sufficient material from these samples was also retained at the Sheffield Centre for International

Drylands Research to permit new measurements of their particle size distributions and carbonate content to be made, to complement the existing geochemical data.

It was thus necessary to collect specific, new samples only in order to characterise the potential local terrestrial sources for the barrier sands. Samples were collected from a variety of settings identified as possible sources for the barrier sands: beach sands, sediment from the back-barrier lagoons, the various bedrock formations local to the Wilderness embayment, sediment carried by rivers debouching into the lagoons or directly to the ocean, and the coversands. Sampling was concentrated predominantly towards the west of the embayment, as the drift direction along the coast is eastward and the dominant dune building wind is westerly, making sediment introduced towards the east of the embayment less likely to have contributed to barrier construction.

Bedrock samples were obtained from each of the major geological units in the vicinity of the Wilderness embayment as identified in chapter 3 (the Kaaimans Group, the TMG and the Woodville granite pluton), with the intention of encompassing as many of the formations within them as possible. Keurbooms Formation conglomerate and Bokkeveld shales were not sampled, as exposures of these formations are extremely limited in extent, particularly in and to the west of the embayment. Also, more importantly, being shales and marls the Keurbooms Formation and Bokkeveld Group comprise predominantly silt- and clay-sized argillaceous material, rather than sand-sized quartz grains similar to those of the barrier sands.

4.6.2 Sediment provenance site selection and sample collection

Broad locations for bedrock samples were established based on the 1:250,000 geological map of the area. Sites were then scouted for suitable surface outcrops of rock, which were typically found at road cuttings or incised river courses (e.g. Figure 4.13a-c). The steep gradients and heavy vegetation of the region made locating suitable exposures problematic, though it was possible to obtain samples from almost all the river valleys within the embayment. Bedrock sample locations are shown in Figure 4.14.

Although predominantly quartz-rich, many of the formations within the TMG and Kaaimans Group contain frequent bands of argillaceous rocks (Visser, 1974; Gresse, 1983). Where possible, these were avoided in preference of sampling the quartzitic materials more likely to have contributed to the quartz-rich Wilderness barrier dune sands. Samples weighing 200-300 g were detached from in situ bedrock outcrops using a hammer and chisel.

4.13 Selected sediment provenance sample sites: (a) TMG sandstone at road cutting (note hammer in centre right for scale); (b) Woodville Granite at road cutting; (c) Kaaimans Group rocks in Kaaimans River channel; (d) Swartvlei lagoon, low tide; (e) Wolwe River channel, showing copious exposed sandy bars and overbank sediment deposits after November 2007 floods; (f) sand bank in Touw River channel.

For the other samples (coversands, beach sands, and river and lagoon sediments), approximately 100 g of material was collected from within 1-2 cm of the surface of the various settings and placed in Ziploc plastic bags. Sample locations are shown in Figure 4.14. Beach samples were acquired from the intertidal zone. Coversand samples were collected from road cutting exposures. The three coversand samples collected for OSL dating purposes were used, and three additional coversand samples were also collected. For logistical reasons lagoon sediments were sampled from the shallows at the edges of the water bodies, though sampling

at low tide enabled sites some distance from the shore to be accessed (Figure 4.13d). When sampling rivers, preferred sampling sites were deposits of sand-sized material from channel bars. The samples collected were not necessarily representative of the total grain size or composition of the river bedload, which at several upstream sites included boulder-sized material, but rather the fraction visually most similar to the barrier dune sediments. In late November 2007, approximately six months prior to the May 2008 field visit, the southern Cape was subjected to a series of heavy storms and associated floods, with the region around Knysna being one of the worst affected. As a consequence, at the time of sampling many of the river channels were particularly rich in sediment (Fig. 4.13e and 4.13f).

4.7 Summary of sediment provenance samples

The locations of samples collected for sediment provenancing purposes (excluding barrier dune sites, which are identical to the OSL sample locations) are shown in Figure 4.14. Numbers correspond with sample descriptions in Table 4.1. In summary, 12 samples of bedrock were obtained: four from the TMG; four from the Woodville granite pluton; and four from the Kaaimans Group. Table 4.1 assigns the bedrock samples to individual members within the TMG and Kaaimans Group according to the geological map and descriptions of Toerien and Roby (1979), but for clarity individual members are not mapped in Figure 4.2. Thirteen samples of the sediment carried by rivers were obtained, covering all the major rivers debouching in the Wilderness embayment excepting the River Knysna, which due to private land ownership it was not possible to gain access to. Five beach sand samples were collected, encompassing the full width of the embayment, and lagoon sediments were obtained from Swartvlei and Knysna lagoons. Six coversand samples were obtained at a variety of locations across the extent of the deposit. The suite of samples represents the most likely terrestrial sources of material for the barrier sands local to the Wilderness embayment.

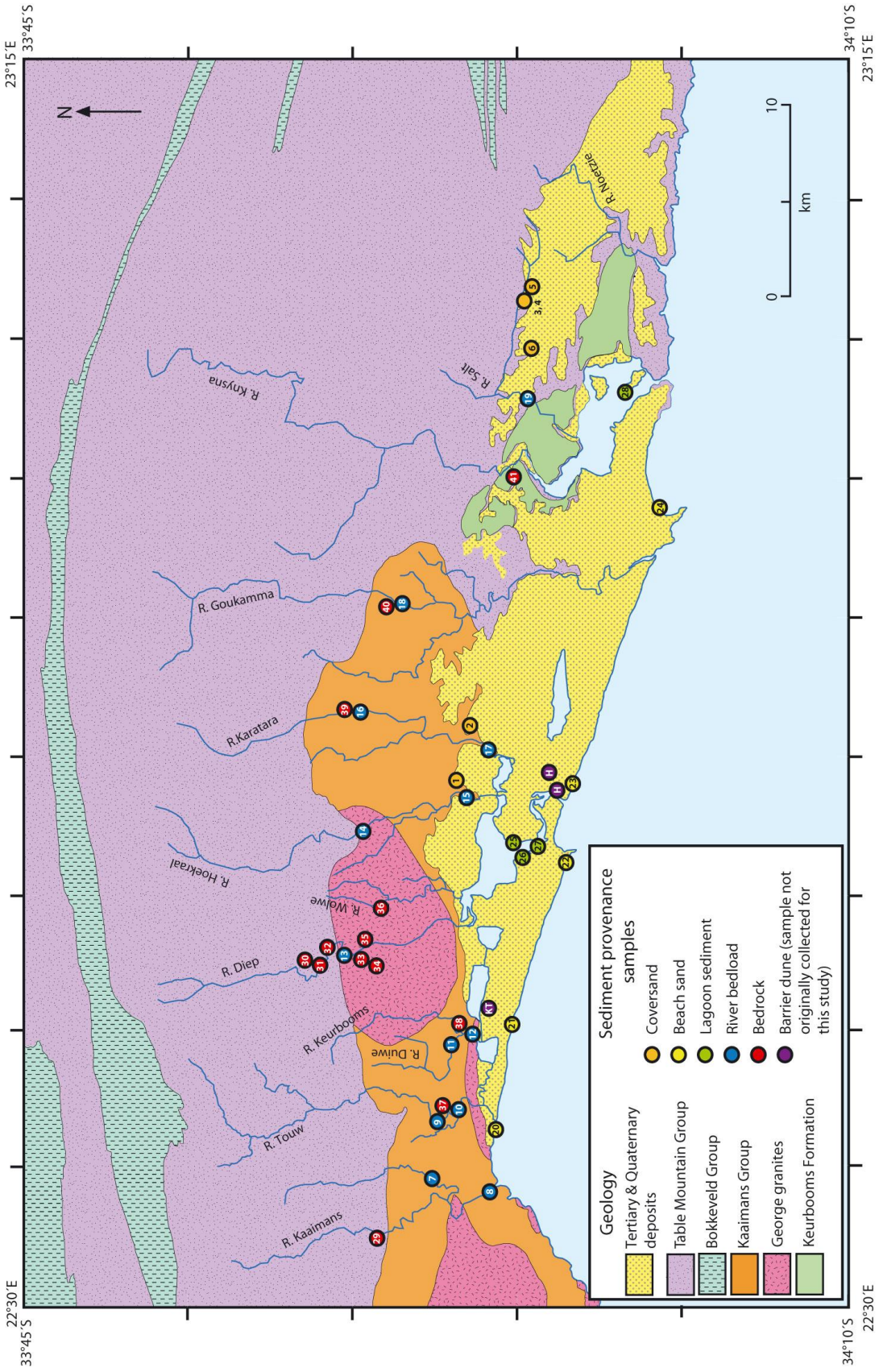

4.14 Sediment provenance sample site locations overlayed on local geology. Note: barrier dune sites sampled in this study are not included, as these are identical to the OSL sample site locations in Figure 4.2. Pre-existing barrier sites (KT section and Holocene dunes) are shown, labelled "KT" and "H" respectively. Sample numbers correspond with descriptions in Table 4.1.

Table 4.1 Sediment provenance samples: locations and brief field descriptions. Sample numbers correspond with sample locations in Figure 4.14. Continues overleaf.

	No.	Field code	Location	Field notes
COVERSANDS	1	Karatara Road	33°59'01 S, 22°48'36 E	Exposure at road cutting. Uncemented structureless sand unit overlying indurated laterised material
	2	Barrington Road	33°59'12 S, 22°50'55 E	Exposure at road cutting due north of former lagoon Ruigtevlei. Unconsolidated sand, some iron pans.
	3	Makhulu Quarry 1	34°00'48"S 23°06'26"E	Considered the typesite for coversands by Holmes et al. (2007). 15 m thick deposit with occasional iron nodules and mottled in colour
	4	Makhulu Quarry 2	34°00'48"S 23°06'26"E	As above, lower down same exposure
	5	Makhulu Quarry 3	34°00'50 S, 23°06'37 E	Exposure at road cutting c. 200 m east of Makhulu Quarry. Extensive piping indicates particularly fine sediment.
	6	Blaricum Heights	34°00'44 S, 23°03'33 E	Road cutting close to crest of slope. Some clay lamellae.
RIVER SEDIMENT	7	Kaaimans upper	33°57'54 S, 22°33'43 E	Exposed sand bank on margins of channel.
	8	Kaaimans lower	33°59'23 S, 22°33'05 E	Sand banked against tree in channel just south of N2 bridge
	9	Touw upper	33°58'03 S, 22°35'48 E	Channel bar near waterfall. Local bedrock granite
	10	Touw lower	33°58'31 S, 22°36'16 E	Coarse sand from channel bar. Local bedrock shale
	11	Duiwe upper	33°58'33 S, 22°39'34 E	Sand from dry backwater channel
	12	Duiwe lower	33°58'56 S, 22°39'07 E	Sand from exposed floodbar in channel (vegetated)
	13	Diep	33°54'59 S, 22°40'18 E	Coarse sand from mostly gravel bar in channel
	14	Hoekraal upper	33°55'32 S, 22°46'41 E	Wide, sinuous channel with multiple bars. Bedload ranges from boulders to sand (sample from the latter).
	15	Hoekraal lower	33°58'43 S, 22°47'59 E	Sand sample from partially vegetated channel bar
	16	Karatara upper	33°55'22 S, 22°51'10 E	Sample of poorly sorted fine-coarse sand from bar. Not as much sediment present as in other river channels.
	17	Karatara lower	33°59'55 S, 22°49'35 E	Channel bar close to Ruigtevlei. Possibly estuarine.
	18	Goukamma	33°56'52 S, 22°55'09 E	Coarse sand from channel bar
	19	Salt	34°01'20 S, 23°01'49 E	Well sorted sand in channel bar
BEACH SAND	20	Wilderness	33°59'45 S, 22°34'26 E	Beach sand from intertidal zone
	21	Klein Krantz	34°00'24 S, 22°39'33 E	Beach sand from intertidal zone
	22	Gerickes Point	34°01'55 S, 22°45'16 E	Beach sand from intertidal zone, in front of OSL sample Shfd08178
	23	Swartvlei	34°01'59 S, 22°47'53 E	Beach sand from intertidal zone
	24	Buffels Bay	34°04'48 S, 22°58'33 E	Beach sand from intertidal zone

Table 4.1 Continued from previous page. Sediment provenance samples: locations and brief field descriptions. Sample numbers correspond with sample locations in Figure 4.14.

LAGOON	25	Swartvlei 1	34°00'02 S, 22°46'31 E	Sandy bank on east shore adjacent to middle barrier
	26	Swartvlei 2	34°01'02 S, 22°46'00 E	Fine sand from tidal marsh on south shore
	27	Swartvlei 3	34°00'32 S, 22°45'52 E	Large sediment bar exposed at low tide
	28	Knysna	34°04'10 S, 23°04'04 E	Sediment exposed at low tide on island in lagoon
BEDROCK	29	TMG Peninsula 1	33°56’25 S, 22°34’02 E	Orange sandstone
	30	TMG Peninsula 2	33°54’49 S, 22°40’26 E	Grey sandstone with fine crystalline structure
	31	TMG Peninsula 3 (weathered)	33°55’01 S, 22°40’17 E	Heavily weathered whitish sandstone
	32	TMG (Tchando)	33°54’28 S, 22°42’06 E	Sandstone highly variable in colour between red/white/grey
	33	Woodville 1	33°56’09 S, 22°42’15 E	Grey unweathered granite
	34	Woodville 2	33°56’11 S, 22°42’12 E	Grey unweathered granite
	35	Woodville 3	33°57’25 S, 22°45’25 E	Grey unweathered granite
	36	Woodville 4	33°56’57 S, 22°43’57 E	Whitish weathered granite
	37	Kaaimans (Skaapkop)	33°58'20 S, 22°36'12 E	Shale, grey w. quartzitic inclusions
	38	Kaaimans (Soetkraal)	33° 58’55 S, 22°39’07 E	Quartzite
	39	Kaaimans (Victoria Bay)	33°55'18 S, 22°51'13 E	Quartzite
	40	Kaaimans (Homtini)	33°56'52 S, 22°55'09 E	V. soft grey/brown shale
	41	Keurbooms		

4.8 Chapter summary

The first part of this chapter explained how the study was designed in order to ensure the objectives of the research are met. The second part described the field sampling methods employed, and the morphology and morphological context of the sample sites.

5 Methods

5.1 Introduction

To meet the site-specific objectives of this research, several analytical techniques were employed. This chapter discusses the rationale for the selection of these techniques, their underlying principles, and details the methods used. It is divided into four main sections: OSL dating (section 5.2), ITL dating (5.3), sediment provenancing (5.4) and statistical analysis (5.5).

5.2 OSL dating

5.2.1 Principles and development of OSL dating

The ability of certain mineral grains to accumulate within them energy emitted from naturally occurring radioactive isotopes (principally potassium, thorium and uranium), and to emit this energy under thermal stimulation as a measurable thermoluminescence (TL) signal, was first recognised as a potential dating technique by Daniels et al. (1949). Determining the amount of radiation the natural luminescence signal of a sample represents (its equivalent dose, or D_e), and dividing this value by an estimation of the annual radiation dose rate the sample has received, provides the basis of the dating method. This can be expressed as:

$$Age\ (a) = \frac{Equivalent\ dose\ (D_e)(Gy)}{Dose\ rate\ (Gy\ a^{-1})} \quad 5.1$$

During the 1960s and 1970s, applications of TL dating were largely focussed on ceramics or otherwise anthropogenically heated materials from archaeological sites (e.g. Aitken, 1974; Fleming, 1979). The high temperatures involved in firing pots, heating hearth stones, etc. reliably resets the TL signal of the quartz and feldspar grains within them, meaning the luminescence observed on heating a sample of said material in the laboratory represents only that accumulated since the date of firing. Extending the utility of TL dating beyond archaeological applications to the geosciences proved problematic as, unlike in the production of ceramics, when sediments are deposited no heating event takes place to reset their TL signal. Not until the realisation in the 1980s that the electron traps in mineral grains (defects in their crystal lattice in which the ionising radiation they are subject to is stored) are of varying sensitivity, and that some are quickly reset by exposure to natural light (Huntley, 1985; Spooner et al., 1988), did the potential for dating natural sedimentary deposits using luminescence become a feasible proposition. Combined with recognition that the most

appropriate means of releasing this "fast" luminescence component in the laboratory was also exposure to light, rather than thermal stimulation, OSL dating was conceived (Huntley et al., 1985).

Since the 1980s, numerous methodological and technological advances have increased the reliability, precision and accuracy of OSL dating (Wintle, 2008). Briefly, these include a shift in focus from dating feldspar grains to quartz grains due to problems of anomalous signal fading with the former (Wintle, 1973; Spooner, 1994); advances in equipment for stimulating quartz grain luminescence signals (Bøtter-Jensen and Duller, 1992; Bøtter-Jensen et al., 1999); and various refinements of the OSL measurement protocol, which are discussed in section 5.2.2 below. OSL dating has proven particularly useful in settings where there is a lack of material suitable for other age determination methods, e.g. organic matter for radiocarbon (^{14}C) dating or corals for uranium-series dating. Numerous studies of sedimentary coastal and shallow-marine environments have consequently employed OSL, with a recent and comprehensive review provided by Jacobs (2008). OSL dating is also frequently applied in other settings where quartz-rich sediments are found. In southern Africa, these include lake shoreline ridges (e.g. Burrough et al., 2007; Thomas et al., 2009), colluvial sediments (Temme et al., 2008), desert dunes (Telfer and Thomas, 2007) and cave deposits (Jacobs et al., 2003b).

5.2.2 OSL measurement protocols

Although Huntley et al. (1985) noted the potential for OSL dating a sample using only a single aliquot (portion of sample), the first iterations of the technique mirrored the established TL protocol. TL dating is destructive, in that each aliquot can only be used once: heating to the high temperatures required (typically 4-500 °C) releases all the electrons trapped in the grains, inducing irreversible sensitivity changes (Murray et al., 1997). Many tens of aliquots are thus required to determine D_e. This causes a number of problems: the procedure is time consuming, large sample sizes are required, and, more fundamentally, problems arise in normalising the responses of the different aliquots (Duller, 1991).

Multiple aliquot procedures have now been superseded by more efficient and precise single aliquot protocols. The first attempts to determine D_e using single aliquots were made by Duller (1991), who suggested a single aliquot additive dose (SAAD) protocol was most promising. In SAAD the luminescence signal is measured following a very short stimulation period (0.1 s of light), and further laboratory doses of radiation are then added to the aliquot and measured to produce an additive-dose curve for determination of D_e. Single-aliquot

protocols were further refined by Murray and Roberts (1998) and Murray and Wintle (2000), who proposed the single aliquot regenerative dose (SAR) protocol. The principal difference between SAAD and SAR is that SAR uses a longer stimulation period to effectively zero (or "bleach") the luminescence signal after each measurement (Figure 5.1a), permitting intermediate measurements of a fixed test dose to be made and used to normalise any sensitivity changes that occur during the sequence. A growth curve is constructed based on the sensitivity-corrected luminescence response of the aliquot to varying known radiation doses (D_i), allowing the value corresponding to the natural signal (D_e) to be interpolated (Figure 5.1b). Wintle and Murray (2006) asserted that SAR "*revolutionised*" OSL dating, and it remains the most widely used form of the technique.

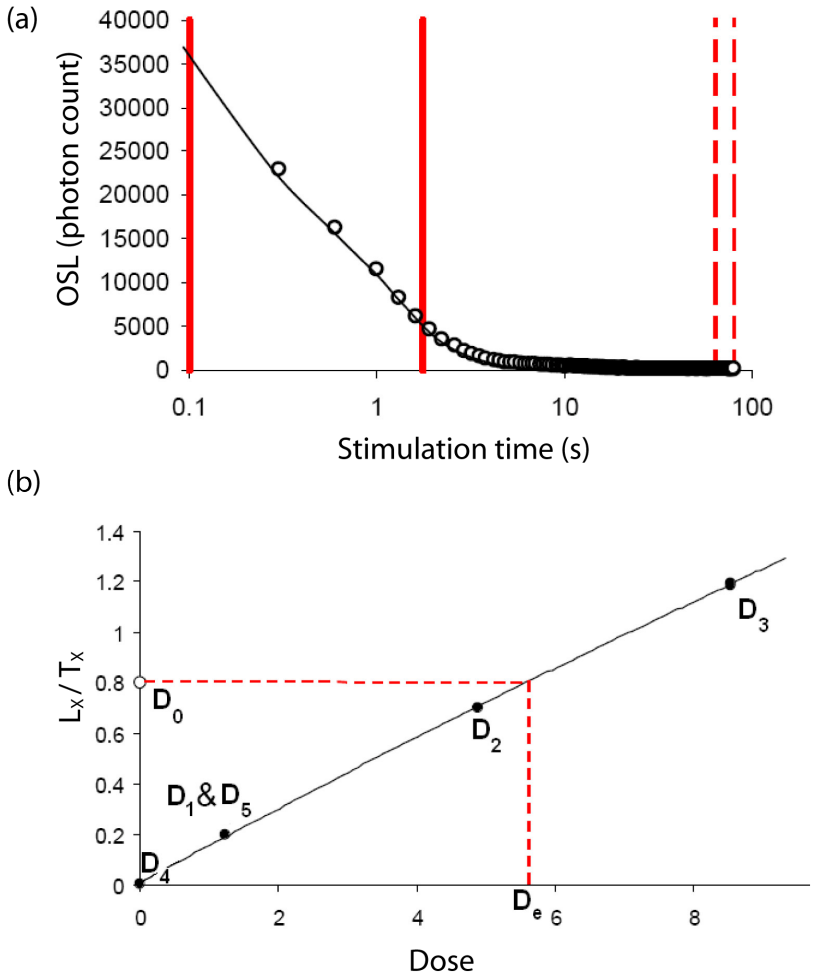

5.1 (a) Typical decay curve generated using SAR OSL. The bold red lines indicate the integration limits for signal measurement, and the dashed lines background measurement once the signal has been zeroed. (b) Growth curve generated using SAR OSL. The luminescence response (L_x) to a series of known doses ($D_{1\text{-}5}$) is normalised by test dose response (T_x) and plotted against dose. The dashed red line represents interpolation of the natural dose (D_e). Modified from Boulter (2007).

A generalised version of the SAR OSL measurement sequence is given in Table 5.1. Five regeneration points ($D_{1\text{-}5}$) are typically used to characterise growth curves, with the first three bracketing the natural dose (so that $D_1 < D_2 \approx D_e < D_3$), a zero point ($D_4$), and D_5 identical to D_1 (Figure 5.1b). The "recycling ratio" produced by D_1/D_5 can be used to assess the efficacy of the test dose normalisation, with aliquots producing values a given percentage (typically >10 %) outside unity being rejected (Murray and Wintle, 2000). The zero point (D_4) enables a test for recuperated signal to be conducted. Recuperation, if it occurs, will result in an overestimation of D_e. Recuperation can arise during: (a) preheating, from thermal transfer of electrons inserted by the test dose into TL traps and their subsequent transferral into OSL traps by the high temperature preheat; and/or (b) OSL shinedown, from transfer of electrons in OSL traps into relatively light-insensitive "refuge traps" and back again (Aitken, 1998). By calculating the L_x/T_x ratio of the zero dose point as a percentage of the L_x/T_x of the natural dose, its magnitude can be established. Murray and Olley (2002) suggest a recuperation value of <5 % is acceptable.

Table 5.1 The SAR OSL protocol, after Murray and Wintle (2000).

Stage	Treatment	Record
1	Administer regeneration dose D_i*	-
2	Preheat for 10 s at T °C†, heating at a rate of 2 °C s^{-1}	-
3	Stimulate for 80 s at 125 °C, heating at a rate of 5 °C s^{-1}	OSL L_x‡
4	Give 50 s fixed test dose D_t**	-
5	Cut heat (160 °C for 0 s, heating at a rate of 2 °C s^{-1})	-
6	Stimulate for 80 s at 125 °C, heating at a rate of 5 °C s^{-1}	OSL T_x‡
7	Repeat steps 1-6	-

* D_i is 0 Gy in the first cycle (i = 0) when D_e is measured.

† Preheat T is between 160-260 °C, with the exact value determined experimentally for each sample (see section 4.2.5).

‡ L_x and T_x are derived from the stimulation curve, and represent the first 1.6 s of OSL signal minus a background value (the last 16 s of the curve) (see Figure 5.1a).

** A standard test dose of 50 s was selected for all samples, irrespective of their D_e. Depending on the dose rate of the Risø reader (see section 5.2.4.2 below) used, this was equivalent to ~3-6 Gy. Test dose size has been found to have no significant effect on the resultant D_e value produced or the size of the recuperated signal (Murray and Wintle, 2000).

The function of the curve fitted to SAR regeneration points is generally most accurately described by the sum of several exponential functions (Bailey et al., 1997; Bulur et al., 2000). However, a single saturating exponential function is commonly fitted to OSL growth curves for age calculation purposes, of the form given in Equation 5.2 (where *I* is the OSL intensity due to

dose D, I_0 is the saturation intensity and D_0 the dose level that is characteristic of the dose response curve).

$$I / I_0 = (1 - \exp^{-D/D_0}) \quad 5.2$$

Adequate description of growth curves with a single saturating exponential function of this form provides confidence they are first-order, i.e. they relate only to the fast component signal desired in OSL (Wintle and Murray, 2006). Use of this function also provides a simple means of assessing whether an aliquot is in saturation, i.e. unable to retain any more charge. If the D_e value interpolated is more than twice its D_0 component, as shown in Figure 5.2, the aliquot should be considered saturated and the D_e value treated as a minimum (Wintle and Murray, 2006). This possibility is discussed further in the next section.

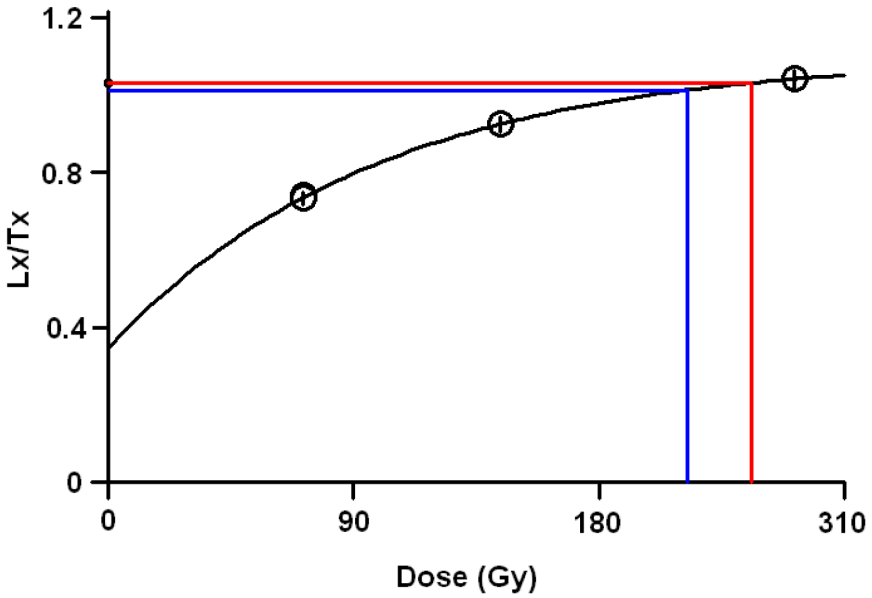

5.2 Growth curve from an aliquot with a saturated natural signal, fitted with a single saturating exponential function. The D_0 value of the function (as per Equation 5.2) is 123 Gy. The blue line represents $2*D_0$ (246 Gy) and the red line represents interpolation of D_e. As it is > $2*D_0$, the interpolated value of 293 Gy should be treated as a minimum estimate of D_e only.

5.2.3 Limitations of OSL

Unfortunately, OSL dating is not appropriate for dating the last exposure to sunlight of all quartz-rich sediments. Although its range exceeds that of ^{14}C dating (c. 40 ka), the electron traps which store the fast luminescence component in quartz eventually become saturated (i.e. unable to retain any more charge), providing an upper age limit for the technique. This typically occurs somewhere between 100-250 Gy, with the absolute age this translates to

being a function of the environmental dose rate: in low radiation settings ages in the region of 800 ka have been obtained (e.g. Banerjee et al., 2003), but usually the limit is much lower.

Although dose rates encountered in southern Cape coastal sediments are consistently relatively low (Carr et al., 2007), saturation issues meant Holmes et al. (2007) were able to obtain only minimum ages (c. 300-500 ka) from the coversands inland of the Wilderness embayment. In order to clarify the relationship between the barriers and the coversands, an isothermal thermoluminescence (ITL) protocol was employed in this study to date the coversands, in addition to conventional OSL dating. ITL is a relatively new technique potentially able to overcome saturation issues, originally proposed by Jain et al. (2005). The ITL dating method is discussed in sections 5.3 and 5.4, following a description of the standard SAR OSL methodology used to date the majority of samples.

5.2.4 OSL methodology

5.2.4.1 Sample preparation

All sample preparation was conducted in red-light conditions. Sample tubes were opened and the potentially light-exposed material at each end removed. The remainder of the material was then prepared following the procedure outlined by Bateman and Catt (1996) in order to isolate pure quartz grains of 125-250 μm size. Briefly, samples were treated with 10 % hydrochloric acid (HCl) and 10 % hydrogen peroxide to remove carbonate and organic content, and dry-sieved at 90, 125, 180, 212 and 250 μm to isolate narrow size fractions. The heaviest of these fractions was selected and its heavy minerals removed by density separation using sodium polytungstate solution with a specific gravity of 2.7. The remaining material was etched in 40 % hydrofluoric acid (HF) for 60 minutes to dissolve feldspar minerals and remove the outer alpha-irradiated layer of the quartz grains. Finally samples were washed in HCl to remove fluorides and re-sieved to remove any remaining feldspar.

5.2.4.2 Instrument specifications

Measurements were conducted on three different configurations of automated Risø luminescence reader: a TL-DA 12 with stimulation provided by a 150W halogen lamp filtered by GG-420 long pass and SWP interference filters; a TL-DA 15 with stimulation provided by blue LEDS; and/or a TL-DA 18 also equipped with blue LED stimulation. Irradiation was from calibrated sealed ^{90}Sr-^{90}Y β sources and luminescence measurements were made through Hoya

U340 filters with peak transmission at 330 nm and a range of 290-370 nm. All measurements were made using 9.6 mm diameter aliquots of sample mounted using silicon oil spray on stainless steel or aluminium discs (depending on machine calibration). Boulter (2007) and Telfer (2006) compared the luminescence measurements from samples measured on the TL-DA 12 and TL-DA 15 instruments and both found no systematic differences between them. Additionally, multiple aliquots from one sample (Shfd09075) were measured on both the TL-DA 15 (17 aliquots) and the TL-DA 18 (13 aliquots). They yielded mean D_es of 202.99 ± 25.57 Gy and 202.29 ± 43.78 Gy respectively, demonstrating the comparability of these instruments.

5.2.4.3 Growth curve fitting

Growth curve fitting and D_e interpolation were both conducted using Risø Analyst version 3.24 software. The function used to describe growth curves was determined on an aliquot-by-aliquot basis based on minimising the error in curve fit as calculated by Risø Analyst. The single saturating exponential function (given in Equation 5.2) was found to best describe the growth curves of the vast majority of aliquots. For a very limited number of samples, alternative functions were more appropriate. At doses well below saturation, the OSL growth curve is known to be linear (Murray and Olley, 2002), and a simple linear curve thus provided the best fit for some aliquots. Carr et al. (2007) used saturating exponential plus linear functions to describe the growth curves of samples from the seaward Wilderness barrier, and these were also found to minimise the error in curve fit for a small number of aliquots in this study. An increased number of regeneration points (up to seven) were used to characterise the growth curves of some samples observed to be close to saturation.

5.2.4.4 Sample testing

Prior to measuring the D_e of a sample using the SAR OSL protocol given in Table 5.1, tests were conducted in order to: (i) confirm the sample had been prepared correctly; and (ii) select the most appropriate values for the regeneration doses D_i and the preheat temperature T. These tests are described in the following sections.

5.2.4.4.1 Sample testing: feldspar contamination

During sample preparation feldspar is removed by etching the sample with HF, to which quartz is more resistant, and then re-sieving to remove any grains that have been

significantly reduced in size (Wintle, 1997). However, the ability of this procedure to remove all feldspar is not guaranteed, particularly if the chosen size fraction of the sample is large and/or the quartz grains contain feldspar inclusions. It is thus necessary to test for feldspar contamination before beginning OSL measurements. A common means of doing this is to make infrared stimulated luminescence (IRSL) measurements: if no IRSL is detectable, it can be assumed feldspar is absent; if a "significant" IRSL signal is obtained, it implies feldspar is present in the sample (Aitken, 1998).

Duller (2003) tested different methods of determining what constitutes a significant level of IRSL in a sample, and concluded the most efficient is to calculate what they termed the OSL IR depletion ratio. First, the natural signal of an aliquot is zeroed. A beta dose of 100 s is then applied, and the OSL signal is measured after an invariant preheat of 260 °C for 10 s. A second OSL measurement is made, identical to the first but for an IR exposure of 100 s before the preheat. If any feldspar is present in the sample, the OSL signal of the second measurement will be lower than the first. Typically, if the ratio of OSL signals (after/before exposure to infrared) is two standard deviations or more less than unity, feldspar contamination is regarded as significant (e.g. Jacobs et al., 2003a; Jacobs et al., 2006a). The OSL IR depletion ratio was calculated for three aliquots of each sample measured. Only one sample (Shfd09071) was found to have significant feldspar contamination, and after re-etching a second IR test confirmed its feldspar content had been successfully removed.

5.2.4.4.2 Sample testing: rangefinder

In order to select appropriate regeneration points for the SAR OSL protocol, and also to determine what laboratory dose to administer in dose recovery preheat tests (discussed in the next section), it is necessary to obtain an initial rough approximation of the D_e of a sample. An abbreviated SAR protocol with only two regeneration points and an invariant preheat of 200 °C was thus conducted on three aliquots of each sample following the IR ratio test.

5.2.4.4.3 Sample testing: dose recovery and preheat temperature

A fundamental assumption of OSL dating is that the electron traps responsible for storing and producing the luminescence signal are stable over the relevant time periods. However, in addition to stable electron traps, quartz grains also contain light-sensitive and thermally unstable traps that do not relate to the geological signal and can contaminate results (Aitken, 1998). For this reason, preheating samples to empty these unstable traps prior to

measurement is an integral part of the protocol. However, different preheat temperatures may induce differing amounts of sensitivity change (Wintle and Murray, 2006). To determine the most appropriate preheat temperature, dose recovery preheat tests were employed. Combining the dose recovery test of Murray and Wintle (2003) and the preheat plateau test of Murray and Wintle (2000), samples were optically bleached at room temperature and given a known laboratory dose (roughly equivalent to D_e, as determined using a rangefinder test), and then measured using SAR OSL with five regeneration points at a series of preheat temperatures. Two criteria were used to assess the results: (i) dose recovery - the ratio of measured to given dose should be as close to unity as possible; and (ii) recycling - the ratio of D_1/D_5 (as described in section 5.2.2) should be as close to unity as possible. A range of preheats from 160-260 °C in 20 °C increments were tested on three aliquots of at least one sample from each site. The results of a typical dose recovery preheat test are shown in Figure 5.3.

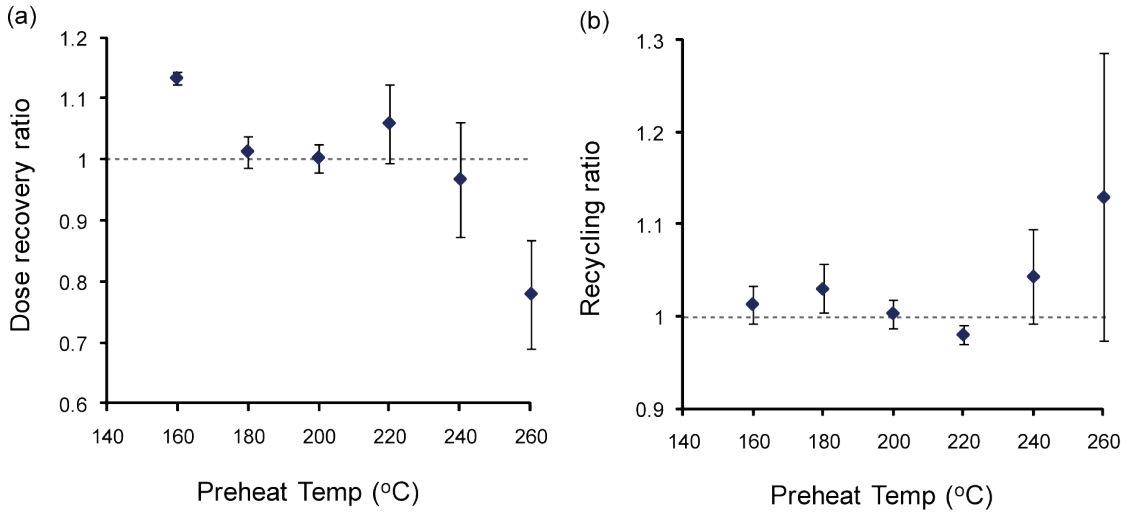

5.3 Results of a typical dose recovery preheat test: (a) shows the ratio of given to measured dose, and (b) shows the recycling ratio. For this sample (Shfd08180 from the seaward barrier at Gerickes Point) a preheat of 200 °C was selected.

5.2.4.4.1 Sample testing: recuperation

To establish whether recuperation poses a problem for the Wilderness samples, the SAR measurements for nine samples were conducted with the incorporation of a zero dose point. An average recuperation value (calculated as per section 5.2.2) of 0.31 ± 0.27 % was obtained. Murray and Olley (2002) suggest a recuperation value of <5 % is acceptable, and as only one aliquot from all nine samples tested exceeded 1 % (an aliquot from Shfd08176 measured 1.04 %), the effects of recuperation are considered as having no significant effect on the calculated D_e values for the suite of samples in this study.

5.2.4.5 Determining D_e

After conducting the above tests and determining appropriate preheat and regeneration dose values, sample D_es were measured using the SAR OSL protocol given in Table 5.1. Following assessment of the D_e values of individual aliquots based on the recycling and saturation criteria discussed above, measurements from 16 to 43 aliquots of each sample were retained for age calculation. A degree of variability in D_e between aliquots is inevitable, due to grain-to-grain variation in luminescence sensitivity, possible interference from microinclusions in quartz, partial bleaching, and several other factors (Felix and Singhvi, 1997), and it is thus necessary to reduce D_e distributions to a single representative value for age calculation. Several statistical methods for achieving this have been proposed (e.g. Olley et al., 1998; Galbraith et al., 1999; Roberts et al., 2000). The appropriate method was selected for each sample based on probability density functions, used to confirm D_e distributions were approximately normal in shape (these are described in the statistical analysis section (5.5) towards the end of this chapter), and overdispersion values, described below.

Overdispersion (OD) quantifies the difference between observed and predicted variance (based on an assumed normal distribution) from the weighted mean, after measurement uncertainties have been accounted for (Galbraith et al., 1999). For samples with zero OD, i.e. in which the D_es of all aliquots are within errors, the common age model of Galbraith et al. (1999) was used. For the much more common scenario, in which sample D_es possess small OD values, Galbraith et al.'s (1999) central age model (CAM) was applied. This model assumes that the D_e values are all centred on some average value (similar to the median), but takes into account that there will be some natural variation in D_e values between aliquots due to water content, microdosimetry etc. in calculating the standard error.

5.2.4.6 Problematic samples

Galbraith et al. (2005) reported that OD values of up to about 18 % could be found for uniformly bleached grains, and other researchers have used an arbitrary value of 20 % as the upper bound for appropriate application of the central age model (e.g. Olley et al., 2004; Mauz et al., 2010). All but four of the samples in this study present OD values below this 20 % threshold (most significantly so), and the four that exceed the threshold do so only marginally. The four samples with OD values of 20 % or greater are:

(a) Shfd08185 from the Buffels Bay seaward barrier site (OD = 21 %)
(b) Shfd08183 from the east Swartvlei middle barrier site (OD = 20 %)
(c) Shfd09070 from the Goukamma landward barrier site (OD = 21 %)

(d) Shfd09082 from the west Swartvlei middle barrier site (OD = 21 %)

Probability density functions for the four samples with OD values ≥20 % are shown in Figure 5.4. None of the samples appears to contain multiple, discrete D_e populations, as might be the case if post-depositional mixing had occurred (e.g. Jacobs et al., 2006a). Thus, applying the finite mixture model of Roberts et al. (2000), which can be used to separate multiple D_e components from composite D_e populations, would be inappropriate.

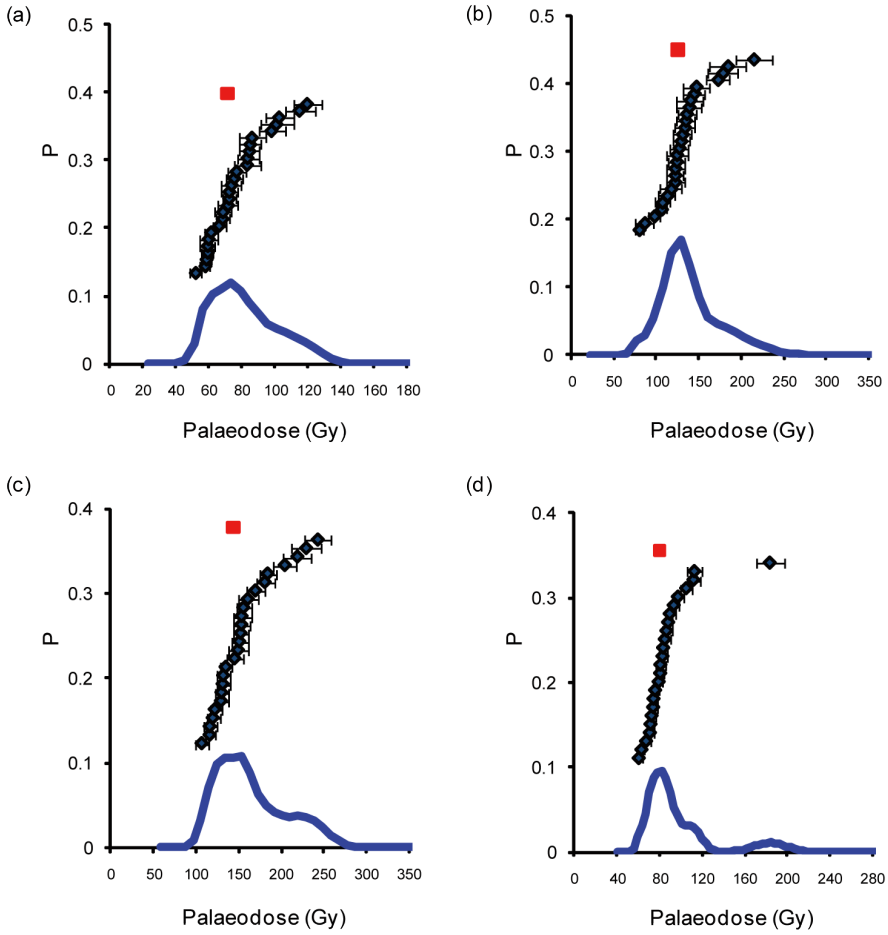

5.4 Probability density functions of aliquot D_es for samples with OD values ≥20 %: (a) Shfd08185; (b) Shfd08183; (c) Shfd09070; (d) Shfd09082.

Samples Shfd08185, Shfd08183 and Shfd09070 display tails of high D_e values (Figure 5.4a, b and c respectively). Such D_e distributions are potentially indicative of partial bleaching (Bateman et al., 2003a), whereby not all of the grains in the sample were exposed to sufficient sunlight during their last exposure to remove their antecedent OSL signal. However, coastal-dune sands are likely to experience multiple bleaching cycles before deposition, leaving them well bleached (Ballarini et al., 2003). Combined with the low OD values of the majority of other samples in the study, the possibility of partial bleaching is thus discounted.

An alternative explanation for the high-tailed D_e distributions in Figure 5.4a-c is that the samples are approaching saturation, and the D_e values have been interpolated from the upper, low gradient part of the growth curve (Murray and Funder, 2003). Murray and Funder (2003) suggest the median D_e value is likely to give the most accurate estimation of the true value in such instances. However, for these samples the difference between the median and CAM D_e values proved negligible. For sample Shfd08185 the median D_e is 72.08 Gy and the CAM D_e is 72.09 Gy. For sample Shfd08183 the median D_e is 125.16 Gy and the CAM D_e is 123.7 Gy, and for sample Shfd09070 the median D_e is 147.42 Gy and the CAM D_e is 143.51 Gy. Carr et al. (2007) also reported negligible differences in median and CAM D_e for samples from the Wilderness barriers with high dose tails. The CAM D_e values were thus used in all cases, as its calculation provides a more rigorous estimation of error.

The relatively high OD of sample Shfd09082 (Figure 5.4d) is attributable to a single outlier falling outside an otherwise approximately normally distributed dataset. For this sample, and in other such cases, the outlier(s) were removed prior to calculating D_e using CAM. The deletion of such values can be justified by the various processes due to which an aliquot can potentially produce a D_e unrelated to burial age, such as the aforementioned possibility for variations in grain sensitivity and/or incomplete bleaching (Felix and Singhvi, 1997), or bioturbation processes (e.g. Bateman et al., 2003a). Outliers were defined as values outside of two standard deviations of the mean (e.g. Bateman et al., 2007).

Determining a reliable estimate of D_e from one other sample, Shfd09075 from the landward barrier, proved problematic. Of the 39 aliquots of this sample measured, six were in saturation (based on the 2 * D_0 criteria discussed in section 5.2.2). Applying CAM to the 30 aliquots that also met other rejection criteria, a D_e of 194 Gy was obtained. This value was treated as a minimum.

5.2.4.7 Determining dose rate

As expressed in Equation 5.1, in addition to a measurement of D_e, determining the age of a sample using luminescence dating also requires an estimation of the dose rate of ionising radiation the sample has received since burial. The primary source of ionising radiation flux to buried sediment is the decay of naturally occurring uranium, thorium and potassium isotopes, which results in the emission of alpha particles, beta particles and gamma radiation. This is referred to as environmental dose rate. Additionally, sediments also receive ionising radiation

from space in the form of cosmic ray muons. This is referred to as cosmic dose rate. The determination of these parameters is discussed in the following sections.

5.2.4.7.1 Determining dose rate: environmental dose rate

For most samples, the concentrations of U, Th and K were determined in situ using an EG&G Micronomad multi channel portable gamma spectrometer with a 2" sodium iodide probe. Elemental concentrations were then converted to annual dose rates using data from Aitken (1985), Adamiec and Aitken (1998) and Marsh et al. (2002). On a small number of occasions, gamma spectrometry (GS) was not possible due to time constraints in the field: measurements require 45 minutes per sample. For these samples radioisotope concentrations were measured later using either: (i) inductively coupled mass spectrometry (ICP-MS) (for U and Th) and inductively coupled plasma atomic spectroscopy (ICP-AES) (for K); or (ii) beta counting. For ICP-MS/AES, material removed from the tube ends of samples was riffled (to 10 g) and pulverised in a Tema mill before being sent to SGS laboratories, Canada. Measurements were made on samples completely digested using sodium peroxide fusion (SGS method code ICM90A), with reporting limits of 0.01 % (K), 0.05 ppm (U) and 0.1 ppm (Th). Beta counting was conducted using a Risø low-level beta GM-25-5A multicounter system on unaltered tube-end material. Unlike GS and ICP-MS/AES, beta counting does not measure the concentrations of the different isotopes, providing instead only a total dose rate.

Using different methods of environmental dose rate determination for different samples within a study is relatively common (e.g. Bateman et al., 2008; Carr et al., 2010a). Boulter (2007) found good agreement between the GS equipment and the Risø low-level beta GM-25-5A multicounter at SCIDR used in this study for aeolian samples from Texas, USA. Their comparability was further assessed here by determining the total dose rates of 16 samples from the Wilderness barriers using both beta counting and GS. Results, shown in Figure 5.5, demonstrate good agreement between the two methods and no systematic differences, with the majority of measurements falling inside or close to ± 10 % of unity.

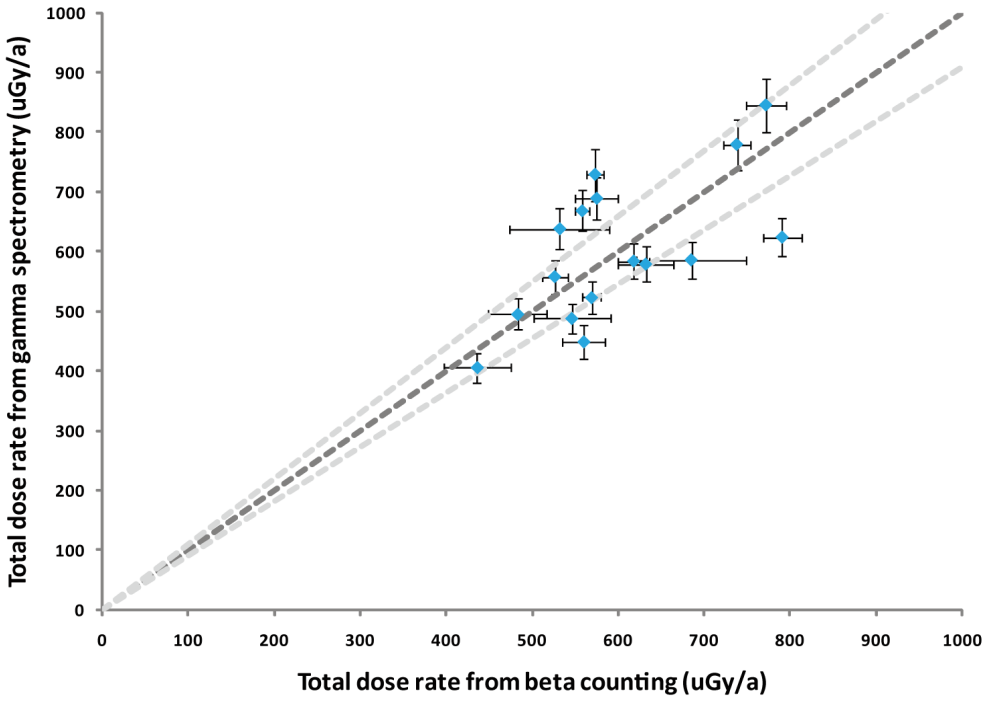

5.5 Comparison of the total dose rates of 16 Wilderness barrier dune samples determined using both gamma spectrometry and beta counting. Dark grey dashed line shows unity and light grey dashes ± 10 % of that value.

5.2.4.7.2 Determining dose rate: U series disequilibrium

Gamma spectrometry is widely regarded as the preferable means of measuring environmental dose rate, chiefly because it can record the radiation dose from a ~30 cm radius surrounding the sample (unlike beta counting or ICP-MS/AES, which are performed on small sub-samples of only a few grams), but it is not without potential problems. As the half-lives of U and Th are in the order of billions of years, GS relies on measurement of the activity of faster-decaying daughter isotopes on their decay chains (thalium 208 and bismuth 214), and total U and Th concentrations are back-calculated from these values. This means GS is unable to account for disequilibrium: a process whereby, if a decay chain is added to or depleted by processes other than radioactive decay, the concentration of daughter isotopes will not provide an accurate measure of that of their parents.

There is little or no risk of disequilibrium in the K or Th decay chains but it is possible in the U-series decay chain, particularly in carbonate-rich environments (Olley et al., 1997; Jacobs et al., 2006b). However, its effects are generally small. In a study of fluvial silt and sand samples in Australia, Olley et al. (1996) found that whilst disequilibrium was common in the U-series decay chain, it was typically ≤20 % and in most cases had an effect of <3 % on total dose rate. Lomax et al. (2003) found U-series disequilibrium of 20-50 % in samples of Australian

dune sand due to calcification of rootlets, which they calculated could result in an error in age calculation of 8 % at worst. Similarly, Jacobs et al. (2006b) noted U-series disequilibrium of 18-40 % in samples of carbonate sand from Blombos Cave, South Africa, but calculated this had an effect of only a few percent at most on calculated ages, even though U comprised ~50 % of total dose rate there. The risk of potential errors in GS dose rate measurements due to U-series disequilibrium are thus tentatively discounted, though where multiple GS measurements were made in close proximity the Th/U ratios produced were compared. Whilst U is a relatively mobile element that can be lost from sediments as they are weathered, Th is much less mobile and its concentration should remain constant under surface weathering conditions (Taylor and McLennan, 1985; Nath et al., 2000). Thus, if U-series disequilibrium affects one sample but not the other, the ratios would likely be different. This is discussed where relevant for individual OSL samples in chapter 6 section 6.1. The relationship between Th/U ratios derived using GS and calculated sample ages was also examined, in order to investigate whether any significant relationship exists between the two (see chapter 6 section 6.3.3.1). No correlation was found (R^2 = 0.08), indicating sample dose rates do not change systematically with sample age.

5.2.4.7.3 Determining dose rate: cosmic dose rate

In addition to radioisotope decay, sediments also receive ionising radiation from space in the form of cosmic ray muons. Cosmic muon flux varies depending on altitude, latitude and burial depth, and typically provides a small, but not negligible, contribution to total dose rate (Prescott and Hutton, 1994). The algorithm given in Prescott and Hutton (1994), which accounts for the aforementioned factors, was used to calculate the cosmic dose for each sample. Whilst altitude and latitude values can be assumed to have remained invariant since sample deposition, the depth parameter requires more careful consideration. For samples with significant burial depths (>180 hectograms, which at a density of 2.5 g cm^{-3} amounts to 72 m), cosmic dose rate is deemed insignificant (Prescott and Hutton, 1994). Cosmic dose declines exponentially with depth and, in practice, variations in depth above 25 m were found to make very little difference to total dose rate: for a typical barrier sample's altitude and latitude, at 25 m depth the cosmic ray contribution is 22 µGy ka^{-1} and at 72 m depth, 18 µGy ka^{-1}.

For most samples the present-day burial depth was considered to provide a reasonable estimation of overburden since burial (such as those from dune crests, or from the base of the seaward barrier where overburden is likely to have been multiple tens of metres for the majority of their history). However, where possible a more sophisticated approach was

adopted. Where multiple samples were obtained in vertical succession, an iterative age-depth model starting with initial estimates of age based on the Prescott and Hutton (1994) algorithm was used to account for increasing burial depth with time (following Roberts et al., 2008). Although failing to take account of any potential erosional episodes, it was considered to give a more accurate estimation than simply using the present-day burial depth.

Several samples were taken from cliff faces likely to have formed not long after burial (such as the wave-cut cliff on the island in Elandsvlei, described in chapter 4). In such instances, a more accurate estimation of the cosmic dose rate was obtained by accounting for the angular distribution of cosmic rays. Average cosmic muon flux distribution can be approximated using $\cos^2(\theta)$, where θ is the angular displacement from the vertical or zenith. This relationship has been used to better estimate dose rates for OSL samples from rock shelters and cave sites, where cosmic ray penetration depends on the zenith angle of the opening (e.g. Smith et al., 1997; Jacobs et al., 2008). For the Elandsvlei sample, the cliff is approximately vertical ($\theta = 0$) and east facing, so there will be negligible attenuation of cosmic dose from the eastern half of the sky (as $\cos^2 0 = 1$), and overburden equal to the depth of the sample from the top of the cliff from the western half of the sky. An average of the cosmic dose calculated from (1) a burial depth of two metres, assuming minor erosion of the cliff face, and (2) the burial depth of the sample from the top of the cliff, was thus used in such cases.

5.2.4.7.4 Determining dose rate: total dose rate

Environmental and cosmic dose rates were combined and converted to a total dose rate. An estimation of the water content of the sample based on the modern value (established by air-drying a known mass of tube-end material at 105 °C for 24 h) plus an error term of ± 5 % was incorporated, as water absorbs radiation that would otherwise reach the grains on which the OSL measurement is made (Aitken, 1998). For the one sample acquired from the intertidal zone (Shfd09149), a temporally weighted average moisture content (e.g. Hoare et al., 2009) was calculated from: (1) the saturated moisture content of the sample; and (2) the average moisture content of the other, subaerially exposed Gerickes Point samples. The average was weighted based on an assumption of 6 ka of saturation (assuming sea level reached present level or above in the Mid-Holocene), and the remainder of the sample age at the average subaerially exposed Gerickes Point sample moisture content.

5.3 ITL dating

5.3.1 Introduction

The functional limit of OSL dating is governed by the time it takes for the light-sensitive electron traps in quartz grains (commonly referred to as the fast component of the luminescence signal) to become saturated, i.e. the point at which they cannot accumulate any more charge. Holmes et al. (2007) found this to be a problem for the coversands inland of the Wilderness embayment, and were able to obtain only minimum ages (c. 300-500 ka) for these deposits. A number of new techniques have been proposed with the intention of extending the limit of luminescence dating, by accessing the less bleachable components of the luminescence signal that the conventional OSL protocol avoids. They include thermally transferred OSL (e.g. Wang et al., 2006b; Wang et al., 2007), red TL (Fattahi and Stokes, 2000), slow-component OSL (Singarayer et al., 2000) and isothermal thermoluminescence (ITL) (e.g. Jain et al., 2005; Choi et al., 2006). All these techniques remain at the experimental stage and, to date, a universally reliable protocol has not been developed for any of them. However, several studies have reported promising results using ITL, and this technique was pursued in this study in order to revise the minimum ages obtained for the coversands by Holmes et al. (2007) and clarify their relationship with the barriers.

The 325 °C thermoluminescence signal forms the basis of the ITL dating technique. TL dating of sediments has been largely superseded by OSL due to concerns over how well the TL signal is reset under natural conditions (Aitken, 1998) and its association with less accurate multiple aliquot measurement protocols. ITL dating attempts to overcome these problems by utilising a SAR protocol akin to standard OSL dating, and by measuring only the signal emitted from the 325°C TL peak (hence "isothermal"), which is known to be bleached by visible light (Franklin, 1997). Although the OSL signal is also thought to originate from the 325 °C TL peak (Spooner, 1994; Murray and Wintle, 2000), the ITL and OSL signals possess very different saturation characteristics. Jain et al. (2005) recorded almost an order of magnitude increase in the saturation dose value for the ITL signal released at 310 and 320 °C compared to the OSL signal from the same sample of sediment from the Himalayan foreland basin (increasing from ~150 Gy to 1.4 kGy). Further promising results were obtained by Jain et al. (2007b), who measured a palaeodose of 440 Gy for a sample of sedimentary quartz from Zambia, which owing to saturation from a high dose rate had recorded an OSL result of only 50 Gy. Choi et al. (2006) were also able to measure a D_e of 550 Gy from a sample of Korean loess beyond the range of conventional SAR OSL. Moreover, they also performed dose recovery tests at 50, 100,

150 and 600 Gy on the sample, obtaining measured doses indistinguishable from the given laboratory doses indicating sensitivity changes were not a problem (Choi et al., 2006).

Two studies have reported less encouraging ITL results. Huot et al. (2006) attempted to date samples from a variety of settings (modern beach, loess, shallow marine, colluvial and periglacial) using ITL. They observed a significant desensitisation at some stage during the first measurement (i.e. of the natural signal) of several samples, precluding the application of a sensitivity correction and resulting in an overestimation of D_e (Huot et al., 2006). Similarly, Buylaert et al. (2006) found that, in spite of good reproducibility of laboratory-induced signals and negligible response at zero dose, ITL produced a significant overestimation of D_e compared with OSL measurements of Chinese loess. It may be the case that whether the ITL protocol yields reliable measurements of D_e is strongly sample dependent (Huot et al., 2006).

5.3.2 ITL methodology

In order to test the validity of ITL dating for the coversand deposits, the technique was first applied to a coversand sample also dated in this study using conventional OSL (Shfd08191, from the Barrington Road coversand site). Results are presented in section 5.3.3 below. After testing the ITL protocol on sample Shfd08191, ITL was then applied to sample Shfd04287 from Makhulu Quarry, the coversand typesite (section 5.3.4). Preceding these sections is a description of the instrument specifications, ITL measurement protocol and sample tests conducted.

The contents of this section were published in Carr et al. (2010b), though some additional material is also presented here (namely the preheat and dose recovery tests performed on sample Shfd04287 detailed in section 5.3.4).

5.3.2.1 Instrument specifications

All ITL measurements were carried out on an automated TL-DA 12 Risø luminescence reader with stimulation provided by a 150W halogen lamp, filtered by GG-420 long pass and SWP interference filters. Irradiation was from a calibrated sealed ^{90}Sr-^{90}Y β source and luminescence measurements were made through a Hoya U340 filter with peak transmission at 330 nm and a range of 290-370 nm. All aliquots were mounted on aluminium discs (9.6 mm diameter) to allow for better thermal contact, as suggested by Jain et al. (2007a; 2007b).

5.3.2.2 ITL measurement protocol

The ITL protocol employed follows the steps of the SAR OSL protocol detailed in Table 5.1, though the stimulation type (thermal rather than optical), measurement time and preheat temperatures differ. A generalised SAR ITL measurement sequence as used in this study is given in Table 5.2. The growth curve fitting procedure is identical to that for conventional OSL dating. Aliquots were also assessed using the same 2 * D_0 saturation criteria given by Wintle and Murray (2006). The rejection limit for recycling ratios was raised from values >10 % outside unity to >20 %. An equivalent reduction in stringency is common in single grain OSL studies (e.g. Feathers, 2003; Jacobs et al., 2003a).

Table 5.2 SAR ITL protocol, after Choi et al. (2006).

Step	Treatment	Record
1	Administer regeneration dose D_i*	-
2	Preheat for 10 s at T °C[†], heating at a rate of 2 °C s^{-1}	-
3	ITL at T°C for 500 s, heating at a rate of 5 °C s^{-1}	ITL L_x
4	Give 100 s fixed test dose D_t[‡]	-
5	Preheat for 10 s at T °C, heating at a rate of 2 °C s^{-1}	-
6	ITL at T °C for 500 s, heating at a rate of 5 °C s^{-1}	ITL T_x
7	Repeat steps 1-6	-

[†] Preheat T is between 240-270 °C and ITL temperature T is 300 or 310 °C Values are determined experimentally for each sample.

5.3.2.3 Sample testing

Prior to measuring the D_e of a sample using the ITL protocol given in Table 5.2, tests were conducted to: (i) confirm the sample was appropriate for dating using ITL; and (ii) select the most appropriate values for the regeneration doses D_i and the ITL and preheat temperature T. These tests are described in the following sections.

5.3.2.3.1 Sample testing: ITL signal bleaching

Fundamental to the validity of the ITL dating procedure is the ability of daylight exposure to reduce the trapped charge to a negligible level. Choi et al. (2006) tested multiple aliquots of modern aeolian and coastal marine samples, obtaining an average residual ITL D_e of ~15 Gy. Vandenberghe et al. (2009) found residual ITL D_es in modern aeolian samples of <1 Gy, and ~3-5 Gy in coastal marine samples. A site-specific test was conducted by exposing seven aliquots of sample Shfd04287 to (UK winter) daylight for 1 week. Following the ITL protocol in Table 5.2, a residual ITL D_e of 4.73 ± 0.34 Gy (n = 7) was determined (Figure 5.6), which given the magnitude of the acquired palaeodoses, was considered small enough to be of negligible significance in determining the age of the coversand samples.

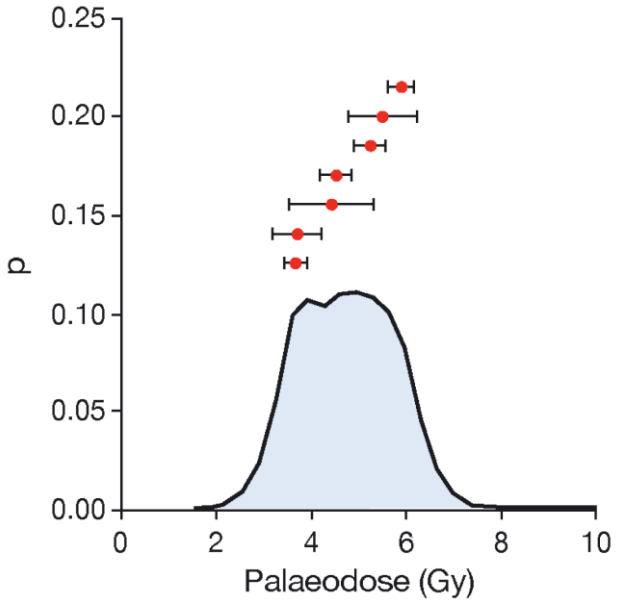

5.6 Probability density function of sample Shfd04287 ITL aliquot D_e distribution after exposure to daylight for seven days. Average D_e = 4.73 ± 0.34 Gy.

5.3.2.3.2 Sample testing: ITL stimulation and preheat temperature test

The majority of previous studies have measured ITL at a stimulation temperature of 310 °C (Buylaert et al., 2006; Choi et al., 2006; and Huot et al., 2006). Vandenberghe et al. (2009) noted that a lower ITL stimulation temperature of 270 °C did not induce the sensitivity change problems reported at 310 °C by Buylaert et al. (2006) and Huot et al. (2006), but equally it did not extend the age range of the technique beyond that of conventional OSL dating. Here, in order to strike a balance between potential desensitisation issues and extending the OSL chronology, ITL stimulation temperatures of 300 °C and 310 °C were tested each with a range of preheats from 240 °C to 270 °C in 10 °C increments.

In order to avoid potential desensitisation issues, the ITL stimulation and preheat temperature test conducted on Shfd08191 was not preceded by optically bleaching the sample and administering a known laboratory dose as per the conventional OSL dose recovery preheat test. Rather, the natural signal of the sample was measured at the various ITL stimulation and preheat temperatures and compared to the mean D_e obtained using OSL (= 242 ± 30 Gy). The results are shown in Figure 5.7. ITL D_es obtained at 310 °C were consistently closer to the OSL D_e than those obtained using ITL at 300 °C. The measurements at 310 °C also produce a D_e plateau at preheats of 260 °C and below. Based on these results, an ITL stimulation temperature of 310 °C and a preheat temperature of 260 °C were selected for full ITL measurement of the sample.

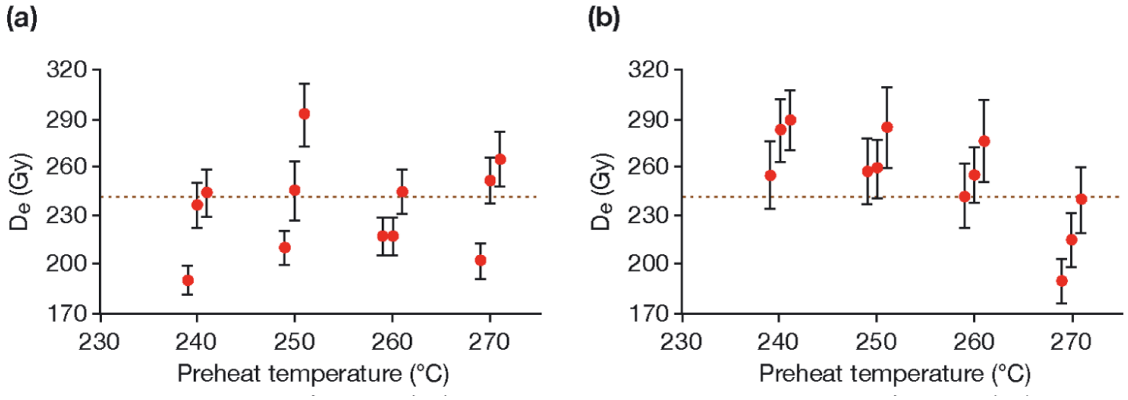

5.7 Preheat plateau tests undertaken to establish the optimum ITL stimulation and preheat temperatures for sample Shfd08191. (a) ITL at 300 °C (b) ITL at 310 °C. Dashed line shows D_e of sample established using conventional SAR OSL. Note that for clarity aliquots measured at the same preheat temperatures are slightly offset.

5.3.3 Comparing OSL and ITL results

Following assessment of the D_e values of individual aliquots based on recycling and saturation criteria, measurements from ten aliquots of sample Shfd08191 were retained for age calculation. All growth curves were fitted with a saturating exponential function. Significantly, while the OSL growth curves for sample Shfd08191 saturate on average at 250 ± 45 Gy (Figure 5.8a), the ITL growth curves for the sample typically grow to more than 550 Gy (Figure 5.8b). However, the mean D_e values for Shfd08191 produced using the OSL and ITL approaches are broadly similar, being within one standard deviation of each other (OSL D_e = 242 ± 30; ITL D_e = 295 ± 50). The slightly higher mean ITL D_e may partly reflect the addition of a small signal contribution from the ITL traps incompletely bleached by sunlight prior to burial.

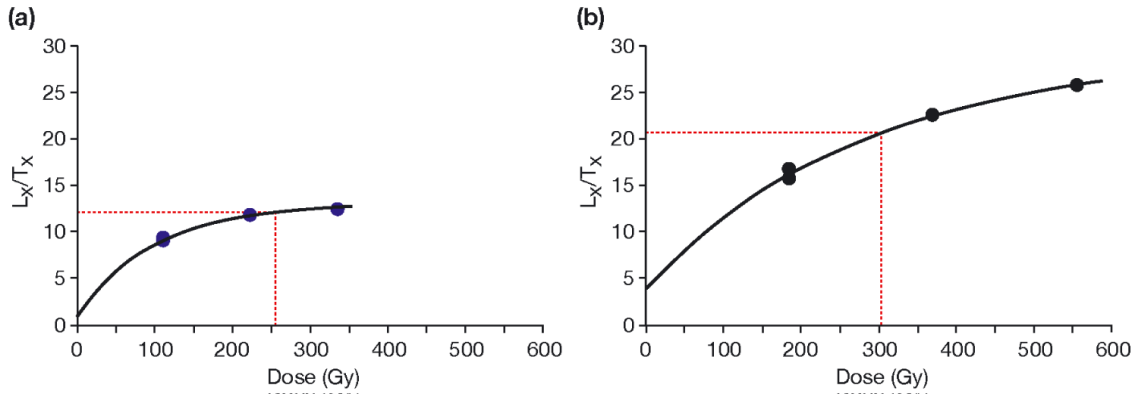

5.8 Example growth curves for individual aliquots from sample Shfd08191: (a) OSL and (b) ITL.

The probability density function for the OSL results from sample Shfd08191 (Figure 5.9a) displays a tail of high D_e values, most likely due to the low gradient of the growth curve (e.g. Murray and Funder, 2003). Whilst the aliquots that comprise the plot are not in saturation, estimating dose from growth curves beginning to flatten reduces the precision of the result obtained (Murray et al., 2002). Conversely, the ITL results (Figure 5.9b) display a more normal distribution of D_e values. As such, and given the favourable comparison of ITL to OSL data, it was inferred that the ITL procedure could potentially provide new age constraints on the Makhulu Quarry sample Shfd04287 originally dated using OSL by Holmes et al. (2007).

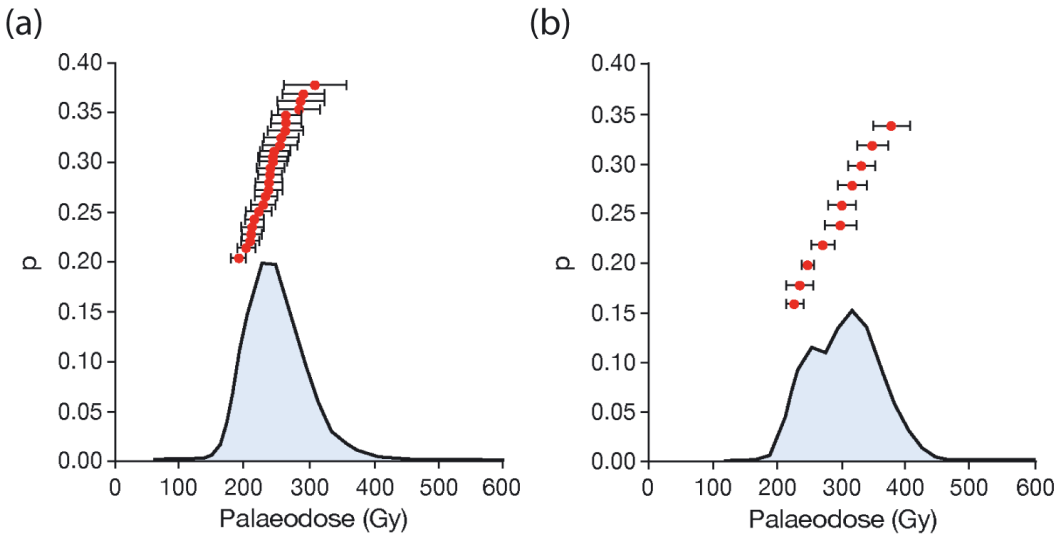

5.9 Probability density functions for sample Shfd08191: (a) measured using OSL. Mean D_e = 242 ± 30; (b)) measured using ITL. Mean D_e = 295 ± 50.

5.3.4 Revising the Makhulu Quarry age

Determining the optimal ITL stimulation and preheat temperature for the Makhulu Quarry sample (Shfd04287) was more challenging than for the test sample Shfd08191. As the D_e of Shfd04287 determined by Holmes et al. (2007) using OSL (248 ± 11 Gy) is only a minimum, it was not appropriate to choose the ITL stimulation and preheat temperatures that recovered the D_e closest to this value. Instead, they were selected based on minimising the standard deviation and error between the three aliquots measured at a range of temperatures. Whilst less rigorous a check than the standard OSL dose recovery preheat test, selection in this way was considered preferable to using invariant preheat and ITL stimulation temperatures.

As per Shfd08191, ITL stimulation temperatures of 300 °C and 310 °C, each combined with a range of preheats from 240 °C to 270 °C in 10 °C increments, were tested. Results were broadly consistent across the full range (Figure 5.10). As previous studies suggest lower ITL stimulation temperatures are less likely to induce sensitivity changes (Vandenberghe et al., 2009: also see section 5.3.2.3.2 above), and several aliquots measured at 310 °C failed to yield any measurement of D_e, an ITL stimulation value of 300 °C and preheat value of 260 °C were chosen.

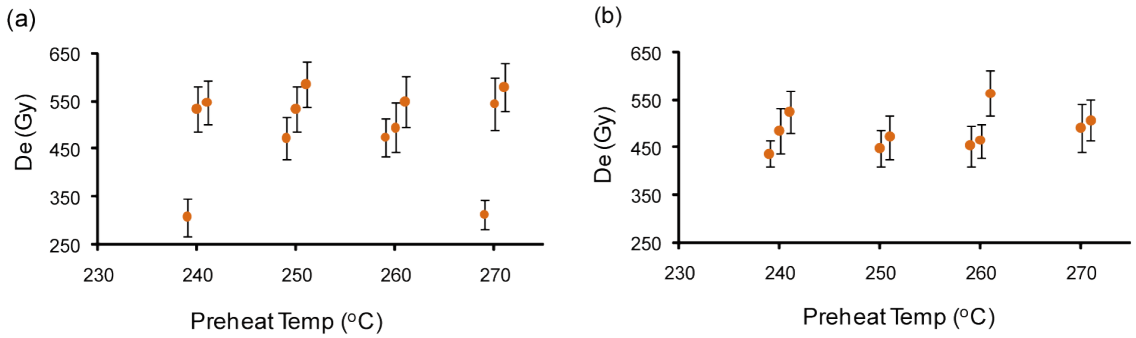

5.10 Preheat plateau tests undertaken to establish the optimum ITL stimulation and preheat temperatures for sample Shfd04287. (a) ITL at 300 °C (b) ITL at 310 °C. Note that for clarity aliquots measured at the same preheat temperatures are slightly offset. ITL stimulation at 300 °C with a preheat of 260 °C was selected.

To check the validity of using these values to date sample Shfd04287, a dose recovery test was performed. Three daylight-bleached aliquots of the sample were given a laboratory dose of 100 Gy and then measured using ITL with stimulation at 300 °C and a preheat temperature of 260 °C. The three aliquots yielded an average D_e of 87.7 ± 7.63 Gy. Whilst being a slight underestimation and therefore not ideal, the result is at odds with the pronounced overestimations of D_e produced in ITL dose recovery tests by Buylaert et al. (2006) and Huot et al. (2006), and gives some assurance in the validity of the technique for the sample.

Having selected the ITL stimulation and preheat temperatures, the natural signal of 20 aliquots of sample Shfd04287 were measured following the protocol outlined in Table 5.2. Results revealed the naturally acquired ITL signal to be very large and for two aliquots this was significantly higher than the maximum administered laboratory dose, which prevented interpolation of a D_e value (Figure 5.11a). These aliquots were rejected from age calculation for the sample both on this basis, and given that D_e values extrapolated from their growth curves formed a distinct population 3-500 Gy higher than the other 18 aliquots of the sample. These aliquots were fitted with saturating exponential growth curves (Figure 5.11b). Eight were in saturation (on average the Makhulu Quarry sample growth curves saturated at 1390 ± 490 Gy), and the remaining ten aliquots, for which a D_e value could be interpolated, produced a mean result of 806 ± 58 Gy (Figure 5.11c). With 40 % of the aliquots measured by ITL in saturation this clearly remains a minimum estimate of D_e. However, it is more than triple the minimum D_e obtained via SAR OSL by Holmes et al. (2007).

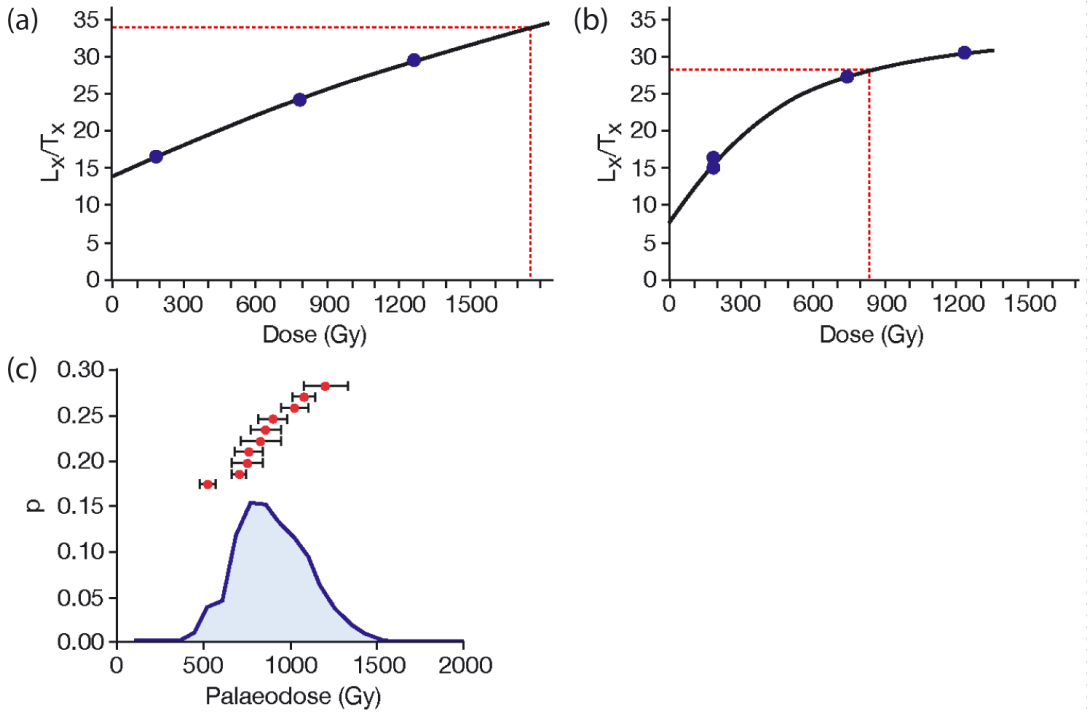

5.11 Sample Shfd04287 from Makhulu Quarry: (a) example ITL growth curve showing aliquot with a naturally acquired ITL signal above the maximum administered laboratory dose, preventing interpolation of D_e; (b) example ITL growth curve showing aliquot fitted with saturating exponential function; (c) probability density function of all suitable aliquot D_es. Mean D_e = 806 ± 58 Gy.

5.4 Sediment provenancing

5.4.1 Introduction

To understand the formation of a landscape it is of great importance to determine the source(s) of the sediment from which it is composed (Yang et al., 2007). The first attempts at establishing sediment provenance, undertaken in the late 19th century, were based on microscopic investigation of the heavy mineral fraction (grains with a density >2.9 gm cm^{-3}) present in beach and river sands, with studies relating the occurrence of single mineral species or varieties to those found in possible parent rocks (Weltje and von Eynatten, 2004 and references therein). In the latter half of the 20th century, technological advances have permitted the development of numerous alternatives to heavy mineral analysis for sediment provenancing. One of the most widely employed is trace element geochemistry. By calculating ratios of elements that are likely to remain stable under surface weathering conditions, the geochemical "signature" of a sediment can be defined and compared to those of its potential sources.

Mange and Wright (2007b) caution that relying on a single line of evidence can yield, at best, only partial resolution of a sediment provenancing question. For this reason, both heavy mineral analysis and trace element geochemistry were employed in this study, along with the complimentary techniques of particle size analysis and calcium carbonate-content determination. The rationale for selecting these techniques, their underlying principles, and the methods used are described in the following sections.

5.4.2 Particle size

The different processes that act to transport and deposit material in aeolian, riverine and littoral settings mean comparisons between the grain size characteristics of the Wilderness barrier dune sands and their various possible local sources cannot be used to determine specific provenance relationships. However, the complete absence of material of equal size fraction to the barrier sands in the possible local source areas could rule out their having contributed. Moreover, comparisons of particle size distributions within the barrier sands may indicate changes in sediment source. For example, Kasper-Zubillaga and Carranza-Edwards (2005) demonstrated it was possible to discriminate between dunes of coastal and terrestrial origin in Sonara, NW Mexico, using particle size distribution data. Similarly, Saye et al. (2006) used particle size data to identify terrestrial input to coastal dunes on the Jutland

coast of Denmark. Particle size can also exert a significant influence on sediment geochemistry (Whitmore et al., 2004) and its accurate characterisation is thus crucial to interpreting comparisons of sediments made using their trace element concentrations.

All samples from the barrier sands and their possible local source areas were subjected to laser diffractometry particle size analysis using a Horiba LA-920 instrument. The limitations of particle size data produced using laser diffractometry are well understood. A principal concern is its tendency to underestimate the clay fraction in a sediment by failing to detect very fine particles (Buurman et al., 1997). This can be particularly pronounced with respect to finer particles in a coarser mixture (Blott and Pye, 2006). There are also difficulties in comparing results with those produced by other methods such as dry-sieving or sieve-pipette particle size determination (Agrawal et al., 1991; Beuselinck et al., 1998). However, the various advantages of laser diffractometry particle sizing over manual techniques (namely improved reproducibility, smaller sample size requirements and faster analysis) mean that it is widely used. In addition, the concerns outlined above are of limited consequence to this study: comparisons with particle size data measured using other techniques are not required, and the minimum detection limit of the Horiba LA-920 instrument is reported as 0.02 μm (Stauffer and Igushi, 1997). This value has been considered adequate to describe the clay-sized fraction of aeolian sediments (e.g. Fitzsimmons et al., 2009).

5.4.2.1 Particle size methodology

Bulk samples were dried in an oven at 105 °C overnight, and then riffled to obtain a ~10 g subsample. River sediment samples were first passed through a 1 mm sieve to remove the coarsest fraction (grains >1 mm were not present in any other samples). To ensure that only non-organic particles were included in the results, subsamples were furnaced at 425 °C for 18 hours to remove organic matter by loss on ignition (LOI). Although Murray (2002) recommends hydrogen peroxide rather than firing for removal of organic matter, LOI values were considered low enough (averaging 0.47 ± 0.29 %) not to warrant concern over potential ash retention.

Prior to measurement the treated subsamples were made into a paste with the addition of a solution containing 1 % sodium hexametaphosphate. This has two purposes: (i) to prevent flocculation of clay particles; and (ii) to prevent the smallest particles from remaining in the container as the sample is added to the machine. Furthermore, results from dry samples may display poorer reproducibility than those moistened prior to measurement (Buurman et

al., 1997). Thirty seconds of sonic agitation was also applied immediately prior to measurement to aid deflocculation. The machine requires approximately 1-5 g of material for each measurement, so the 10 g subsamples permitted two, three or four aliquots to be measured for most samples.

To assess the reproducibility of the results, the coefficient of variation of the mean particle size produced from different aliquots of each subsample was calculated, following Pye and Blott (2004). Results are shown in Table 5.3. The lagoon sediments and beach sands were found to be the most reproducible, with average coefficients of variation around the mean size of each sample of 1.2 % and 0.5 % respectively. The barrier dune sands and the coversands were slightly more variable, with values of 3 % and 1.9 % respectively. River sediments were the least consistent, displaying an average coefficient of variation for the mean size of 5.4 %. Visual inspection of the samples indicates this variation can be attributed to varying degrees of parent sample heterogeneity, and all values are considered low enough to provide confidence that the measurements are representative.

Table 5.3 Average standard deviation (σ) and coefficient of variation (C.V.) prdocued from multiple aliquots of individual samples, averaged amongst sample groups.

	Statistical measure		
Sample group	**Average mean (μm)**	**Average σ (μm)**	**Average C.V. (%)**
Barrier sands	254.5	7.4	3
Coversands	171.1	1.7	1.9
River sediments	411.9	21.9	5.4
Beach sands	281.4	1.4	0.5
Lagoon sediments	312.6	3.6	1.2

Raw data from the Horiba LA-920 instrument (percentage volume of material in 93 bins ranging from 0.011 μm to 3 mm) was converted to the percentage of clay, silt, fine-, medium- and coarse-grained sand in each sample, according to the Udden-Wentworth particle size scale as reproduced in Gale and Hoare (1991). The graphic distribution measures of Folk and Ward (1957) (mean, median, sorting, skewness and kurtosis) were also calculated. There is some debate concerning the validity of the Folk and Ward statistics, chiefly concerning their reliance on the often incorrect assumption that particle size distributions are log-normal (Bagnold and Barndorffnielsen, 1980; Hartmann and Christiansen, 1992). However, they are widely accepted as the most appropriate means of routine grain size analysis (Blott and Pye, 2001). This is especially the case when they are regarded simply as a means of comparing grain

size distributions between samples, as is their purpose in this study, rather than absolute measures of the particle size characteristics (Gale and Hoare, 1991).

5.4.3 Calcium carbonate content

The calcium carbonate content of samples was determined gasometrically by measuring the volume of carbon dioxide evolved during their reaction with 4 mol hydrochloric acid, following the procedure described in Jones and Kaiteris (1983). An Eijkelkamp calcimeter was used, calibrated using measurements of the volume of gas produced on reacting known quantities of pure $CaCO_3$ prior to making sample measurements. To test reproducibility, measurements on multiple aliquots (either two or three) of ten samples were made, yielding an average standard deviation of 1.43 %.

As stated in previous chapters, the calcium carbonate fraction of the Wilderness barrier dune sands is considered to be solely of marine origin. This assumption is generally implicit in studies concerning carbonate coastal-dune provenance on the southern African coast and elsewhere (e.g. Franceschini et al., 2003; Andreucci et al., 2009; Muhs and Budahn, 2009), and is confirmed at Wilderness by thin-section micromorphological analyses of the barrier sands conducted by Bateman et al. (2011).

5.4.4 Trace element geochemistry

The geochemical signature of a sediment is a reflection not only of its source material but also of a number of processes within the sedimentary cycle that can result in chemical fractionation. Chemical weathering, physical weathering and diagenesis may all alter the original geochemical fingerprint of a source rock, so that identifying sediment derived from it can be hard to achieve (Taylor and McLennan, 1985). Careful selection of elements that remain, as far as possible, immobile under near-surface weathering conditions is thus fundamental in using geochemistry for provenancing purposes. Comparisons of appropriate trace elements and trace element ratios have been used to identify the importance of atmospheric dust inputs to soil formation on carbonate substrates (Muhs et al., 2007a; Muhs et al., 2007b), to distinguish contributions of sediment from different sources to river and delta sediments (Vital and Stattegger, 2000; Huntsman-Mapila et al., 2005), and to relate desert sands to their sources (Muhs and Holliday, 2001; Pease and Tchakerian, 2003).

Provenancing studies of coastal-dune sands using trace element geochemistry are rarer, for several reasons. Many of the largest coastal-dune systems form in association with marine carbonate provinces, and their provenance is thus self-evident. Where the non-carbonate sediment content of coastal dunes is significant, it is often well mixed and derived from numerous sources (e.g. local coastal erosion, fluvial and/or aeolian transport from inland, authigenic input, longshore drift, the seabed, etc.), making identification of specific provenance relationships problematic. Studies that have successfully determined the provenance of coastal-dune sands are concentrated in areas where sediment transport pathways are relatively simple, and/or in areas which possess contrasting geology (e.g. Saye and Pye, 2000; Saye and Pye, 2006; Kasper-Zubillaga and Zolezzi-Ruiz, 2007). At Wilderness, and across the entire southern Cape region, rocks are exclusively siliciclastic and felsic in nature, a setting less than ideal for determining specific provenance relationships. However, the objectives of the sediment provenancing aspect of this study are slightly simpler: (i) to establish whether the relative importance of terrestrial vs. marine sediment input to the Wilderness barriers has changed with time; and (ii) to establish whether or not sediment from local terrestrial sources has been significant in their formation. The methodology used to address these questions is described in the following sections.

5.4.4.1 Particle size fraction selection

In addition to weathering and diagenesis processes, geochemical sediment signatures can also be obscured by hydraulic sorting during transport, which can separate sediments into compositionally distinct size fractions (Whitmore et al., 2004). Whilst the most common approach in studies investigating sediment geochemistry is to isolate a relatively narrow size fraction for analysis, a number of studies have successfully utilised bulk (i.e. unsieved) material for provenancing purposes (e.g. Huntsman-Mapila et al., 2005; Kasper-Zubillaga and Zolezzi-Ruiz, 2007; Kasper-Zubillaga et al., 2007; Muhs and Budahn, 2009; Hanson et al., 2010).

A large volume of trace element data pertaining to unsieved samples of the seaward Wilderness barrier has already been generated via ICP-MS/AES for OSL dose rate determination purposes from previous studies (Bateman et al., 2004; Carr et al., 2007; Bateman et al., 2008; Bateman et al., 2011). In addition to U, Th and K, the ICM90A package from SGS used in these studies provides concentrations of a suite of 52 other elements. The high reproducibility of sodium peroxide digestion ICP-MS measurements for trace elements concentrated in even the most resistant mineral species (e.g. zircon and tourmaline) has been demonstrated (Meisel et al., 2002), and in light of the provenancing studies that have used

unsieved material mentioned in the previous paragraph, and the aeolian (i.e. well sorted) nature of the sediments, this was considered an appropriate dataset to describe the geochemistry of the barriers.

Valid geochemical comparisons to aeolian sands can only be made on source sediments that are of the same size fraction (Muhs et al., 1996). The particle size distributions of the barrier dune sands and the samples of their potential source sediments were thus measured using laser particle size analysis (see section 5.4.2) and compared, to determine what fractions should be sent to SGS for ICP-MS/AES. River samples were consequently sieved to remove material >1 mm (very coarse sand and above), and lagoon, coversand and beach samples were left unsieved due to the similarity of their particle size distributions to those of the barrier dune sands. Samples of the hard-rock geology were also analysed in bulk. All samples were riffled (excluding bedrock) to 10 g and pulverised in a Tema mill prior to being sent to SGS.

The possibility of particle size influencing the element concentrations present in sediment samples was further investigated using least squares regression. Each of the elements selected for analysis was compared to the percentage of material in each particle size class across all samples (barriers and their possible sources), in order to identify any elements whose concentration is strongly controlled by particle size. This approach was used by Muhs et al. (2008) to identify elements appropriate for analysis in a study of the origin of Nebraskan loess. The highest correlation they observed was between Ti and clay content (R^2 = 0.37), which they still deemed a sufficiently low value to retain the element for analysis (Muhs et al., 2008). A similar degree of stringency was used here.

5.4.4.2 Element selection and analysis

Underlying the use of element geochemistry for sediment provenancing purposes is the assumption that certain elements are largely unaffected by the processes which cause chemical fractionation in the sedimentary cycle, and thus retain a record of source rock composition in the sediment of interest (Taylor and McLennan, 1985). This assumption is informed by the principle of ionic potential, which is the ratio of electric charge to ionic radius. Soluble cations are formed by elements with both very low ionic potentials and very high ionic potentials, but elements with intermediate ionic potential are assumed to remain relatively immobile in surficial environments (Muhs et al., 2007b). The mobility of various elements under low temperature, near-surface conditions is illustrated in Figure 5.12.

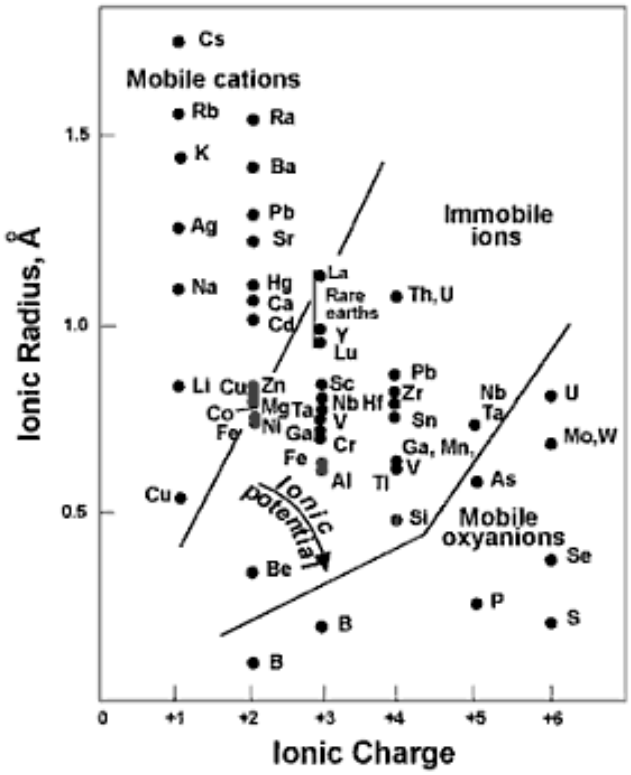

5.12 Mobility of elements in the surficial environment as a function of ionic potential. The least mobile elements are those with intermediate ionic potentials. From Rose et al. (1979).

The elements selected for provenancing purposes in this study are limited to those that are understood to be immobile in near-surface environments, and that have been demonstrated as useful in previous sediment provenancing studies. The elements and element ratios considered are also necessarily a function of the data available. For example, whilst ternary plots of La-Sc-Th and Zr-Sc-Th have been widely demonstrated as powerful sediment provenancing tools (e.g. Bhatia and Crook, 1986; Nath et al., 2000; Muhs and Budahn, 2009), Sc was found to be completely absent from all samples tested in this study, precluding the use of these plots. Sc is a marker element for mafic igneous rocks (Hessler and Lowe, 2006) and as all the southern Cape bedrock formations are felsic, its absence is unsurprising. The elements selected for analysis comprise Zr, Hf, Co, Cr, Th, Ti and the rare earth elements (REE), the group of 15 elements from lanthanum to lutetium in Group IIIA of the periodic table.

Zr and Hf are hosted almost exclusively in zircon grains, which are highly resistant to mechanical abrasion and diagenetic dissolution (Hubert, 1962; Garzanti and Andò, 2007). The ratio of Zr/Hf should consequently remain constant between source and sediment and be unaffected by hydraulic sorting, making it particularly valuable for sediment provenancing purposes (e.g. Moreno et al., 2006; Muhs and Budahn, 2006). Ti is found in low concentrations in biotite, hornblende and zircon and is a major constituent of various metamorphic minerals

(e.g. sphene, ilmenite, and rutile) (Parker and Fleischer, 1968 c.f. Muhs et al., 2008), several of which have been identified as components of the geology local to Wilderness (see chapter 3). Niobium commonly substitutes for Ti and thus Ti/Nb ratios will vary primarily with the mineralogy and source rocks of Ti-bearing heavy minerals, a characteristic which allowed Muhs et al. (2008) to discriminate between loess from different sources in North America. Co, Cr and Th are also all relatively immobile elements that have been demonstrated as effective indicators of sediment provenance in sand-sized grains within aeolian and fluvial settings (e.g. Vital and Stattegger, 2000; Wolfe et al., 2000; Pease and Tchakerian, 2003) and, crucially, are all present in the felsic minerals of the southern Cape.

The REE are found in an array of heavy minerals (Muhs and Budahn, 2009), and all fifteen (La, Ce, Pr, Nd, Sm, Eu, Gd, Tb, Dy, Ho, Er, Tm, Yb and Lu) have very similar geochemical properties (Henderson, 1984). The elements from La to Sm are often referred to as the light REE (LREE), and those from Eu to Lu as the heavy REE (HREE) (Xing and Dudas, 1992). There is some debate regarding the utility of REE for sediment provenancing: whilst several studies have found significant changes in REE within weathering profiles (e.g. Condie et al., 1995; Compton et al., 2003), numerous others maintain they are relatively immobile and insoluble in low-temperature, near-surface environments, and therefore a valid tool for relating sediments to their sources (e.g. Taylor and McLennan, 1985; Huntsman-Mapila et al., 2005; Muhs and Budahn, 2006; Yang et al., 2007). Several studies have used REE to distinguish sediment provenance relationships in areas lacking strongly contrasting geology, such as is the case on the Southern Cape. Yang et al. (2007) used differences in REE and other trace- and major-element characteristics to recognise that the coarse fraction of the Taklamakan desert sands differs from area to area, corresponding to the varying (felsic) geology of the local fluvial systems (sandstone, granite and metamorphic). Similarly, Muhs and Budahn (2006) examined the REE content of silts from three rivers in investigating the source of central Alaskan loess. Though their chondrite-normalised[‡] REE plots all displayed patterns typical of felsic upper continental crust (UCC) material, by calculating and comparing certain ratios of the REE they were able to ascertain the river most likely to have made the largest contribution to the loess (Muhs and Budahn, 2006). This approach is widely used: common ratios considered are the

[‡] REE concentrations are commonly presented as values normalised to those in a chosen reference material independent of the sample, usually chondritic meteorites (Henderson, 1984).

Europium (Eu) anomaly, given by $Eu_N/(Sm_N*Gd_N)^{0.5}$[§] and the ratio of LREE to HREE, given by La_N/Yb_N. These ratios were utilised in this study.

In addition to the REE and other immobile elements discussed above, the mobile element U was also selected for analysis. Although mobile elements are, by definition, not of use for determining sediment provenance relationships, they can be used to assess the degree of weathering sediment has undergone. The Th/U ratio is commonly used for this purpose (e.g. Taylor and McLennan, 1985; Nath et al., 2000), as whilst U is oxidised and lost from sedimentary rocks as they are weathered, concentration of the immobile element Th should remain constant.

5.4.5 Heavy mineralogy

Although the trace element geochemistry of quartz-rich sediments is predominantly derived from their heavy mineralogy (quartz contains little or no REE: Taylor and McLennan, 1985), examining the heavy minerals themselves can yield additional and important information for sediment provenancing purposes that is not available from geochemistry alone (Mange and Wright, 2007a). Rare minerals diagnostic of particular geological sources, authigenic minerals indicative of environmental conditions sediment has been subjected to, and concentration of resistant mineral species highlighting sediment "maturity" (discussed further in the following section), are some of the possibilities. One of the strengths of heavy mineral analysis is the extremely broad variety of detrital minerals (50+ species of translucent heavy mineral are described in Mange and Maurer, 1992), many of which have specific and restricted parageneses (Morton and Hallsworth, 1999). However, it is this characteristic which limits reliable description of heavy mineral assemblages to highly skilled practitioners. The heavy mineral fraction was thus extracted from a limited number of samples (coversands = 2; barrier dunes = 5; rivers = 3; beach = 2; lagoon = 1) and sent to Dr. Bethan Davies at Durham University for identification and counting.

[§] The subscript "N" denotes the concentrations are normalised to chondrite.

5.4.5.1 Heavy mineral identification and counting

Samples were dry-sieved to isolate the 63-280 µm size fraction and heavy minerals were separated using sodium polytungstate solution with a specific gravity of 2.9. The heavy minerals were air dried and weighed to 2 d.p. to allow the percentage of heavy minerals in the sample to be determined. The material was then sent to Dr. Davies, who mounted the minerals in clove oil and identified mineral species under a petrological microscope in plane and cross-polarised light. Between 302 and 405 translucent grains[**] were counted for each sample.

5.4.5.2 Heavy mineral analysis

The same processes that can modify trace element geochemistry from source to sediment also act upon heavy mineral assemblages. To recap, these are: *mechanical abrasion*, which takes place during transport and reduces grain size; *hydraulic sorting*, which takes place as a result of the hydrodynamic processes operative during transport and final deposition, and can fractionate the relative abundance of minerals with different hydraulic behaviour; and *dissolution/diagenesis*, which can occur at several stages in the sedimentation cycle and may cause partial or total loss of mineral grains (Morton and Hallsworth, 1999).

Although considerable research has been conducted on determining the relative mechanical stability of heavy mineral species, evidence suggests the effects of abrasion during transport on heavy mineral proportions are negligible (Morton and Smale, 1991; Morton and Hallsworth, 1999) More problematic for provenancing purposes are hydraulic sorting and dissolution. Heavy minerals are denser than the light minerals, quartz and feldspar, and consequently have different hydrodynamic properties. Differences also occur within the suite of heavy minerals, due to variations in density, size and shape (Komar, 2007). Coastal environments, such as considered in this study, are particularly conducive to hydraulic segregation of HM (e.g. Komar and Chi, 1984; Peterson et al., 1986). Whilst analysing heavy minerals within a specific size fraction will minimise grain size dependencies, it is not likely to eliminate selective sorting due to differences in grain densities (Komar et al., 1989). To account for these factors, ratios of minerals with similar hydraulic and diagenetic behaviour can be

[**] Opaque heavy mineral species are much harder to identify and almost universally disregarded in provenancing studies.

calculated. Morton and Hallsworth (1994) proposed several mineral ratios suitable for this purpose, which are given in Table 5.4. These were used to compare the barrier sand samples to those from their potential sources, with the exception of the ATi index. Morton and Hallsworth (1999) identify apatite as a very unstable or unstable mineral in most environments, so this ratio was excluded from consideration.

Table 5.4 Provenance-sensitive heavy mineral ratios. From Morton and Hallsworth (1994).

Index		Definition
ATi	apatite–tourmaline index	100 × apatite count/(total apatite plus tourmaline)
GZi	garnet–zircon index	100 × garnet count/(total garnet plus zircon)
RZi	TiO_2 group–zircon index	100 × TiO_2 group count/(total TiO_2 group plus zircon)
RuZi	rutile–zircon index	100 × rutile count/(total rutile plus zircon)
MZi	monazite–zircon index	100 × monazite count/(total monazite plus zircon)
CZi	chrome spinel–zircon index	100 × chrome spinel count/(total chrome spinel plus zircon)

In addition to calculating the ratios given in Table 5.4, the zircon-tourmaline-rutile (ZTR) index of the Wilderness samples was also considered. Originally proposed by Hubert (1962), the ZTR index is intended to quantitatively define the maturity of a heavy mineral assemblage. Zircon, tourmaline and rutile are considered chemically "ultrastable", and high ZTR values very commonly characterise ancient or polycyclic sands, because of extensive diagenetic dissolution of less stable species (Garzanti and Andò, 2007). Muhs (2004) investigated the potential for using mineralogical maturity (assessed using bulk mineralogy rather than isolating the heavy fraction) to investigate the origin and history of aeolian sand bodies, and was able to make inferences about dunefields in North America, Africa and Australia. The final means of utilising the heavy mineral data was a qualitative consideration of the mineral species identified in the samples. They were compared to those found in the regional hard-rock geology as described in the literature (reviewed in chapter 3 section 3.2), and the volume of glauconite was considered. Glauconite is an authigenic marine mineral which forms at water depths of 50-500 m (Wigley and Compton, 2007), and its presence in a sediment thus provides an absolute indicator of marine input.

5.5 Statistical analysis

Various statistical models and methods of analysis were applied in order to facilitate a more detailed and quantitative interpretation of the data produced. They are described in the following sections.

5.5.1 Regression

In order to investigate the relationship between pairs of variables assumed to have a linear relationship, ordinary least squares regression was conducted using the regression analysis toolpack in Microsoft Excel 2007. The R^2 value (which describes the proportion of variability in the dataset described by linear regression) and significance of the relationship (at the $p<0.05$ level) were considered.

5.5.2 Probability density functions

Probability density functions (PDFs) provide a means of incorporating the precision of individual measurements in histogram-like plots. They were used: (i) to confirm that the D_e distributions of the aliquots measured for each OSL sample are approximately normal in shape and thus appropriate for the application of other statistical models (see section 5.4.2.5); and (ii) to visually represent the distribution of OSL ages from the Wilderness barriers (in chapter 7). In a PDF each D_e value (or OSL age) is represented by a normal distribution whose centre is the D_e value itself, and the width of the distribution is determined by its precision. Similar to plotting histograms, a bin width must be chosen to represent the data. Bateman et al. (2003a) used a value based on the median uncertainty of the measurements, and that approach was also applied here.

There has been some criticism of PDFs as a statistical method: they can make distributions look unreasonably broad and, as they do not display individual data points, it is not easy to see if they are unduly altered by a few results (Duller, 2008). However, despite these limitations, they provide a simple method of visually displaying data and its surrounding uncertainties, and are widely used in the OSL literature.

5.5.3 Finite mixture modelling

Finite mixture modelling (FMM) was originally proposed by Galbraith and Green (1990) in order to isolate multiple D_e components from composite D_e populations. In FMM, each D_e is logged, as is its error, and assumed to form part of a normal distribution from a total population composed of an unknown number of normal distributions, each with a common OD value defined by the user (Roberts et al., 2000) The number of populations is increased iteratively, and goodness of fit is assessed using the Bayesian Information Criterion, with the number of components for which this value is closest to zero representing the best fit.

As stated in section 5.2.4.6, none of the OSL samples in this study contain multiple, discrete D_e populations, as might be the case if post-depositional mixing had occurred (e.g. Jacobs et al., 2006a), and applying FMM would thus be inappropriate. However, FMM was applied to the finalised OSL chronology in order to identify whether any discrete phases of deposition could be isolated within it.

5.5.4 Principal component analysis

All of the sediment provenancing techniques utilised in this study result in the generation of suites of multiple data variables associated with single samples. Methods of multivariate statistical analysis, which facilitate easier consideration of such data, are widely used in sediment provenancing studies (e.g. Vital and Stattegger, 2000; Pease and Tchakerian, 2002; Pe-Piper et al., 2008). Here, principal component analysis (PCA) was employed to investigate multivariate data. PCA reduces multidimensional datasets to a smaller number of artificial variables called "principal components" (PCs) composed of differently weighted iterations of the original data. Each PC represents a linear combination of weighted observed variables, and a small number of them should account for most of the variance in the dataset (typically two are sufficient). Samples can thus be represented graphically using biplots instead of requiring consideration of values for tens of variables (Ringner, 2008). PCA is catered for in most statistical computing packages: here, CAP III v3.01 software from Pisces Conservation Ltd. was used. Before conducting PCA it was necessary to consider a number of factors, which are explained in the following two sections.

5.5.4.1 Transforming the data

If variables representing the same or similar entities display large differences in their scale, those variables that possess the largest amounts of variance will dominate the results. This is true of trace element geochemical data, where certain elements will have concentrations orders of magnitude larger than others. In such cases it is necessary to perform some sort of transformation to normalise the dataset. Typically, variables are normalised by subtracting the variable mean from each sample observation, and dividing the results by that variable's standard deviation. The outcome of this is that PCs are actually extracted from a correlation matrix instead of what would otherwise be a variance-covariance matrix (Krzanowski and Marriott, 1994). This method was used here.

For compositional data, where each variable represents a percentage of the entire sample (such as the heavy mineral and particle size datasets in this study), a more complex method of data transformation is required. Due to the unit-sum constraint, the analysis of compositional data is subject to a "closure effect" whereby at least one negative correlation must exist between the variables (e.g. as the percentage of fine sand increases, the percentage of coarse sand correspondingly decreases) (Zhou et al., 1991). In order to avoid this type of spurious correlation, Aitchison (1982) suggested a centred logratio (CLR) transformation be applied to such data. The technique has subsequently been widely used to permit statistical analysis of compositional data (e.g. Zhou et al., 1991; Noda, 2005; Pe-Piper et al., 2008), and was employed here. Zero data values are not permitted when conducting CLR transformations, so where variables of a sample are empty they must be represented by a small positive value before performing the transformation. Replacement techniques can cause problems, such as spurious clusters around the replacement values (e.g. Tauber, 1999). Martin-Fernandez et al. (2003) attempted to address these with the multiplicative replacement approach, which was used in this study. Both CLR and zero replacement transformations were performed using the freeware Microsoft Excel add-on CoDaPack (Thio-Henestrosa and Martin-Fernandez, 2005).

5.5.4.2 Which principal components should be retained?

As previously mentioned, the number of PCs extracted from a dataset is equal to the number of variables being analysed. For PCA to be of use, the number of these must be reduced to a more manageable level. Typically, the "eigenvalues" of the PCs are considered. An eigenvalue represents the amount of variance that is accounted for by a given component, with a value greater than 1.00 typically used to indicate a PC worthy of being retained (Stevens, 2002). The two PCs possessing the highest eigenvalues are typically displayed on a standard biplot, and that convention was followed here.

5.6 Chapter summary

This chapter has justified the selection of the various analytical techniques employed, and described their underlying principles. The steps taken to ensure the validity of the ITL dating results were discussed in particular detail, as the protocol is novel and there are few published applications of its use.

6 Results

This chapter presents the results of both the chronological and sediment provenancing aspects of this study. The first part (section 6.1) encompasses both OSL and ITL dating results. The second part of the chapter covers the sediment provenancing results, and is divided into three sections according to analysis method: (6.2) sediment characteristics; (6.3) trace element geochemistry; and (6.4) heavy mineralogy.

6.1 Luminescence dating results

6.1.1 Introduction

This section presents the results of the 36 OSL age determinations conducted on samples from the Wilderness barrier dunes, and the three OSL and two ITL age determinations conducted on samples from the coversand deposits inland of the Wilderness embayment. The reliability of the dose rate and finalised D_e values used to calculate sample ages are discussed on a sample-by-sample basis. Samples with problematic OD values or saturation issues were addressed individually in chapter 5, and the remaining samples all display approximately normal distributions of aliquot D_es with OD values of <20 % (OD values are included in the results tables in the following sections). It was thus not considered necessary to present regeneration curves and D_e probability density functions for individual samples here.

All ages are reported in years from the date of measurement (2009) with confidence limits of ± 1 standard deviation (σ). Confidence limits are based on uncertainties associated with all aspects of measurement and calculation, combined in quadrature (see Armitage et al., 2006). Ages are presented graphically, and any site details or field observations potentially relevant to their validity are discussed. Where stratigraphic relationships can be inferred between multiple samples, the appropriateness of the calculated ages is considered in this context. The particle size distributions and carbonate contents of samples are also discussed where useful, though these data are considered in detail in section 6.2. Results are organised into separate sections for samples from the seaward, middle and landward barriers, and finally the coversands.

6.1.2 Seaward barrier

Summaries of all the OSL ages obtained from the seaward Wilderness barrier are presented in Table 6.1.1 and Figure 6.1.1. Table 6.1.1 is organised from west to east, with the first two rows (Klein Krantz samples) the western-most seaward barrier sites and the last row (the Buffels Bay sample) the farthest east. For each sample Table 6.1.1 also includes dose rate data and the parameters used in calculating its age (burial depth, moisture content), the Th/U ratio (potentially useful for assessing the possibility of U-series disequilibrium, as explained in chapter 5 section 5.2.4.7), the number of aliquots the age calculation is based on, the OD value of the D_e distribution and the finalised D_e value ± 1 σ. The numbers preceding the sample site names in Table 6.1.1 correspond with their locations as shown in Figure 6.1.1, which presents seaward barrier sample ages on both a morphological map of the Wilderness embayment and on the stratigraphic columns originally presented in chapter 4. Ages are discussed on a site-by-site basis in the following sections.

6.1.2.1 Klein Krantz

The two samples from Klein Krantz are 2.7 km apart and at similar elevations, with Shfd09072 (the farthest-west sample from the seaward barrier) taken from aeolianite at 2.4 m amsl and Shfd09073 from aeolianite at 8 m amsl (Figure 6.1.2 sites 1a and 1b). Despite a relatively large difference in D_e between the two samples (84.1 ± 1.6 Gy and 103.4 ± 1.5 Gy respectively), their total dose rates also differ correspondingly (see Table 6.1.1) to produce almost identical ages of 131 ± 7 ka and 133 ± 7 ka. This concordance in the sample ages, despite differences in both D_e and dose rate, bolsters confidence that they are accurate.

6.1.2.2 East Elandsvlei and Elandsvlei Island

Three samples were obtained in vertical succession from the exposure on the eastern shore of Elandsvlei, directly inland of the Klein Krantz sites. The exposure extends from lake level at 1.5 m amsl to the barrier crest at 50 m amsl. An oblique view of the sample locations and ages is provided in Figure 6.1.2. Towards the base of the East Elandsvlei exposure, at 5 m amsl, marine herringbone bedding is present (Figure 6.1.1 site 2b). A sample obtained from beneath this marine facies at 3.9 m amsl (Shfd09076) yielded an age of 120 ± 7 ka. Sample Shfd09077, from directly above the marine facies (8.5 m amsl) ~150 m south of Shfd09076, dates to 129 ± 8 ka, and Shfd08184, from 24 m amsl, to 127 ± 8 ka.

Table 6.1.1 Dose rate data, D_e values, and calculated ages for OSL samples obtained from the seaward Wilderness barrier. Numbers by sample sites correspond with sample locations in Figure 6.1.1.

Sample details		Dosimetry							Palaeodose			
Sample code	Burial depth (m)	Water content (%)	K (%)	U Ppm	Th ppm	Th/ U	Cosmic dose rate (μGy a^{-1})	Total dose rate (μGy a^{-1})	D_e (Gy)	n	OD (%)	Age (ka)
1. Klein Krantz												
Shfd09072	28.6	3.2	0.33	0.75	1.86	2.48	17 ± 1	641 ± 32	84.1 ± 1.6	21	12	**131 ± 7**
Shfd09073	29	1.9	0.30	1.25	2.27	1.82	16 ± 1	775 ± 39	103.4 ± 1.5	21	11	**133 ± 7**
2a. Elandsvlei Island												
Shfd09065	14.2	0.9	0.16	1.04	1.58	1.52	76 ± 4	599 ± 28	68.2 ± 1.4	22	12	**114 ± 6**
Shfd09066	4.9	0.3	0.22	1.26	1.6	1.27	113 ± 6	750 ± 35	82.2 ± 1.7	29	11	**110 ± 6**
2b. East Elandsvlei												
Shfd08184	26	0.2	0.13	0.85	1.54	1.81	44 ± 2	494 ± 29	62.8 ± 1.8	28	18	**127 ± 8**
Shfd09076	46.1	0.6	0.22	1.38	1.93	1.4	22 ± 1	710 ± 37	85.5 ± 2.2	21	11	**120 ± 7**
Shfd09077	41.5	0.7	0.14	1.1	1.4	1.27	25 **± 1**	531 ± 28	68.6 ± 1.9	18	13	**129 ± 8**
3. Gerickes Point												
Shfd08173	125.5	1.9	0.29	0.79	1.85	2.34	1 ± 0	613 ± 31	84.9 ± 1.8	23	8	**138 ± 8**
Shfd08174	127.7	0.9	0.26	0.84	1.62	1.93	1 ± 0	587 ± 31	83.7 ± 1.4	22	8	**143 ± 8**
Shfd08175	128.4	0.3	0.17	0.64	1.06	1.66	14 ± 1	420 ± 25	62.2 ± 1.7	23	12	**148 ± 10**
Shfd08176	128.7	2.5	0.22	0.83	1.70	2.05	1 ± 0	541 ± 27	60.6 ± 1.3	23	9	**112 ± 6**
Shfd08177	127.6	2.4	0.28	1.04	2.13	2.05	1 ± 0	669 ± 34	82.1 ± 1.2	22	7	**123 ± 6**
Shfd08178	126.8	3.6	0.23	0.56	1.96	3.5	12 ± 1	508 ± 25	78.1 ± 1.5	21	9	**154 ± 8**
Shfd08179	126.4	4	0.29	0.75	1.81	2.41	1 ± 0	585 ± 30	87 ± 1.2	15	0	**149 ± 8**
Shfd08180	128.3	2.1	0.37	0.86	2.41	2.8	1 ± 0	742 ± 38	95.4 ± 1.6	15	5	**129 ± 7**
Shfd09068	65	0.8	0.34	1.38	2.29	1.66	4 ± 0	849 ± 44	94.5 ± 1.1	17	5	**112 ± 6**
Shfd09067	81	0.9	0.27	0.88	1.34	1.52	3 ± 0	581 ± 31	76.9 ± 0.9	15	11	**132 ± 7**
Shfd09149	130	3.1[$]	0.34[*]	1.38[*]	2.29[*]	1.66	1 ± 0	816 ± 42	75.1 ± 1.2	21	7	**92 ± 7**
4. Groenvlei												
Shfd08186	28.1	1.6	0.19	0.76	1.29	1.7	17 ± 1	475 ± 24	48.5 ± 0.6	21	5	**102 ± 5**
Shfd08187	24.3	1.2	0.26	0.71	1.29	1.82	21 ± 1	544 ± 28	44.3 ± 1.1	17	8	**82 ± 5**
Shfd08189	17	2.7	-	-	-		35 ± 2	619 ± 67[#]	49.1 ± 1.7	15	13	**79 ± 9**
Shfd08188	30	2.1	0.22	0.69	1.41	2.04	30 ± 1	518 ± 25	70.4 ± 1.5	25	13	**136 ± 7**
Shfd09071	35.2	3	0.21	0.82	1.36	1.66	12 ± 1	507 ± 25	46.1 ± 0.6	14	11	**91 ± 5**
5. Buffels Bay												
Shfd08185	5	3.6	0.31	1.22	2.11	1.73	108 ± 5	835 ± 37	72.1 ± 2.7	24	21	**86 ± 5**

[#] Dose rate determined using beta counting

[*] Element concentrations determined using ICP-MS

[$] Confidence limits of ± 10 % were applied to the moisture content of Shfd09149 rather than the standard ± 5 % used for all other moisture contents (see section 6.1.1.3)

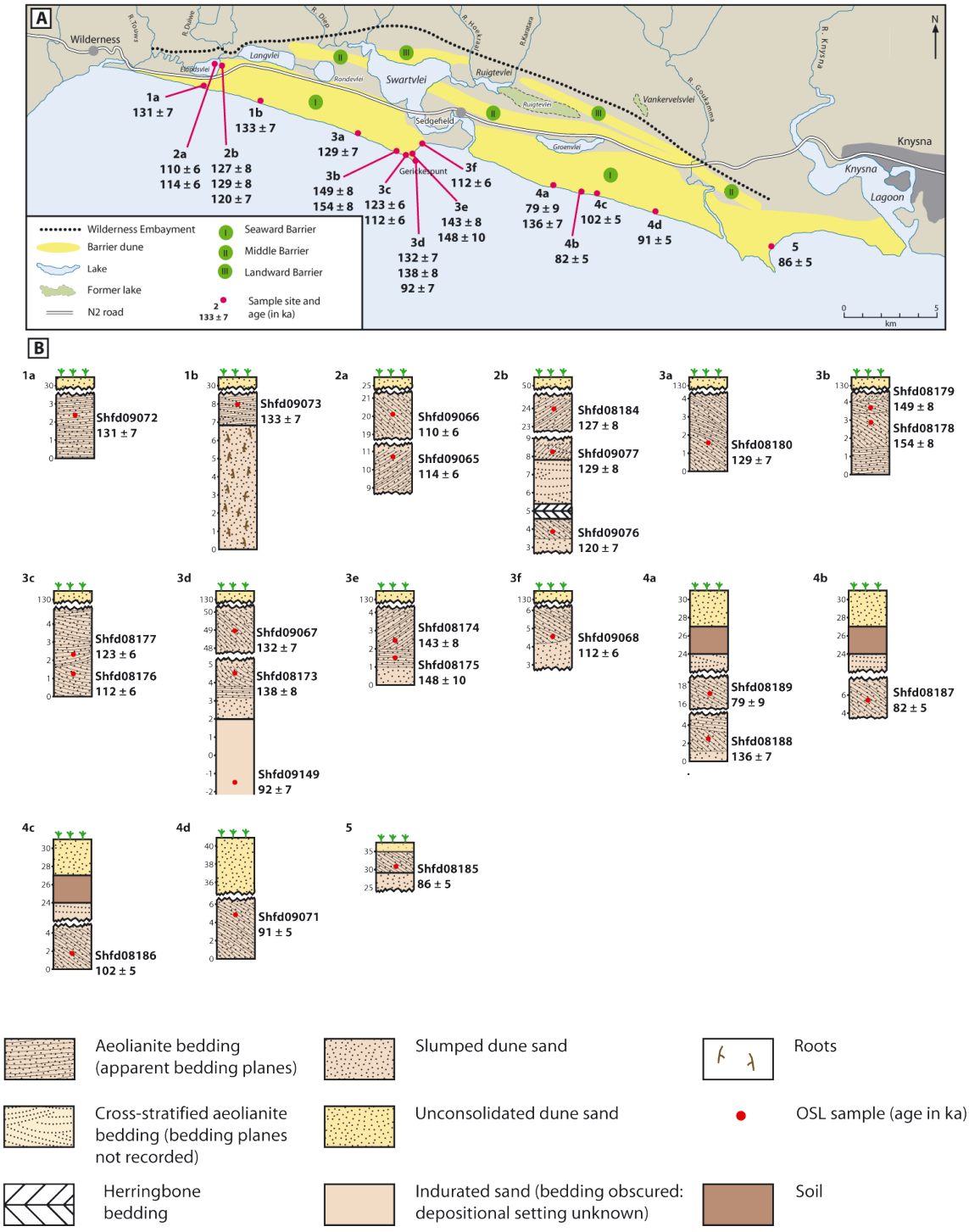

6.1.1 OSL age determinations from seaward barrier samples, shown on: (a) morphological map of the Wilderness embayment; and (b) stratigraphic sections. Site numbers on the map correspond with those on the stratigraphic sections and in Table 6.1.1. All ages are expressed in ka. The scale on the left of the stratigraphic sections indicates the height of the samples in m amsl.

The dose rate of Shfd09076, the youngest and stratigraphically lowest sample at East Elandsvlei, is greater than those of the two stratigraphically higher samples (Shfd08184 and Shfd09077) by ~200 uGy a^{-1} (Table 6.1.1). The sea-level incursion responsible for depositing the marine facies overlying Shfd09076 would have saturated the underlying aeolianites, and it is

possible that uranium in the carbonate fraction of the sand was mobilised during this episode, disrupting the U-series decay chain in material around the sample. However, its Th/U ratio falls between those of Shfd09077 and Shfd08184 (Table 6.1.1), tentatively suggesting that disequilibrium is not an issue. Moreover, the fact that the overlying samples are within errors of Shfd09076 suggests that the marine incursion occurred relatively soon after underlying aeolianites were deposited. Any alterations to the environmental dose rate of Shfd09076 would thus apply to the vast majority of its burial period, making the contemporary measurement of dose rate appropriate. That deposition was concentrated between 120-129 ka (notwithstanding errors) is further supported by a sample collected from the marine facies itself by Bateman et al. (2011), dating to 128 ± 7 ka (Shfd05049: chapter 7 Table 7.1).

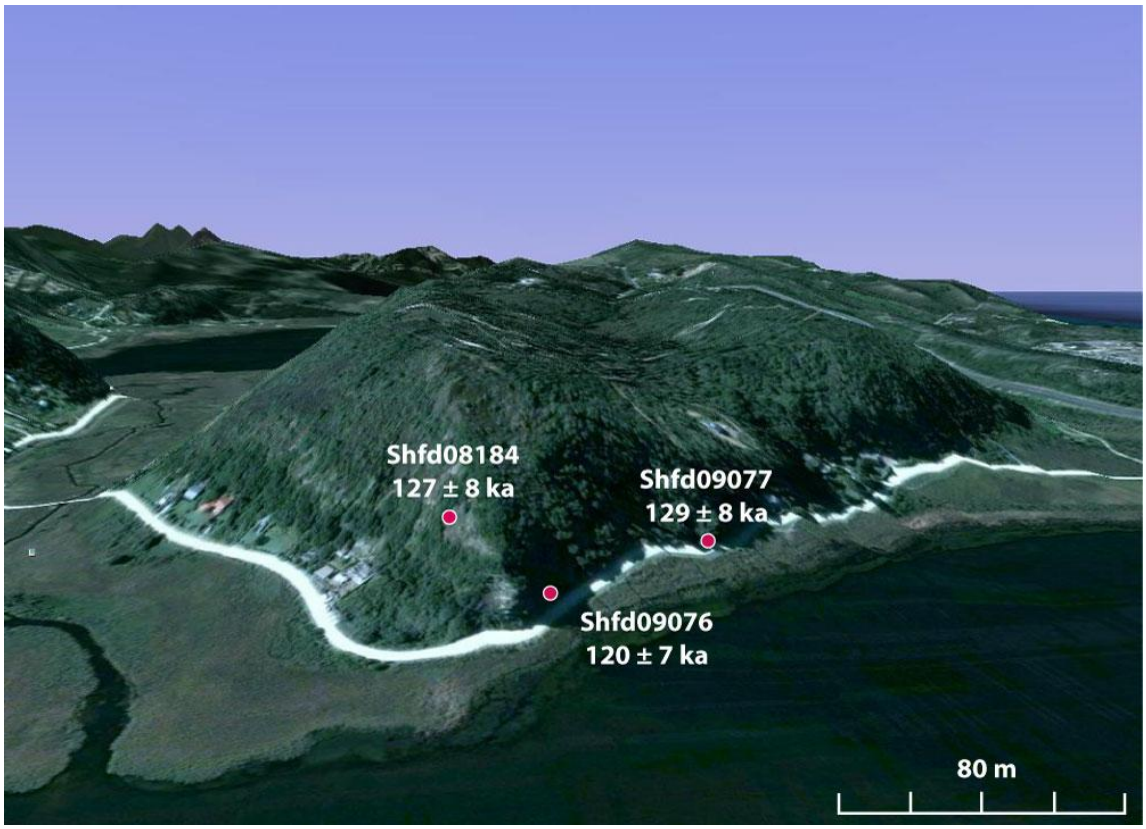

6.1.2 Oblique view, facing east south east, of the seaward barrier exposure at East Elandsvlei. Ages indicate rapid dune accumulation between 120-129 ka (notwithstanding errors), with this period also inclusive of a marine incursion stratigraphically between Shfd09076 and Shfd09077 reaching ~5 m amsl. The marine facies were dated by Bateman et al. (2011) to 128 ± 7 ka. Figure based on Google Earth image using data from DigitalGlobe Data SIO, NOAA, U.S. Navy, HGA and GEBCO. Note scale applies to horizontal direction only and image has been vertically exaggerated by a factor of three.

The two samples from Elandsvlei Island report slightly younger ages than those from the adjacent exposure at East Elandsvlei, of 114 ± 6 ka (Shfd09065) and 110 ± 6 ka (Shfd09066). Here, similar to the Klein Krantz samples, a relatively large difference in D_e (68.2 ± 1.4 Gy and

82.2 ± 1.7 Gy respectively) is matched by a corresponding difference in dose rate to produce sample ages well within errors, providing confidence they are representative of true burial age.

6.1.2.3 Gerickes Point

Sampling of the seaward barrier was most intensive around the Gerickes Point headland west of Sedgefield (Figure 6.1.1 sites 3a-3f). Ages indicate the depositional history of this area is complex, with aeolianite samples spanning the period 112 ± 6 ka (Shfd08176 and Shfd09068) to 154 ± 8 ka (Shfd08178). The youngest sample, Shfd09149 (92 ± 7 ka), was chiselled as a block from the intertidal zone and bedding structures were obscured by marine flora, meaning it was not possible to visually identify whether it was originally deposited in an aeolian, marine or beach setting. However, its slightly coarser particle size distribution relative to the other Gerickes Point samples (see section 6.2) indicates one of the latter two is more likely. Shfd09149 is discussed at greater length later in this section.

In order to assess the rate at which smaller parabolic dunes coalesce to form the barriers, paired samples were collected at three localities around Gerickes Point bracketing bounding surfaces within the bedding (Figure 6.1.1 sites 3b, 3c and 3e). Photos of sampled sections and ages are shown in Figure 6.1.3. At all three sites the paired samples yield ages within errors of one another, indicating no discernable pause in sedimentation (within the limits of the OSL dating technique) between the formation of one parabolic dune and its subsequent truncation by the formation of another dune above.

At Gerickes Point site 3d, it was possible to sample the sea cliff approximately one third of the way up the barrier face at 49 m amsl (Shfd09067). A sample was also obtained 300 m south of Shfd09067 and close to sea level, from the headland at the very tip of Gerickes Point (Shfd08173). The location of these two samples is shown in Figure 6.1.4. Whilst not in direct stratigraphic succession, the relationship between them allows the rate of vertical and horizontal barrier accumulation to be inferred over a relatively large distance. The age of Shfd09067 (from 49 m amsl) falls within errors of sample Shfd08073 obtained at 4.5 m amsl (132 ± 7 ka and 138 ± 8 ka respectively). This further indicates the rapidity of accretion within the seaward barrier, as suggested by the paired samples and those from the East Elandsvlei exposure discussed previously.

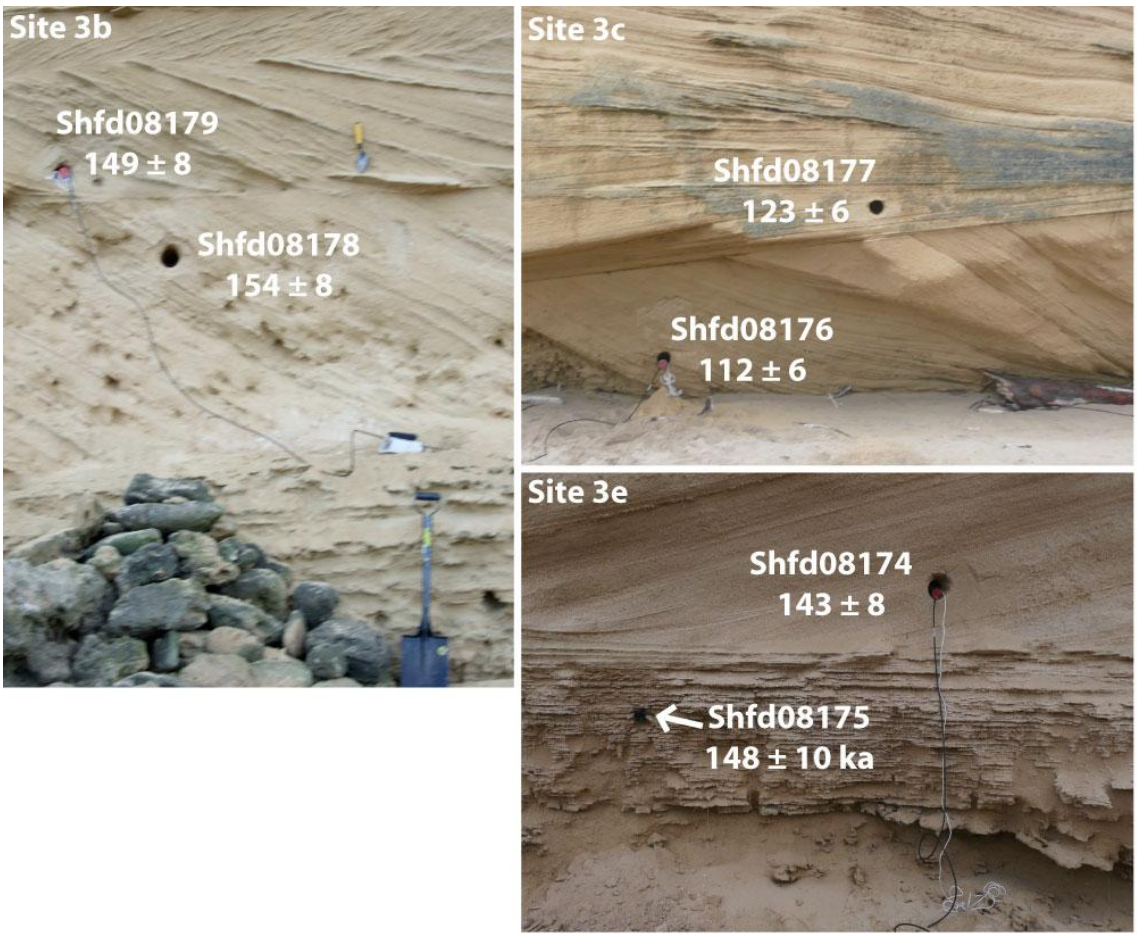

6.1.3 Paired OSL samples from various seaward barrier localities around Gerickes Point, annotated with sample code and age. That the paired ages fall within errors at all sites indicates no significant temporal break occurs between one parabolic stacking on top of another as the barriers accumulate.

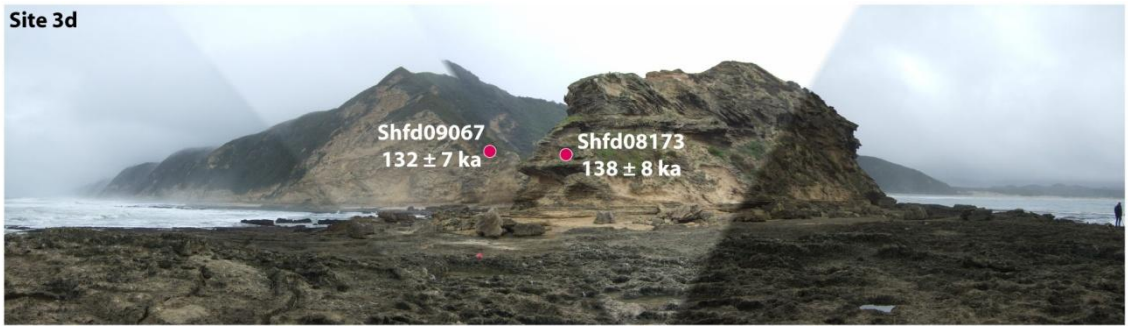

6.1.4 Samples from the Gerickes Point headland area (site 3d), indicating the rapidity of horizontal and vertical accumulation within the seaward barrier. Shfd09067 is 44.5 m higher than Shfd08173 and 300 m further north. Both samples were obtained from high-angle bedded aeolianite. See person on far right for scale.

In Figure 6.1.1b, sample Shfd09149 (92 ± 7 ka) is included in the stratigraphic section for site 3d alongside Shfd08173 and Shfd09067, giving rise to an apparent age inversion. However, although collected in close proximity to Shfd08173, as stated earlier in this section the coarse particle size distribution of Shfd09149 relative to other barrier dune samples

suggests it is of marine or beach, rather than aeolian, origin. The spatial relationship between it and the other Gerickes Point samples is illustrated in Figure 6.1.5.

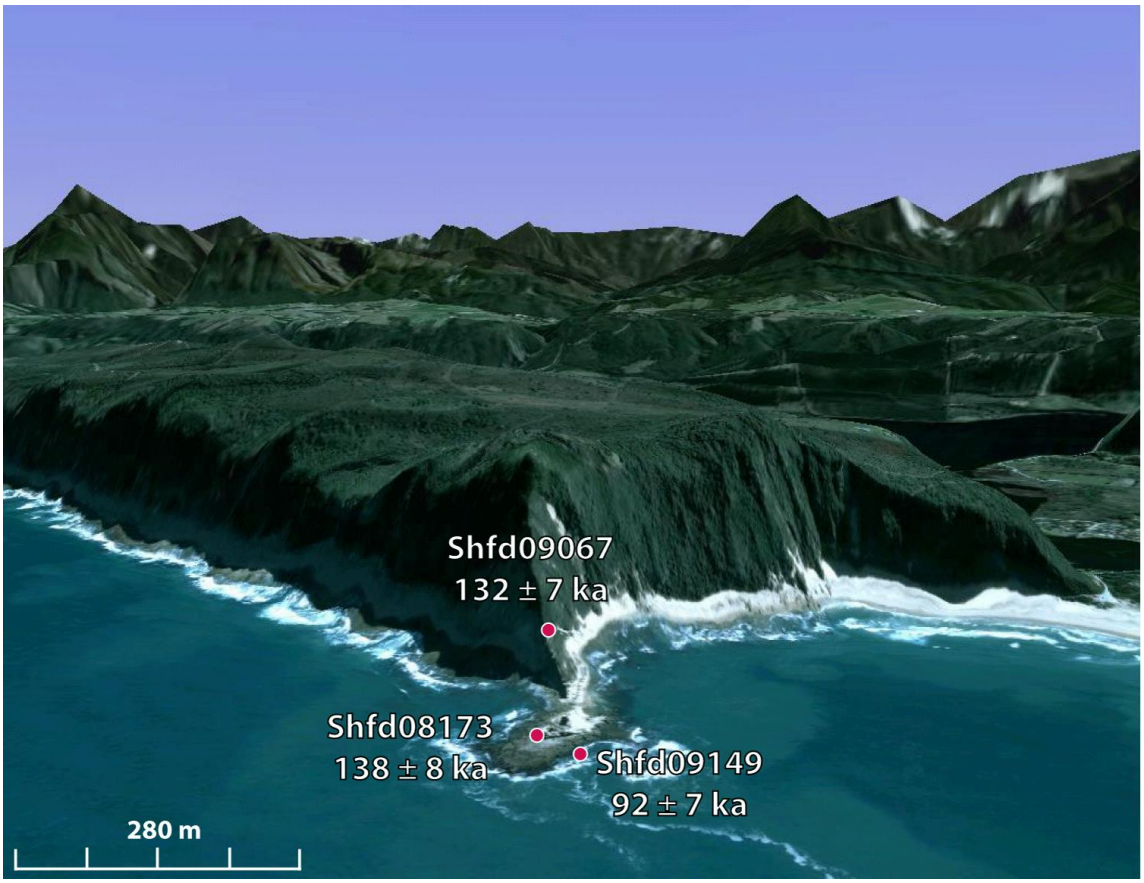

6.1.5 Oblique view of Gerickes Point headland illustrating the stratigraphic relationship between samples Shfd09067, Shfd08173 and Shfd09149. Shfd09149 is tentatively interpreted as being of marine or beach origin, whereas Shfd08173 and Shfd09067 are aeolianite. Figure based on Google Earth image using data from DigitalGlobe Data SIO, NOAA, U.S. Navy, HGA and GEBCO. Note scale applies to horizontal direction only and image has been vertically exaggerated by a factor of three.

The dose rate of Shfd09149 is significantly higher than most other seaward barrier samples, at 816 ± 42 μGy a^{-1} (Table 6.1.1). The location of the sample in the intertidal zone increases the risk that this high dose rate is a reflection of disruption in the U-series decay chain. The estimated moisture content for Shfd09149 also induces additional uncertainty to the calculated age. It is based on a weighted average of: (1) the average moisture content of the other, subaerially exposed Gerickes Point samples (1.94 %); and (2) the saturated moisture content of the sample (assuming 6 ka of saturation, since the Mid-Holocene) (14.9 %), producing a value of 3.1 %. Confidence limits of ± 10 % were applied to this figure, rather than the ± 5 % used for all other sample moisture contents. However, even with the increased moisture content error and the potential for a few percent error in age calculation due to U-series disequilibrium, the age of Shfd09149 apparently represents a later stage of deposition than the other material at Gerickes Point. Its close proximity to the much older Shfd08173

sample indicates that Shfd09149 represents material “welded” on to pre-existing aeolianite, and its relatively coarse particle size suggests this may have occurred in a beach or shallow marine setting.

6.1.2.4 Groenvlei

Five samples were obtained from the Groenvlei area, spanning a horizontal distance of 4 km along the sea cliffs in the eastern half of the embayment (Figure 6.1.1 sites 4a to 4d). The majority of the Groenvlei samples are younger than those from the western half of the Wilderness embayment (Klein Krantz, Elandsvlei and Gerickes Point sites), being concentrated between 80–100 ka (Table 6.1.1). However, one Groenvlei sample (Shfd08188) is significantly older than the other four at 136 ± 7 ka, and is directly overlain by the much younger Shfd08189 sample (79 ± 9 ka). A photo showing the stratigraphic relationship between these two samples, which are separated by 13 m vertically, is given in Figure 6.1.6. Shfd08189 is the only sample from the seaward barrier with a dose rate determined by beta counting. The possibility that this less precise means of determining environmental dose rate has resulted in an under- or over-estimation of the true dose rate cannot be ruled out. However, the sample was obtained from the centre of a unit of very finely bedded aeolianite at least 1.5 m thick, in an attempt to minimise the potential risk for heterogeneities in surrounding radionuclide content that would not be measured by beta counting. The D_e of Shfd08189 is also consistent with the other Groenvlei samples (which all fall between 44-49 Gy), as opposed to Shfd08188 which has a significantly larger D_e of 70.4 ± 1.5 Gy (Table 6.1.1). In the absence of any evidence to the contrary, the ages are thus interpreted as reflecting the true burial ages of the deposits.

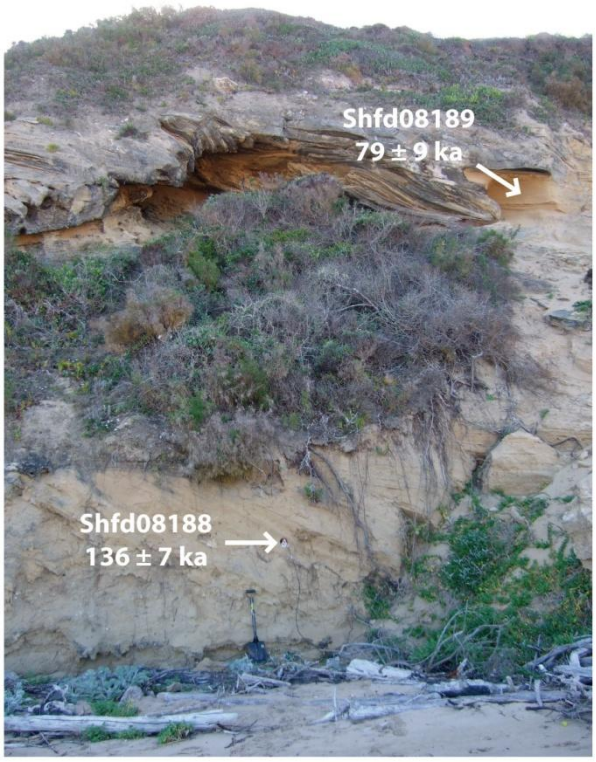

6.1.6 Location and age of samples Shfd08188 and Shfd08189 at Groenvlei site 4a. The large difference in age between two samples relatively close to one another contrasts with the rapid vertical accretion of the barrier at Gerickes Point sites.

6.1.2.5 Buffels Bay

Similar to the majority of the Groenvlei samples, at 86 ± 5 ka Shfd08185 from Buffels Bay is younger than the material from the western half of the Wilderness embayment (Figure 6.1.1 site 5). Its age is corroborated by a sample from Bateman et al. (2011) taken from a similar stratigraphic position ~150 m farther east, which dates to 91 ± 5 ka.

6.1.3 Middle barrier

Summaries of all the OSL ages obtained from the middle Wilderness barrier are provided in Table 6.1.2 and Figure 6.1.7, which follow the same conventions used for the seaward barrier data. Ages are discussed on a site-by-site basis in the following sections.

Table 6.1.2 Dose rate data, D_e values, and calculated ages for OSL samples obtained from the middle Wilderness barrier. Numbers by sample sites correspond with sample locations in Figure 6.1.7.

Sample details		Dosimetry							Palaeodose			
Sample code	Burial depth (m)	Water content (%)	K (%)	U Ppm	Th ppm	Th/ U	Cosmic dose rate (μGy a^{-1})	Total dose rate (μGy a^{-1})	D_e (Gy)	n	OD (%)	Age (ka)
6. Rondevlei												
Shfd09078	2.75	0.7	0.22	0.76	1.48	1.95	143 ± 7	655 ± 28	90.5 ± 2.9	28	16	**138 ± 7**
Shfd09079	4.2	1.6	0.25	0.82	1.71	2.09	127 ± 6	684 ± 29	111.9 ± 3.1	19	15	**163 ± 8**
7. West Swartvlei												
Shfd08080	24.8	0.4	0.21	0.57	1.25	2.19	51 ± 3	493 ± 26	75.8 ± 2.3	19	19	**154 ± 9**
Shfd09081	2.6	3.9	0.5	1.81	6.56	3.62	146 ± 7	1480 ± 66	137.7 ± 5.4	26	18	**93 ± 6**
Shfd09082	44.2	0.6	0.21	0.61	1.31	2.15	27 ± 1	482 ± 25	79.5 ± 2.3	21	21	**165 ± 10**
8. East Swartvlei												
Shfd08182	57.2	0.6	-	-	-	-	16 ± 1	604 ± 75[#]	85.8 ± 2.5	18	16	**142 ± 18**
Shfd08181	64	0.3	0.21	0.80	1.43	1.79	32 ± 2	548 ± 30	87.5 ± 2.7	16	19	**160 ± 10**
Shfd08183	1.3	0.4	0.20	1.64	2.58	1.57	167 ± 8	946 ± 43	123.7 ± 3	20	20	**131 ± 7**

[#] Dose rate determined using beta counting

6.1.3.1 Rondevlei

The two Rondevlei samples were obtained from a core extracted from the crest of the middle barrier west of Swartvlei (Figure 6.1.7 site 6). Coring ceased at 4.2 m depth when aeolianite fragments started to be retrieved from the hole, preventing the corer from penetrating further. Sample Shfd09078 was extracted at 2.75 m depth from unconsolidated sand. Shfd09079, obtained from 4.2 m depth, was collected by hammering the corer into the indurated aeolianite. Although the samples are stratigraphically close to one another (separated by only 1.45 m vertically) there is a reasonably large difference in age between them, with Shfd09078 dating to 138 ± 7 ka and Shfd09079, 1.45 m lower, dating to 163 ± 8 ka.

The carbonate content of the two Rondevlei samples suggests the boundary between aeolianite and unconsolidated sand material is not due to weathering, with almost identical values for the two samples (Shfd09079 has 16.3 % $CaCO_3$ and Shfd09078 has 15.7 %) indicating no leaching has taken place (n.b. carbonate contents for all samples are given in Appendix 1). Moreover, the OD values of both samples indicate they have not been subjected to bioturbation or partial reactivation, their dose rates are within errors of one another, their Th/U ratios are similar and their D_e distributions are normal in shape (Table 6.1.2). All of these factors combine to indicate the calculated ages represent true burial ages, and the Rondevlei samples thus represent two phases of deposition.

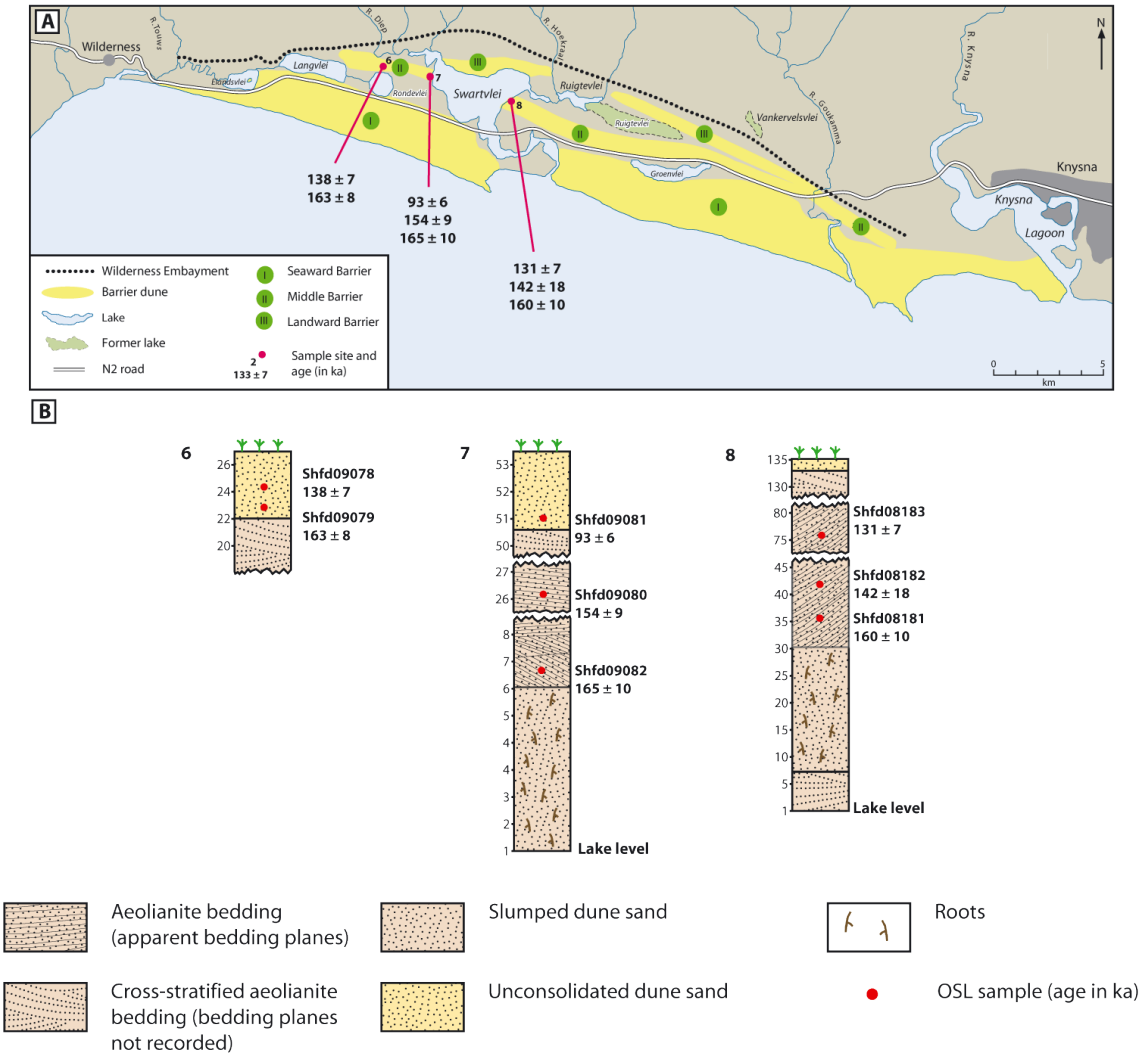

6.1.7 Sample locations and OSL age determinations from middle barrier sites: (a) morphological map of the Wilderness embayment showing sample site locations; (b) stratigraphic sections showing sample positions and finalised ages. Site numbers on the map correspond with those on the stratigraphic sections and in Table 6.1.2. All ages are expressed in ka. The scale on the left of the stratigraphic sections indicates the height of the samples in m amsl and, where appropriate, lake level.

6.1.3.2 West Swartvlei

Three samples were obtained in vertical succession from the middle barrier on the western shore of Swartvlei (Figure 6.1.7 site 7): from exposures of aeolianite at 6.8 m amsl and 26.2 m amsl (Shfd09082 and Shfd09080 respectively) and from a core at the crest of the barrier at 51 m amsl (Shfd09081). Sample locations and ages are illustrated in Figure 6.1.8. The samples from the base and middle of the exposure, Shfd09082 and Shfd09080, are consistent in their D_e and dose rate, with both being within errors of one another. However, the dose rate of Shfd09081, from the barrier crest, is unusually high at 1480 ± 66 µGy a^{-1} (Table 6.1.2). Its Th/U ratio is 3.62, which is close to the upper continental crustal (UCC) average of 3.82 (Taylor and McLennan, 1985) but significantly larger than most other barrier samples in this study.

Also, the carbonate content of sample Shfd09081 is only 0.06 %, compared to 19.6 % for Shfd09082 and 14 % for Shfd09080 (sample carbonate contents are listed in Appendix 1), suggesting its elevated Th/U ratio has most likely arisen from leaching of U along with carbonate. Its dose rate, and consequently its calculated age of 93 ± 6 ka, is therefore treated with caution.

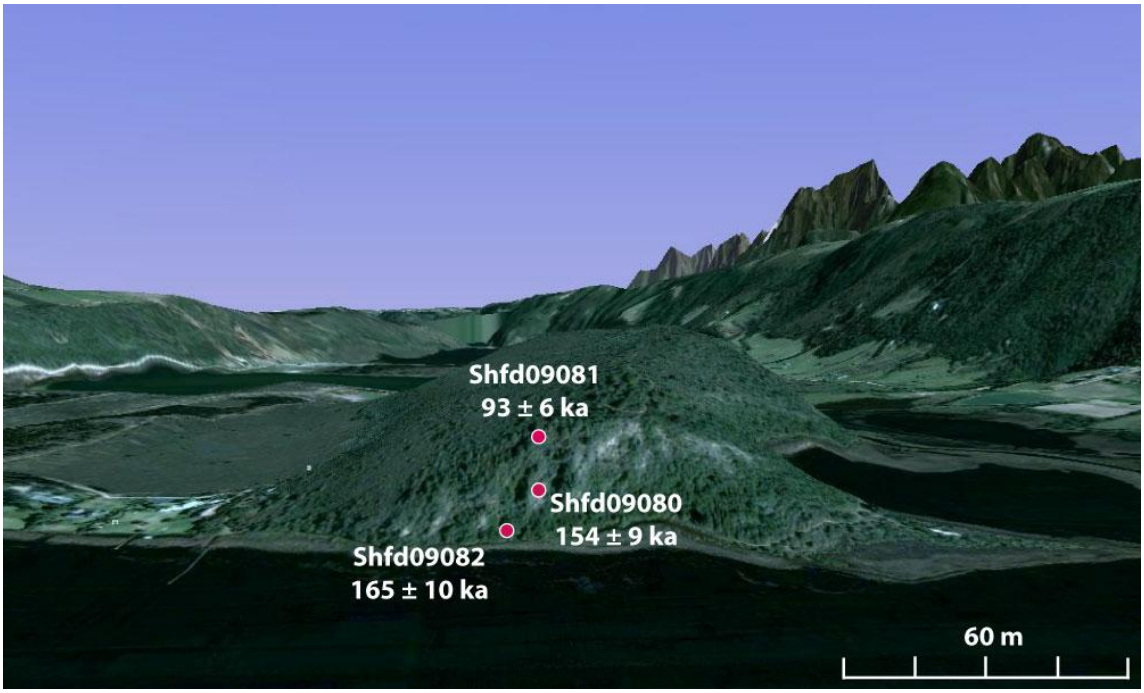

6.1.8 Side-on view, facing west, of the middle barrier exposure at West Swartvlei. The age of sample Shfd09081, obtained from a core the crest of the dune, is considered potentially unreliable. Figure based on Google Earth image using data from DigitalGlobe Data SIO, NOAA, U.S. Navy, HGA, GEBCO. Note scale applies to dune cross-section and image has been vertically exaggerated by a factor of three.

6.1.3.3 East Swartvlei

In approximate stratigraphic correspondence with the samples obtained from the west Swartvlei exposure, three samples were also obtained from the middle barrier exposure on Swartvlei's eastern shore (Figure 6.1.7 site 8). They comprise Shfd08181 and Shfd08182 from aeolianite exposed at 36 and 42.8 m amsl, and Shfd08183 from aeolianite at 78 m amsl. Sample locations and ages are illustrated in Figure 6.1.9. The dose rates and D_e values of the lower two samples are within errors of one another, providing confidence that their finalised ages represent the true burial age of the deposits: 160 ± 10 ka for Shfd08181 and 142 ± 18 ka for Shfd08182. The large confidence intervals surrounding Shfd08182 are due to uncertainties in dose rate, which was measured using the less precise beta counting procedure. Nevertheless, the similarity in age between Shfd08181 and Shfd08182 from East Swartvlei to Shfd09080 and Shfd09082 from similar stratigraphic positions at West Swartvlei strongly suggests the middle barrier formed concurrently along the length of the embayment.

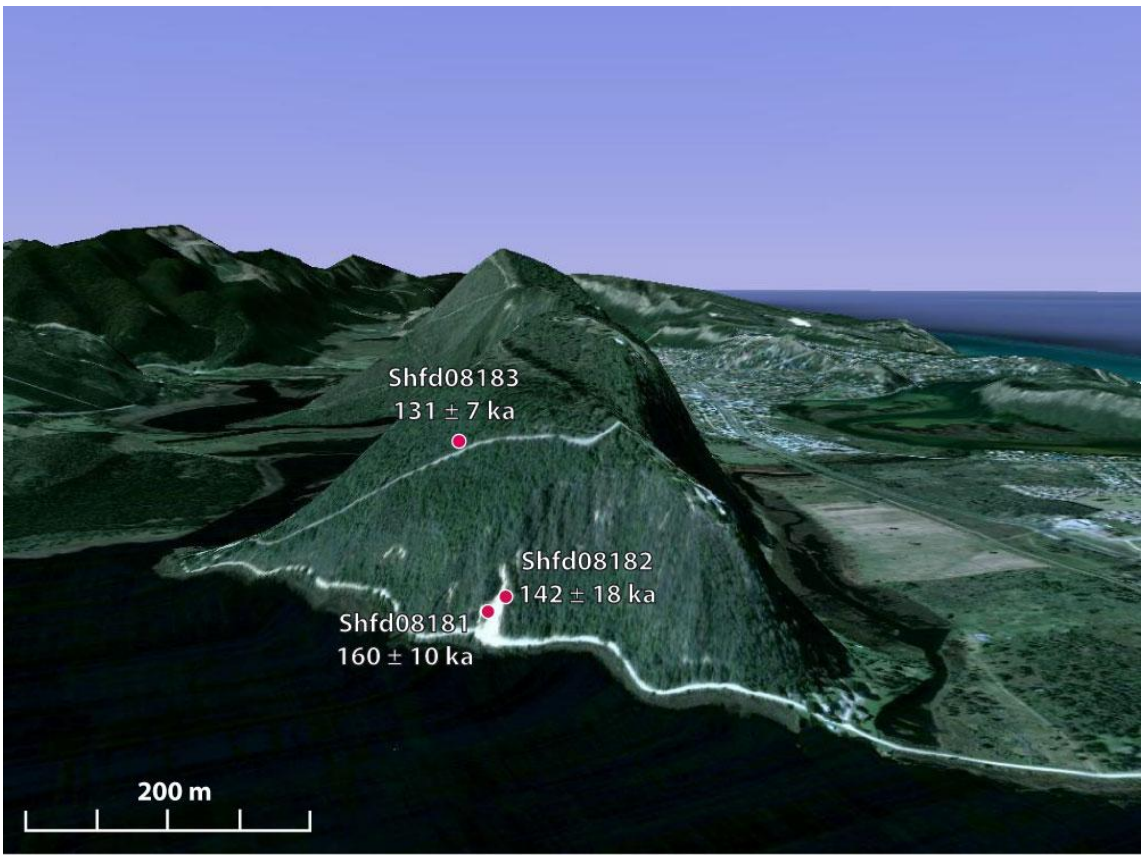

6.1.9 Side-on view, facing east, of the middle barrier exposure at East Swartvlei. Ages indicate two phases of dune accumulation. Basal ages correspond well with those at west Swartvlei (Figure 6.1.8). Figure based on Google Earth image using data from DigitalGlobe Data SIO, NOAA, U.S. Navy, HGA, GEBCO. Note scale applies to dune cross-section and image has been vertically exaggerated by a factor of three.

The dose rate of sample Shfd08183, obtained from a road cutting close to the crest of the barrier is relatively high (946 ± 43 µGy a^{-1}), akin to its crestal counterpart Shfd09081 from the west Swartvlei exposure (Table 6.1.2). However, Shfd08183 was collected from visible high-angle aeolianite bedding and possesses a carbonate content of 24.6 % (compared to 22.6 % and 21.7 % for the underlying Shfd08181 and Shfd08182), indicating that leaching has not taken place. The measured dose rate is thus considered reliable. The age calculated for Shfd08183 (131 ± 7 ka) is also corroborated by a sample obtained by Bateman et al. (2011) from further along the same road cutting (Shfd05048), dated to 139 ± 8 ka .

6.1.4 Landward barrier

Summaries of all the OSL ages obtained from the landward Wilderness barrier are provided in Table 6.1.3 and Figure 6.1.10, which follow the same conventions used for the seaward and middle barrier data. Ages are discussed on a site-by-site basis in the following sections.

Table 6.1.3 Dose rate data, D_e values, and calculated ages for OSL samples obtained from the landward Wilderness barrier. Numbers by sample sites correspond with sample locations in Figure 6.1.10.

Sample details		Dosimetry							Palaeodose			
Sample code	Burial depth (m)	Water content (%)	K (%)	U ppm	Th ppm	Th/ U	Cosmic dose rate (µGy a^{-1})	Total dose rate (µGy a^{-1})	D_e (Gy)	n	OD (%)	Age (ka)
9. North Swartvlei												
Shfd09074	39.6	1.1	0.27	0.91	1.61	1.77	27 ± 1	626 ± 31	128.2 ± 2.4	50	15	**205 ± 11**
Shfd09075	40.8	0.5	0.3	2.23	6.2	2.78	26 ± 1	1301 ± 65	>194[$]	28	14	**>149**
10. Goukamma												
Shfd09069	166	1.9	0.32	1.05	4.50	4.29	1 ± 0	889 ± 44	222.5 ± 3.6	21	8	**250 ± 13**
Shfd09070	123	3.4	0.27	0.79	1.94	2.46	1 ± 0	580 ± 29	143.5 ± 4.9	22	21	**247 ± 15**

[$] D_e value excludes saturated aliquots and as such represents a conservative estimate of minimum palaeodose

6.1.4.1 North Swartvlei

Samples Shfd09074 and Shfd09075 were collected from aeolianite exposures on the north shore of Swartvlei (Figure 6.1.10 sites 9a and 9b respectively). Although obtained from similar stratigraphic positions, material (high-angle bedded aeolianite) and altitudes (10.4 m amsl and 9.2 m amsl), Shfd09075 has a dose rate almost double that of Shfd09074 (Table 6.1.3). As reported in chapter 5 section 5.2.4.6, several aliquots from Shfd09075 were found to be in saturation, meaning only a minimum age of >149 ka could be calculated. Fortunately Shfd09074 exhibited no such problems, producing an age of 205 ± 11 ka that is considered reliable.

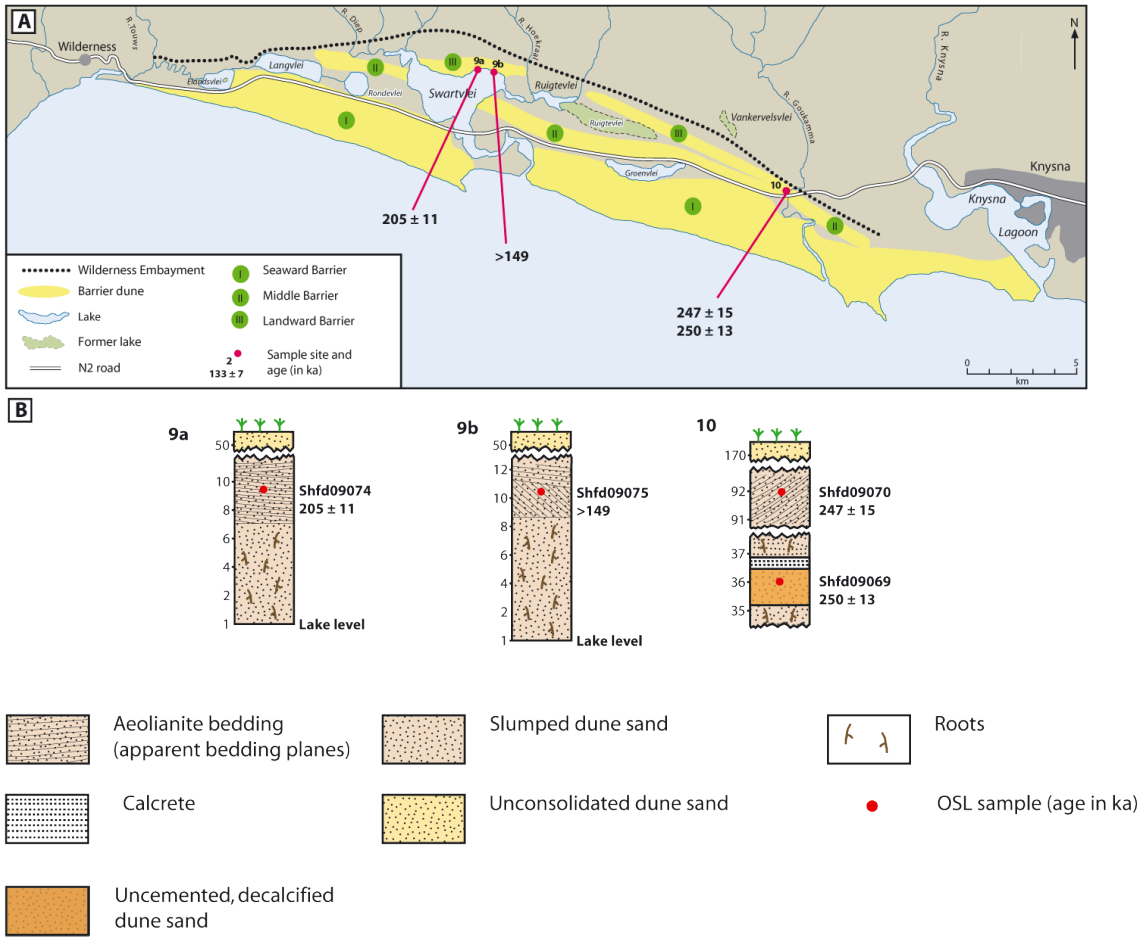

6.1.10 Sample locations and OSL age determinations from landward barrier sites: (a) morphological map of the Wilderness embayment showing sample site locations; (b) stratigraphic sections showing sample positions and finalised ages. Site numbers on the map correspond with those on the stratigraphic sections. All ages are expressed in ka. The scale on the left of the stratigraphic sections indicates the height of the samples in m amsl and, where appropriate, lake level.

6.1.4.2 Goukamma

The Goukamma site is located on the eastern side of the Wilderness embayment where the lower flanks of the landward and middle barrier dunes overlap (Figure 6.1.10 site 10). Two samples were obtained, both from the seaward flank of the landward barrier: Shfd09069 from a small burrow pit towards its base at 36 m amsl; and Shfd09070 from a road cutting approximately two thirds of the way up the dune at 92 m amsl. The Th/U ratio of the lower sample (Shfd09069) is particularly high at 4.29 (Table 6.1.3). Given the unusual colour of the sample, its lack of aeolian bedding, low carbonate content (0.52 %, compared to 19 % for Shfd09070: Appendix 1), and the calcrete layer above (Figure 6.1.10b site 10), it is unsurprising that it appears to be subject to U-series disequilibrium. However, despite large differences in dose rate between Shfd09069 and Shfd09070, their D_e values differ accordingly and the ages of the two samples are almost identical: 250 ± 13 ka and 247 ± 15 ka respectively. It is possible that any disruption to the U-series decay chain of Shfd09069 occurred soon after burial, and

the contemporary measurement of dose rate (and thus the calculated age) is accurate. If Shfd09069 and Shfd09070 both represent the true burial age of the deposits, their large difference in elevation suggests the landward barrier accumulated as rapidly as the seaward and middle barriers.

6.1.5 Coversands

The coversands inland of the Wilderness embayment were dated using samples obtained from two sites: Karatara Road and Barrington Road. A coversand sample originally collected by Holmes et al. (2007) from Makhulu Quarry, for which they obtained a minimum age of >522 ka using OSL dating, was also re-dated using ITL. A morphological map showing the location of the three sites is provided in Figure 6.1.11a, and stratigraphic columns illustrating the stratigraphy and calculated ages of the Karatara Road and Barrington Road sites are presented in Figure 6.1.11b. A diagram showing the stratigraphy of the Makhulu Quarry site is included in Holmes et al. (2007). Ages for the three coversand sites are discussed in the following sections.

6.1.5.1 Karatara Road

Close to the Swart River and the north east corner of Swartvlei, the Karatara Road site represents the point furthest west at which a coversand exposure suitable for OSL sampling could be located. One sample (Shfd08192) was obtained from a road cutting at 59 m amsl (Figure 6.1.11 site 11). It yielded an age of 66 ± 4 ka, considerably younger than the coversands are widely assumed to be. None of the values used in the age calculation indicate Shfd08192 should be treated as unreliable, with the sample possessing a low OD value and an approximately normal D_e distribution, with no evidence of multiple peaks as would be expected in a sample subject to bioturbation (e.g. Bateman et al., 2007). The particle size distribution of samples from the Karatara Road site is also similar to those from all other coversand sites (see Table 6.2.3 in section 6.3), suggesting the young age of Shfd08192 is not a consequence of reworking. The date is thus interpreted as representing either original deposition or aeolian reactivation of the coversands at this time.

Table 6.1.4 Dose rate data, D_e values, and calculated age for the Karatara Road coversand sample. Number by sample site corresponds with its location in Figure 6.1.11.

Sample details		Dosimetry							Palaeodose			
Sample code	Burial depth (m)	Water content (%)	K (%)	U ppm	Th ppm	Th/ U	Cosmic dose rate (µGy a^{-1})	Total dose rate (µGy a^{-1})	D_e (Gy)	n	OD (%)	Age (ka)
11. Karatara Road												
Shfd08192	1.9	0.1	0.19	1.08	3.74	3.46	161 ± 8	889 ± 44	58.4 ± 1.7	15	15	**66 ± 4**

6.1.5.2 Barrington Road

The Barrington Road site is further east than the Karatara Road site and possesses deeper coversand deposits. Two samples were collected, from adjacent coversand units separated by a laterised and red-tinged layer 0.6 m thick incorporating several iron pans and nodules (Figure 6.1.11b site 12). The sample from the upper coversand unit, Shfd08190, yielded an age of 17 ± 2 ka. As with the Karatara Road sample, there is no evidence to indicate the age is unreliable, and it is thus similarly interpreted as indicating either original deposition or an aeolian reactivation event.

The second Barrington Road sample (Shfd08191) was obtained from the lower coversand unit beneath the iron pans (Figure 6.1.11b site 12). Shfd08191 was measured using both OSL and ITL dating techniques. The results of both methods are included in Table 6.1.5. As discussed in chapter 5, the lower D_e produced by the OSL measurement most likely reflects the OSL signal approaching saturation, and the ITL result is thus assumed to be the more accurate of the two.

6.1.5.3 Makhulu Quarry sample

Details of the ITL measurement of Shfd04287 were discussed in detail in chapter 5. Briefly, with 40 % of the aliquots measured in saturation, the calculated D_e of 806 ± 58 Gy remains a minimum estimate, and as such so too is the age of >1.6 Ma. However, it is more than triple the minimum age obtained via SAR OSL for the sample by Holmes et al. (2007). Makhulu Quarry represents the type site for the coversands around Knysna (Holmes et al., 2007), and if accurate its calculated Early Quaternary age provides support that the relatively young ages of the Karatara Road and upper Barrington Road deposits (and possibly even the lower Barrington Road sample, dating to 362 ± 35 ka) represent reactivated material.

Table 6.1.5 Dose rate data, D_e values, and calculated age for the Barrington Road and Makhulu Quarry coversand samples. Includes both OSL and ITL measurements for samples measured using both techniques. Number/letter by sample sites corresponds with their location in Figure 6.1.11.

Sample details		Dosimetry			OSL data				ITL data			
Sample code	Burial depth (m)	Water content (%)	Cosmic dose rate (µGy a^{-1})	Total dose rate (µGy a^{-1})	D_e (Gy)	n	OD (%)	Age (ka)	D_e (Gy)	n	OD (%)	Age (ka)
12. Barrington Rd												
Shfd08190	1.5	0.1	171 ± 9	747 ± 71#	12.4 ± 0.3	24	14	**17 ± 2**				
Shfd08191	3	4.2	169 ± 8	804 ± 66#	232 ± 6	23	7.9	**292 ± 25**	291 ± 15	10	15	**362 ± 35**
F. Makhulu Quarry												
Shfd04287	1.6*	4.8*	174 ± 9*	475 ± 20*	248 ± 11*	12*	-	**>0.522***	806 ± 58$	9	21	**>1600**

*Published in Holmes et al. (2007)

Dose rate determined using beta counting

$ D_e value excludes saturated aliquots and as such represents a conservative estimate of minimum palaeodose

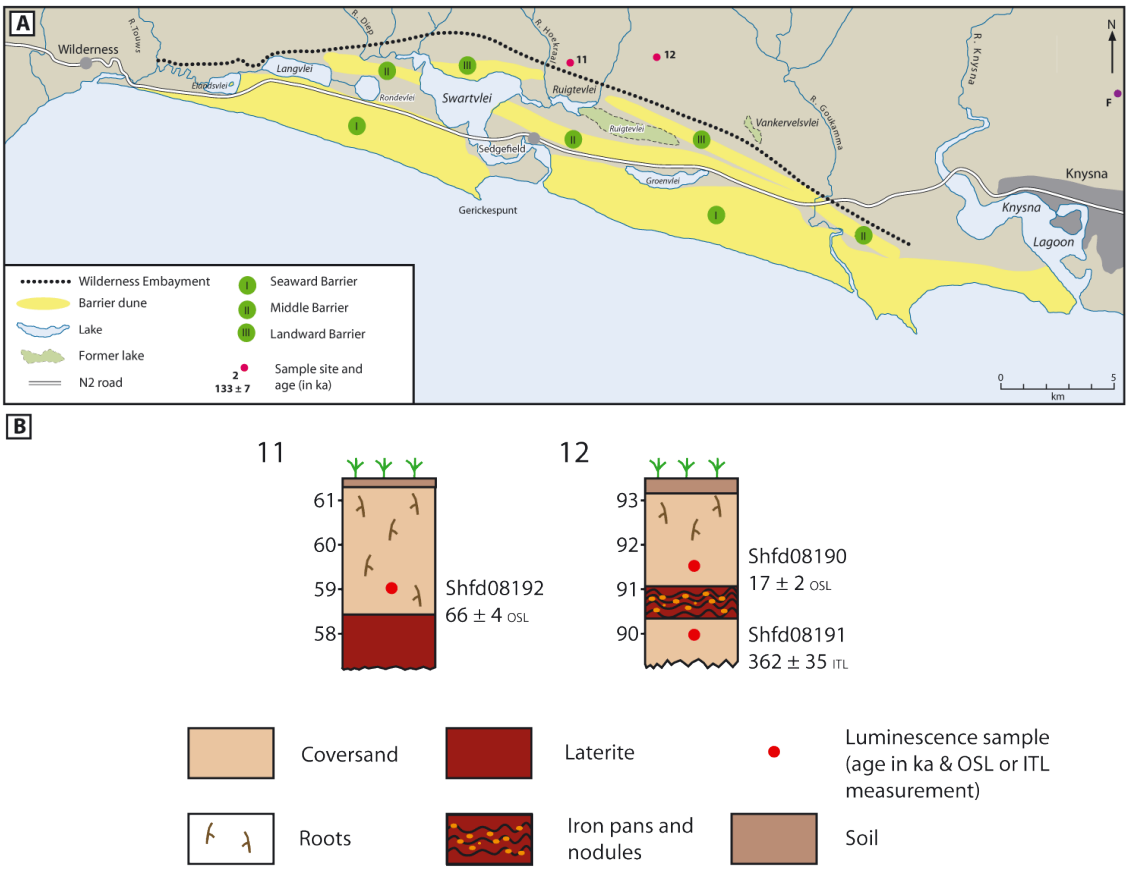

6.1.11 Sample locations and age determinations from coversand sites. (a) Morphological map of the Wilderness embayment showing sample site locations: site 11 (Karatara Road); Site 12 (Barrington Road); and site F (Makhulu Quarry, as originally sampled by Holmes et al. (2007)). (b) Stratigraphic sections showing sample positions and finalised ages. Site numbers on the map correspond with those on the stratigraphic sections. All ages are expressed in ka, and subscript indicates whether they were determined using OSL or ITL. The scale on the left of the stratigraphic sections indicates the height of the samples in m amsl.

6.1.6 Luminescence dating summary

This section has presented the results of the 36 OSL age determinations conducted on samples from the Wilderness barrier dunes, and the two OSL and two ITL ages determinations conducted on samples from the coversand deposits inland of the Wilderness embayment. Their reliability has been considered and the overall well behaved and undisturbed nature of the samples provides confidence that the calculated ages are representative of true burial age, with few exceptions. It was possible to retrieve only minimum ages from two samples (Shfd04287 from the Makhulu Quarry coversand site and Shfd09075 from the landward barrier) due to saturation issues. Also the dose rate for one sample from the middle barrier crest (Shfd09081 from the West Swartvlei site) was anomalously high, indicating possible U-series disequilibrium issues. The age of this sample (93 ± 6 ka) is significantly lower than samples obtained from similar settings close to the middle barrier crest at East Swartvlei (Shfd08183 at 131 ± 7 ka) and Rondelvei (Shfd09078 at 138 ± 7 ka), and is thus treated with caution in discussing and synthesising the results in the following chapter.

6.2 Sediment provenancing results: sediment characteristics

6.2.1 Introduction

This section presents the results of particle size analysis and calcium carbonate-content determination conducted on samples of the barrier sands and their various possible local sources (coversands, river sediments, beach sands and lagoon sediments). Barrier samples include all those collected for luminescence dating, and additional samples from two other seaward barrier sites: (1) Kirsten Tulleken quarry on the landward face of the seaward barrier ("KT section"), originally sampled by Carr et al. (2007); and (2) Holocene dunes on the seaward barrier crest ("Holocene dunes"), originally sampled by Bateman et al. (2011) and Carr et al. (2010a). The location of these two sites is illustrated in chapter 4 Figure 4.2.

The sedimentary characteristics of the barrier samples are first considered in isolation, in order to investigate what similarities and/or differences can be identified between the seaward, middle and landward barriers. The particle size characteristics of the barrier sands are then compared to those of the potential local sources of sediment, in order to determine whether or not any of them could have contributed to the dunes. Whilst the different processes that act to transport and deposit material in dune, river, lagoon and beach settings mean comparisons between their particle size distributions cannot be used to determine

specific provenance relationships, observing a total absence of material of equal size fraction to the barrier sands in the possible source areas can rule out their having contributed.

6.2.2 Barrier sands

Previous studies by Bateman et al. (2004) and Carr et al. (2010a) describe sediments from the seaward Wilderness barrier as being well sorted, fine to medium grained sands with negligible skewness and slightly leptokurtic distributions. These descriptions were both based on measurements made using a settling column and, as noted in chapter 5 section 5.6.1, comparisons between different methods of particle size determination can be problematic. However, the particle size measurements of the barrier sands conducted in this study using laser diffractometry compare quite favourably, including those of the middle and landward barriers. The results, averaged by site, are presented in Table 6.2.1. On average, the barrier dune sands were found to comprise moderately well sorted fine to medium grained sands, which are slightly skewed towards coarse material and possess mesokurtic to leptokurtic distributions. The average mean grain size is 289.5 µm, sorting is 0.66, skewness is -0.11 and kurtosis is 1.34. These characteristics are broadly typical of coastal-dune sands (e.g. Kasper-Zubillaga and Carranza-Edwards, 2005; Saye et al., 2006).

Exceptions to the average particle size characteristics of the barrier sands are provided by the Groenvlei, West Swartvlei, KT section and Goukamma sample groups. At Groenvlei and West Swartvlei, the sampled material contains a larger proportion of coarse grains than the barrier average (20.1 % and 18 % respectively, compared to the total barrier dune average of 9.6 %), and a corresponding greater degree of negative skew (Table 6.2.1). Conversely, the KT section samples contain a greater proportion of silt and clay sized material than average, are poorly sorted, very negatively skewed, and very leptokurtic. The two Goukamma samples are quite different to one another (see site description in section 6.1.4.2), and for this reason are listed individually in Table 6.2.1. Shfd09070 is a well sorted, medium grained sand with a nearly symmetrical mesokurtic distribution, similar to the majority of the other barrier sands. Conversely, Shfd09069 has much more in common with the KT section samples, being a poorly sorted, finer grained sand with a strong negative skew and a very leptokurtic distribution.

Table 6.2.1 Grain size parameters of the barrier dune samples. N = number of samples results are averaged from. Note that where multiple samples were collected from a single site data has been averaged, and overall barrier averages are based on all individual samples not site averages.

	N	Coarse sand (%)	Medium sand (%)	Fine sand (%)	Silt (%)	Clay (%)	Median (μm)	Mean (μm)	Sort	Skew	Kurtosis	Carbonate (%)
Seaward barrier												
Klein Krantz	2	3.4	39.4	53.8	3.2	0.2	233.7	235.3	0.61	-0.05	1.28	29.9
Elandsvlei	5	8.8	66.8	23.2	1.2	0	313.8	314.2	0.51	-0.02	1.13	18.7
KT section	7	7.4	56.5	27.6	7.9	0.7	291.4	260.3	1.06	-0.4	2.02	8.1
Gerickes Point	11	8	38.5	51.2	2.3	0	259	257.7	0.62	-0.05	1.24	29.3
Groenvlei	5	20.1	62.7	14.8	2	0.4	369.3	361.8	0.67	-0.11	1.43	32.5
Buffels Bay	1	0.8	34.8	61.6	2.8	0	224.1	222.9	0.49	-0.09	1.27	33.2
Holocene dunes	6	5.4	55.7	38.9	0	0	275.8	277.8	0.5	0	1.1	27
Avg	**37**	**8.7**	**51.7**	**36.5**	**2.9**	**0.2**	**287.8**	**281**	**0.67**	**-0.11**	**1.37**	**23.8**
Middle barrier												
Rondevlei	2	10.8	64.8	24.4	0	0	323.3	322.1	0.49	-0.02	1.08	16
W Swartvlei	3	18	56.9	22.1	2.9	0.1	350.2	342.4	0.64	-0.17	1.33	11.2
E Swartvlei	3	10.5	67.9	18.4	1.8	0	348.7	344.7	0.58	-0.12	1.28	23
Avg	**8**	**15.2**	**61.7**	**21.3**	**1.8**	**0**	**342.9**	**338.2**	**0.58**	**-0.11**	**1.25**	**16.8**
Landward barrier												
N Swartvlei	2	8.4	62.3	29.2	0.1	0	304.2	304.5	0.51	0	1.05	13.3
Goukamma (Shfd09069)	1	4.2	44	38.5	12.6	0.7	244.5	194.9	-1.32	-0.53	1.84	0.5
Goukamma (Shfd09070)	1	5.1	58.3	36.4	0.2	0	280.3	281.2	-0.5	0.01	1.06	19
Avg	**4**	**6.5**	**56.7**	**33.3**	**3.2**	**0.2**	**283.3**	**271.2**	**0.71**	**-0.13**	**1.25**	**11.5**
Total barrier dune avg	**49**	**9.6**	**53.8**	**33.7**	**2.7**	**0.2**	**296.5**	**289.5**	**0.66**	**-0.11**	**1.34**	**21.8**

The carbonate content of the barrier sands varies widely both within and between the different barriers. The seaward barrier sands average 23.8 % carbonate, though the KT section average is only 8.1 % (Table 6.2.1). Bateman et al. (2004) found similarly carbonate-poor sands at the nearby Otto Sands site, which they described as showing no evidence of leaching or residual calcification, and thus attributed to a possible switch from marine to terrestrial sediment supply.

The average carbonate content of the middle and landward barriers is 16.8 % and 11.5 % respectively. Whilst their lower values compared to the seaward barrier average could reflect the smaller number of samples analysed, it could also be a result of longer-term decalcification via meteoric water undersaturated in carbonate percolating through the dunes. This is supported by the low carbonate content (0.1 %) of sample Shfd09081 obtained from 2.6 m depth at the crest of the middle barrier at the West Swartvlei site, compared to two samples obtained from greater burial depths at the same site (Shfd08080 and Shfd08082 at 24.8 m and 44.2 m, with carbonate contents of 14 % and 19.6 % respectively) (sample carbonate contents are listed individually in Appendix 1). However, samples from elsewhere on the middle barrier

crest retain relatively high carbonate contents (Shfd09078 and Shfd09079 from Rondevlei, at 15.7 % and 16.3 % and Shfd08183 from east Swartvlei at 24.6 %).

Least squares regression of sample OSL ages vs. carbonate content (Figure 6.2.1a) reveals a weak negative correlation between the two (R^2 = 0.12) that is statistically significant at the $p<0.05$ level. The correlation between carbonate content and burial depth is weaker (R^2 = 0.06) and insignificant at $p<0.05$ (Figure 6.2.1b). However, importantly, if the KT section samples are considered separately the correlation between carbonate content and depth is strong (R^2 = 0.66, statistically significant at $p<0.05$), clearly demonstrating the relatively low carbonate content of these samples is due to post-depositional modification.

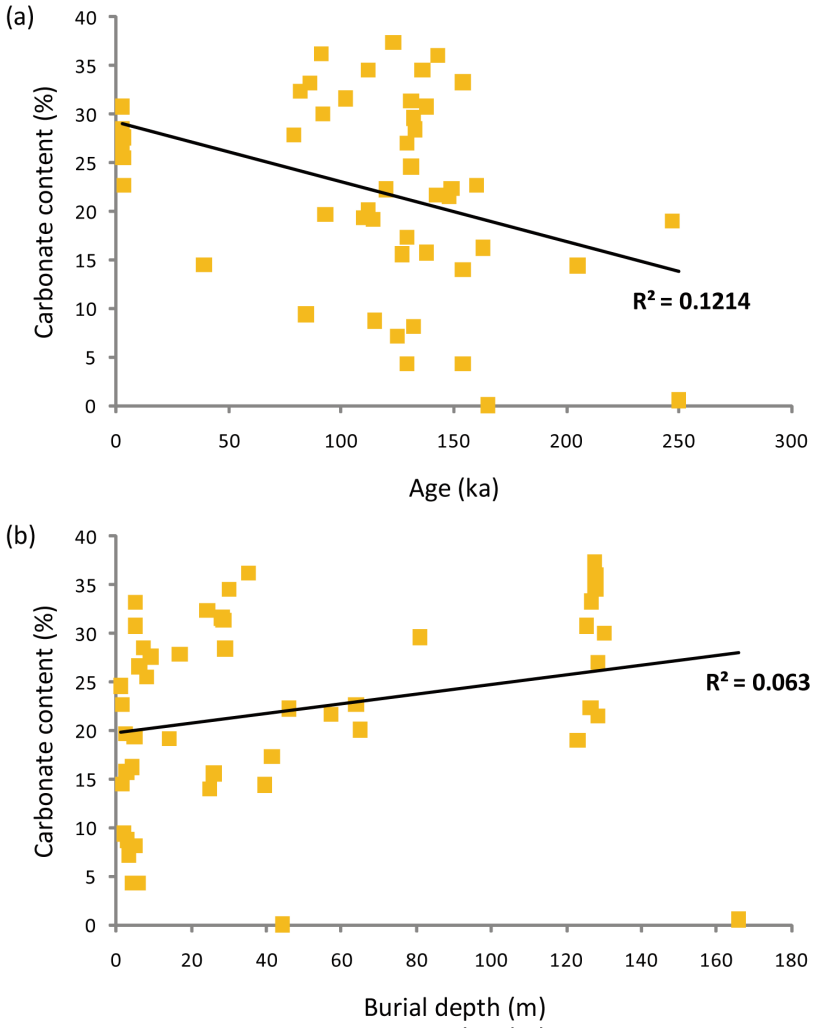

6.2.1 Biplots of: (a) carbonate content vs. sample OSL ages; and (b) carbonate content vs. burial depth for all barrier dune samples from this study plus KT section samples (data from Carr et al. (2007)) and Holocene dunes (data from Bateman et al. (2011) and Carr et al. (2010a)).

6.2.2.1 Similarity of the seaward, middle and landward barrier sands

Principal component analysis was used to assess the degree of similarity between the particle size distributions of the seaward, middle and landward barrier sands, with the results

shown in Figure 6.2.2. A CLR transformation was performed on the dataset prior to analysis in order to avoid autocorrelation issues. Although the first two PCs extracted are able to explain 86 % of variance within the dataset, Figure 6.2.2 illustrates that PCA fails to separate between the barriers, with the fields defined by all three overlapping one another.

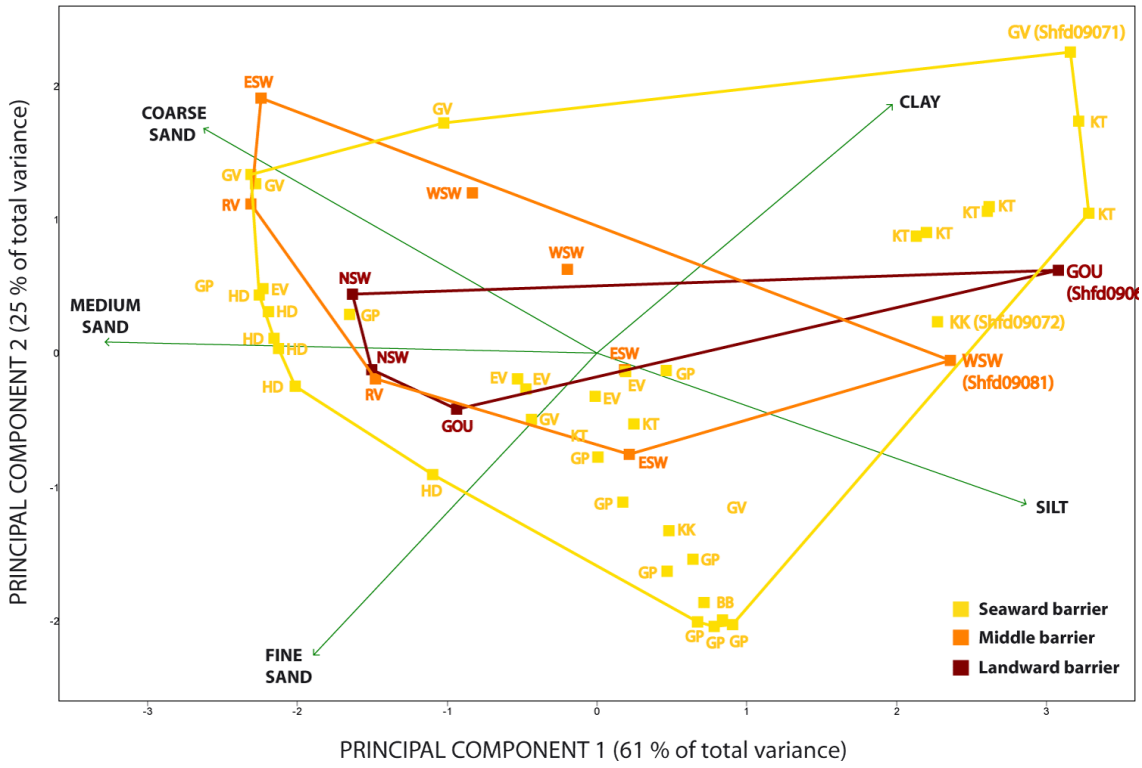

6.2.2 Biplot of PCA performed on grain size distribution data for the barrier dune samples. Loadings for the PCs are given in Table 6.2.2. Certain samples referred to in text are labelled individually. Others are labelled by site: HD = Holocene dunes; KK = Klein Krantz; EV = Elandsvlei; KT = KT section; GP = Gerickes Point; GV = Groenvlei; BB = Buffels Bay; RV = Rondevlei; WSW = West Swartvlei; ESW = East Swartvlei; NSW = North Swartvlei; GOU = Goukamma.

It is possible to make some distinctions within the PCA results, particularly within the seaward barrier. These can be assessed according to the loadings of each PC, given in Table 6.2.2. PC 2 has strong negative weightings on fine sand and silt, concentrating the majority of Gerickes Point samples between these poles (Figure 6.2.2). Conversely, PC 1 has strong negative weighting on coarse and medium grained sands, highlighting the importance of these size fractions in the Holocene dune samples. PC 1 also has positive weighting on silt and clay, and displaces the KT section and Goukamma (Shfd09069) samples towards these poles, along with samples from Groenvlei (Shfd09071) and West Swartvlei (Shfd09081). It is interesting to note that all of these samples, except Shfd09071, were previously noted as possessing relatively low carbonate contents, suggesting their increased fine fractions may be a result of increased weathering. This possibility is explored further below.

Table 6.2.2 Loadings of first two principal components produced using PCA of grain size distribution data for the barrier dune samples, as plotted in Figure 6.2.2.

Variable	PC1	PC 2
Coarse sand	-0.45	0.47
Medium sand	-0.56	0.02
Fine sand	-0.33	-0.63
Silt	0.5	-0.31
Clay	0.34	0.52

If the silt and clay contents of the barrier sands are primary deposits that were transported along with the sand fraction, they should show a positive correlation with the fine sand fraction: conversely, if they represent authigenic material produced by *in situ* weathering or pedogenesis of the dune sands, then concentrations should be unrelated to fine sand content (Muhs et al., 1996). Least squares regression of the silt and clay content vs. fine sand fraction of all barrier dune samples (excluding the four samples that contain zero silt and clay) yields an R^2 value of only 0.02 (Figure 6.2.3). The relationship is insignificant at the $p<0.05$ level, strongly indicating that variation in the clay and silt content of the samples is attributable to post-depositional processes rather than a change in sediment source or transport regime.

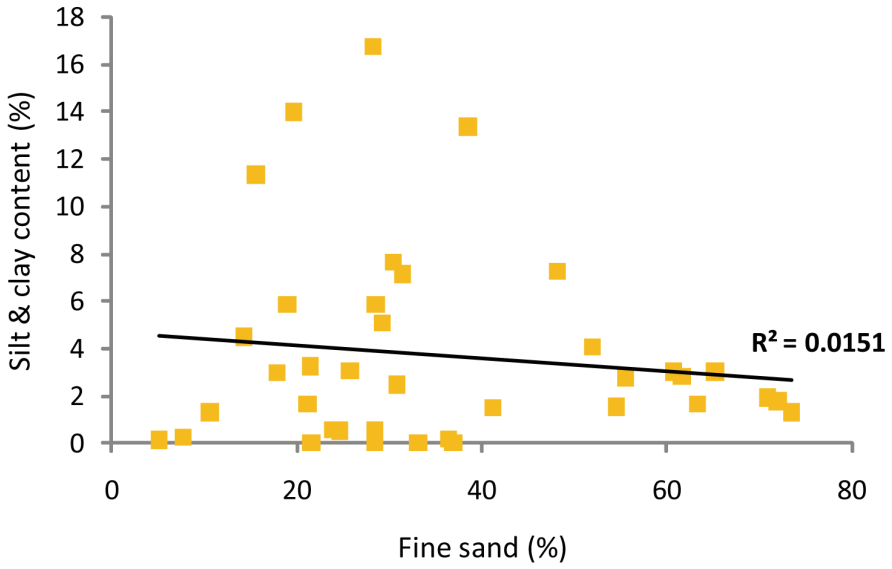

6.2.3 Biplot of combined silt and clay content as a function of the fine sand fraction for barrier dune samples. Plot excludes ten samples which possess zero combined silt & clay content: five of the six Holocene dune samples, Shfd08184 from Elandsvlei, Shfd08188 and Shfd08189 from Groenvlei, Shfd08181 from East Swartvlei, and Shfd09078 from Rondevlei.

As per the particle size data, the graphical moment statistics calculated from the barrier dune sands (given in Table 6.2.1) do not demonstrate any consistent differences or trends between the seaward, middle and landward barriers. Least squares regression of mean

grain size against the various graphical moment statistics reveal no statistically significant correlations between any of these variables, with R^2 values of 0.06 (mean size vs. sorting), 0.04 (mean size vs. kurtosis) and 0.04 (mean size vs. skewness), all of which are insignificant at the P<0.05 level. Biplots of these variables are shown in Figure 6.2.4.

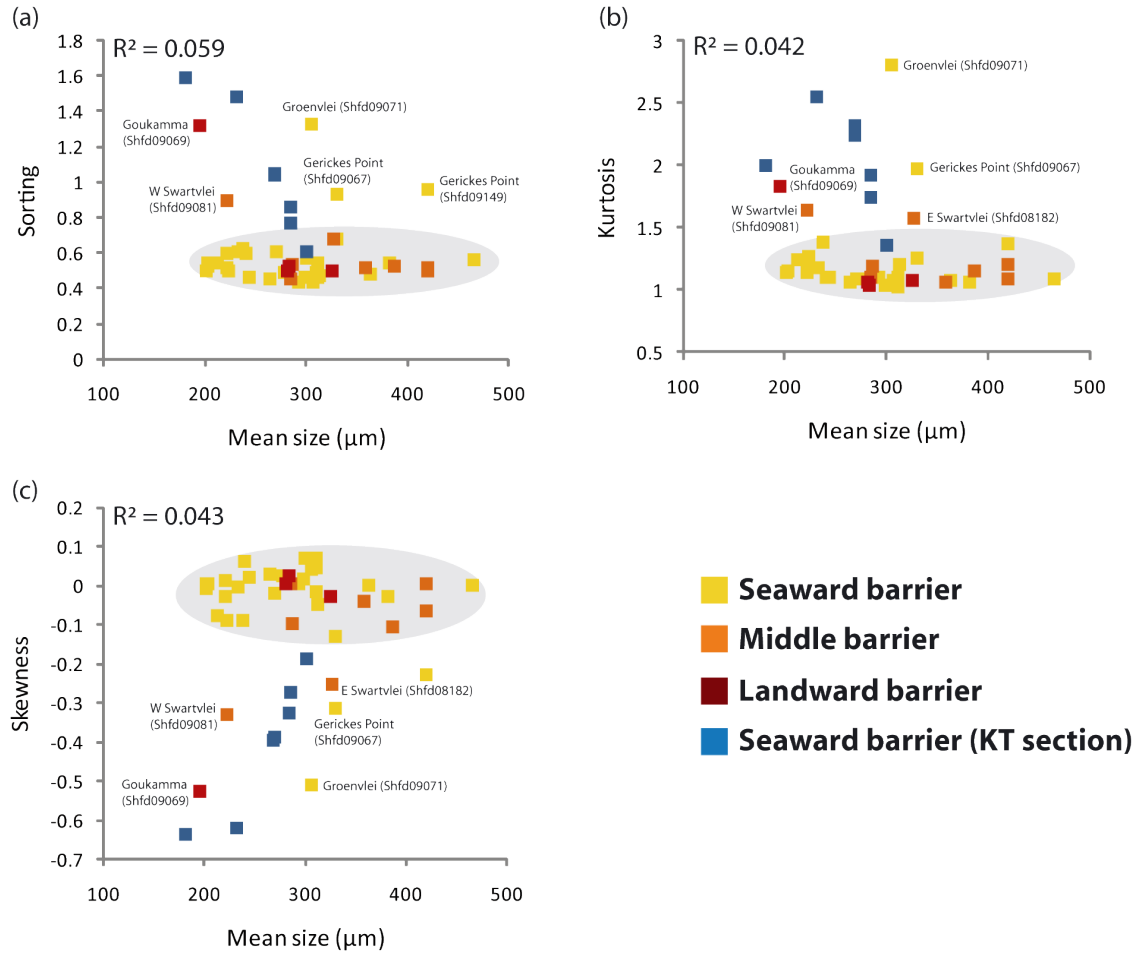

6.2.4 Biplots of mean grain size vs. (a) sorting; (b) kurtosis; and (c) skewness for the barrier dune samples. Shaded areas encompass majority of barrier samples. Certain outliers referred to explicitly in the text are labelled individually.

The seaward barrier sands are slightly more leptokurtic than the middle or landward barriers, but this is primarily due to the KT section samples (which have a kurtosis value of 2.02, compared to the seaward barrier average of 1.37) (Table 6.2.1). The KT section samples are thus plotted as a separate group in Figure 6.2.4 and appear quite distinct to the majority of other samples, except those outliers identified previously on the basis of particle size distribution and carbonate content: Shfd09069 (Goukamma) and West Swartvlei (Shfd09081); and also single samples from Gerickes Point (Shfd09067) and East Swartvlei (Shfd08182). All of these samples, labelled individually in Figure 6.2.4, display greater kurtosis, poorer sorting and increased negative skew relative to the barrier dune average. Shfd09081 was obtained from

closer to the surface than the majority of other barrier samples (burial depth of 2.6 m) as were the KT section samples (burial depths of 1-6 m: Carr et al., 2007) and their deviation from the average barrier characteristics are thus interpreted as reflecting increased pedogenesis/weathering rather than a change in provenance.

6.2.2.2 Summary

A relative increase in the fine sand fraction of dune sands suggests either a change in sediment source or increased transport distance (Muhs et al., 1996). The majority of the Gerickes Point samples have an increased fine fraction relative to the barrier sand average, but given the similarly fine particle size distributions of samples from some other sites (e.g. Buffels Bay and Klein Krantz), and the coarser nature of several other Gerickes Point samples (illustrated in Figure 6.2.2), these differences are interpreted as reflecting small-scale variations in sediment transport rather than a major change in transport regime and/or sediment source. The same is true for the coarser nature of the Groenvlei samples, which also fall within the field defined by other barrier samples (Figure 6.2.1). The KT section samples can be distinguished based on kurtosis, skewness and sorting values significantly different from the average, but these characteristics are also shared by other barrier crest samples (Figure 6.2.4), and in all instances the differences can be associated with lesser burial depths and/or reduced carbonate content. They are thus interpreted as reflecting increased pedogenesis/weathering rather than a change in sediment source. There also seems to be a general age-related reduction in carbonate content, with the middle and landward barriers containing successively less than the seaward barrier. Particle size distributions are thus interpreted as indicating no significant changes in provenance or transport regime between the seaward, middle and landward barriers, or between the KT section, Holocene dunes and other seaward barrier samples.

6.2.3 Possible local sediment sources

The particle size distributions, graphical moment statistics and carbonate contents of the possible local source sediments for the barrier sands are given in Table 6.2.3 (averaged by site), and are described in the following paragraphs.

The characteristics of the coversands are largely consistent across the three sample sites, comprising poorly sorted fine grained sands with very negative skew and very leptokurtic distributions. Their average mean grain size is 190.5 µm, sorting is 1.39, skew is -0.48 and

kurtosis is 1.73 (Table 6.2.3). This contrasts slightly with the results of Holmes et al. (2007), who reported the coversands as having broadly similar grain size distributions to the results obtained in this study but found them to be well or very well sorted. The difference is attributed to different measurement techniques (Holmes et al. used the settling column method), and the new results presented here are assumed to be reliable. Least squares regression of the fine sand content of the coversands vs. their silt and clay content yields an R^2 value of only 0.03 (with the relationship insignificant at the $p<0.05$ level), suggesting that, like the barrier sands, this material represents post-depositional breakdown of larger grains rather than primary deposition. The carbonate content of all the coversand samples analysed was minimal (<0.2 %). Holmes et al. (2007) reported two samples with slightly higher carbonate contents from Makhulu Quarry (2.3 % and 5 %), and interpreted the coversands in general to be decalcified rather than devoid of carbonate in the first instance.

The upstream river sediments are all poorly or moderately sorted coarse sands (mean size = 615.2 µm), with varying degrees of skew and kurtosis (Table 6.2.3). As the particle size distribution of river bedload depends on a variety of factors (channel morphology, stream power etc.) and can vary within single sampling sites (Noda, 2005), a greater degree of intra-sample variation compared to material obtained from other depositional settings is expected. All the downstream river sediments are medium grained sands (mean = 394.1 µm) except for the Kaaimans and Karatara river samples, which possess coarser means closer to the upstream material (589 µm and 530.2 µm respectively). Similar to their upstream counterparts, the downstream river samples are poorly to moderately sorted and display varying degrees of skew and kurtosis. As would be expected carbonate is largely absent from all the river samples, supporting the assertion that its presence in the barriers is attributable to marine input.

The lagoon sediments comprise moderate to well sorted medium grained sands, with approximately symmetrical mesokurtic distributions (mean size = 313.4 µm, sorting = 0.52, skew = 0, kurtosis = 1.04). They contain a significant amount of carbonate (averaging 14.7 %). The beach sands are very similar to the lagoon sediments, also being moderate to well sorted medium grained sands with nearly symmetrical mesokurtic distributions (mean size = 300.1 µm, sorting = 0.48, skewness = 0.03, kurtosis = 1.09) (Table 6.2.3).

Table 6.2.3 Grain size parameters of possible local source areas for the Wilderness barrier dune sands. N = number of samples results are averaged from. Note that where multiple samples were collected from a single site data has been averaged, and overall barrier averages are based on all individual samples not site averages

	N	Coarse sand (%)	Medium sand (%)	Fine sand (%)	Silt (%)	Clay (%)	Median (μm)	Mean (μm)	Sort	Skew	Kurtosis	Carbonate (%)
Coversands												
Karatara Road	4	4.3	45	38.1	11.5	1.2	224.3	195.3	1.38	-0.43	1.99	0.04
Barrington Road	4	5.4	45.2	37.1	11.6	0.7	249.9	196.5	1.37	-0.49	1.58	0.14
Makhulu Quarry	3	7.1	48.7	29.4	13.9	0.9	236.6	176.1	1.43	-0.53	1.56	0.18
Avg	**11**	**5.5**	**46.1**	**35.4**	**12.2**	**0.9**	**237**	**190.5**	**1.39**	**-0.48**	**1.73**	**0.12**
River sediments – upstream												
Kaaimans upper	1	73.7	12.1	9.2	4.9	0	749.5	633.4	1.17	-0.48	1.77	0.04
Touw upper	1	69.8	22.5	7.3	0.4	0	666.9	635.5	0.82	-0.18	1.16	0.02
Hoekraal upper	1	61.5	33.3	5.1	0.2	0	572.8	569.4	0.69	-0.04	1.05	0.06
Karatara upper	1	60.2	36.6	3.2	0	0	556.3	560.8	0.62	0.03	1.04	0.03
Goukamma	1	75	21.4	2.9	0.8	0	688	677.1	0.69	-0.07	1.09	0
Avg	**5**	**68**	**25.2**	**5.5**	**1.2**	**0**	**646.7**	**615.2**	**0.8**	**-0.15**	**1.22**	**0.03**
River sediments – downstream												
Kaaimans lower	1	65.3	25.1	6.1	3.5	0	612	589	0.91	-0.24	1.47	0
Touw lower	1	48.5	41.8	9.2	0.5	0	491.4	486	0.71	-0.07	1.11	0.11
Duiwe	1	32	30.8	32.2	5	0	352.1	299.2	1.25	-0.27	0.9	0.23
Diep	1	36.9	43.7	15.7	3.7	0	416	409.6	0.9	-0.13	1.21	0
Wolwe	1	30.8	45.3	23.5	0.4	0	371.3	377.9	0.86	0.03	1.04	0.1
Hoekraal Lower	2	19.2	40.7	34.6	5.6	0	300.2	287	1.1	-0.2	1.2	0.04
Karatara lower	1	63.9	18.6	11.6	5.8	0	644.3	530.2	1.24	-0.46	1.44	0.17
Knysna	1	24.3	61.1	13.8	0.8	0	381.1	381.5	0.59	0	1.07	0
Salt	1	8.6	58.2	32.9	0.4	0	294.8	293.9	0.58	-0.04	1.12	0.05
Avg	**10**	**34.9**	**40.6**	**21.4**	**3.1**	**0**	**416.4**	**394.1**	**0.92**	**-0.16**	**1.18**	**0.08**
Beach sands												
Wilderness	1	8.4	69.4	22.2	0	0	317.3	318.4	0.47	0.01	1.09	25
Klein Krantz	1	29.9	63.7	6.4	0	0	419.8	422.5	0.49	0.03	1.09	26.9
Gerickes Point	1	11.1	68.1	20.8	0	0	328.4	328.6	0.49	0	1.06	26.9
Sedgefield	1	3.8	49.3	46.8	0.1	0	256.4	259.2	0.5	0.05	1.06	33.2
Buffels Bay	1	0.7	27.8	71.3	0.2	0	210.8	212.3	0.45	0.03	1.13	32
Avg	**5**	**10.8**	**55.7**	**33.5**	**0.1**	**0**	**306.5.3**	**308.2**	**0.48**	**0.03**	**1.09**	**28.8**
Lagoon sediments												
Knysna	1	5.9	54.7	39.3	0.1	0	274.8	277.3	0.52	0.04	1.04	18.7
Swartvlei 1	1	10.8	61.3	27.7	0.2	0	313.9	311.7	0.56	-0.04	1.04	11.9
Swartvlei 2	1	14.4	70.6	15.2	0	0	351.2	351.1	0.48	0	1.05	13.4
Avg	**3**	**10.3**	**62.2**	**27.4**	**0.1**	**0**	**313.3**	**313.4**	**0.52**	**0**	**1.04**	**14.7**

Whether any spatial variation is apparent in beach sand size was explored by plotting particle size data according to distance along the embayment coastline, shown in Figure 6.2.5. Although based on only a small number of samples, the plot demonstrates that beach sands exhibit a gradual fining towards the east, which is to be expected given the eastward direction

of littoral drift along the southern Cape. The pattern is interrupted by the presence of coarser material at Klein Krantz than Wilderness. This likely reflects input of new sediment by the Touw River (the mouth of which is located between Wilderness and Klein Krantz), though no such coarsening occurs between the Sedgefield and Buffels Bay sample sites, which are separated by the Goukamma River. It is interesting to note that the particle size distribution of beach sands does not reflect the adjacent seaward barrier characteristics, which as discussed in the previous section are particularly fine at Gerickes Point and coarser at Groenvlei. The carbonate content of the beach sands is reasonably consistent, with the average value (28.8 %) very similar to that of the seaward barrier (which is 27.8 % if the KT section samples are excluded).

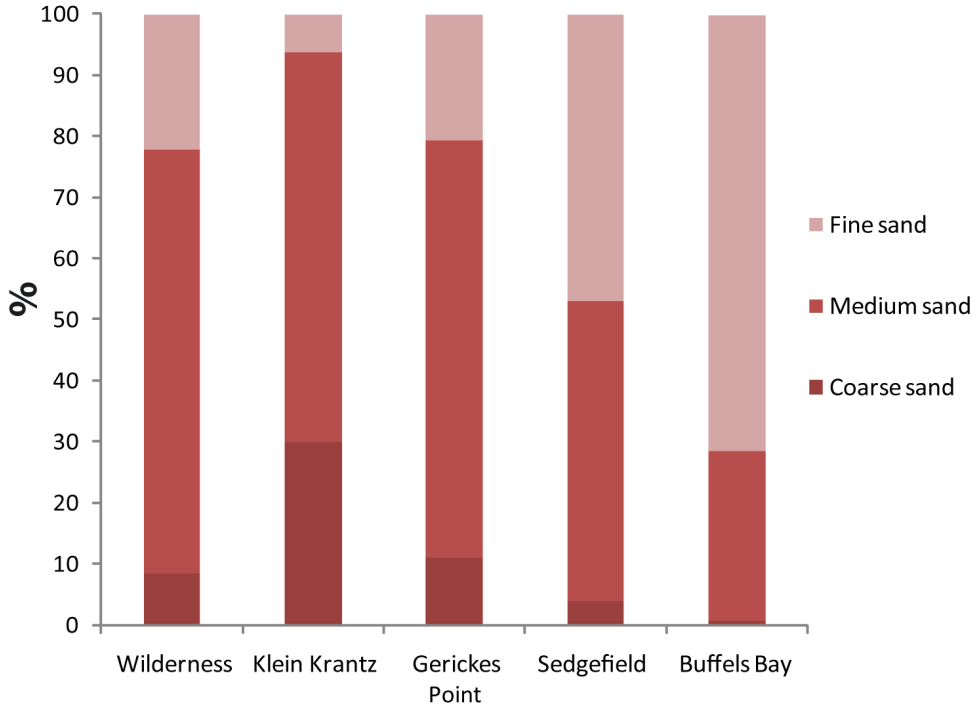

6.2.5 Grain size distribution of beach sand samples. Samples are arranged along the x-axis according to their position west-east along the Wilderness embayment. Distances of sample sites from the embayment's western edge are: Wilderness 0.9 km, Klein Krantz 8.9 km, Gerickes Point 18.2 km, Sedgefield 22 km, Buffels Bay 38 km. Note: silt content is excluded as it is ≤0.2 % for all samples.

6.2.4 Comparison of barrier dune and possible sediment source area particle size characteristics

Comparisons of the particle size distributions of the barrier dune sands and their possible local source areas are shown in Figure 6.2.6, and the graphical moment statistics in Figure 6.2.7. Figure 6.2.6 illustrates the overall high degree of similarity between the barrier

sands and the beach, lagoon and coversand samples, confirming that any of these potential sources could have provided material for dune building at Wilderness. Likewise, although the river sediments are considerably coarser than the barrier sands, they contain in both their upper and lower reaches significant quantities of fine and medium grained material. Sorting during nearshore transport once river sediment debouches into the bay and aeolian transport from the beach would, of course, select this fraction for incorporation into the dunes. Note that PCA was not conducted on the data, as to infer any specific provenance relationships based on particle size data would be spurious: aeolian entrainment and transport of sediment from any of the potential sources would concentrate their fine and medium sand fractions, making alteration of their original size distributions a certainty.

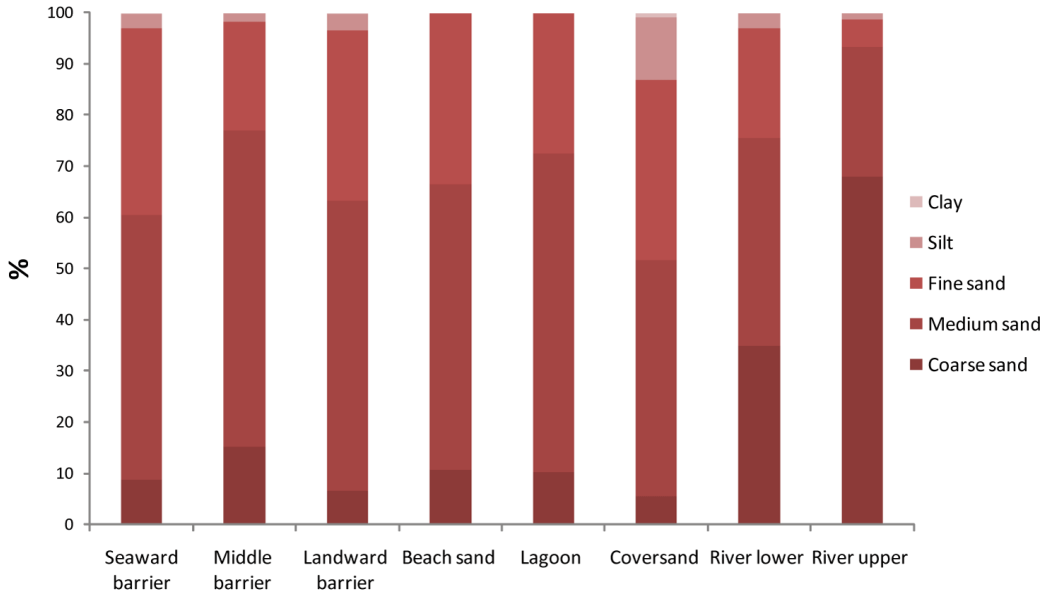

6.2.6 Comparisons of the barrier dunes and their various possible local source areas with respect to their particle size distributions. Plotted values are site averages.

That the graphical moment statistics of the lagoon sediments are uniformly much closer to those of the beach and barrier sands than the river sediments (Figure 6.2.7) suggests they represent either eroded barrier material or material from the beach, rather than sediment introduced to the lagoons by rivers. This is also supported by the high carbonate content of the lagoon sediments, contrasting with the absence of such material in the river sediment samples. For logistical reasons the lagoon samples were collected from locations close to the shoreline (see map of sample locations in chapter 4 Figure 4.14), increasing the likelihood that they are eroded barrier material. The same could potentially also be true of the beach sands: as mentioned in chapter 3 (section 3.3.1), Martin and Flemming (1986) assert erosion of the existing seaward barrier has provided a significant source of material for the

Holocene nearshore sediments at Wilderness. The similarity of the barrier sands to the lagoon and beach sands, along with the other possible sediment sources, is considered further using sediment geochemistry and heavy mineralogy in the following sections.

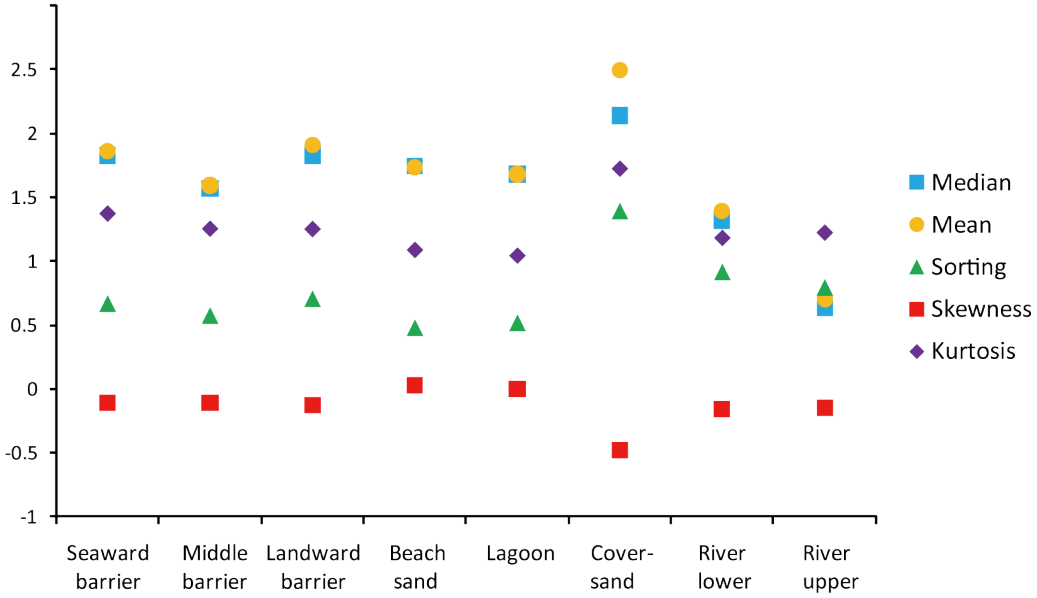

6.2.7 Comparisons of the barrier dunes and their various possible local source areas with respect to their graphical moment statistics. Plotted values are site averages.

6.2.5 Particle size summary

This section has presented the results of particle size analysis and calcium carbonate-content determination conducted on samples of the barrier sands and their various possible local sources. Differences in particle size distributions between the three barriers are generally negligible, indicating no significant changes in transport regime or sediment source between them. The KT section samples from the landward flank of the seaward barrier can be distinguished based on kurtosis, skewness and sorting values significantly different from the average barrier characteristics, but these characteristics are shared by certain other samples from barrier crests, and in all instances they can be associated with lesser burial depths and/or reduced carbonate content. They are thus interpreted as reflecting increased pedogenesis/weathering, rather than a change in sediment source.

With regard to the possible local sources of sediment for the barriers, all of them (coversands, beach sands and river and lagoon sediments) contain significant quantities of fine- and medium-grained sands, and could consequently have contributed material to the Wilderness barriers. The graphical moment characteristics of the beach, lagoon and barrier sands are almost identical, indicating a close relationship between the three.

6.3 Sediment provenancing results: geochemistry

6.3.1 Introduction

This section presents the results of geochemical analyses of the provenance of the barrier dune sands. In using trace element geochemistry for sediment provenancing purposes, there is a danger that variation can be dominated by particle size rather than parent material (e.g. Whitmore et al., 2004; Pe-Piper et al., 2008). The first stage of the analysis was thus to screen for any correlation between grain size and the elements preliminarily selected for use as provenance indicators in chapter 5. This is described in section 6.3.2. Having assessed the reliability of the dataset, selected elements were then used to explore any differences in weathering within the barrier sands, as indicated by the particle size and carbonate data considered previously. These results are presented in section 6.3.3.1. Next, trace element ratios considered to remain stable under surface weathering conditions were compared to determine whether any changes in provenance can be distinguished within the seaward barrier sands (section 6.3.3.2). Finally, the geochemical signature of the seaward barrier was compared to samples from various possible local sediment sources (local bedrock, coversands, river sediments, beach sands and lagoon sediments), in order to identify whether any of them have contributed to it (section 6.3.4). The contents of this section represent a development of the material presented in Dunajko and Bateman (2010), with the incorporation of new data and additional analyses.

6.3.2 Assessment of grain size effect on element concentrations

The elements preliminarily selected for provenance analysis in chapter 5 were Co, Cr, Hf, Nb, Th, Ti, Zr and the REE ratios La_N/Yb_N and Eu/Eu* (which incorporates the elements Gd and Sm). U was also identified as a mobile element that could be used to consider weathering. In order to identify any elements whose concentrations are primarily controlled by particle size (and are thus unsuitable for analysis), least squares regression was conducted on element concentrations vs. the percentage of material in each particle size class for all samples (barrier dunes and possible sediment sources). Due to the absence of silt and clay sized material in many of the samples, it was necessary to combine the silt, clay and fine sand fractions into a single group for comparison. Correlation between element concentrations and the fine sand fraction was also assessed separately. An example biplot is provided in Figure 6.3.1 (Cr vs. fine sand + silt + clay fractions) and the results for all size fractions and elements in Table 6.3.1.

Bedrock samples were not incorporated in this analysis as their geochemistry was established from analysis of whole-rock samples

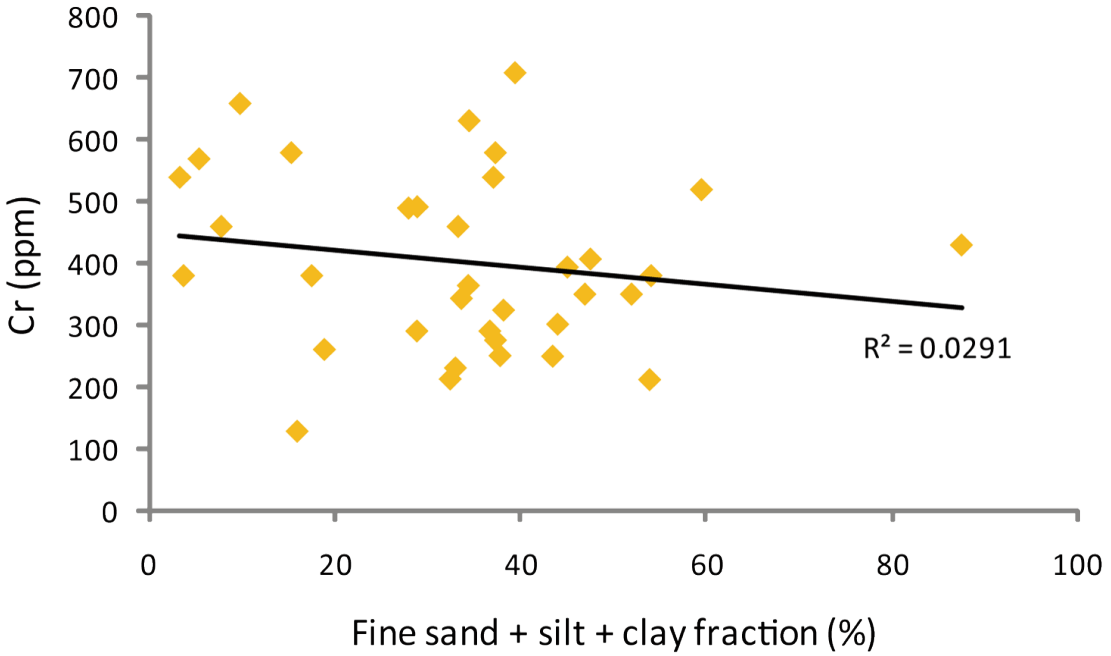

6.3.1 Biplot of Co concentration vs fine sand + silt + clay size fractions for all geochemistry samples. Relationship is insignificant at $p<0.05$ level. Note: plot excludes five samples subject to geochemical analysis (KT2-4, Shfd05026, Swartvlei Estuary aeolianite, Makhulu coversand 2 and Swartvlei lagoon 1) as sufficient sample material was not available to measure their particle size distributions.

Muhs et al. (2008) used least squares regression of element concentrations vs. particle size classes to identify elements appropriate for analysis in a study of the origin of Nebraskan loess. The highest correlation they observed was between Ti and clay content ($R^2 = 0.37$), which they still deemed a sufficiently low value to retain the element for provenance analysis (Muhs et al., 2008). Whilst many of the elements considered here have statistically significant correlations with the fine sand, and fine sand plus silt and clay fractions, all of them possess R^2 values of 0.35 or less (Table 6.3.1). This is interpreted as indicating the trace element concentrations present in the samples are primarily controlled by factors other than particle size, and they are consequently considered appropriate for investigating (with caution) provenance and weathering.

Table 6.3.1 Degree of correlation according to least squares regression (R^2) between trace element concentrations and percentage of material in different particle size fractions. Note: calculations exclude five samples subject to geochemical analysis (KT2-4, Shfd05026, Swartvlei Estuary aeolianite, Makhulu Quarry 2 and Swartvlei lagoon 1) as sufficient sample material was not available to measure their particle size distributions.

Element	Correlation with size fraction							
	Clay + silt + fine sand (R^2)	Significant at p<0.05	Fine sand (R^2)	Significant at p<0.05	Medium sand (R^2)	Significant at p<0.05	Coarse sand (R^2)	Significant at p<0.05
Co	0.01	N	0.01	N	-0.05	N	0	N
Cr	-0.03	N	-0.06	N	-0.06	N	0.09	N
Hf	0.17	Y	0.23	Y	0	N	-0.08	N
Nb	0.22	Y	0.02	Y	0	N	-0.11	N
Th	0.35	Y	0.29	Y	-0.07	N	-0.09	N
Ti	0.32	Y	0.33	Y	0	N	-0.18	Y
U	0.22	Y	0.35	Y	0.01	N	-0.17	Y
Zr	0.15	Y	0.22	Y	0	N	-0.08	N
La	0.13	Y	0.22	Y	0	N	-0.11	N
Eu	0.12	Y	0.21	Y	0.01	N	-0.11	Y
Gd	0.13	Y	0.21	Y	0	N	-0.09	N
Sm	0.12	N	0.21	Y	0	N	-0.10	N

6.3.3 Geochemistry of the seaward barrier sands

Using the elements discussed in the previous section, the geochemistry of samples obtained from three settings within the seaward Wilderness barrier was compared to determine whether any changes in provenance or weathering could be distinguished between them. The settings comprise: (1) aeolianites from the seaward flank of the barrier; (2) the KT section dune sands, from a sand quarry on the landward flank of the barrier; and (3) the Holocene dunes on the barrier crest. In addition to sample location, the three groups are also partly separable based on age, with the Holocene dune samples dating to ≤3.7 ka, the seaward flank samples aged between 86-128 ka, and the KT section samples 39-154 ka. A list of the barrier samples, their ages, and the trace element concentrations used in analysis is provided in Table 6.3.2. Results are discussed in the following sections.

Table 6.3.2 Location, age (where available) and trace element concentrations used in analysis for samples from the seaward Wilderness barrier dune.

Sample	Age (ka)	Co	Cr	Hf	Th	Nb	Zr	Ti (ppm)	U	Eu	Sm	Gd	La	Yb
Detection limit (ppm)		0.5	10	1	0.1	1	0.5	100	0.05	0.05	0.1	0.05	0.1	0.1
Seaward flank														
Shfd05026	86 ± 5[$]	1.8	220	4	2.4	3	160	800	1.95	0.42	1.9	1.87	13.5	1
Shfd05039	95 ± 4[#]	1.4	275	1	1.1	1	44	300	0.95	0.19	0.8	0.88	5.7	0.4
Shfd09149	92 ± 5	1.9	260	2	1.5	2	77	500	0.85	0.18	1.1	1.05	6.5	0.5
Shfd05049	128 ± 7[$]	0.8	212	4	2.4	4	161	1000	1.41	0.39	2.2	1.72	11.5	0.7
Swartvlei Estuary	-	1.3	198	1	1.5	1	58	400	0.95	0.19	1	0.92	6.7	0.5
KT section														
KT2-2	39 ± 2[~]	1.3	394	6	3	5	188	1500	0.83	0.56	4	2.66	16.9	0.7
KT2-3	84 ± 4[~]	0.7	343	6	1.7	5	222	1100	0.84	0.41	2.2	1.83	14.4	1
KT2-4	104 ± 5[~]	3.1	451	5	1.7	2	170	1100	0.67	0.31	1.7	1.23	10.5	0.7
KT2-6	125 ± 7[~]	1	364	4	1.5	2	146	1200	0.78	0.41	2.1	1.62	12.5	0.7
KT2-8	129 ± 7[~]	1.3	324	6	2	4	231	1500	0.88	0.52	2.9	2.13	16.2	0.8
KT2-9	132 ± 7[~]	1.8	632	6	2.3	4	221	1200	0.79	0.4	2.2	1.63	12.1	0.8
KT2-11	154 ± 8[~]	2.5	492	2	1.9	2	63	700	0.51	0.3	1.6	1.22	10.6	0.5
Holocene dunes														
Shfd05040	3.7 ± 0.1[#]	1.4	211	16	4.4	6	650	1700	2.12	0.39	2.9	2.48	17.8	1.3
Shfd04279	2.9 ± 0.2[$]	1.5	250	20	3.9	13	860	2800	2.84	1.09	6.8	4.5	31.2	1.7
Shfd04280	2.5 ± 0.1[$]	1.5	290	8	2.6	6	338	1700	2.24	0.63	3.8	2.73	17.5	1
Shfd04281	2.6 ± 0.2[$]	0.8	249	7	2.9	5	272	1600	1.85	0.47	2.4	1.9	13.1	0.9
Shfd04282	3 ± 0.2[$]	1.7	230	15	4.2	11	615	2900	2.61	1.02	6.5	4.47	28.8	1.8
Shfd04283	3.1 ± 0.2[$]	1.7	290	21	4.1	10	907	2800	2.70	0.92	5.4	4.25	23.1	1.6

[$] Age from Bateman et al. (2011)

[#] Age from Carr et al. (2010a)

[~] Age from Carr et al. (2007)

6.3.3.1 Weathering

Weathering of the seaward barrier samples was assessed by considering their Th/U ratio, which tends to increase with weathering as U is oxidised and lost whilst concentration of the immobile element Th remains constant. In Dunajko and Bateman (2010) differences were noted in the Th/U values of the samples from the three different seaward barrier settings, with the seaward flank and Holocene dune samples possessing similar values but those of the KT section being higher, indicating they have undergone increased weathering (Figure 6.3.2a). The elevated Th/U ratios of the KT section samples was interpreted as reflecting their greater age. Incorporating the Th/U ratios of additional barrier samples generated using GS for dosimetry purposes (as presented in section 6.1) makes the relationship between Th/U and sample age less distinct (Figure 6.3.2b), though the KT section samples still remain towards the high end of the range. Th possesses a positive correlation of 0.35 with finer size fractions (Table 6.3.1), so it is likely that the elevated Th/U ratio of the KT section samples is a reflection of their increased silt and clay content relative to the other barrier sands (see section 6.2.2). However, the particle size data confirms that their increased clay and silt content is attributable to post-depositional processes such as weathering (Figure 6.2.3)

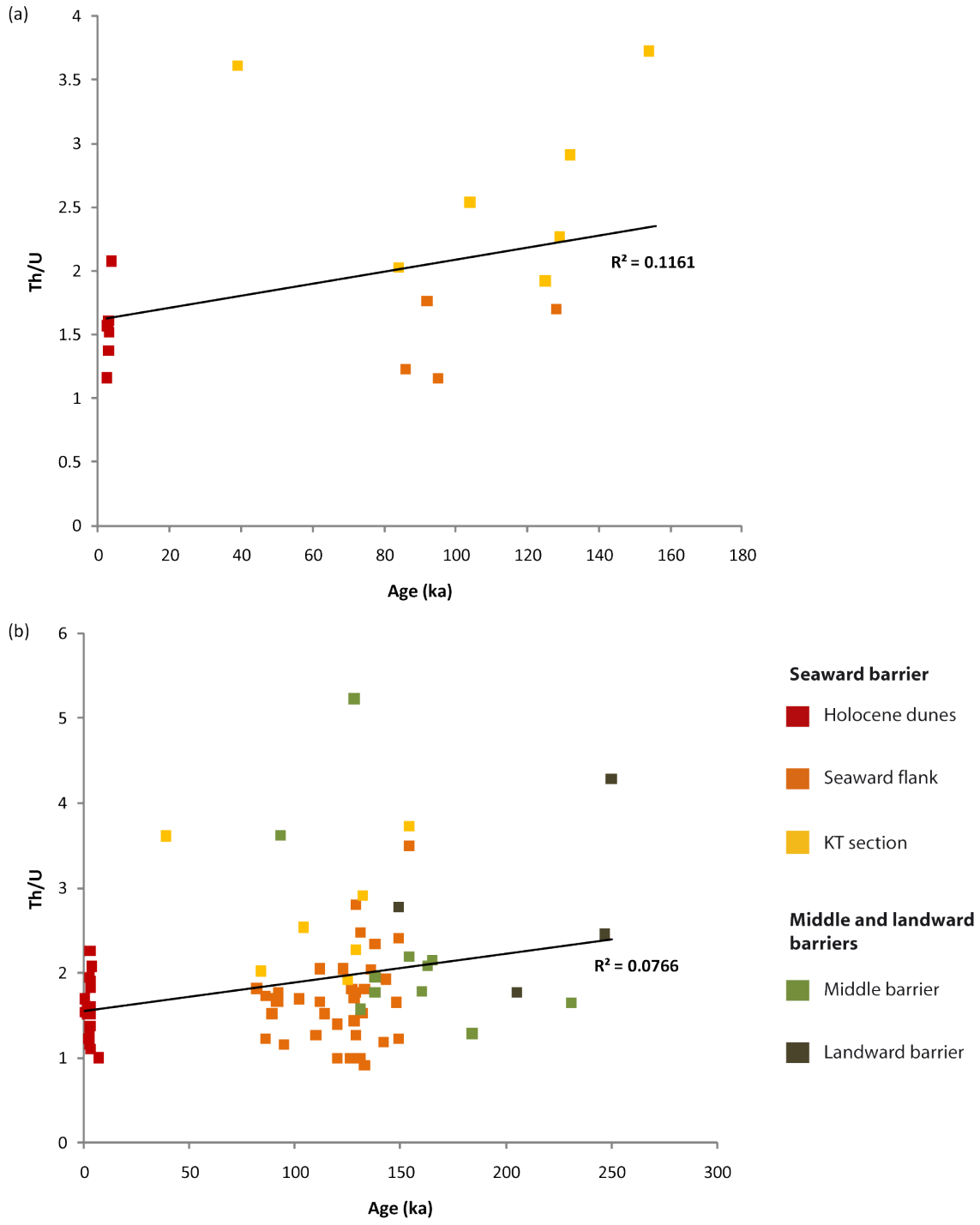

6.3.2 Biplots of Th/U vs. sample age: (a) seaward barrier samples only (element concentrations determined using ICP-MS), originally presented in Dunajko and Bateman (2010); (b) incorporating additional samples with Th/U ratios measured using GS for OSL dating purposes, from this study and from Bateman et al. (2011). Note: in both plots one sample from the seaward flank (Swartvlei estuary) is excluded as it is undated. Its Th/U ratio is 1.7, within the range defined by the other seaward flank samples.

Although the KT section samples are more weathered than the younger Holocene dune samples, least squares regression of all the barrier sample ages vs. Th/U values indicates the two variables are not related (R^2 = 0.08) (Figure 6.3.2b). There is also no statistically

significant relationship between Th/U and sample burial depth (Figure 6.3.3), though the small number of samples with particularly high Th/U ratios (arbitrarily defined as >3) (KT2-2, KT2-11, Shfd09081, Shfd05046 and Shfd09069) all have burial depths of ≤6 m, with the exception of Shfd09069 (landward barrier, Goukamma site). This sample was identified previously as displaying unusually pedogenised characteristics (section 6.1.4.2), indicating it may have undergone surfical weathering before later being buried by additional barrier accumulation.

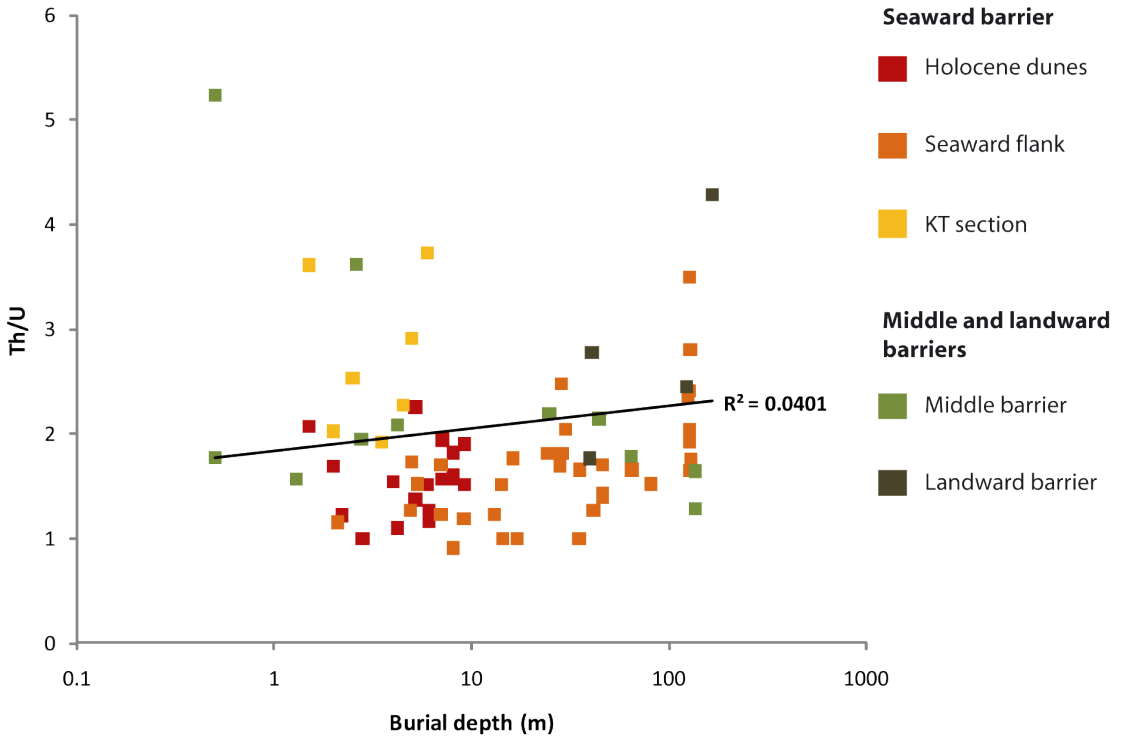

6.3.3 Biplot of Th/U vs. sample depth for barrier dune samples, incorporating seaward barrier samples with element concentrations determined using ICP-MS and additional samples with Th/U ratios derived using gamma spectrometry for OSL dating purposes, from this study and from Bateman et al. (2011).

6.3.3.2 Provenance

The chondrite-normalised average REE compositions of the seaward flank, KT section and Holocene dune seaward barrier samples are shown in Figure 6.3.4, where they are compared to the UCC average (the individual REE concentrations of the samples are provided in Appendix 2). All the barrier sample groups display characteristics similar to typical quartz-rich sediments and sandstones, as described by Taylor and McLennan (1985): relative enrichment in the LREE (La to Sm), a negative Eu anomaly, depleted heavy REE (Eu to Lu), and low overall REE abundances compared to the UCC average. However, all sample groups also exhibit a significant negative Ce anomaly atypical of average coarse-grained quartzitic material.

Seawater is characterised by a pronounced negative Ce anomaly, which is inherited by marine carbonates and authigenic marine minerals (e.g. Nothdurft et al., 2004; Wigley and Compton, 2007). Its occurrence in the barrier samples thus potentially reflects the presence of marine carbonate (see section 6.2) and glauconite (see section 6.4) within them.

The Holocene dunes are relatively more enriched in REE than the KT section and seaward flank samples (Figure 6.3.4). REE are typically concentrated in the clay-sized fraction of sediments (Henderson, 1984), but as silt and clay sized material is absent from the Holocene dune samples (Table 6.2.1) this cannot be the reason for their greater REE enrichment. Rather, it is interpreted as reflecting the higher concentration of zircon (in which REE are also relatively enriched) present in the Holocene dunes (discussed later in this section and in section 6.4).

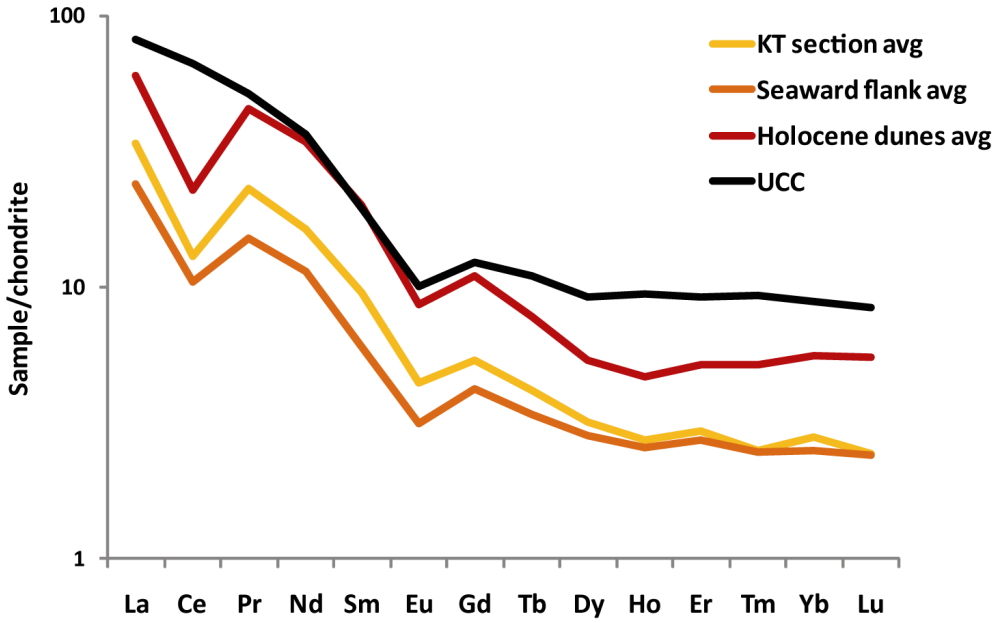

6.3.4 Chondrite-normalised REE concentrations of seaward barrier samples (values averaged from all samples within each group). The upper continental crust (UCC) average is also shown (values from Taylor and McLennan, 1985).

Comparing Eu/Eu* and La_N/Yb_N permits a more quantitative analysis of differences in REE concentrations, and consequently whether or not a change in sediment provenance can be inferred from them. A biplot of these ratios is given in Figure 6.3.5. Typical UCC material possesses an Eu anomaly of 0.6-0.7 and a La_N/Yb_N value of ~9.2 (McLennan et al., 1993). Most of the barrier samples fall within or just outside the UCC Eu/Eu* range, and are slightly more enriched in LREE (higher La_N/Yb_N). The three outliers with significantly lower Eu anomalies comprise one sample from each seaward barrier group (Shfd09149, KT2-2 and Shfd05040), none of which share anything extraordinary in common with respect to their sedimentary

characteristics or depositional settings. Several of the KT section samples have a relatively high La_N/Yb_N ratio (KT2-2, KT2-8 and KT2-11), but overall the plot does not clearly discriminate between any of the sample groups. Taylor and McLennan (1985) counsel that the analytical uncertainty inherent in evaluating the low REE abundances of typical quartz-rich sediments (see detection limits in Table 6.3.2) can explain such variability.

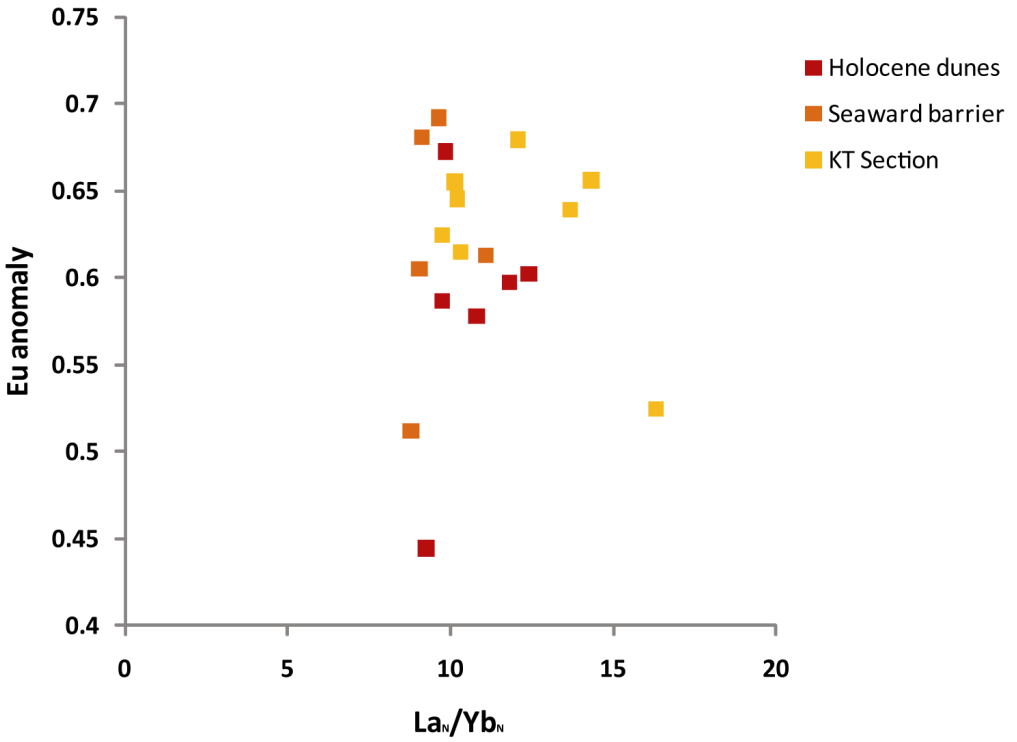

6.3.5 Eu/Eu* vs La_N/Yb_N for samples from the seaward barrier.

Ternary plots of Th-Co-Hf and Th-Cr-Zr are presented in Figure 6.3.6. All of these elements occur in association with heavy minerals, though Zr and Hf are hosted almost exclusively in the most stable of mineral species, zircon. Enrichment of Zr and/or Hf can thus be interpreted as indicating a greater concentration of zircon, and in turn a more mineralogically mature sediment. Sediment maturity can be a reflection of several possible factors. These are: (i) inheritance of mature material from sediment source; (ii) physical weathering during transport; and/or (iii) post-depositional chemical weathering during long periods of dune stability (Muhs, 2004). Hydraulic sorting can also result in a concentration of zircon grains (Garzanti and Andò, 2007), but as all the samples considered here are of aeolian origin differences due to sorting should be minimal.

Of the three barrier sample groups, the Holocene dunes are displaced most significantly towards the Hf and Zr poles (Figure 6.3.6). Though the abundance of Hf and Co are

low relative to the element detection limits (Table 6.3.2), the consistency of the grouping across the two plots provides confidence the ratios reflect actual sediment characteristics. Increased chemical weathering can be discounted as the cause of enriched zircon in the Holocene dunes according to the Th/U ratios discussed previously. Another possible explanation is provided by Martin and Fleming (1986), who assert that erosion of existing seaward Wilderness barrier aeolianite has provided a significant source of material for the Holocene nearshore sediments at Wilderness. It follows the Holocene dunes on the seaward barrier crest would be derived from these sediments, and recycling of sediment in this way would increase concentration of the stable mineral zircon.

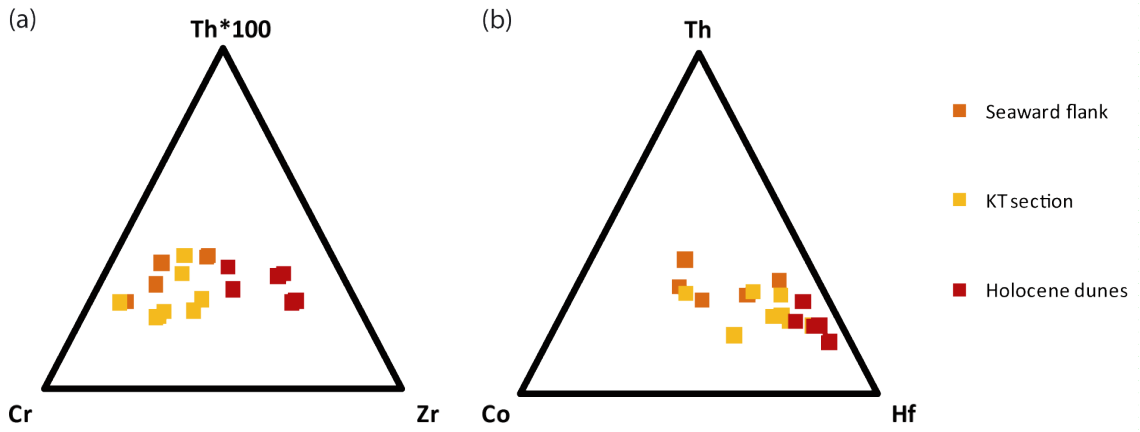

6.3.6 Ternary plots of (a) Th*100-Cr-Zr and (b) Th-Co-Hf for seaward barrier samples. In plot (a) the scaling factor was used to bring the fields closer to the centre of the diagram (after Bhatia and Crook, 1986).

The question of whether the relative importance of Zr and Hf in the Holocene dunes represents: (i) a concentration of stable zircon grains derived from recycling of seaward barrier aeolianites; or (ii) a change to an entirely different sediment source, was addressed by examining Zr/Hf ratios. Because these elements are hosted almost exclusively in zircon grains, this ratio is arguably the most reliable of provenance indicators. If the seaward barrier sands all originate from the same source, the ratio should be approximately equal. Results are shown in Figure 6.3.7a plotted against Cr/Co, another immobile trace element ratio that should also be indicative of provenance. Figure 6.3.7a demonstrates quite a different pattern to the ternary plots in Figure 6.3.6, with the Holocene dune and seaward flank samples largely overlapping. This suggests no change in source between the two, and consequently that the concentration of zircon in the Holocene dune samples most likely represents a loss of less stable mineral species as seaward barrier aeolianites have been recycled to form the younger dunes on the barrier crest, rather than a shift to a different sediment source.

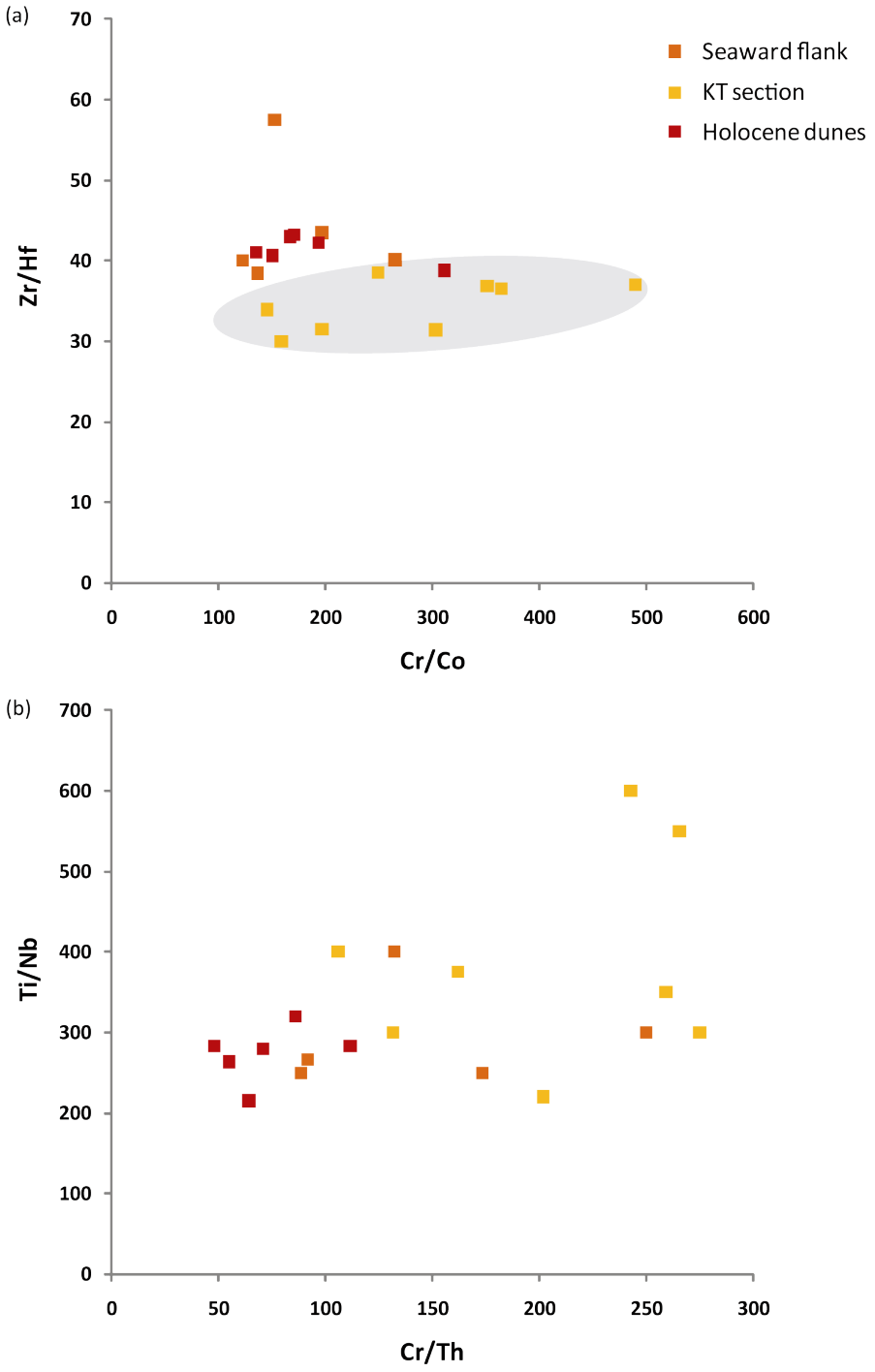

6.3.7 Biplots of immobile element ratios from seaward barrier samples: (a) Zr/Hf vs. Cr/Co; (b) Ti/Nb vs. Cr/Th. Shaded area in (a) encompasses KT section samples.

Interestingly, the KT section samples are distinguishable based on their Zr/Hf ratios and, partly, their Cr/Co ratios (Figure 6.3.7a), suggesting that this component of the barrier may have a different source to the seaward flank and Holocene dune samples. This was further explored by considering additional immobile element ratios, Ti/Nb and Cr/Th. However, these ratios fail to discriminate between the KT section and the other samples (Figure 6.3.7b), with

only two KT section samples plotting as outliers (KT2-4 and KT2-6). It is worth noting that these are not the same two KT section samples identified as outliers based on their Th/U ratios.

6.3.3.3 Summary of seaward barrier geochemistry

Th/U ratios were interpreted in Dunajko and Bateman (2010) as indicating the KT section samples have undergone a greater amount of weathering than sands from elsewhere in the seaward barrier. This is supported with the inclusion of additional data here. Weathering appears most significant in samples with particularly shallow burial depths.

With regard to the immobile elements considered, the relatively high concentration of Zr and Hf in the Holocene dunes indicates these samples are enriched in zircon, most likely a consequence of their formation from recycled seaward barrier aeolianite (during which less stable minerals would have been lost). Their Zr/Hf ratios overlap with those from the seaward flank of the barrier, which is currently undergoing erosion, supporting this assertion. The KT section samples are distinguishable from the other seaward barrier sands based on their Zr/Hf and, partly, Cr/Co ratios, indicating a possible change in parent material between these sands and the Holocene dune and seaward flank samples. However, Ti/Nb and Cr/Th values fail to separate the three sample groups, as do the REE ratios Eu/Eu* and La_N/Yb_N. The barrier samples almost all fall within or just outside the range typical of UCC material with respect to these ratios. Likewise, the chondrite-normalised REE plots of all samples from the seaward barrier display a pattern consistent with typical coarse-grained quartz-rich sediments, with the exception of their negative Ce anomalies. This latter characteristic is interpreted as reflecting the presence of a marine sediment component within the barriers.

6.3.4 Barrier sands compared to possible local sediment sources

In this section the geochemical characteristics of the barrier sands are compared to those of the possible local sediment sources, in order to identify whether any of them have contributed to the barrier. The possibility of whether the KT section samples have a different source to the seaward flank and Holocene dune samples, as tentatively suggested by their Zr/Hf ratios, is also explored. A list of the possible sediment source samples and their trace element concentrations used in analysis is provided in Table 6.3.3.

Table 6.3.3 Trace element concentrations of samples from the various possible sediment sources for the barrier dune sands.

Sample	Co	Cr	Hf	Th	Nb	Zr	Ti (ppm)	Eu	Sm	Gd	La	Yb
Detection limit (ppm)	0.5	10	1	0.1	1	0.5	100	0.05	0.1	0.05	0.1	0.1
Coversands												
Karatara Road	2.4	430	20	9.1	12	733	3200	0.55	3.1	3.14	18.1	2.3
Barrington Road	2.4	520	30	4.6	11	1190	3200	0.58	3.9	2.84	18.7	1.6
Makhulu Quarry 1	0.7	407	5	2.1	5	157	1900	0.19	0.8	0.78	5.1	0.8
Makhulu Quarry 2	1	336	-	1.8	-	28	500	0.17	0.6	0.5	3.3	0.3
Makhulu Quarry 3	2.2	380	24	8.2	11	865	3300	0.47	2.9	2.66	16.4	2.1
Blaricum Heights	0.6	301	9	2.6	8	295	2000	0.31	1.9	1.31	12.7	0.6
River sediments												
Touw upper	1.6	460	1	1.6	2	40.7	300	0.16	0.9	0.83	5.1	0.4
Karatara upper	1.7	540	2	1.6	2	75.9	500	0.14	0.9	0.91	4.8	0.6
Goukamma	1.7	380	2	2.2	3	74.4	700	0.22	1.3	1.31	7.9	0.7
Touw lower	2.3	660	2	2.1	3	50.9	700	0.15	0.9	1.05	5.8	0.5
Duiwe 1	2.7	610	2	2.4	3	69.2	800	0.19	1.2	1.13	6.6	0.7
Duiwe 2	2.3	580	5	4.1	3	181	700	0.2	1.9	1.74	9.6	0.7
Diep	1.8	480	5	3.4	4	174	1000	0.28	2.1	1.67	11.4	0.7
Hoekraal lower 1	1.8	570	2	1.6	3	63.2	500	0.14	0.9	0.83	5.4	0.5
Hoekraal lower 2	1.8	540	4	3.1	3	122	700	0.18	1.4	1.4	6.1	0.9
Karatara lower	1.5	380	2	2.1	2	54.5	400	0.15	1.1	1.18	5.9	0.8
Salt	2.2	460	3	1.9	3	102	600	0.19	1.1	0.95	7.2	0.4
Beach sands												
Wilderness	3.1	350	115	14.8	37	4730	8100	3.26	20.4	15.3	98.1	6.8
Sedgefield	1.7	350	2	2	2	51.1	500	0.27	1.4	1.42	8.4	0.5
Lagoon sediments												
Swartvlei 1	2.4	570	15	2.9	6	601	1200	0.47	2.6	2.36	12.8	1
Swartvlei 2	2.6	490	5	2.1	4	225	900	0.29	1.8	1.74	9.7	0.7
Swartvlei 3	2	580	1	1.3	1	52	300	0.15	0.8	0.75	5.1	0.4
Knysna	2.5	710	3	1.8	3	108	600	0.29	1.5	1.25	8.2	0.6
Bedrock – TMG												
Peninsula 1	2	510	2	2.3	1	51.1	300	0.22	1.3	1.21	7.8	0.6
Peninsula 2	1.8	460	2	1.8	2	43.7	600	0.38	1.8	1.3	10.6	0.8
Tchando	1.8	500	3	3.7	4	111	900	0.18	1.2	1.11	6.5	0.8
Bedrock – Woodville Granite												
Woodville 1	1.8	350	3	18.3	10	65.1	400	0.3	6.7	7.87	16.7	6.6
Woodville 2	2	380	3	19.3	12	64	500	0.36	7.9	8.62	20.2	6.6
Woodville 3	2.2	720	2	4.7	-	45.3	100	0.23	1.5	1.54	7	1.3
Woodville 4	1.5	450	5	1.6	-	78.7	-	0.09	0.5	0.42	3.5	0.4
Bedrock – Kaaimans												
Homtini	6.1	110	6	17.1	21	188	4500	1.26	6.7	7.71	29.4	4.5
Victoria Bay	4	220	4	10.1	8	114	1200	1.2	6.7	7.23	24.1	4
Soetkraal	1.9	220	5	15.6	10	154	1300	0.73	2.6	2.47	23.6	2.6
Skaapkop	1.1	230	2	4.1	1	27.8	-	0.14	1.9	2	5.3	1.2

The chondrite-normalised REE composition of the seaward barrier samples is compared to bedrock samples in Figure 6.3.8a and possible local sediment sources in Figure 6.3.8b (individual REE concentrations of the samples are provided in Appendix 2). It was noted in section 6.3.3.2 that samples from the seaward barrier all possess chondrite-normalised REE patterns typical of coarse-grained quartz-rich sediments. The TMG bedrock samples display a similar pattern, though with lower overall REE abundances (Figure 6.3.8a), and it also possesses a slight negative Ce anomaly. The TMG was originally laid down in a shallow marine setting (chapter 3 section 3.2), which could explain this. The heavy mineral apatite also possesses a negative Ce anomaly, arising during igneous or metamorphic crystallisation

(Puchelt and Emmermann, 1976). Whilst apatite is not identified in the TMG, it is present in the Woodville Granite and Kaaimans Group rocks (chapter 3 section 3.3), explaining their negative Ce anomalies. Apart from this characteristic, the Woodville Granite and Kaaimans Group bedrock types appear much less similar to the barrier sands than the TMG, with enriched HREE (Eu to Lu) and much greater negative Eu anomalies (Figure 6.3.8a).

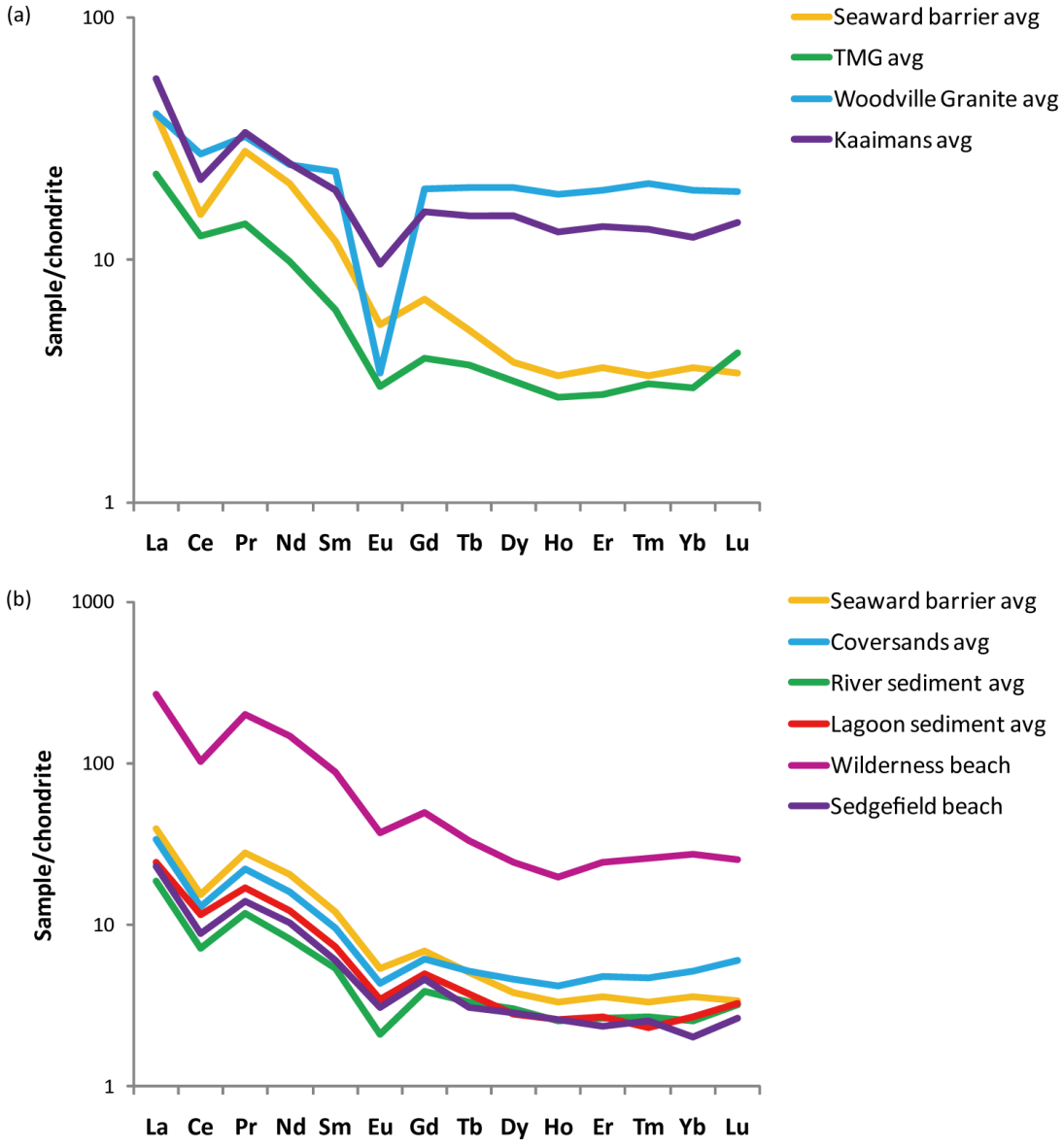

6.3.8 Chondrite-normalised REE curves of the seaward barrier sands (average of all samples) compared to: (a) local bedrock; and (b) other possible local sediment sources.

Figure 6.3.8b demonstrates the high degree of similarity between the barrier sands and all the possible local sediment source samples, with the exception of the Wilderness beach sand (plotted separately). As can be noted from Table 6.3.2, the Wilderness beach sample has concentrations of several elements up to an order of magnitude higher than most other

samples, strongly suggesting a beach placer deposit (concentration of heavy minerals due to hydraulic sorting) was inadvertently sampled. The lagoons, coversands and river sediments all possess chondrite-normalised REE curves characteristic of coarse-grained quartzitic sediments, similar to the barriers. However, given the ubiquity of such REE distributions, it is not interpreted as necessarily indicating a provenance relationship between them.

Comparisons of the Eu/Eu* and La_N/Yb_N ratios of the bedrock samples and barrier sands are shown in Figure 6.3.9. Similar to the REE curve in Figure 6.3.8a, the Woodville Granite and Kaaimans Group samples deviate significantly from the barrier characteristics, most likely reflecting fractionation of their REE during metamorphism. Their distinction from the barrier samples strongly indicates they do not represent their parent material. However, the TMG Peninsula Formation 1 sample falls within the field defined by the barrier sands (and the TMG Peninsula Formation 2 sample just outside). As discussed in the previous paragraphs, whilst this could indicate a provenance relationship, such REE characteristics are typically possessed by all coarse-grained quartz-rich sediments and sandstones.

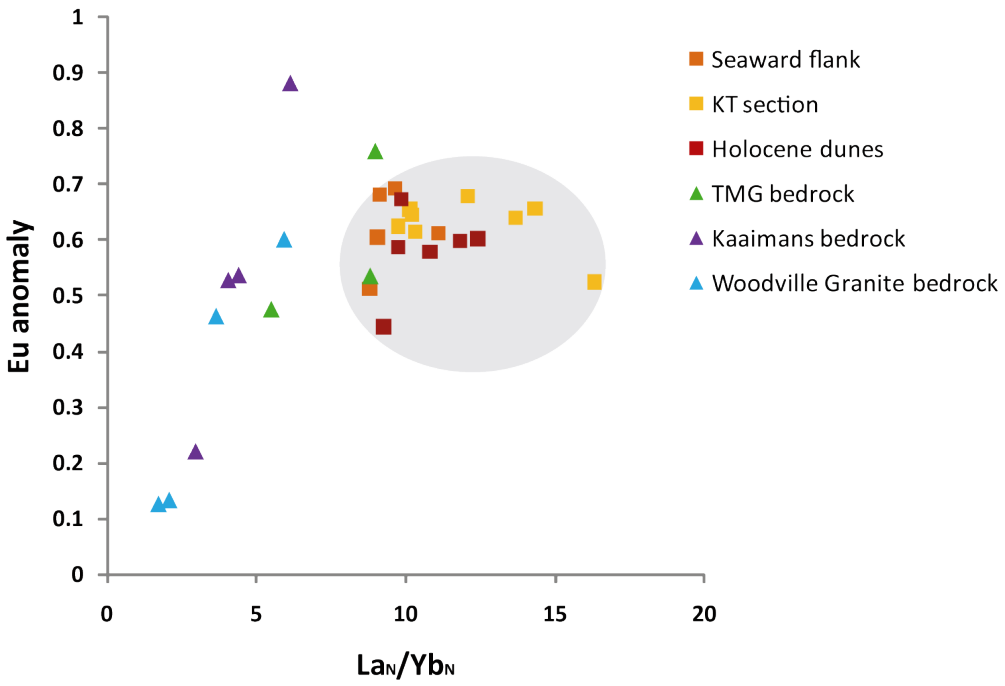

6.3.9 Eu/Eu* vs La_N/Yb_N ratios of barrier sands and bedrock samples. Shaded area encompasses barrier samples.

Unsurprisingly, most of the river sediment samples have Eu/Eu* and La_N/Yb_N values similar to the majority of bedrock samples (Figure 6.3.10). Only the Salt, Touw Upper and Diep river sediment samples overlap with the barrier sands. Figure 6.3.10 also illustrates the dissimilarity of most of the coversand samples (excepting the Barrington Road (labelled BR in

the plot) and Blaricum Heights (labelled BH) samples) to the barriers. The lagoon sediments have consistently similar REE characteristics to the barriers. Despite the high REE concentrations in the Wilderness beach sample evident in Figure 6.3.8b, it plots very closely to the Sedgefield beach sample, and both the beach sands are indistinguishable from the barriers.

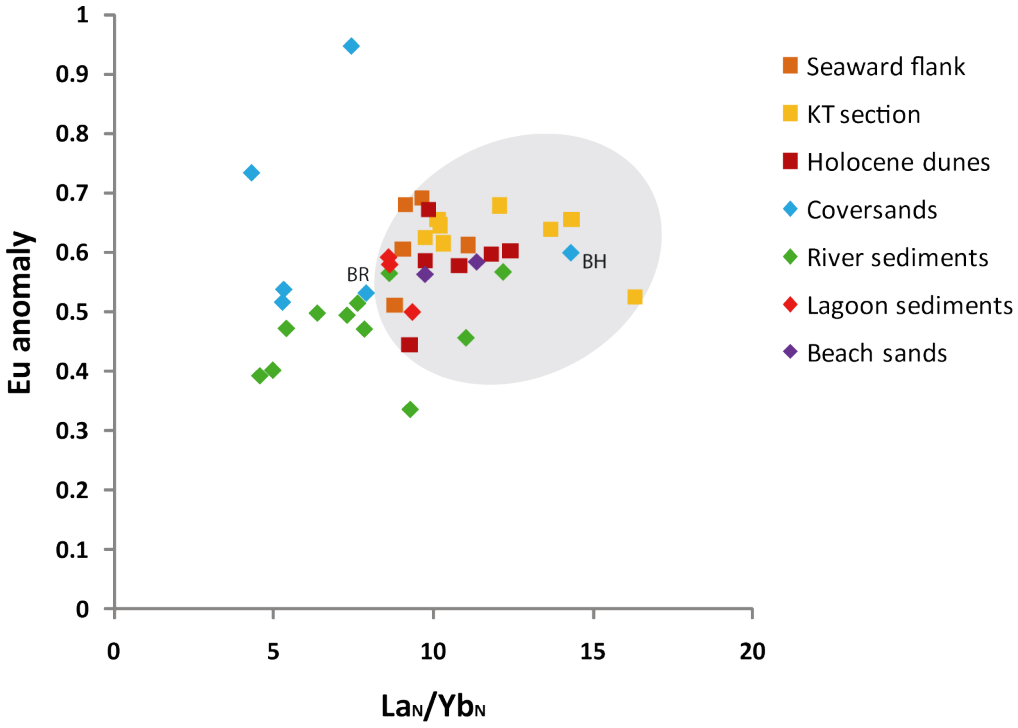

6.3.10 Eu/Eu* vs La_N/Yb_N ratios of barrier sands and possible sediment source samples. Shaded area encompasses barrier samples. Labels identify Blariucm Heights (BH) and Barrington Road (BR) coversand samples.

The Zr/Hf, Cr/Co, Ti/Nb and Cr/Th ratios of the barrier sands are compared to the bedrock samples in Figure 6.3.11a and 6.3.11b. With respect to Zr/Hf and Cr/Co only a single bedrock sample (TMG Tchando Formation) overlaps with the dune sands (Figure 6.3.11a). However, according to Ti/Nb and Cr/Th ratios the TMG bedrock samples are very similar to the barrier sands (Figure 6.3.11b), strongly suggesting they are related. The Kaaimans Group and Woodville Granite bedrock samples appear quite distinct in both plots, providing further evidence they are not the parent material of the barrier sands. Note that Ti and/or Nb were entirely absent from two of the Woodville Granite samples (Woodville Granite 3 and 4: see Table 6.3.3), so they are not plotted.

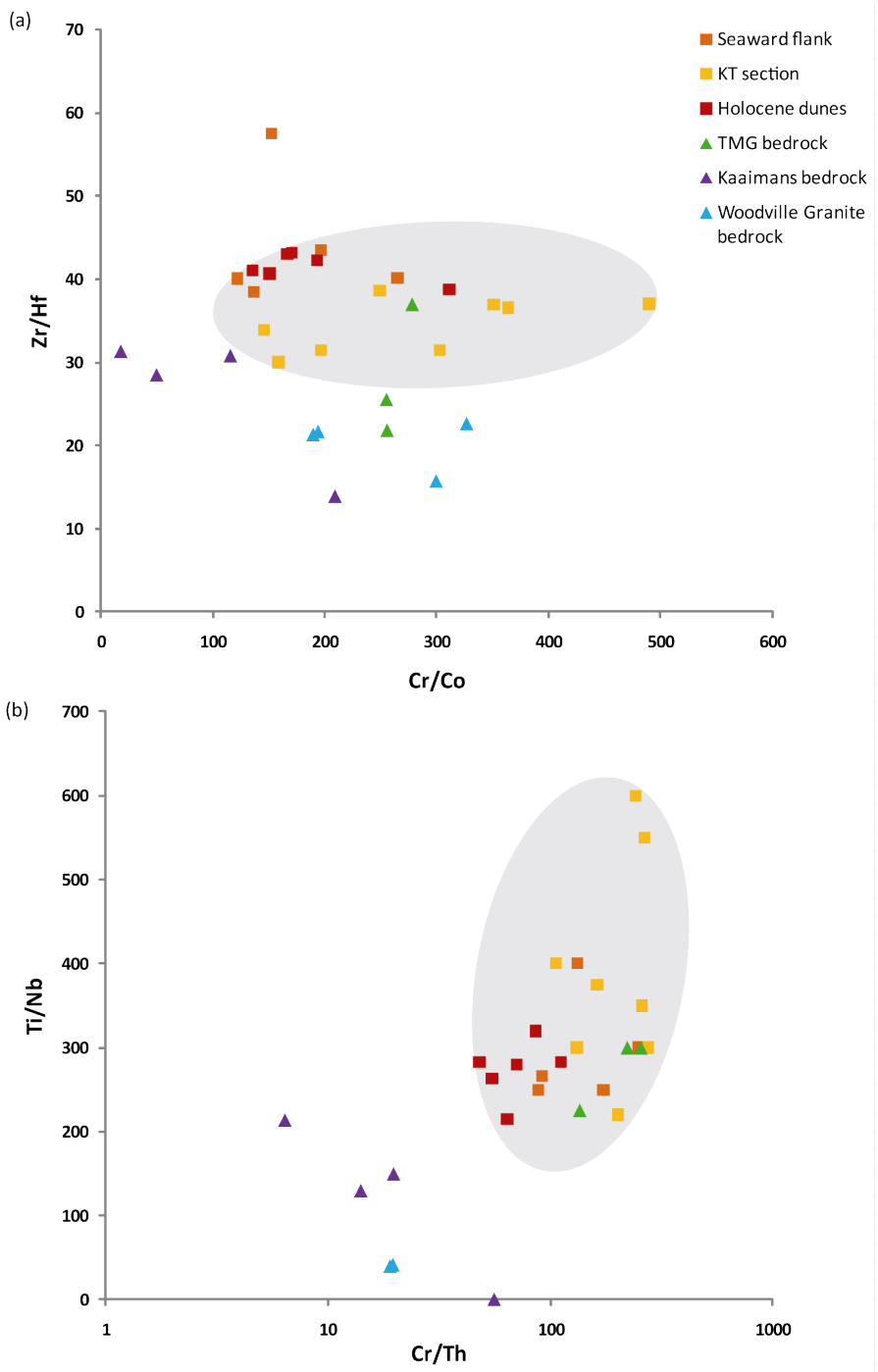

6.3.11 Barrier sand samples compared to local bedrock according to: (a) Zr/Hf and Cr/Co ratios; and (b) Ti/Nb and Cr/Th ratios. Shaded areas encompass barrier samples.

The barrier sands are compared to the other possible local sediment sources according to the various immobile element ratios in Figure 6.3.12a and 6.3.12b. In the plot comparing Zr/Hf and Cr/Co (Figure 6.3.12a), the most notable aspect is the overlap of the river sediments with the KT section barrier samples. Conversely, the Holocene dunes and seaward flank samples mostly fall outside the field defined by the river sediments. This was interpreted in Dunajko and Bateman (2010) as indicating the KT section part of the seaward barrier

incorporates a contribution from fluvial sediment sources local to Wilderness, whereas the seaward flank and Holocene dunes do not.

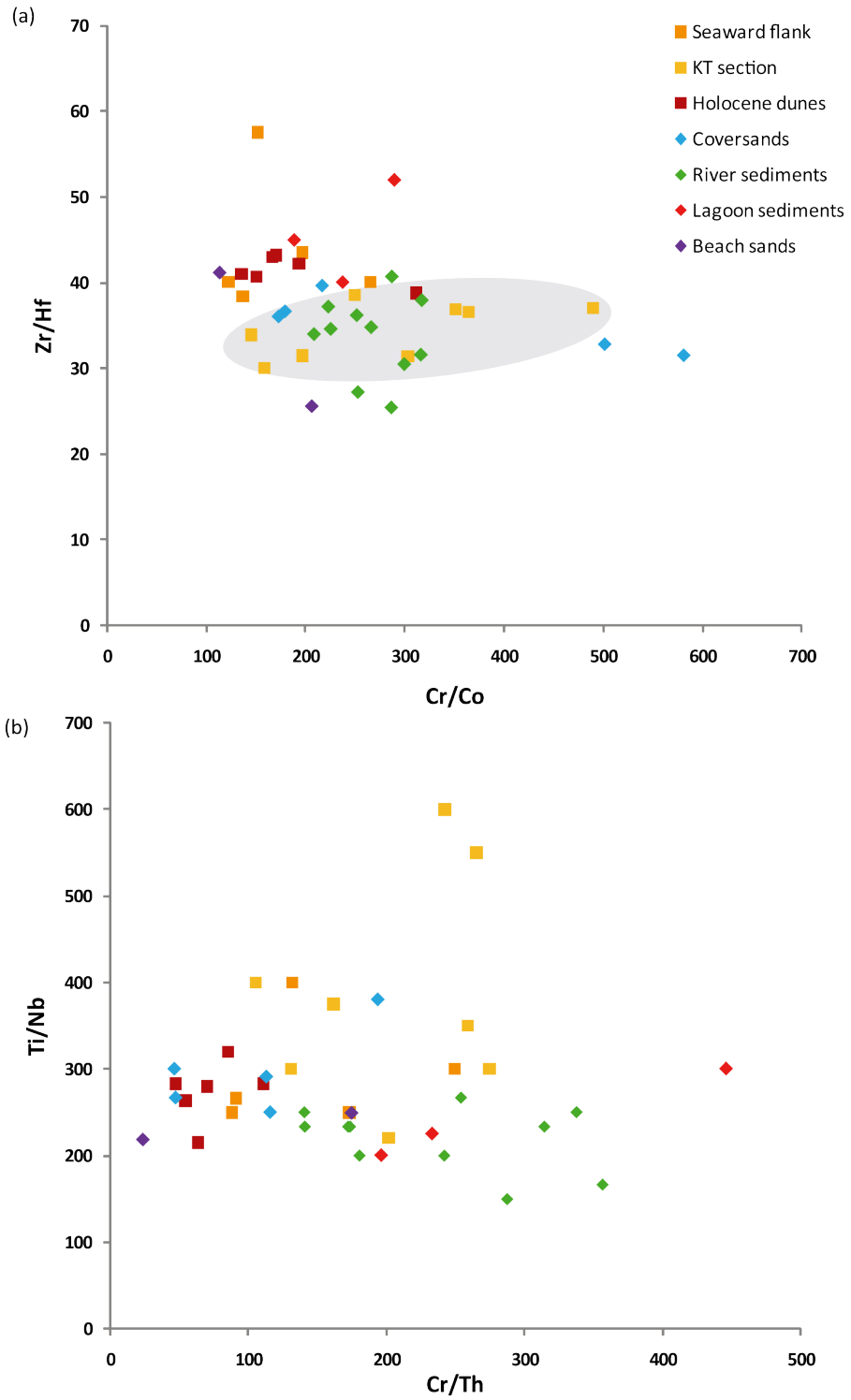

6.3.12 Barrier sand samples compared to other possible local sediment sources: (a) Zr/Hf vs. Cr/Co; (b) Ti/Nb vs. Cr/Th. Shaded area in (a) encompasses KT section barrier samples.

Figure 6.3.12a also shows that, whilst the lagoon and beach sands display quite a lot of variability, they largely overlap with the field defined by the barrier samples, further indicating

they are related. The coversand display a bimodal distribution, with some samples very similar to the barrier sands (Makhulu Quarry 2, Barrington Road and Karatara Road) but two others (Makhulu Quarry 1 and Blaricum Heights) separate with respect to their Cr/Co ratios. Comparisons of Ti/Nb and Cr/Th are much less distinct, with few clear separations between any of the sample groups, and little overlap between the river sediments and KT section samples (Figure 6.3.12b). Interestingly, however, there is some overlap between the lagoon sediments and the river sediments in this plot.

6.3.5 Principal component analysis

Considered with respect to one another, the immobile element ratios discussed in the previous section present a slightly confusing picture of whether the three seaward barrier sample groups provide evidence for any potential changes in provenance between them, and whether they can be related to any of the potential local sediment sources. In order to assess the geochemical similarity (or otherwise) of the samples in aggregate, PCA was used to combine the various immobile element ratios (Cr/Co, Cr/Th, Ti/Nb, Zr/Hf, Eu/Eu* and La_N/Yb_N). Prior to analysis a CLR transformation was performed on the data, in order to prevent any autocorrelation issues that might otherwise arise from the use of Cr in two of the ratios. Results are presented in Figure 6.3.13a (barrier sands vs. bedrock samples) and Figure 6.3.13b (barrier sands vs. other possible sediment sources). The loadings of the two PCs plotted in each figure are given in Table 6.3.4.

The comparison of the barrier and bedrock samples (Figure 6.3.13a) confirms the Kaaimans Group bedrock is geochemically distinct from the barrier sands. Conversely, the TMG bedrock samples overlap with the barrier samples (and in particular the KT section samples), demonstrating that their overall immobile element geochemistry is very similar. This provides a strong indication that the TMG bedrock has contributed to the seaward barrier sands. Overlap is most significant on PC 1, which has strong loadings on Cr/Th, Eu/Eu* and Zr/Hf (Table 6.3.4), so importantly the similarity is not only a reflection of REE composition. Two of the unweathered Woodville granite samples (Woodville Granite 1 and 2) also appear quite similar to the barrier. Both of these samples were obtained from exposures close to the Diep River, though all four of the granite samples were obtained in relatively close proximity (≤6 km apart: see chapter 4 Figure 4.14), indicating the geochemical (and thus mineralogical) variability of the Woodville granite pluton is large.

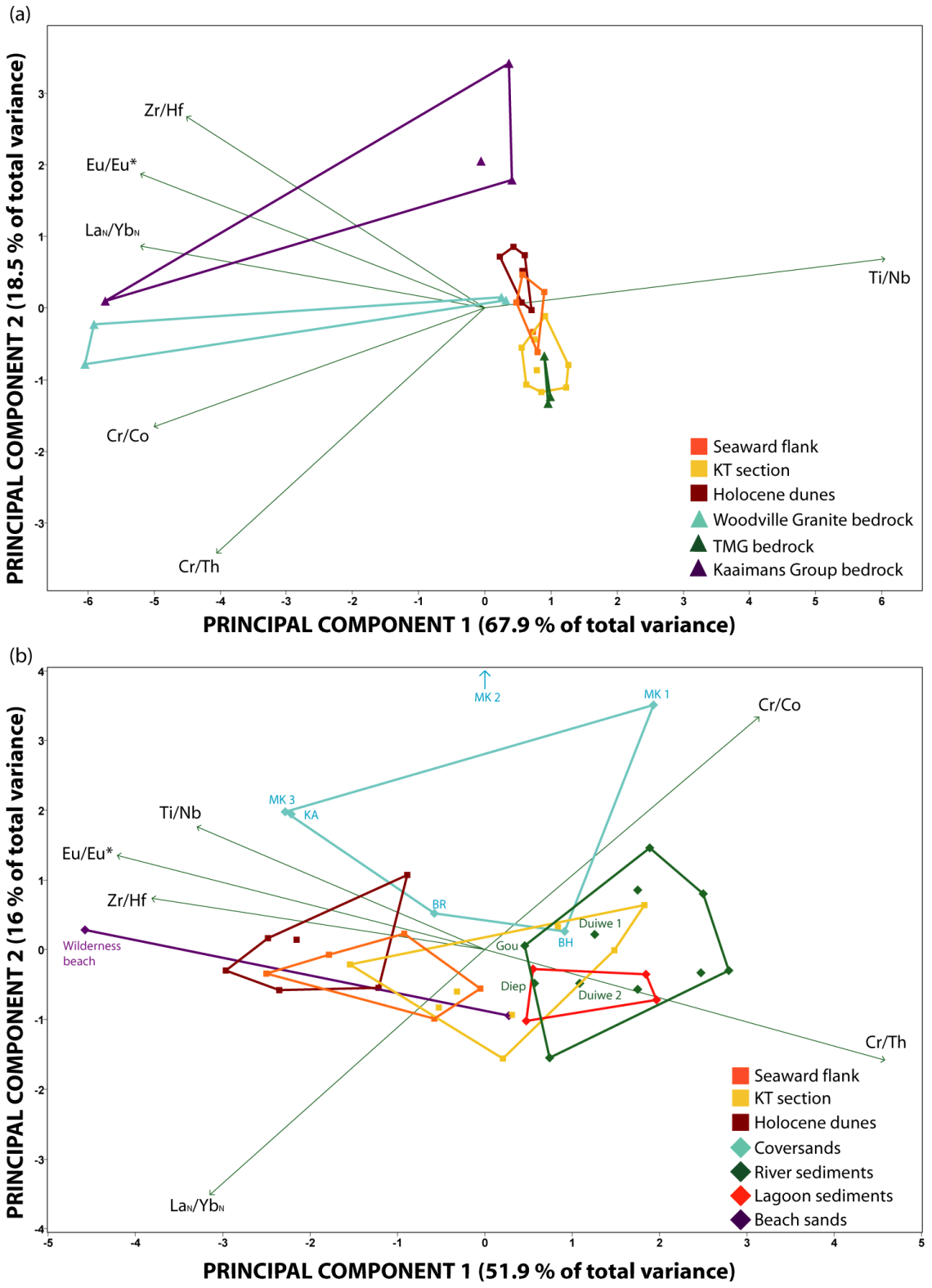

6.3.13 Biplot of PCA performed on trace element ratios considered to be indicative of provenance, comparing: (a) barrier dune samples to local bedrock; (b) barrier dune samples to other possible local sediment sources. In (b) certain samples referred to in the text are labelled individually. Loadings for the PCs are given in Table 6.3.4.

Table 6.3.4 Loadings of PCs plotted in Figure 6.3.13a (barrier vs. bedrock) and Figure 6.3.13b (barrier vs. other possible sources).

Variable	Barrier vs. bedrock		Barrier vs. other possible sources	
	PC1	PC 2	PC1	PC 2
Cr/Co	0.34	0.59	0.34	0.59
Ti/Nb	-0.36	0.32	-0.36	0.32
Cr/Th	0.5	-0.28	0.5	-0.28
Zr/Hf	-0.42	0.13	-0.42	0.13
Eu/Eu*	-0.46	0.24	-0.46	0.24
La_N/Yb_N	-0.34	-0.63	-0.34	-0.63

PCA highlights the large variability within the coversand sample group, and also the relatively significant dissimilarity of the Makhulu Quarry and Karatara Road coversand samples to the barrier sands. It was necessary to remove the Makhulu Quarry 2 coversand sample from the results plotted in Figure 6.3.13b, as its extreme difference to all the other samples according to PC 2 necessitated too large a y-axis scale. Its position is thus indicated by an arrow (labelled MK 2). The remaining two Makhulu Quarry samples are labelled MK 1 and MK 2, and the Karatara Road sample KA. Conversely, the Blaricum Heights (BH) and Barrington Road (BR) coversand samples appear quite similar to the barriers.

Figure 6.3.13b also confirms the similarity of certain river sediments (the Diep, Goukamma and Duiwe) to the KT section seaward barrier samples. The Duiwe River runs adjacent to the KT section site, but the Diep and Goukamma river course are further east (Figure 6.1.2). Also, the Duiwe headwaters rise in Kaaimans Group rocks, whereas the Diep traverses the TMG and the Woodville Granite pluton, and the Goukamma the TMG and the Kaaimans Group (see chapter 4 Figure 4.14), highlighting the difficulty of discriminating provenance relationships between sediments derived from exclusively felsic rocks of similar metamorphic grade. Interestingly, the river sediments also overlap almost entirely with the lagoon sediments. The Wilderness beach sample, previously identified as a placer deposit, plots quite distinctly from the barriers, though the Sedgefield beach sample falls within the field defined by the KT section barrier samples.

6.3.6 Trace element geochemistry summary

To summarise, according to all methods of geochemical analysis conducted the lagoon sediments are geochemically similar to the barrier sands, clearly suggesting they are related to one another. The beach sand samples are also inseparable from the barriers in most respects, despite the anomalously high concentrations of most elements in the Wilderness beach sample due to its status as a placer deposit. The TMG bedrock is geochemically

indistinguishable from the barrier samples according to Ti/Nb ratios and the PCA results, suggesting the barrier sands are ultimately likely to have been derived from this bedrock type. The TMG bedrock and barrier samples are also similar with respect to their REE abundances, though this is a much less reliable indicator of provenance. Conversely, the Kaaimans Group bedrock samples possess geochemical characteristics significantly different to those of the barrier sands in almost all respects, strongly suggesting they are not related. Two of the unweathered Woodville Granite bedrock samples appear similar to the barrier sands in the PCA analysis, though this is not apparent when considering the various trace element ratios in isolation.

The relationship of the coversands and river sediments to the barrier sands is harder to interpret. River sediments overlap the KT section samples with respect to their Zr/Hf ratios, indicating local fluvial sources have contributed material to this part of the barrier. PCA also identifies certain river samples that are more similar to the KT section samples than others (namely the Diep, Goukamma and Duiwe). However, these rivers each traverse different bedrock types, and various other indicators of provenance (Ti/Nb, Cr/Th and the REE ratios) do not discriminate between the KT section samples and the other seaward barrier sands. On balance, and also considering the results of the particle size analysis, whilst the KT section samples may include a component derived from the adjacent Duiwe River, it is considered that they do not represent material of significantly different provenance to the other seaward barrier sands. The coversand samples display quite variable geochemistry, with some samples similar to the barriers (Barrington Road and Blaricum Heights) and others (Makhulu Quarry) quite distinct. The relationship between the coversands and the barrier sands, along with the other possible sources, is considered further in the next section using heavy mineral analysis.

6.4 Sediment provenancing results: heavy minerals

6.4.1 Introduction

The trace element concentrations present in quartz-rich sediments are predominantly a function of their heavy mineralogy. However, considering the heavy mineral (HM) species themselves can yield additional and important information for sediment provenancing purposes that is not available from geochemistry alone (Mange and Wright, 2007a). This section presents the results of analyses conducted on the HM present in the 63-280 μm fraction of a limited number of samples (barrier dunes = 5; coversands = 2; rivers = 3; beach = 2; lagoon = 1). The mineralogy of the barrier dune samples was first considered in isolation (section 6.4.2), and then compared to: (i) the samples of the possible sediment sources (section 6.4.3); and (ii) descriptions of local bedrock mineralogy from the literature (section 6.4.4).

6.4.2 HM present in the barrier dunes

The HM of three samples from seaward barrier aeolianites, one sample from a Holocene dune on the seaward barrier crest and one sample from middle barrier aeolianite was established. Unfortunately, as the KT section seaward barrier samples considered elsewhere in this chapter were originally sampled by Carr et al. (2007) without HM analysis in mind, insufficient sample material was left to extract a sufficient quantity of HM for point counting. Results are presented in Table 6.4.1. The HM spectrum of the seaward barrier aeolianite samples is extremely diverse, containing a variety of mineral species ranging from unstable to ultrastable. Averaged across the three samples, dominant constituents are biotite (30.8 %), garnet (11.9 %) and glauconite (11.6 %). Significant subordinate species present include minerals identified as highly unstable or unstable during burial by Morton and Hallsworth (2007), including olivine (3.8 %), epidote (2.5 %) and the aluminium silicate minerals kyanite, sillimanite and andalusite (totalling 13.1 %). The middle barrier aeolianite and Holocene dune samples are less mineralogically diverse, both containing greater proportions of stable and ultrastable minerals such as zircon (27.4 % of the Holocene dune sample and 20.3 % of the middle barrier sample), garnet and rutile. Glauconite is also entirely absent from the Holocene dune and middle barrier samples.

Table 6.4.1 Heavy mineral species present in samples from the barrier dunes (63-280 µm fraction).

MINERAL GROUPS		SAMPLE	Seaward barrier								Middle barrier	
			Holocene dune sand (Shfd05040)		Gerickes Point aeolianite (Shfd08178)		Gerickes Point aeolianite (Shfd08180)		Buffels Bay aeolianite (Shfd08185)		East Swartvlei aeolianite (Shfd08183)	
		Age	3.7 ± 0.1 ka[#]		154 ± 8 ka		129 ± 7 ka		86 ± 5 ka		131 ± 7 ka	
		Mineral species	*Raw*	*%*	*Raw*	*%*	*Raw*	*%*	*Raw*	*%*	*Raw*	*%*
		n	**394**		**649**		**511**		**424**		**475**	
		Opaques	*87*	*22.1*	*316*	*48.7*	*201*	*39.3*	*111*	*26.2*	*140*	*29.5*
		Non Opaques	*307*	*77.9*	*333*	*51.3*	*310*	*60.7*	*313*	*73.8*	*335*	*70.5*
SILICATES	Silicates	*Olivine Group*	20	6.5	5	1.5	20	6.5	11	3.5	14	4.2
		Zircon	84	27.4	11	3.3	4	1.3	2	0.6	68	20.3
		Sphene			10	3			6	1.9		
		Garnet Group	81	26.4	42	12.6	23	7.4	49	15.7	141	42.1
		Sillimanite	3	1	11	3.3	18	5.8	11	3.5	5	1.5
		Andalusite	11	3.6	3	0.9	18	5.8	20	6.4	5	1.5
		Kyanite	3	1	6	1.8	16	5.2	21	6.7		
		Staurolite	2	0.7	12	3.6	1	0.3	2	0.6	1	0.3
		Chloritoid	1	0.3			3	1	3	1	1	0.3
	Epidotes	*Zoisite/ clinozoisite*	3	1	3	0.9	3	1	5	1.6		
		Epidote	5	1.6	10	3	9	2.9	5	1.6	8	2.4
		Lawsonite					1	0.3				
		Pumpellyte			2	0.6						
		Allanite			5	1.5			1	0.3		
		Piemontite							1	0.3		
		Axinite							3	1		
		Tourmaline	4	1.3	10	3	2	0.6	5	1.6	3	0.9
	Pyroxenes	*Enstatite*	3	1	1	0.3	20	6.5	7	2.2	1	0.3
		Hypersthene	1	0.3	4	1.2	2	0.6			1	0.3
		Clinopyroxene	2	0.7	6	1.8	2	0.6	1	0.3		
	Amphiboles	*Tremolite*	1	0.3			11	3.5	5	1.6		
		Ferriactinolite							3	1		
		Hornblende					1	0.3				
	Micas	*Muscovite*			3	0.9	3	1	3	1		
		Glauconite			36	10.8	30	9.7	45	14.4		
		Biotite	15	4.9	119	35.7	93	30	83	26.5	14	4.2
		Chlorite Group	19	6.2	6	1.8	3	1	5	1.6	9	2.7
OXIDES		*Rutile*	25	8.1	7	2.1	4	1.3	3	1	31	9.3
		Brookite	5	1.6	3	0.9	1	0.3				
		Chromian Spinel			1	0.3						
		Anatase					1	0.3			29	8.7
CARBONATES		*Dolomite/ Calcite*	11	3.6	14	4.2	20	6.5	10	3.2		
SULPHATES		*Baryte*			1	0.3						
PHOSPHATES		*Apatite*	3	1	1	0.3	1	0.3	1	0.3	2	0.6
		Monazite	5	1.6	1	0.3			2	0.6	2	0.6

[#] Age from Carr et al. (2010a)

One of the basic tenets of using heavy minerals to identify sediment provenance is that the diversity of the mineral assemblage present in a sediment will decrease as it is

subjected to weathering (Boswell, 1933). The relatively limited number of mineral species present in the Holocene dune sample thus supports the assertion made in section 6.3, that the Holocene dunes are formed from material eroded from the seaward barrier aeolianites. During the recycling process, less resistant mineral species will have been removed by weathering, whilst remaining preserved in the lithified aeolianite below. Glauconite is one such relatively unstable mineral (McRae, 1972). It forms authigenically in water depths from 50-500 m (Wigley and Compton, 2007), and its presence in the seaward barrier aeolianite samples confirms that they contain a marine component. The lack of glauconite in the Holocene dune sample most likely reflects dissolution of the mineral due to weathering, rather than its absence in the first instance.

The lack of HM diversity in the middle barrier sample (Shfd08183) is probably also due to increased weathering relative to the seaward barrier aeolianite samples. The location of sample Shfd08183 on the exposure east of Swartvlei (see Figure 6.1.9) mean it is likely to have been subaerially exposed for longer than the seaward barrier samples, which were obtained from the rapidly eroding sea cliffs at the rear of the modern beach.

6.4.3 HM of possible sediment source areas compared to the barrier dunes

The HM present in the samples from the various possible local sediment sources are presented in Table 6.4.2. PCA was used to compare these samples to those from the barrier dunes, and the results are shown in Figure 6.4.1. A CLR transformation was performed on the dataset prior to analysis for statistical rigour. Morton and Hallsworth (1999) caution against such uncritical use of entire HM assemblages in attempts to characterise provenance relationships, due to the various “overprinting” processes known to modify the heavy mineralogy of sediments compared to their sources (namely weathering, diagenesis and hydraulic sorting during transportation). However, similar multivariate statistical analyses of entire HM assemblages have been used to establish the similarity (or otherwise) of sediments in other studies (e.g. Pirkle et al., 1989; Hota and Maejima, 2009), and if nothing else the analysis provides a useful means of graphically displaying the relative importance of different mineral species within the various samples.

Table 6.4.2 Heavy mineral species present in samples from the possible local sediment sources (63-280 µm fraction). Continues overleaf.

MINERAL SPECIES		SAMPLE	Beach sands				Lagoon		Coversands			
			Wilderness Beach		Buffels Bay Beach		Knysna Lagoon		Makhulu Quarry		Barrington Road	
			Raw	*%*	*Raw*	*%*	*Raw*	*%*	*Raw*	*%*	*Raw*	*%*
		n	**502**		**434**		**445**		**704**		**711**	
		Opaques	*180*	*35.9*	*109*	*25.1*	*126*	*28.3*	*388*	*55.1*	*334*	*47*
		Non Opaques	*322*	*64.1*	*325*	*74.9*	*319*	*71.7*	*316*	*44.9*	*377*	*53*
SILICATES	Silicates	*Olivine Group*	24	7.5	22	6.8	7	2.2				
		Zircon	71	22	8	2.5	27	8.5	172	54.4	276	73.2
		Sphene					20	6.3				
		Garnet Group	107	33.2	28	8.6	23	7.2	16	5.1	1	0.3
		Sillimanite	13	4	24	7.4	27	8.5				
		Andalusite	3	0.9	5	1.5	4	1.3				
		Kyanite	5	1.6	13	4	9	2.8	10	3.2	2	0.5
		Dumortierite										
		Staurolite			1	0.3					2	0.5
		Chloritoid	1	0.3	5	1.5	7	2.2	2	0.6	1	0.3
	Epidotes	*Zoisite/ clinozoisite*	8	2.5	4	1.2	1	0.3	8	2.5	1	0.3
		Epidote	6	1.9	8	2.5	9	2.8	3	0.9	4	1.1
		Lawsonite										
		Pumpellyte										
		Allanite					3	0.9				
		Piemontite										
		Axinite					1	0.3				
		Tourmaline	5	1.6	5	1.5	6	1.9	7	2.2	8	2.1
	Pyroxenes	*Enstatite*			4	1.2	1	0.3				
		Hypersthene	2	0.6	3	0.9	1	0.3				
		Clinopyroxene			2	0.6						
	Amphiboles	*Tremolite*			16	4.9	1	0.3				
		Ferriactinolite			1	0.3						
		Hornblende			1	0.3	1	0.3			1	0.3
		Glaucophane										
	Micas	*Muscovite*			1	0.3	2	0.6	1	0.3		
		Glauconite			40	12.3	43	13.5				
		Biotite	14	4.3	51	15.7	49	15.4	1	0.3	2	0.5
		Chlorite Group	9	2.8	3	0.9	8	2.5				
OXIDES		*Rutile*	10	3.1	2	0.6	10	3.1	62	19.6	67	17.8
		Brookite	7	2.2	1	0.3					1	0.3
		Chromian Spinel	1	0.3	1	0.3	6	1.9				
		Anatase					3	0.9			1	0.3
CARBONATES		*Dolomite/ Calcite*	26	8.1	71	21.8	46	14.4	2	0.6	8	2.1
PHOSPHATES		*Apatite*	6	1.9	2	0.6			29	9.2		
		Monazite	4	1.2	3	0.9	4	1.3	3	0.9	2	0.5

Table 6.4.2 Continued from previous page.

MINERAL SPECIES		SAMPLE	River sediment					
			Hoekraal lower		Salt		Touw lower	
			Raw	*%*	*Raw*	*%*	*Raw*	*%*
		n	**1072**		**1405**		**895**	
		Opaques	*667*	*62.2*	*1077*	*76.7*	*593*	*66.3*
		Non Opaques	*405*	*37.8*	*328*	*23.3*	*302*	*33.7*
SILICATES	**Silicates**	*Olivine Group*					2	0.7
		Zircon	125	30.9	104	31.7	14	4.6
		Sphene					6	2
		Garnet Group	7	1.7	23	7	22	7.3
		Sillimanite					1	0.3
		Andalusite					15	5
		Kyanite	4	1	8	2.4	3	1
		Dumortierite	2	0.5	2	0.6		
		Staurolite	1	0.2	5	1.5	1	0.3
		Chloritoid	14	3.5	9	2.7	1	0.3
	Epidotes	*Zoisite/ clinozoisite*	9	2.2	8	2.4	4	1.3
		Epidote	7	1.7	3	0.9	4	1.3
		Lawsonite						
		Pumpellyte					1	0.3
		Allanite					2	0.7
		Piemontite						
		Axinite						
		Tourmaline	134	33.1	67	20.4	40	13.2
	Pyroxenes	*Enstatite*					2	0.7
		Hypersthene	22	5.4			12	4
		Clinopyroxene	1	0.2				
	Amphiboles	*Tremolite*						
		Ferriactinolite					3	1
		Hornblende	12	3	17	5.2	1	0.3
		Glaucophane					1	0.3
	Micas	*Muscovite*	4	1	16	4.9	40	13.2
		Glauconite						
		Biotite	4	1	12	3.7	95	31.5
		Chlorite Group			9	2.7	10	3.3
OXIDES		*Rutile*	28	6.9	20	6.1	9	3
		Brookite	6	1.5	9	2.7	3	1
		Chromian Spinel					7	2.3
		Anatase			3	0.9		
CARBONATES		*Dolomite/ Calcite*			6	1.8		
SULPHIDES		*Sphalerite*					1	0.3
PHOSPHATES		*Apatite*	15	3.7	2	0.6		
		Monazite	10	2.5	5	1.5	2	0.7

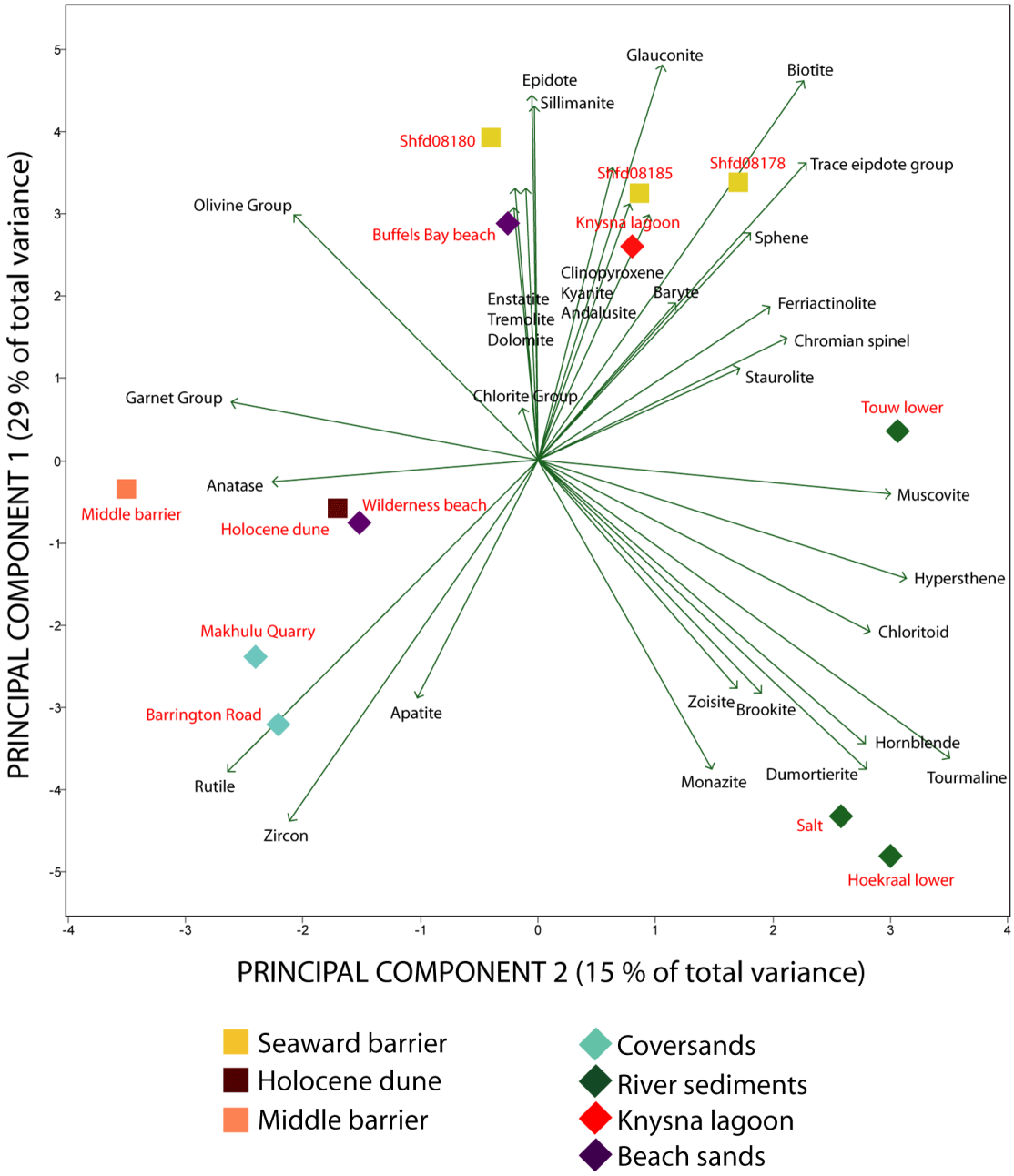

6.4.1 PCA of PCA performed on HM assemblages of barrier dune and possible source sediment samples. PC1 explains 29 % of total variance and PC 2 15 %. Loadings for the PCs are given in Table 6.4.3.

Figure 6.4.1 confirms the mineralogy of the seaward barrier samples are similar to one another, with biotite, epidote, sillimanite and glauconite most significant in determining their positions on the plot (see Table 6.4.3). The Knysna lagoon and Buffels Bay beach sample also plot close by, confirming the assertion inferred from the geochemistry data that the lagoons and beach sands are strongly related to the seaward barrier sands. Unsurprisingly the Wilderness beach sample, identified as a placer deposit according to its geochemistry in section 6.3, has a rather different HM assemblage that is closer to the middle barrier, Holocene dune and coversand samples. All these samples are displaced towards the stable

minerals zircon, rutile and apatite, which have significant negative loadings on both PC 1 and PC 2 (Table 6.4.3). The Salt and Hoekraal lower river sediments plot quite separately to all the other samples considered, evidently possessing significantly different HM assemblages. The Touw lower sample appears slightly more similar to the barrier sands. Tourmaline is particularly abundant in all three river sediment samples (averaging 22.2 %). The apparent difference between the river sediments and the barrier sands could be because the former have not contributed to the latter, or it could be a consequence of the aforementioned overprinting processes that serve to modify HM assemblages during transport and following deposition. For this reason, several other methods of analysing the HM data more widely proven to be capable of elucidating provenance relationships were also explored. These are discussed in the following sections.

Table 6.4.3 Loadings of first two PCs plotted in Figure 6.4.1.

Mineral	PC 1	PC 2	Mineral	PC 1	PC2
Glauconite	0.28	0.10	Zircon	-0.25	-0.19
Biotite	0.26	0.21	Rutile	-0.22	-0.24
Sillimanite	0.25	-0.01	Monazite	-0.22	0.13
Epidote	0.25	0.00	Dumortierite	-0.22	0.25
Trace epidote group minerals	0.21	0.21	Tourmaline	-0.21	0.32
Andalusite	0.20	0.06	Hornblende	-0.20	0.25
Tremolite	0.19	-0.02	Apatite	-0.17	-0.09
Enstatite	0.19	-0.01	Brookite	-0.16	0.17
Kyanite	0.18	0.07	Zoisite/ clinozoisite	-0.16	0.15
Dolomite/ Calcite	0.18	-0.02	Chloritoid	-0.12	0.26
Olivine Group	0.17	-0.19	Hypersthene	-0.08	0.28
Clinopyroxene	0.17	0.09	Muscovite	-0.02	0.27
Sphene	0.16	0.16	Anatase	-0.01	-0.20
Baryte	0.11	0.11	Chlorite Group	0.04	-0.01
Ferriactinolite	0.11	0.18	Garnet Group	0.04	-0.24
Chromian spinel	0.09	0.19	Staurolite	0.06	0.16

6.4.3.1 Zircon-tourmaline-rutile (ZTR) index

Defined by Hubert (1962), the ZTR index is intended to quantitatively define the maturity of a heavy mineral assemblage. Zircon, tourmaline and rutile are considered chemically ultrastable, and high ZTR values very commonly characterise ancient or recycled sands as less stable species are removed over time (Garzanti and Andò, 2007). Hubert (1962) proposed the ZTR index should omit authigenic minerals and this approach was followed here,

with glauconite being removed from the calculations. Results are shown in Table 6.4.4 and Figure 6.4.2. The plot confirms the coversands are the most mature of all the samples considered, which is unsurprising given their great age (>1.6 Ma for a sample from Makhulu Quarry: section 6.1.5). The maturity of their HM assemblages demonstrates the coversands cannot have formed a significant source for the barrier dune sands, as they are unable to explain the diversity of minerals present within them. Figure 6.4.2 also demonstrates the increased maturity of the Holocene dune and middle barrier samples relative to the seaward barrier samples. Interestingly the Touw lower river sample is considerably less mature than the Salt and Hoekraal lower river samples (ZTR of 20.8 % compared to 58.2 % and 70.9 % respectively). The Touw and Hoekraal river courses traverse very similar suites of bedrock (see chapter 4 Figure 4.14), suggesting differences in the HM assemblages of the two samples are likely due to variations in local hydraulic sorting. This could also explain the relative maturity of the Salt River sediment, though this river is the shortest of the three and its headwaters are within the extent of the Knysna coversands (chapter 4 Figure 4.14). It is thus possible that sediment in the Salt River contains a contribution from the coversands as well as the underlying bedrock, which would also account for its increased maturity relative to the Touw lower sample.

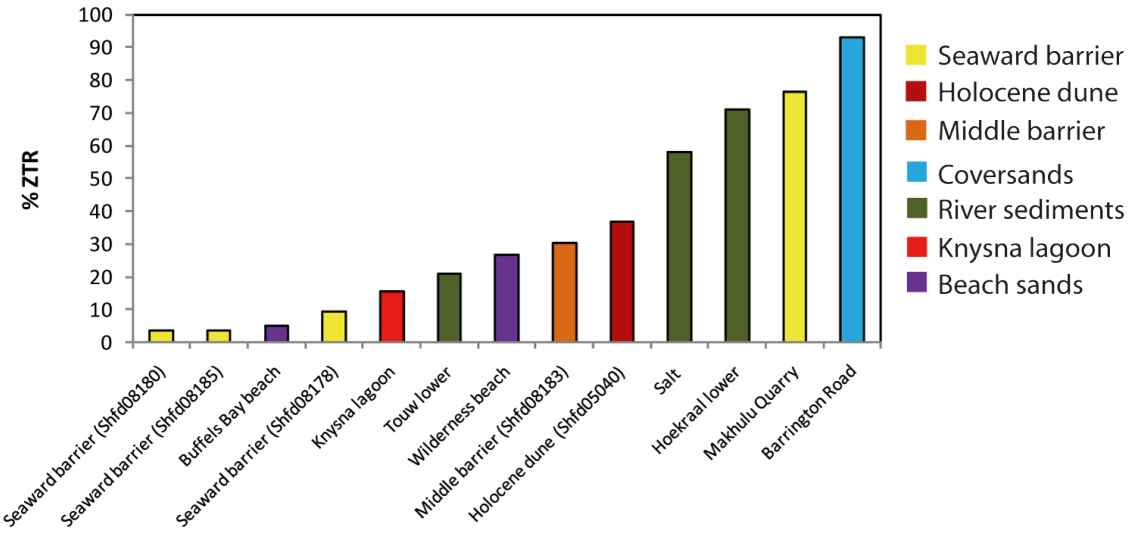

6.4.2 Percentage of zircon, tourmaline and rutile amongst entire HM assemblage (excluding the authigenic marine mineral glauconite) (ZTR index) for Wilderness barrier dune samples and possible sediment sources. Samples organised along x-axis in order of increasing ZTR value. Bar colours indicate sample group (see legend).

6.4.3.2 *Other mineral indices*

Morton and Hallsworth (1994) proposed several HM indices that, by only incorporating minerals with similar hydraulic behaviour that are also stable during diagenesis, should retain a good reflection of source characteristics in sediments derived from them. They are garnet: zircon (Gzi), rutile: zircon (RuZi), monazite: zircon (MZi) and chrome spinel: zircon (CsZi). Values for the Wilderness samples are illustrated in Figure 6.4.3 and given in Table 6.4.4.

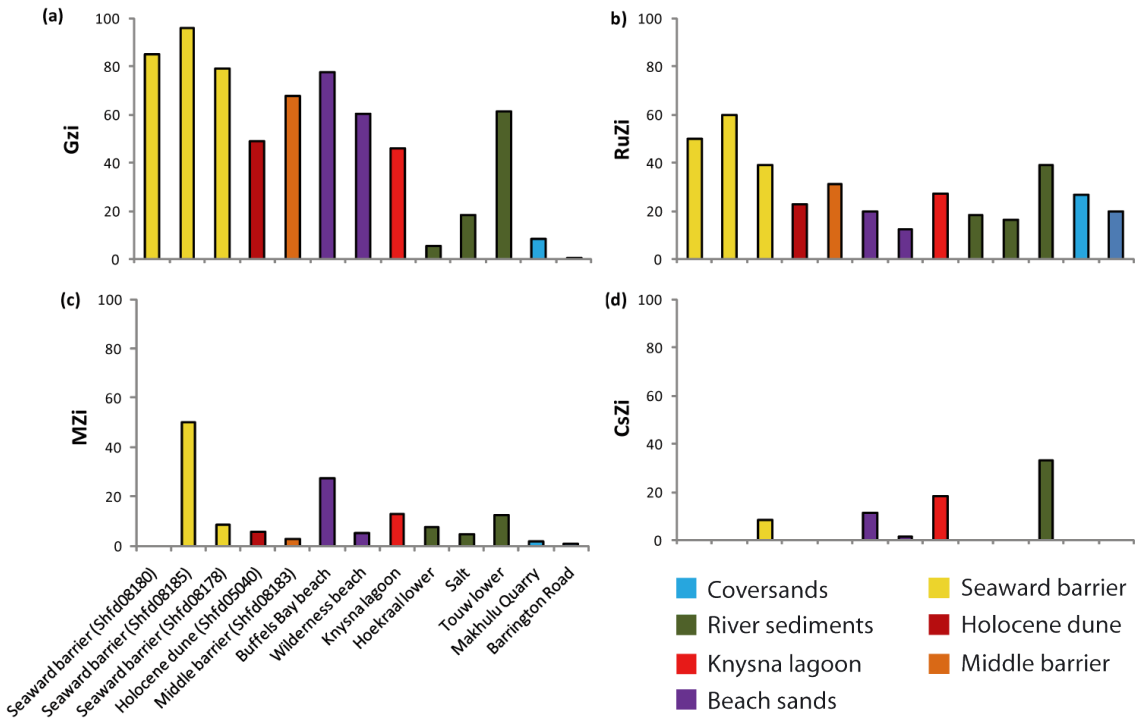

6.4.3 HM indicies comparing Wilderness barrier dune samples and possible sources: (a) garnet: zircon; (b) rutile: zircon; (c) monazite: zircon; and (d) chromian spinel: zircon. X axis labels on (c) apply to all charts. Samples are organised along the x-axis by group, and can be distinguished by bar colour (see legend).

The GZi index (Figure 6.4.3a) confirms the marked difference of the coversands to the barriers, suggesting the coversands have not made a significant contribution to them. Figure 6.4.3a also demonstrates the greater similarity of the Touw lower river sediment to the barrier dune sand samples, relative to the much lower GZi values of the Salt and Hoekraal lower river samples. The RuZi index largely mirrors the GZi, though differences are less pronounced (Figure 6.4.3b). The MZi index (Figure 6.4.3c) is less useful in distinguishing between the different sample groups, with most samples largely similar except for the seaward barrier (Shfd08185) and Wilderness beach samples, which are enriched in monazite. It is interesting to note that the Touw lower sample is the only river sediment which contains chromian spinel (Figure 6.4.3d), a mineral indicative of metamorphic rocks which also occurs in the beach sands, lagoon sediment and seaward barrier (Shfd08178) sample.

Table 6.4.4 Provenance and maturity indices comparing Wilderness barrier dune samples and possible sources. Plotted in Figures 6.4.2 and 6.4.3.

Sample	Index				
	ZTR	Garnet: zircon	Rutile: zircon	Monazite: zircon	Chromian spinel: zircon
Seaward barrier (Shfd08180)	3.57	85.19	50	0	0
Seaward barrier (Shfd08185)	3.73	96.08	60	50	0
Seaward barrier (Shfd08178)	9.43	79.25	38.89	8.33	8.33
Holocene dune (Shfd05040)	36.81	49.09	22.94	5.62	0
Middle barrier (Shfd08183)	30.45	67.46	31.31	2.86	0
Buffels Bay beach	5.26	77.78	20	27.27	11.11
Wilderness beach	26.71	60.11	12.35	5.33	1.39
Knysna lagoon	15.58	46.00	27.03	12.9	18.18
Hoekraal lower	70.86	5.30	18.30	7.41	0
Salt	58.23	18.11	16.13	4.59	0
Touw lower	20.86	61.11	39.13	12.5	33.33
Makhulu Quarry	76.27	8.51	26.50	1.71	0
Barrington Road	93.10	0.36	19.53	0.72	0

6.4.4 Comparisons with local bedrock mineralogy

The mineralogy of the bedrock local to the Wilderness embayment was discussed in chapter 3, but a brief recap of each of the three major bedrock types is provided here. The Kaaimans Group bedrock comprises rocks of low- to medium-metamorphic grade, displaying increasing metamorphism (and consequently increased diversity of mineral species) towards the coast. Primary HM are biotite, chlorite, muscovite and albite. The suite of accessory HM species includes amphibole, andalusite, apatite, chloritoid, epidote, hematite, microcline, plagioclase, sphene, tourmaline, zircon and zoisite/clinozoisite. Garnet is also present close to the granite intrusions (Gresse, 1983; Frimmel and Vanachterbergh, 1995). TMG bedrock is limited to low metamorphic grade. Potgieter (1950) identified zircon as the most common accessory HM in the TMG, rutile, tourmaline, hematite, chlorite and magnetite as fairly abundant, and hornblende, muscovite, garnet and titanite as sparingly present. Krynauw (1983) broadly summarised the petrography of the Woodville granite, identifying biotite as the primary HM, in places altered to chlorite, muscovite and/or clinozoisite. Accessory minerals in

the Woodville granite are identified as garnet, zoisite, calcite, epidote, rutile, zircon, apatite, tourmaline, ilmenite, sphene and magnetite.

Most of the more abundant HM species in the barrier samples, such as chlorite, garnet, tourmaline and zircon are present in all three of the local bedrock types, and thus cannot be used to discriminate any of them as a dominant source for the barrier sands. The vast majority of the other minerals present in the barrier samples are all indicative of metamorphic rocks (e.g. olivine, sphene, garnet, sillimanite, andalusite, kyanite, dumortierite, staurolite, chloritoid, clinozoisite, epidote and others), which could also have originated from any of the local bedrock types. Biotite, a dominant component of the seaward barrier samples, is present in both Kaaimans Group rocks and the Woodville Granite, but not the TMG. The similarity of certain Woodville Granite samples according to PCA of trace element ratios (Figure 6.3.13) suggests that it is more likely to have contributed the mineral to the barriers than the Kaaimans Group.

Ultimately, the HM data presented in this study highlight the paucity of detailed mineralogical studies of southern Cape geology. Numerous mineral species were identified in the extremely limited number of river sediment samples considered here (e.g. kyanite, dumortierite, staurolite, pyroxene group minerals and others) which, given their small catchments, must have originated from one of the three bedrock types considered, but are not mentioned in the literature.

6.4.5 Heavy mineral analysis summary

Given the small number of samples analysed using HM, the findings of this section are treated tentatively. However, for the most part they support the relationships indicated by the geochemistry data in section 6.3. The maturity of the Holocene dune sample relative to the other seaward barrier samples supports the assertion that the Holocene dunes are formed from recycling of seaward barrier aeolianites. The presence of the authigenic marine mineral glauconite in the seaward barrier aeolianites confirms they contain a marine component. The Knysna Lagoon and beach samples appear very similar to the barrier sands in most respects, confirming they are related. The Knysna Lagoon sample also contains a relatively large proportion of glauconite (13.5 %), demonstrating it contains sediment of marine origin, though its broad suite of silicate minerals is indicative of a terrestrial component as well. The maturity of the coversand samples demonstrates they cannot have formed a significant source for the barrier dune sands, as they are unable to explain the diversity of minerals present within them.

Of the three river sediment samples, the Touw appears most similar to the barrier sands, though the differences between the Touw and Hoekraal river samples are interpreted as most likely reflecting local hydraulic sorting effects, rather than their derivation from different parent materials.

Many of the dominant HM species present in the barrier samples are present in two or all three of the major local bedrock groups, preventing the inference of any provenance relationships between barriers and bedrock. However, biotite is an important constituent of the barrier sands, and whilst present in the Woodville Granite and the Kaaimans Group it is absent from the TMG. In combination with the trace element geochemistry data presented in section 6.3, its presence in the barrier sands is interpreted as most likely reflecting a contribution of material from the Woodville Granite. The small number of samples analysed, and the lack of detailed HM descriptions of the bedrock local to the Wilderness embayment in the literature, precludes more detailed analysis in this area.

6.5 Chapter summary

This chapter has presented the results of 36 OSL age determinations conducted on samples from the seaward, middle and landward Wilderness barrier dunes. This represents the longest and most detailed chronology of barrier dune accumulation in the Wilderness embayment yet produced. Two OSL and two ITL ages from the coversands inland of the Wilderness embayment were also obtained, and extend the chronology of this deposit in both directions. The minimum age of >1.6 Ma for the Makhulu Quarry coversand sample more than triples the age of the sample previously obtained by Holmes et al. (2007). Conversely, the ages of 17 ± 2 ka and 66 ± 4 ka from the Barrington Road (Shfd0819) and Karatara Road (Shfd08192) samples provide evidence for Late Quaternary reactivation of the coversands, with the older of these two ages falling very close to the youngest date obtained for seaward barrier accumulation.

The sediment provenancing results present the first detailed, evidence-based consideration of the source of the Wilderness barrier sands. Key findings are:

- Differences in particle size distributions between the three barriers are negligible, indicating no significant changes in transport regime or sediment source between them.

- The KT section samples from the landward flank of the seaward barrier can be distinguished based on particle size distributions and, to some extent, Th/U ratios different from the average barrier characteristics. However, these characteristics are shared by certain other samples from barrier crests, and in all instances they can be associated with lesser burial depths and/or reduced carbonate content. They are thus interpreted as reflecting increased pedogenesis and/or weathering, rather than a change in sediment source or transport pathway.
- The possible local sediment sources for the barrier sands (coversands, river sediment, beach sands and lagoon sediments) all contain significant quantities of fine- and medium-grained sands, and could all consequently have contributed material to the Wilderness barriers.
- Zr/Hf (and to a lesser extent Cr/Co) ratios were interpreted by Dunajko and Bateman (2010) as indicating the KT section of the seaward barrier contains input of material from fluvial sources of sediment local to Wilderness, whereas the seaward flank of the barrier and the Holocene dunes on its crest do not. PCA also identifies certain river samples that are more similar to the KT section samples than others (namely the Diep, Goukamma and Duiwe). However, various other indicators of provenance (Ti/Nb, Cr/Th and the REE ratios) do not discriminate between the KT section samples and the other seaward barrier sands. On balance, whilst the KT section samples may include a component derived from the adjacent Duiwe River, it is considered that they do not represent material of significantly different provenance to the other seaward barrier sands.
- Various immobile trace element ratios, considered in isolation and using PCA, strongly suggest the TMG bedrock may represent the major source of the barrier sands.
- The Kaaimans Group bedrock samples possess geochemical characteristics significantly different to those of the seaward barrier sands according to all methods of analysis, demonstrating they do not represent their parent material. The geochemistry of the Woodville Granite samples is variable, with some more similar to the barriers than others. The importance of biotite in the barrier sands indicates they contain a contribution of material derived from the Woodville Granite pluton.
- The geochemistry of the coversands is extremely variable, with the Makhulu Quarry samples most geochemically distinct from the barrier sands.

Coversand samples from other locations display a greater degree of similarity with the barriers (Barrington Road and Blaricum Heights), but heavy mineral data demonstrates that the coversands are ultimately too mineralogically mature to represent a significant source of material for the barrier sands.

- Sediments from the lagoons and beaches within the Wilderness embayment are indistinguishable or very similar to the barrier sands in almost all respects, clearly indicating the three are related.

7 Discussion

7.1 Introduction

This chapter seeks to synthesise the previously presented chronological and sediment provenancing results into a coherent reconstruction of the emplacement and evolution of the Wilderness barriers. Before presenting the reconstruction, its component elements are discussed individually. The long-term OSL chronology of the barriers is summarised and compared to the global eustatic sea-level record, and the manner in which dunes have accumulated on top of the seaward barrier aeolianites during the Holocene is also considered (evidenced by a compilation of dates from the literature). Other factors possibly responsible for influencing the timing of barrier formation at Wilderness are then examined, namely: (i) shifts from marine to terrestrial sediment supply; (ii) the potential for offshore bathymetry to modulate coastline position; and (iii) regional deviations from the global sea-level record.

The latter part of the chapter (section 7.7) considers the results of this research in a broader context. The history of barrier accumulation at Wilderness is compared with records of Quaternary coastal aeolian activity elsewhere in southern Africa, and with respect to barrier systems globally. A generalised model of barrier accumulation based on this data is also presented. Parts of this chapter have been published in Bateman et al. (2011) but some additional material and detail is incorporated here, including within the reconstruction of barrier emplacement and evolution at Wilderness (section 7.6 and Figure 7.7).

7.2 A chronology of barrier accumulation at Wilderness

7.2.1 Introduction

In order to construct the best possible chronology of barrier formation at Wilderness, all previously published OSL ages from the Wilderness barriers were compiled (from Bateman et al., 2004; Carr et al., 2007; Bateman et al., 2008; Carr et al., 2010a; and Bateman et al., 2011), and are listed in Table 7.1. A combined dataset of 87 ages, comprising these ages and the new dates produced in this study (listed in chapter 6 Tables 6.1.1, 6.1.2 and 6.1.3), is presented in Figure 7.1a and utilised for discussion in the following sections. Locations of the previously published OSL sample sites were given in chapter 4 Figure 4.2, and a schematic of all site names (new and previously published) is provided in Figure 7.1b as an aide-memoire.

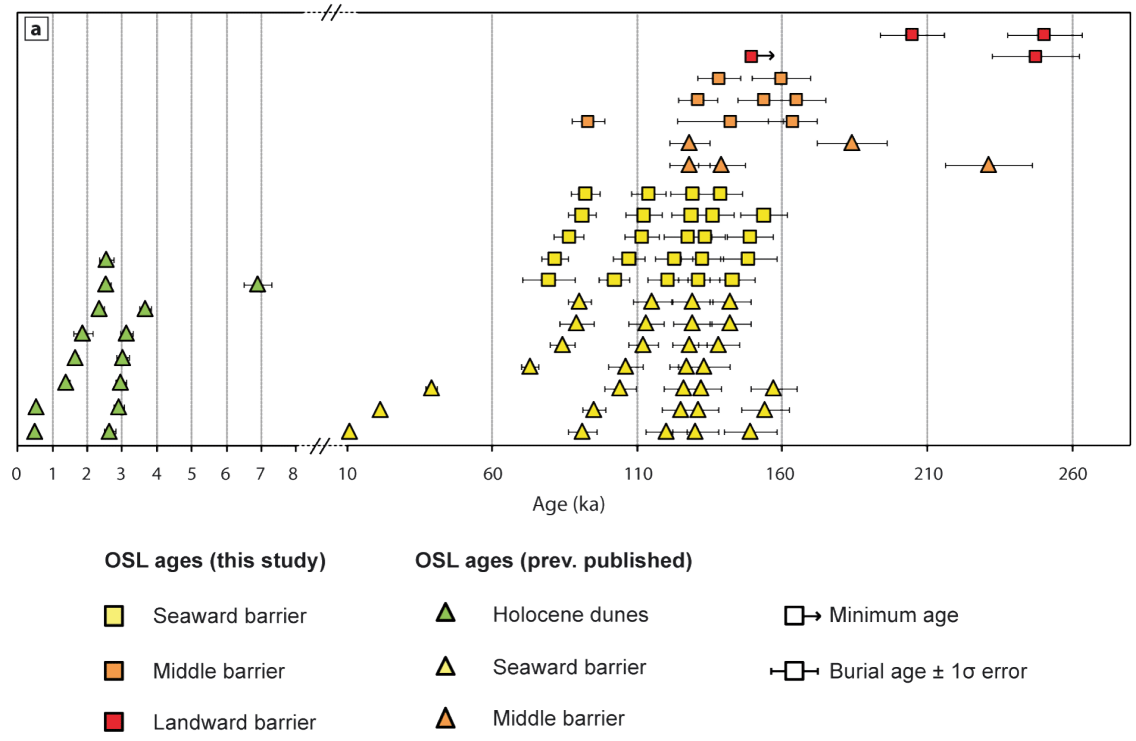

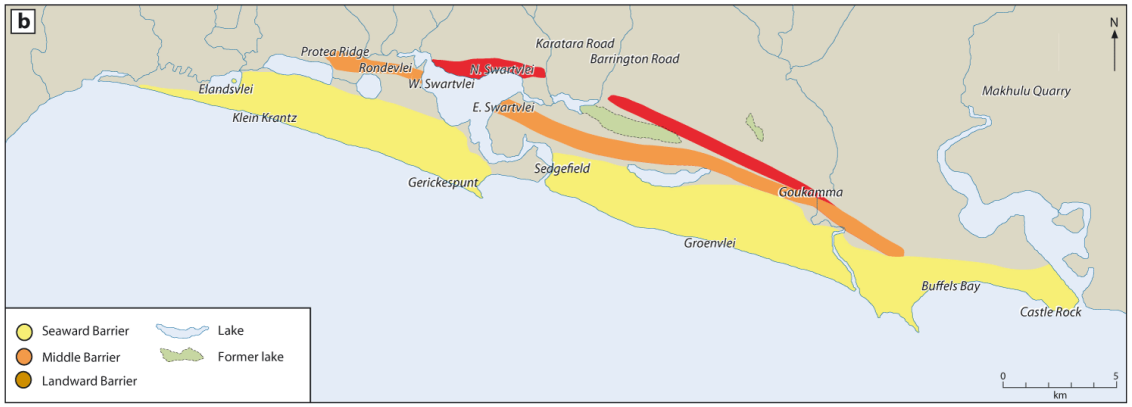

7.1 (a) Compilation of OSL ages from the Wilderness barriers. New ages generated in this study are represented by squares, and previously published ages (listed in Table 7.1) by triangles. Note change in scale on X axis. Y axis scale is arbitrary to improve clarity. (b) Schematic showing broad locations of all new and previously published OSL sample sites by name. Barrier shading corresponds with symbol colours in (a). Coversand OSL/ITL sample site locations are also shown. Note that Holocene dunes are located on top of the seaward barrier, and are not mapped separately.

To provide a frame of reference for the chronology presented here, Illenberger's (1996) model of barrier formation is referred to. Illenberger used a presumed accumulation rate for the barriers (based on radiocarbon dating of the nearby Alexandria coastal dunes and estimations of sand volume) to conclude the seaward barrier formed in the Holocene and last interglacial highstands (MIS 1 and 5: <10 ka and ~120 ka), the middle barrier in the second- and third-last interglacials (MIS 7 and 9: ~200 and ~320 ka), and the landward barrier in MIS 11 and 13 (~410 and ~500 ka). Prior to the undertaking of this research, Illenberger's (1996) model represented the most recent published estimations of middle and landward barrier age.

Table 7.1 Previously published OSL ages from the Wilderness barriers. Broad locations of sample sites are illustrated in Figure 7.1b by name (letters/numbers preceding sample site names correspond with exact site locations shown in chapter 4 Figure 4.2). Continues overleaf.

Sample site and context	Sample code	Altitude (m)	Depth from surface (m)	Age (ka)	Reference
A. Kirsten & Tulleken Quarry (KT section), seaward barrier					
Dune sand	KT2-1	79	1	21.3 ± 0.97	Carr et al. (2007)
Dune sand	KT2-2	78.5	1.5	39 ± 1.9	
Dune sand	KT2-3	78	2	84.2 ± 4.3	
Dune sand	KT2-4	77.5	2.5	104 ± 5.4	
Dune sand	KT2-5	77	3	115 ± 6.6	
Dune sand	KT2-6	76.5	3.5	125 ± 6.5	
Dune sand	KT2-7	76	4	142 ± 7.2	
Dune sand	KT2-8	75.5	4.5	129 ± 6.5	
Dune sand	KT2-9	75	5	132 ± 6.8	
Dune sand	KT2-10	74.5	5.5	157 ± 7.9	
Dune sand	KT2-11	74	6	154 ± 8.2	
Aeolianite	Shfd05032	71.9	8.1	133 ± 9	Bateman et al. (2011)
Aeolianite	Shfd05033	70.85	9.15	142 ± 7	
Aeolianite	Shfd05034	66.95	13.05	149 ± 9	
Aeolianite	Shfd05035	63.85	16.15	129 ± 7	
B. Otto Sands Quarry, seaward barrier					
Dune sand	Shfd02006	72.2	0.8	10.7 ± 0.5	Bateman et al. (2004)
Dune sand	Shfd02007	67.9	5.1	73 ± 3	
Aeolianite	Shfd02008	64	2.65	90 ± 4	
Aeolianite	Shfd02009	59	7.85	128 ± 6	
C. Sedgefield, unconsolidated dune on top of seaward barrier					
Dune sand	Shfd05036	29	20.5	1.87 ± 0.27	Bateman et al. (2008)
Dune sand	Shfd05037	30.1	21.1	2.55 ± 0.2	
D. Swart Estuary, seaward barrier					
Dune sand	Shfd05040	15.2	1.5	3.67 ± 0.17	Carr et al. (2010a)
Aeolianite	Shfd05039	14.7	2.1	95 ± 4	
Aeolianite	Shfd05038	11.7	5	112 ± 5	
Aeolianite	UoW-236	7	6	106 ± 6	
Aeolianite	UoW-235	6.5	6	113 ± 6	
Tidal inlet facies	UoW-234	6	7	127 ± 6	
Tidal inlet facies	Shfd07072	4.5	13.25	130 ± 8	
Tidal inlet facies	Shfd04288	0.5	16.25	138 ± 7	
E. Sedgefield Ridge 1, unconsolidated dune on top of seaward barrier					
Dune sand	Shfd04277	81.8	2.2	2.35 ± 0.13	Bateman et al. (2011)
Dune sand	Shfd04278	79.5	4.5	3.02 ± 0.17	
Dune sand	Shfd04279	78.8	5.2	2.91 ± 0.16	
Dune sand	Shfd04280	77.9	6.1	2.54 ± 0.14	
Dune sand	Shfd04281	76.9	7.1	2.64 ± 0.16	
Dune sand	Shfd04282	75.9	8.1	2.96 ± 0.16	
Dune sand	Shfd04283	74.8	9.2	3.13 ± 0.17	
F. Sedgefield Ridge 2, unconsolidated dune on top of seaward barrier					
Dune sand	Shfd05032	30	2	0.54 ± 0.06	Bateman et al. (2011)
Dune sand	Shfd05033	28	4	0.5 ± 0.07	
Dune sand	Shfd05034	26	6	1.39 ± 0.09	
Dune sand	Shfd05035	24	8	1.66 ± 0.09	
G. Buffels Bay, seaward barrier					
Aeolianite	Shfd05026	30	7	91 ± 5	Bateman et al. (2011)

Table 7.1 Continued from previous page.

Sample site and context	Sample code	Altitude (m)	Depth from surface (m)	Age (ka)	Reference
H. Castle Rock, seaward barrier					
Dune sand	Shfd04275	33.5	2.8	6.9 ± 0.4	
Aeolianite	Shfd04276	28.2	5.3	89 ± 6	
Aeolianite	Shfd04273	19.1	14.4	131 ± 7	Bateman et al. (2011)
Aeolianite	Shfd04272	16.5	17	120 ± 7	
Aeolianite	Shfd04274	0.5	35	126 ± 7	
I. Protea Ridge, middle barrier					
Dune sand	Shfd05046	36	0.5	128 ± 7	Bateman et al. (2011)
2b. East Elandsvlei, seaward barrier					
Marine facies	Shfd05049	3.9	46.1	128 ± 7	Bateman et al. (2011)
8. East Swartvlei, middle barrier					
Aeolianite	Shfd04284	2.5	136	231 ± 15	
Aeolianite	Shfd04285	2.5	136	184 ± 12	Bateman et al. (2011)
Aeolianite	Shfd05048	134.5	0.5	139 ± 8	

7.2.2 The timing of barrier accumulation compared to the sea-level record

The full suite of ages from the Wilderness barriers is compared to the eustatic sea-level curve of Waelbroeck et al. (2002) in Figure 7.2. In interpreting the chronology, it is important to consider the nature of the information provided by OSL dating: that is, it records the timing of the last exposure to sunlight of the dated material. Parabolic dunes, such as those that have coalesced to form the majority of the Wilderness barriers, are migratory in nature. OSL dating of such features records the cessation, rather than initiation, of aeolian activity (Chase and Thomas, 2006), and the distribution of ages must be considered with this in mind. At the same time, the high preservation potential of carbonate coastal dunes (discussed in chapter 2 section 2.3) strongly suggests episodes of reactivation are unlikely to have occurred within the barrier aeolianites. Likewise, their universally low water content at the time of sampling (<4 %: chapter 6 Tables 6.1.1, 6.1.2 and 6.1.3), in spite of the current proximity of the coastline, indicates variations in water table position within the barriers are unlikely to have been responsible for determining whether accumulation is preserved or eroded. Gaps in the chronology should thus reflect true hiatuses in accumulation, as opposed to zeroing of OSL signals during episodes of reworking as is a risk in desert dunes (e.g. Bateman et al., 2003b; Telfer et al., 2010), or episodes of deflation controlled by water table position (e.g. Kocurek and Havholm, 1993).

Beginning with the oldest deposits, OSL samples from the landward barrier Goukamma site, located towards the eastern edge of the embayment (Figure 7.1b), record ages of 250 ± 13 ka and 247 ± 15 ka (Shfd09069 and Shfd09070). The relatively large errors around these dates mean it is not possible to state whether they correspond to the MIS 7e sea-level highstand, to earlier rising sea levels in the MIS 7/8 transition, or to MIS 8. The landward

barrier samples from the northern shoreline of Swartvlei are younger, with Shfd09074 falling firmly within the MIS 7 highstand (205 ± 11 ka) and Shfd09075 at >149 ka. Clearly, none of the four ages fits the MIS 11 and 13 time span suggested for landward barrier accumulation by Illenberger (1996) and, also contrary to Illenberger's model, they tentatively suggest some degree of overlap with the timing of middle barrier formation (Figure 7.2).

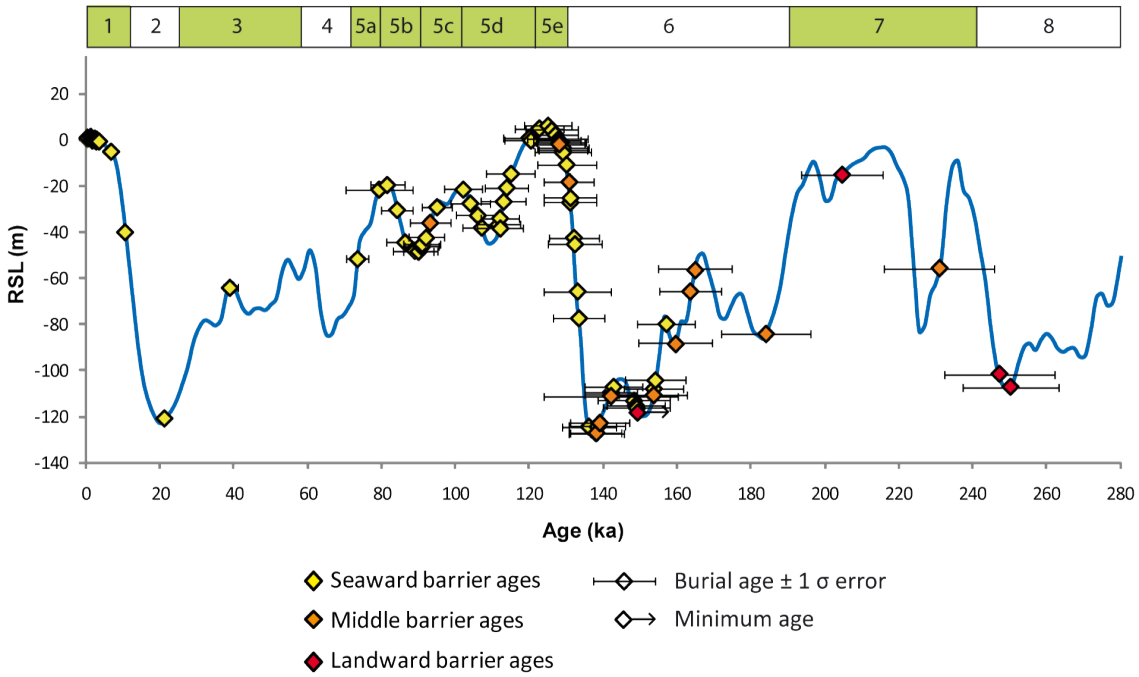

7.2 OSL ages from the Wilderness barriers compared to the global eustatic sea-level curve of Waelbroeck et al. (2002). Figure includes dates from this study and previously published ages compiled from Bateman et al. (2004), Carr et al. (2007), Bateman et al. (2008), Carr et al. (2010a) and Bateman et al. (2011) (see Table 7.1). Note that the OSL ages were not used as index points in constructing the curve, but are located on it for clarity. Bar above plot indicates MIS stages.

Eight new OSL ages were obtained from the middle barrier, making a total of 12 including those from Bateman et al. (2011), from four sites (Figure 7.1b). Two samples from 2.5 m amsl at the base of the middle barrier exposure at East Swartvlei record ages of 231 ± 15 and 184 ± 12 ka (Shfd04284 and Shfd04285: Table 7.1), placing the core of the barrier within the MIS 7 interglacial and broadly contemporaneous with parts of the landward barrier. The lowest sample obtained from the middle barrier exposure at West Swartvlei is slightly higher in altitude at 6.8 m amsl (Shfd09082) and dates to MIS 6 (165 ± 10 ka), suggesting MIS 7 material is only present at the very base of the barrier. As sea levels in MIS 7 reached only -5 to -15 m compared to present (Siddall et al., 2007: see also Figure 7.2), a relatively small volume of barrier accumulation dating to this period is to be expected.

MIS 6 material is also found in the middle barrier, at the East Swartvlei exposure (Shfd08181: 160 ± 10 ka) and at Rondevlei to the west (Shfd09079: 163 ± 8 ka), indicating accumulation of the middle barrier spanned much of the length of the embayment at this time. Significant middle barrier accumulation can also be identified during MIS 5e and the MIS 5/6 transition. Ages from various elevations at the East Swartvlei exposure fall within this period: Shfd08182 at 142 ± 18 ka and 42.8 m amsl; Shfd08183 at 131 ± 7 ka and 78 m amsl; and Shfd05048 at 139 ± 8 m amsl and 134.5 m amsl. Stratigraphically these three samples are almost directly above one another, demonstrating barrier accretion at this time was rapid. MIS 5/6 accumulation was also identified further west at Rondevlei (Shfd09078: 138 ± 7 ka).

Shfd09081, the middle barrier sample from the West Swartvlei barrier crest, was identified in chapter 6 as being potentially unreliable due to its anomalously high dose rate. It is evident in Figure 7.2 that its age of 93 ± 6 ka falls well outside the range defined by the other middle barrier samples. Assuming Shfd09081 is indeed unreliable, accumulation of the middle barrier spanned MIS 7, MIS 6 and the MIS 5/6 transition, and ceased during MIS 5e, at which point aeolian activity continued on the seaward barrier only.

The majority of seaward barrier ages fall within MIS 5, in accordance with Illenberger's (1996) model. Aeolian activity ceased around 75 ka, coincident with eustatic sea level falling below approximately -50 m amsl (Figure 7.2). Ages corresponding with the low sea levels of MIS 2-4 are almost completely absent: only samples KT2-1 and KT2-2 from the KT section date to this period, at 21.3 ± 0.97 and 39 ± 1.9 ka respectively (Table 7.1). Dune accumulation resumed on the seaward barrier crest during the Holocene as sea levels once again reached a highstand position (Figure 7.2). Perhaps the most striking feature of the seaward barrier chronology is the lack of evidence for barrier formation under low sea levels in MIS 2-4, in contrast to the number of barrier ages coinciding with similarly low sea levels in MIS 6 and the MIS 5/6 transition (Figure 7.2). Moreover, the MIS 6 paired samples obtained from either side of bounding surfaces at Gerickes Point fall within errors of one another, indicating accumulation at that time was rapid (Shfd08179 and Shfd08178 at 149 ± 8 and 154 ± 8 ka, and Shfd08174 and Shfd08175 at 143 ± 8 and 148 ± 10 ka).

7.2.3 Synthesising the chronology

In order to identify whether discrete phases of deposition can be isolated within the entire OSL chronology, and to consider more thoroughly the uncertainties surrounding the ages, various statistical analyses were performed. A probability density function of the

seaward, middle and landward barrier ages was constructed (excluding the unreliable Shfd09081 middle barrier sample) using a bin size based on the median uncertainty of the ages (= 5 %), and is shown in Figure 7.3. The main phases of accumulation clearly fall in MIS 5e and 5b. Figure 7.3 also displays the results of FMM applied to the ages >70 ka. Using an OD value of 0.05 (again, based on the median uncertainty surrounding the 68 OSL ages analysed), the best fit for FMM was produced by extracting four phases of deposition from the chronology. These span 245-217 ka, 155-143 ka, 128-121 ka and 91-86 ka. Whilst the small number of ages in the 245-217 ka phase (and their large errors) make this episode difficult to associate with a particular sea-level position, the two MIS 5 depositional phases are clearly associated with relatively high sea levels. The much lower eustatic sea-level position during the MIS 5/6 episode of accumulation from 159-143 ka thus forms something of an anomaly. Possible explanations for barrier accumulation at Wilderness during this period are explored in sections 7.3-7.5 below, following a more detailed consideration of the Holocene dune chronology, which forms another discrete phase of deposition post 6 ka (Figure 7.2).

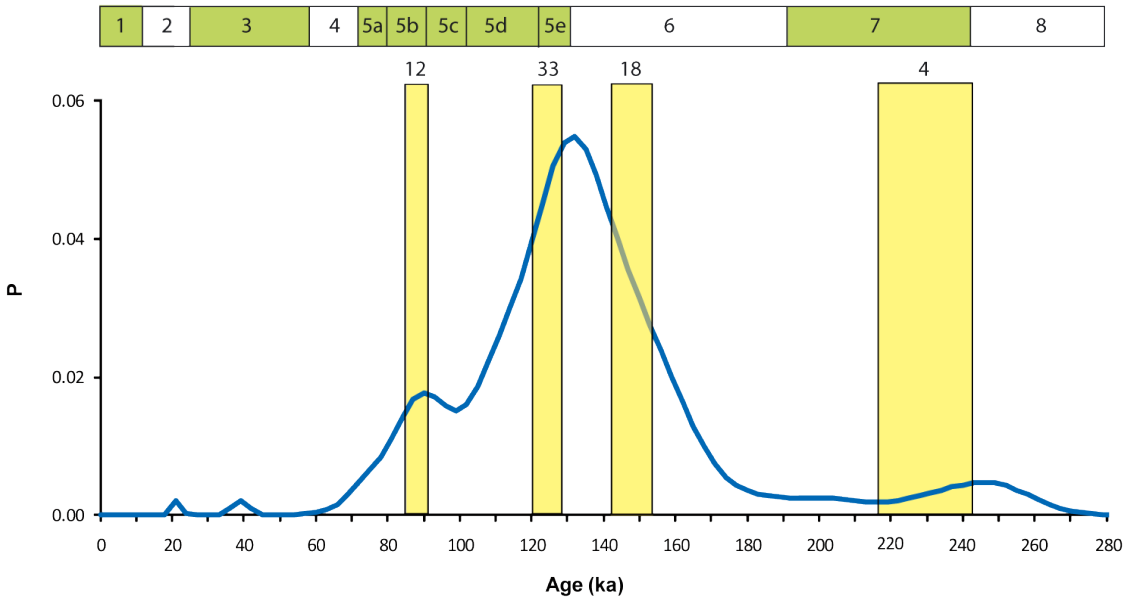

7.3 Probability density function of the seaward, middle and landward barrier OSL ages, using a bin size based on the median uncertainty of the ages (= 5 %). Overlying the PDF are shaded boxes indicating where FMM isolated components within the dataset (conducted using OD = 0.05). Numbers at the top of the boxes indicate number of OSL ages contained within each component. Bar above plot indicates MIS stages.

7.2.4 Holocene dune accumulation

Previously published OSL ages from Holocene dunes located on top of the seaward barrier, as listed in Table 7.1, are compared to the relative sea-level curve for South Africa of Compton (2001) in Figure 7.4. The greater precision afforded by the Holocene ages and sea-

level curve permits a more detailed analysis of the relationship between aeolian activity and sea level than for the older samples, and provides a potential analogue for earlier episodes of barrier accumulation at Wilderness.

The vast majority of Holocene dune activity has been concentrated in the last 4 ka, following the sea-level highstand of +3 m at 6.5 ka and its subsequent regression to -0.5 m at 5 ka (Figure 7.4). Most of the Holocene dune samples were obtained by coring (Bateman et al., 2011), and the paucity of ages from 8-4 ka may simply reflect the depth reached. However, samples Shfd05036 and Shfd05037 (dating to 1.87 ± 0.27 and 2.55 ± 0.2 ka) are from the same dune as the cored samples Shfd04277-Shfd04283 (dating from 2.35 ± 0.13 to 3.13 ± 0.17 ka), but stratigraphically ~50 m lower (Table 7.1) and resting very close to the underlying MIS 5 aeolianites. This indicates material >4 ka is indeed absent from the dune.

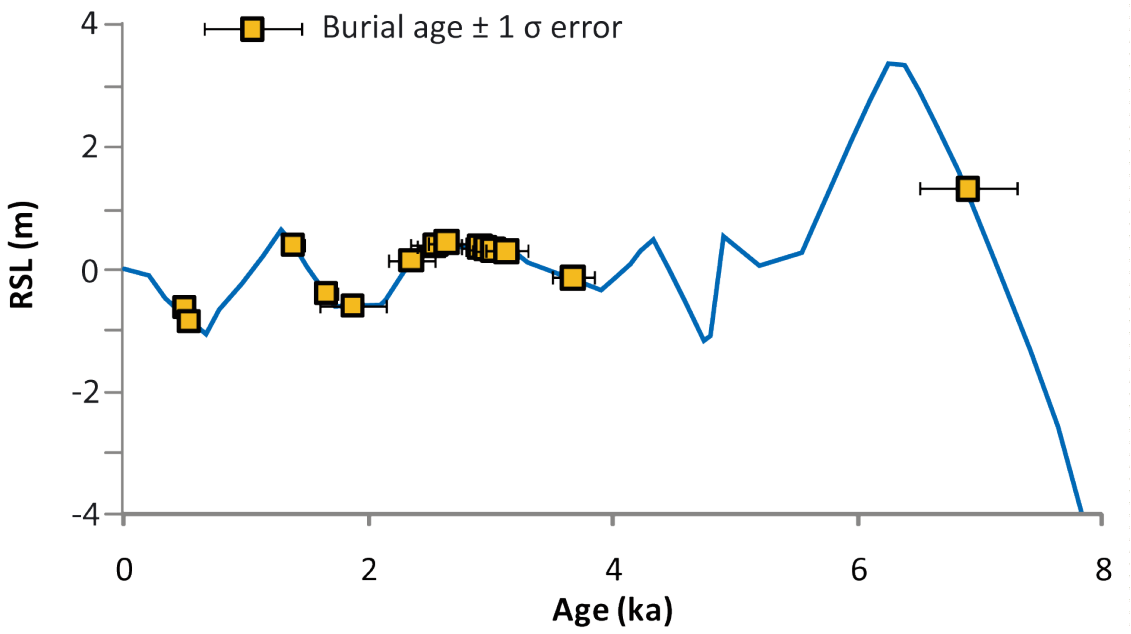

7.4 Comparison of the distribution of OSL ages from Holocene dunes located on the crest of the seaward barrier (compiled from Bateman et al., 2008; Carr et al., 2010a; and Bateman et al., 2011: see Table 7.1) to the South African relative sea-level curve of Compton (2001). Note that the OSL ages were not used as index points in constructing the curve, but are located on it for clarity.

An alternative explanation for the lack of Early Holocene ages is provided by the increased mineralogical maturity of the Holocene dunes sands relative to the older aeolianites (discussed in greater detail in section 7.3.4 below). The greater maturity of the younger deposits suggests that recycling of sediment has been more important in the Holocene than in previous episodes of barrier formation. Commencement of the OSL record c. 4 ka could correspondingly be interpreted as reflecting continued dune activity on the barrier crest around the Mid-Holocene sea-level highstand, with the preservation of aeolian strata

occurring only once sea levels lowered and stabilised. The single Holocene dune age pre-dating the Holocene sea-level maxima, Shfd04275 at 6.9 ± 0.4 ka, was obtained from the Castle Rock site at the very edge of the embayment (Figure 7.1b) and at a relatively high elevation of 33.5 m overlying a MIS 5 aeolianite sea cliff (Table 7.1). Jennings (1967) proposed coastal dunes in cliff-top settings form as dunes advance up pre-existing slopes that are subsequently eroded. This age is interpreted as having either formed in such a manner, or having otherwise somehow been protected from erosion/recycling by virtue of its position at the embayment edge abutting the hard rock geology of the Knysna headland.

7.2.5 Summary

Combining the paucity of barrier ages corresponding with low sea levels during MIS 2-4, the distribution of Holocene dune ages, and the MIS 5b and 5e episodes of accumulation extracted using FMM, the OSL chronology is interpreted as indicating a proximal coastline is important in controlling the position of barrier accumulation at Wilderness. Whether the sediment provenancing results provide further evidence for this, along with possible explanations for the anomalous MIS 5/6 episode of accumulation coinciding with low eustatic sea level, is explored in the following sections.

7.3 Provenance of the barrier sands

7.3.1 Introduction

Whilst the manner of Holocene dune accumulation at Wilderness discussed in the previous section can also be applied to the barrier ages dating to the MIS 5 and MIS 7 highstands, it fails explain the significant number of MIS 6 and MIS 5/6 transition ages coinciding with relatively low eustatic sea levels. Bateman et al. (2004) hypothesised that increased input of terrestrial sediment may have been more important for dune building at Wilderness during such periods. A possible precedent for barrier construction in this manner is provided by dunefields located down-drift of river mouths at several other locations on the Cape coast, e.g. False Bay (Roberts and Brink, 2002), the barrier islands on the Mozambique coast (Armitage et al., 2006) and the Alexandria coastal dunefield (Illenberger and Rust, 1988). This possibility is explored in the following sections, in which the provenance of the barrier sands is discussed.

7.3.2 Weathering and carbonate content

The highly variable carbonate content of the seaward Wilderness barrier was cited by Bateman et al. (2004) as potentially indicating that barrier construction at Wilderness during periods of low sea level was sustained by a shift from marine to terrestrial sediment supply. This was investigated by comparing the sedimentary characteristics of the relatively carbonate-poor KT section seaward barrier samples, which record deposition from MIS 2-4 and MIS 6 as well as MIS 5 (Table 7.1), to samples from various other locations within the barriers. Whilst the KT section samples are distinct from the other barrier sands according to their increased kurtosis and skewness values, these characteristics are also shared by other samples exhibiting evidence of pedogenisation (e.g. Shfd09081 from the West Swartvlei barrier crest and Shfd09069 from the Goukamma site) (chapter 6 Figure 6.2.4). Shfd09081 and Shfd09069 are similarly depleted in carbonate, suggesting its relative paucity in the KT section may too be due to post-depositional modification. Most tellingly, the correlation between carbonate content and depth amongst the KT section samples is strong (R^2 = 0.66) (chapter 6 section 6.2.2), clearly demonstrating their carbonate content has been reduced post-depositionally rather than differing in the first instance.

The relatively low carbonate content of the KT section samples, and by extension the other carbonate-depleted barrier sands, is thus attributed to increased weathering rather than a shift from marine to terrestrial sediment supply. That the KT section samples are more weathered than the other seaward barrier sands is confirmed by their elevated Th/U ratios (chapter 6 Figure 6.3.2). Both lines of evidence (carbonate content and Th/U) indicate burial depth is more significant than age in controlling the degree of weathering within the barriers.

7.3.3 Can changes in provenance be distinguished within the seaward barrier sands?

Whilst the reduced carbonate content of the KT section samples cannot be interpreted as indicating they contain a greater proportion of terrestrial material relative to the barrier average, they are also distinct from other seaward barrier sands according to their Zr/Hf ratios. In turn, the Zr/Hf ratios of the KT section samples overlap with the sediment of certain rivers debouching within the Wilderness embayment (chapter 6 Figure 6.3.12), indicating a possible provenance relationship between the two. Further evidence in support of this is provided by PCA analysis of multiple immobile trace element ratios (Cr/Co, Cr/Th, Ti/Nb, Zr/Hf, Eu/Eu* and La_N/Yb_N), which confirms the similarity of certain river sediments (from the Diep, Goukamma and Duiwe) to the KT section material (chapter 6 Figure 6.3.13). However, whilst the Duiwe River runs adjacent to the KT section site, the Diep and Goukamma river courses lie further

east (chapter 4 Figure 4.14). Given the eastward direction of longshore drift, it is not conceivable how sediment from these three rivers could be concentrated at the KT section site, but not have contributed to other parts of the barrier. Moreover, despite the apparent similarity of the Duiwe, Diep and Goukamma river sediments' geochemistry, the headwaters of the Duiwe River rise in Kaaimans Group rocks, whereas the Diep traverses the TMG and the Woodville Granite pluton, and the Goukamma the TMG and the Kaaimans Group (chapter 4 Figure 4.14). In settings where possible sediment sources are geologically relatively similar, there is a risk that geochemical variation attributable to factors other than parent material, e.g. particle size or hydraulic sorting, may obscure provenance signals (Pe-Piper et al., 2008). Whilst the elements selected for analysis were screened for particle size controls on their concentrations, the similarity of the Duiwe, Diep and Goukamma river sediments, despite the different bedrock types they traverse, suggests non-provenance related factors have most likely influenced their geochemistry.

On balance, it is concluded that whilst the KT section samples may include a component derived from the adjacent Duiwe River, they do not represent material of significantly different provenance to the other seaward barrier sands. Additionally, the similarity of particle size distributions amongst samples from all three barriers (demonstrated to be largely indistinguishable by PCA) is interpreted as indicating no significant changes in transport regime have occurred throughout their accumulation from the Holocene to MIS 7.

7.3.4 Have local sediment sources been important in barrier formation?

The presence of significant amounts of carbonate in all unaltered barrier samples further confirms that the transport pathway of material to them must involve the nearshore zone and, by extension, a proximal coastline. Excepting erosion and recycling of the coastal aeolianites themselves, a terrestrial source for the carbonates can be ruled out by its absence from published descriptions of local geology (see chapter 3 section 3.3). This is further confirmed by the lack of carbonate observed in samples of river sediments (chapter 6 Table 6.2.3). Particle size distributions and graphical moment statistics provide additional evidence that the barrier sands and beach sediments are closely related (chapter 6 section 6.2.4).

The authigenic marine mineral glauconite, characteristic of formation on continental shelves at water depths of 50-500 m, was also observed in reasonably significant quantities in samples of seaward barrier aeolianites (averaging 11.6 % of the non-opaque HM fraction of the sands: chapter 6 section 6.4.2), indicating another small marine component additional to

the carbonate fraction. Glauconite and carbonate are also present in the lagoon sediments, indicating that they represent either eroded barrier material or overwash from the beach, rather than "fresh" sediment introduced to the lagoons by rivers.

All three groups of seaward barrier samples (the aeolianites, the KT section samples, and the Holocene dunes on the barrier crest) possess REE characteristics in line with typical quartz-rich sediments and sandstones, consistent with a siliciclastic, terrigenous source for their non-carbonate/non-glauconite fraction. On the basis of combined evidence from various geochemical provenance indicators (REE curves and the immobile element ratios Eu/Eu*, La_N/Yb_N, Zr/Hf, Ti/Nb and Cr/Th), it is possible to rule out the outcrop of pre-Cape metasedimentary rocks local to Wilderness (the Kaaimans Group) as having made a major contribution to the barrier sands. Conversely, samples of TMG bedrock are geochemically indistinguishable from the barrier sands according to PCA analysis of multiple immobile trace element ratios (Cr/Co, Cr/Th, Ti/Nb, Zr/Hf, Eu/Eu* and La_N/Yb_N: chapter 6 Figure 6.3.13a), strongly suggesting they represent their parent material. There is a risk that the geochemical similarity of the barrier sands and the TMG is the result of equifinality: the homogenising effects of sedimentary processes are known to result eventually in very similar REE distributions in sediments originally derived from different sources, ultimately reflecting the average UCC abundances of these elements (Taylor and McLennan, 1985). However, the likeness of the TMG samples and the barrier sands is most apparent with respect to immobile element ratios limited to certain HM species (Ti/Nb and Cr/Th in particular: chapter 6 Figure 6.3.11b), rather than the REE, suggesting the provenance relationship is real.

TMG bedrock is exposed in a 30-60 km broad belt along much of the southern Cape coast (chapter 3 Figure 3.1), and it is consequently impossible to determine whether or not the barrier sand material was derived from outcrops local to Wilderness. The Gouritz River, debouching ~75 km to the west, traverses TMG rocks and is a much greater contributor of material to the nearshore zone off Wilderness than the small river catchments within the embayment itself (Martin and Flemming, 1986), suggesting it probably represents the dominant source of the barrier sands.

Interestingly, biotite is a dominant constituent of the HM assemblages of the barriers (averaging 30.8 %: chapter 6 section 6.4.2), despite it not being reported as present in the TMG (Potgieter, 1950). Biotite is, however, a major component of both the Kaaimans Group and the Woodville Granite pluton (Gresse, 1983; Krynauw, 1983). The relative similarity of certain Woodville Granite samples to the barrier sands according to PCA of trace element ratios (chapter 6 Figure 6.3.13a) suggests it, rather than the Kaaimans Group, is responsible for

contributing this mineral to the barrier sands. Sand derived from the Woodville Granite would be transported to the nearshore zone off Wilderness by local rivers, where it mixes with both authigenic marine material and sediment derived from TMG rocks. The TMG sediment probably also includes a local component, though is likely sourced predominantly from the Gouritz River to the west. The resultant combination of sediment comprises the beach sands in the embayment and thus, ultimately, the barrier material. An additional input to the barrier sands is almost certainly provided by erosion of pre-existing aeolianites deposited in the embayment. Amino acid racemisation data from coastal aeolianites at Still Bay, ~120 km west of Wilderness, demonstrates such recycling of sediment was important in MIS 5 barrier formation there (Roberts et al., 2008). At Wilderness, the mineralogical maturity of the Holocene dunes sands relative to older samples (as evidenced by their high ZTR values) suggests that recycling has been more important in the Holocene than during previous episodes of barrier formation.

7.3.5 The relationship between the Wilderness barriers and the coversands

The final possible local sediment source for the Wilderness barrier sands is the coversand deposits inland of the embayment. OSL data presented by Holmes et al. (2007) demonstrated the coversands to be at least Mid Quaternary in age. With application of ITL dating to a sample from the coversand typesite at Makhulu Quarry (Figure 7.1a), this is pushed back to >1.6 Ma. Stable isotope data from the underlying lignites, which the coversands grade into, supports the assertion that they are at least Early Quaternary in age (Carr et al., 2010b). The geotechnical properties of the coversands indicate they are vulnerable to erosion (Marker and Holmes, 2005), and remobilisation of the deposits into estuaries and onto floodplain terraces has been observed during recent rainfall events (Marker, 2003). Ages of 17 ± 2 ka (Shfd08190), 66 ± 4 ka (Shfd08192) and 362 ± 15 ka (Shfd08191) from the Barrington Road and Karatara Road coversand sites (Figure 7.1a) may also represent episodes of reactivation, and it is possible that sediment released in these events could have been transported to the nearshore zone, and consequently recycled to form the barriers. However, HM analysis demonstrates the coversands are extremely mature, being dominated by the ultrastable HM species zircon, tourmaline and rutile. They are unable to account for the much greater diversity of HM species present in the barrier sands, and consequently have most likely not made a major contribution of material to them.

7.4 Offshore bathymetry and coastline position

Since it has been demonstrated that barrier accumulation at Wilderness outside of interglacial sea-level highstands was not sustained by a shift from marine to terrestrial sediment sources, an alternative explanation for the MIS 6 and MIS 5/6 transition seaward and middle barrier OSL ages must be found. As discussed in chapter 2, nearshore bathymetry controls the magnitude of shifts in coastline position caused by changes in sea level and, consequently, the position of the ultimate sediment source for coastal-dune building (i.e. the beach). Considerations of continental shelf topography have proven useful in interpreting aeolian and archaeological records found at other southern Cape locations and elsewhere (e.g. Dillenburg et al., 2000; Fisher et al., 2010; Compton, 2011). Bateman et al. (2011) produced a DEM of the nearshore continental shelf around the Wilderness embayment and, in conjunction with the eustatic sea-level curve of Waelbroeck et al. (2002), reconstructed the coastline position at various points in time corresponding with sea-level high- and lowstands (Figure 7.5).

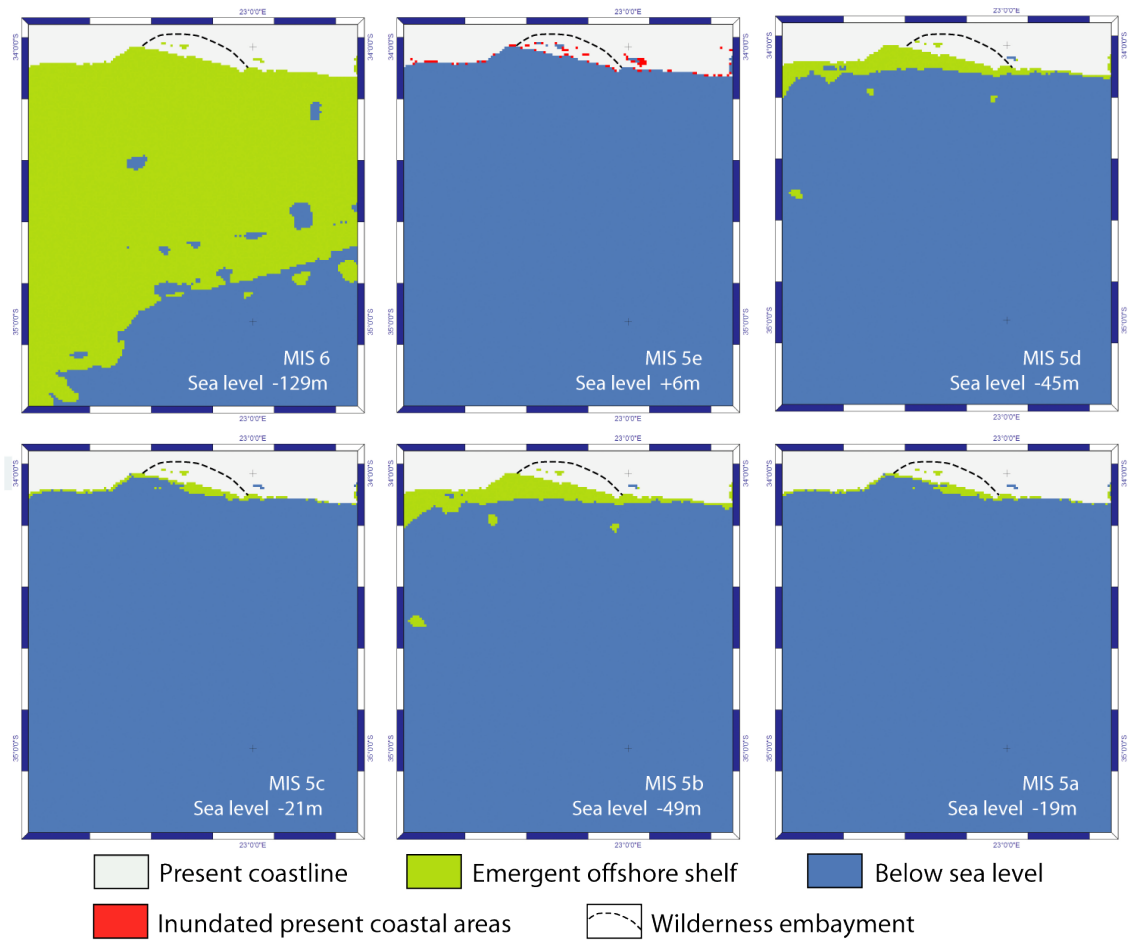

7.5 Modelled shifts in coastline position at Wilderness in response to eustatic sea-level changes from MIS 6 (c. 137 ka) to MIS 5a (c. 80 ka). Time slices selected to represent interglacial sea-level highstands and glacial sea-level lowstands. Modified from Bateman et al. (2011).

The reconstruction of coastline position at Wilderness shown in Figure 7.5 demonstrates that there are clear bathymetric differences between the east and west sides of the embayment, with the gentle shelf slope in the west causing the coastline there to recede southward quite quickly in response to the relatively small falls in sea level during MIS 5d and 5b. Conversely, the steeper shelf slope on the east side of the embayment allowed the corresponding section of coastline to remain close to its present position throughout MIS 5. The differences in seaward barrier chronology related to nearshore bathymetry are illustrated in Figure 7.6, which plots OSL ages from sample sites adjacent to the current coastline vs. their distance from the western edge of the embayment.

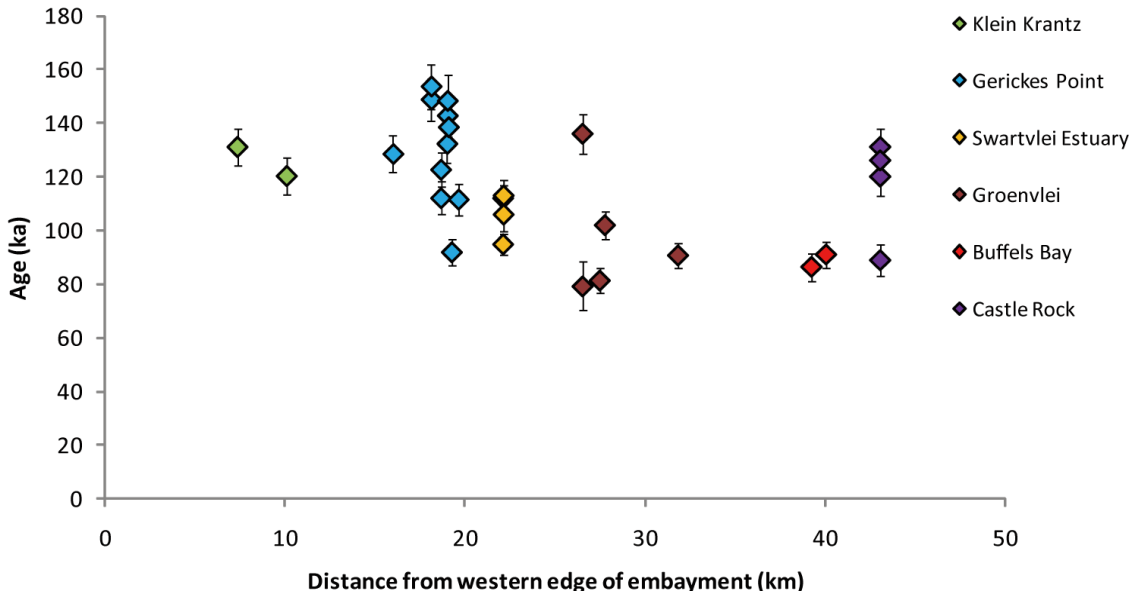

7.6 Seaward barrier ages organised according to sample sites and their distance from the western edge of the Wilderness embayment, illustrating the difference in timing of barrier construction between the east and west sides of the embayment. Sample site locations shown in Figure 7.1b.

Towards the east of the embayment, Figure 7.6 illustrates that MIS 5 deposition continued to the very end of MIS 5 (sub-stage 5a at c. 80 ka). Conversely, it ceased earlier in the west, contiguous with earlier sea-level regression (and thus, withdrawal of sediment supply) there. The pattern is slightly complicated slightly by an age of 92 ± 7 ka at Gerickes Point (Shfd09149), located in the western half of the embayment, though this sample is the farthest south of all those obtained from the site (see chapter 6 Figure 6.1.5), and would thus be expected to be the youngest. Bateman et al. (2011) suggested the age could be related to the palaeo-valley of the Swart River, visible in the high-resolution DEM shown in chapter 3 Figure 3.11. The steep gradient of the river valley would have kept the estuarine shoreline within it closer to its present position as sea levels receded, allowing barrier construction to

continue during more of the regression (similar to the generally steeper shelf slope in the east). The long period of MIS 5 accumulation permitted at Gerickes Point may also explain the high altitude of the barrier there.

7.5 Regional deviations from the eustatic sea-level record

Whilst explaining the distribution of ages within the seaward barrier following the MIS 5e sea-level highstand, consideration of offshore bathymetry fails to provide an explanation for the preceding MIS 5/6 episode of deposition. Moreover, the close association of MIS 5 ages with coastline position further confirms the importance of beach proximity in barrier construction, compounding the puzzle of the MIS 6 and MIS 5/6 transition ages. According to the global eustatic sea-level curve of Waelbroeck et al. (2002), at 170 ka sea levels were at -49 m amsl, and they continued to fall to below -100 m amsl until rising rapidly at 132 ka.

Using strontium isotope ratios in speleothems from southern Cape caves as a proxy for distance to the ocean, Fisher et al. (2010) inferred a brief transgressive event around 167 ka that moved the coastline there to within ~5 km of its current position. Further evidence of a regional sea-level transgression at this time is provided by the archaeological record at Pinnacle Point Cave, located on the present coastline ~56 km WSW of Wilderness, which includes evidence of humans utilising marine resources at 164 ± 12 ka (Marean et al., 2007). The MIS 5/6 OSL ages at Wilderness, which begin at 154 ± 8 ka on the seaward barrier (Shfd08178) and 160 ± 10 ka on the middle barrier (Shfd08181), are thus interpreted as reflecting this pre-MIS 5 transgression, which is absent from the global eustatic sea-level curve of Waelbroeck et al. (2002). The termination of the last glacial was also marked by an episode of rapid sea-level rise followed by an abrupt, but brief return to glacial conditions (the Bølling-Allerød warm interval and the Younger Dryas stadial), inferred from far-field sea-level records and interpreted as reflecting a large meltwater pulse from the Laurentide ice sheet and subsequent disruption of the thermohaline conveyor (Weaver et al., 2003). Similarly, Siddall et al. (2006) report evidence of a brief, early sea-level highstand prior to MIS 5 from the oxygen isotope ratio of Red Sea sediment cores.

7.6 A reconstruction of barrier emplacement and evolution at Wilderness

Through drawing together the above lines of evidence, a thorough reconstruction of the emplacement and evolution of the Wilderness barriers through the Mid- to Late-Quaternary has been produced (Figures 7.7 and 7.8). Though the age of the Wilderness embayment itself is unknown, it likely significantly pre-dates the oldest (MIS 7) OSL ages obtained from the barriers within it. Evidence suggests that the MIS 11 sea-level highstand, c. 400 ka, was one of the highest and longest of the Quaternary, with sea levels reaching in excess of 21 m above present (Olson and Hearty, 2009). Given the magnitude of barrier erosion that has taken place at Wilderness during the Holocene, it is plausible that an older generation of Early-Mid Quaternary barriers occupying the embayment were entirely removed by the MIS 11 transgression.

Accumulation of the oldest extant aeolian feature present in the embayment, the landward barrier, began no later than 250 ka (MIS 7). No ages corresponding with MIS 9 were obtained from the landward barrier, though this may reflect the limited number of sites located and dated within it. Given that the middle and seaward barriers both formed over multiple interglacials, and that sea levels in MIS 9 were comparable to or slightly higher than present (Siddall et al., 2007), material of MIS 9 age is probably present at the core of the landward barrier (Figure 7.7a).

The geomorphology of the landward barrier is more akin to a sand ramp banked against the rear of the embayment than a “true” coastal barrier dune, but its high-angle, cross-bedded aeolianite (observed at both the North Swartvlei and Goukamma sites) is identical to the stratigraphy of the middle and seaward barriers, indicating it too formed from vertical and lateral stacking of parabolic dunes. The landward barrier reaches a maximum of ~250 m elevation towards its western-most point, is more subdued towards the centre of the embayment, and is absent from the east entirely. Its extension westward is curtailed by the Hoekraal and Karatara Rivers, before it resumes on the north shore of Swartvlei and ceases completely where it meets the Diep and Wolwe (Figure 7.7a). The lower elevation of the barrier to the west is interpreted as reflecting its continued erosion by migration of these rivers, similar to the subdued nature of the seaward barrier around the Goukamma and Swart river mouths.

Assuming that the younger barriers provide an appropriate analogue, accumulation of the landward barrier after MIS 9 will have resumed once rising sea levels in the MIS 7/8

transition reached a position approximately -50 m amsl. Also using the seaward barrier as an analogue, the beach sands in MIS 7 and 9, and thus by extension the landward barrier material, comprised a mixture of marine carbonate and terrigenous sediment, with the latter predominantly derived from TMG sandstone. The major source of the terrigenous fraction was most likely the Gouritz River, debouching ~75 km to the west, with its load transported to the beaches of the Wilderness embayment via alongshore drift. The beach sands also included a component provided by local rivers, and probably material recycled from previous generations of barrier as well. Evidence suggests that this mixture of sediment sources has remained largely constant across the formation of all three barriers.

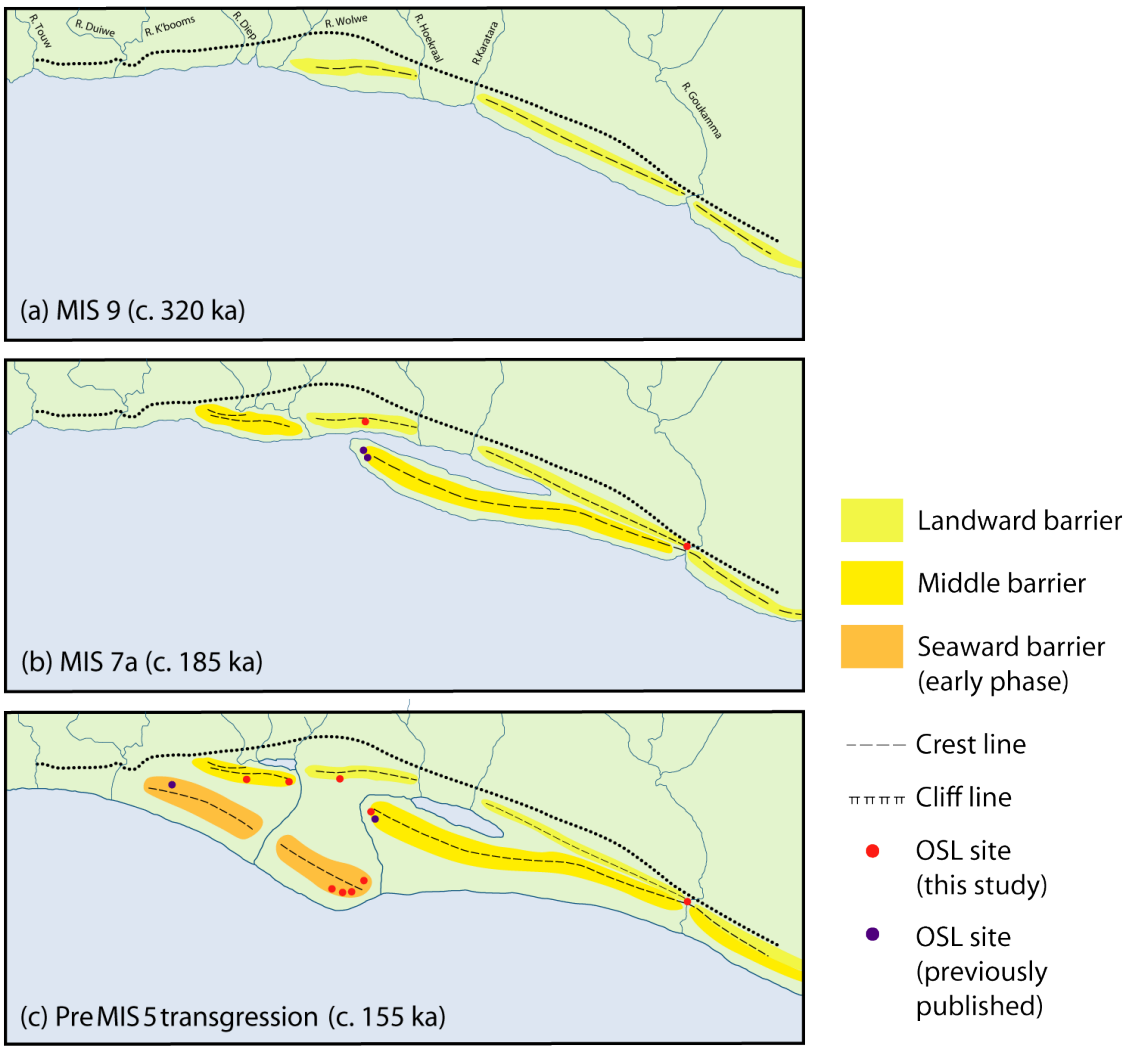

7.7 Model of Mid- to Late-Quaternary barrier emplacement and evolution at Wildernesss from MIS 9 to the pre-MIS 5 transgression.

The chronology of the middle barrier suggests its preservation began later than the landward barrier, and in response to falling sea levels in MIS 6 following the MIS 7 highstand. Free from the constraints of the hard-rock geology at the rear of the embayment, the middle barrier initiated as a true coastal barrier, rather than mirroring the sand-ramp morphology of

the landward barrier (Figure 7.7b). Sea levels in MIS 7 reached only -5 to -15 m compared to present (Siddall et al., 2007), explaining the relatively small volume of MIS 7 barrier accumulation compared to subsequent phases of accumulation. Additionally, it is well known that periods in which aeolian activity is most enhanced are the least likely to be preserved in the palaeorecord (Nanson et al., 1992; Telfer et al., 2010), and the paucity of middle barrier ages dating to the MIS 7 highstand itself may reflect continued activity (and thus frequent resetting of OSL signals) during this period. Alternatively, MIS 7 accumulation may have subsequently been removed and/or reworked towards the beginning of the next phase of accumulation. This initiated in the pre-MIS 5 transgression around 160 ka, anchored on the site of the previous deposits.

More of the MIS 5/6 episode of middle barrier accumulation remains preserved than that from MIS 7, and corresponding ages are present at the Rondevlei, West Swartvlei and East Swartvlei sites (Figure 7.7c). The first evidence of seaward barrier formation also falls within the pre-MIS 5 transgression, with corresponding ages obtained from the Gerickes Point and KT section sites. They are slightly younger than the middle barrier ages (c. 155-160 ka vs. 160-165 ka), indicating seaward barrier preservation initiated only once sea level had fallen sufficiently to cut off sediment supply to the middle barrier. Seaward barrier accumulation at this time is labelled “early phase” in Figure 7.7c. The shallower nearshore bathymetry on the west side of the embayment has preserved this pre-MIS 5 material, whereas contemporaneous deposits to the east are assumed to be either submerged or eroded.

As discussed in chapter 3, various features indicative of partial submergence of the barriers have been identified. From the east shore of Swartvlei to the Goukamma river the seaward flank of the middle barrier is over-steepened, interpreted by Illenberger (1996) as reflecting partial slumping of a fossil sea cliff. This cliff must have formed in the absence of a significant seaward barrier, otherwise the middle barrier would have been protected from wave attack. It is thus attributed to early MIS 5e, an episode also interpreted to have eroded much of the pre-MIS 5 seaward barrier accumulation (Figure 7.8a).

The pattern of barrier construction during MIS 5 was complex, and requires detailed consideration of sea levels at the time. A high-resolution sea-level curve for MIS 5e, averaged from 15 far-field localities, was produced by Hearty et al. (2007) (chapter 3 Figure 3.11). It indicates oceans equalled their present level at c. 135 ka and rapidly rose to 2-3 m amsl, before returning to 0 m amsl around 125 ka and finally reaching a maximum peak of 6-9 m amsl at 120 ka, consistent with multiple inundations of the embayment. The marine facies dating from 128-139 ka at Sedgefield (UoW-234, Shfd07072 and Shfd04288) and East Elandsvlei

(Shfd05049) (Table 7.1) fit well with the first highstand. Martin (1962) also noted the presence of beach terraces and fossil sea cliffs cut into the seaward barrier at several locations, including Gerickes Point and the Swartvlei Estuary mouth. These features could reflect the second MIS 5e highstand at c. 120 ka, though the Mid-Holocene sea-level maxima of 2-3 m amsl may alternatively (or additionally) be responsible for them.

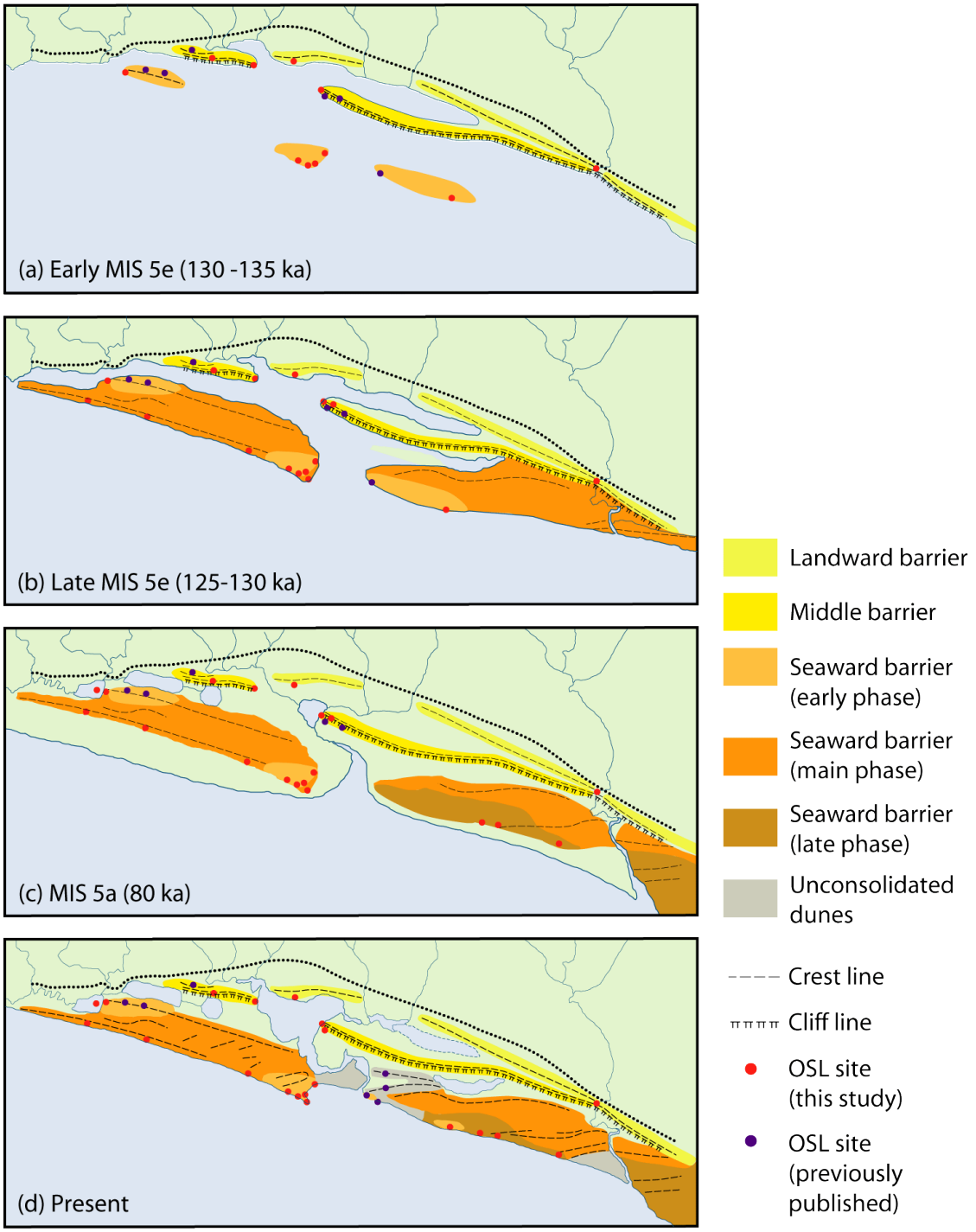

7.8 Model of Mid- to Late-Quaternary barrier emplacement and evolution at Wildernesss from early MIS 5e to the present.

As sea levels receded from the first MIS 5e highstand, accumulation of the middle barrier resumed briefly, but sediment supply subsequently withdrew to a point which facilitated dune building on the seaward barrier only. Numerous seaward barrier ages (from Elandsvlei, Gerickes Point and Castle Rock) fall in the period between 120-130 ka, and accumulation at this time is labelled “main phase” in Figure 7.8b. The earliest age obtained from Elandsvlei Island places it at 114 ± 6 ka (Shfd09065), though its morphology indicates its accumulation must have initiated earlier, contemporaneous with East Elandsvlei (see description in chapter 4 section 4.4.1.2). The wave-cut platform on the southern side of the island is thus most likely associated with the 120 ka 6-9 m amsl highstand maxima of Hearty et al. (2007), around which time it is hypothesised this part of the barrier also became an island. However, the difficulty of dating erosional episodes means this is particularly hard to establish.

Seaward barrier formation continued through MIS 5c and MIS 5a, particularly in the eastern half of the embayment where sea levels receded less quickly than in the west due to the steeper shelf gradient there (labelled “late phase” deposition in Figure 7.8c). MIS 5e accumulation was buried. The series of submerged aeolianite ridges to the west of the embayment (surveyed by Birch et al. (1978) and described in chapter 3 section 3.7.2) most likely track sea-level regression at the end of MIS 5, and probably continue (or continued, prior to their erosion by rising sea levels in the Holocene) much further offshore than revealed in Birch et al.’s survey. The large barrier-like feature ~100 km south associated with the LGM sea-level lowstand observed in the offshore DEM produced by Bateman et al. (2011) is potentially an example of this (chapter 3 Figure 3.13).

Following barrier construction on the continental shelf through MIS 2-4, sea level (and consequently dune building) returned to the present shoreline at Wilderness around 6 ka. Erosion of the seaward barrier during the Mid-Holocene sea-level maxima exposed MIS 5e material previously buried by later MIS 5 accumulation (Figure 7.8d). Illenberger (1996) estimated the volume of Holocene dune accumulation on the seaward barrier to equal only around a third of the underlying MIS 5 material, and this is immediately apparent in considering the small scale of the unconsolidated dunes on the barrier crest relative to the aeolianite sea cliffs below. The paucity of Holocene dune accumulation is interpreted as potentially reflecting the lack of accommodation space left within the embayment. Whilst in previous interglacials the embayment would have represented a major re-entrant on an otherwise relatively smooth coastline, it is now entirely filled with previous generations of aeolianite. The erosion presently experienced by the seaward barrier, and the recycling of seaward barrier sediments to form the Holocene dunes (as evidenced by the greater mineralogical maturity of the latter), supports this hypothesis.

7.7 The Wilderness barriers in a regional and global context

7.7.1 Coastal-dune activity, sea-level position and the sea-level record

Early researchers assumed coastal dunes on the southern Cape formed during glacial sea-level lowstands (e.g. Dingle and Rogers, 1972; Tankard and Schweitzer, 1974), but this hypothesis was subsequently discounted as others argued that vegetation would have rapidly covered the continental shelf when exposed during glacial lowstand periods, preventing significant aeolian transportation of sediment inland (Barwis and Tankard, 1983; Illenberger, 1996). The relationship between dune accumulation and sea-level position on the southern Cape coast was again brought into question by Bateman et al. (2004) and Carr et al. (2007), who reported OSL ages from coastal aeolianites falling not only within the MIS 5 sea-level highstand, but also during the preceding MIS 6 glacial period between 142-159 ka.

This research has shown that the transport pathway of material to the Wilderness barriers has remained similar throughout their formation from MIS 7 to the Holocene, and must involve the nearshore zone. Combined with the close association observed between Holocene dune accumulation and sea level returning to a highstand position, the currently submerged aeolianite ridges south of the embayment surveyed by Birch et al. (1978), and the barrier-like feature associated with the LGM sea-level position revealed in the offshore DEM produced by Bateman et al. (2011), the importance of a proximal coastline in controlling the position of barrier construction at Wilderness is clearly demonstrated. Coastal barrier systems possessing chronologies similarly associated with sea level are located in Brazil (Tomazelli and Dillenburg, 2007), Bermuda and the Bahamas (Hearty and Kindler, 1995), southern Australia (Murray-Wallace et al., 2001), eastern Africa (Armitage et al., 2006) and elsewhere. That ages from these deposits are concentrated predominantly in the Holocene and MIS 5 is a reflection of: (i) the tendency for Late Quaternary interglacial sea-level maxima to repeatedly return to approximately the same point; and (ii) the vulnerability of previous episodes of deposition to erosion by subsequent high sea levels.

Coastal aeolianites dating to sea-level lowstands are rare (Brooke, 2001), and where they do occur it is in sparsely vegetated, arid regions such as Mallorca (Clemmensen et al., 2001; Fornos et al., 2009), parts of SE Australia (Zhou et al., 1994) and Israel (Sivan and Porat, 2004). In most instances these lowstand deposits can be associated with topographic features such as cliffs (e.g. Clemmensen et al., 2001) or aeolianite barriers deposited during previous sea-level highstands (e.g. Zhou et al., 1994; Price et al., 2001), that have served to trap migratory dunes formed from carbonate sediments exposed on unvegetated continental

shelves. Southern Africa's year-round rainfall zone, within which the southern Cape coast falls, is understood to have been slightly drier during glacial periods (Chase and Meadows, 2007). However, the lack of MIS 2-4 ages from the Wilderness OSL record suggests that the degree of aridity was insufficient to prevent the exposed coastal plain being colonised by vegetation.

In light of the above points, the large volume of Wilderness barrier material dating to 140-160 ka is interpreted as providing evidence in support of a regional pre-MIS 5 sea-level transgression, rather than reflecting a change from marine to terrestrial sediment supply during a sea-level lowstand as suggested by Bateman et al. (2004). Evidence for a pre-MIS 5 transgression in the southern Cape region c. 167 ka, absent from the global eustatic sea-level record, has also been presented by Marean et al. (2007) and Fisher et al. (2010). That the Wilderness barrier ages all fall after 167 ka mirrors the Holocene chronology of dune accumulation at the site, in which the OSL record commences c. 2 ka after the Holocene sea-level maxima. The delay neatly illustrates the tendency for aeolian features to record the latter phases of deposition at a site (Kocurek, 1999).

Given mounting evidence for the occurrence of a sea-level transgression c. 167 ka, reinterpretation of pre-MIS 5 aeolianite ages found elsewhere on the southern Cape may be necessary. Roberts et al. (2008) attributed OSL and AAR ages of c. 140 ka from the Still Bay barrier to "*very early*" MIS 5e deposition, though they could equally relate to the pre-MIS 5 transgression. So too could the 150 ± 24 ka age obtained from the base of Inhaca barrier island, Mozambique by Armitage et al. (2006). This date was assumed by the authors to be unreliable, an interpretation based in part on the apparent absence of coastal sediment supply at the time (Armitage et al., 2006).

7.7.2 Accommodation space and coastal-dune morphology

Some of the studies discussed in the previous section highlight the risk of deriving chronologies of coastal-dune activity from limited numbers of samples, and/or from sampling schemes with low horizontal and vertical resolution. The more extensive chronology utilised in this research, permitted by sampling of multiple sites and compilation of a wide range of dates from existing literature, has enabled a detailed reconstruction of barrier emplacement and evolution at Wilderness to be produced. However, in turn, the extensive sampling scheme at Wilderness was facilitated in part by the spatial separation of different episodes of aeolian activity there into geomorphologically separate barriers. Of the coastal barriers present

elsewhere on the southern South African coast, e.g. at Bredasdorp, Still Bay, Port Elizabeth and Mozambique, none are comparable in number or size to those found at Wilderness.

Two factors are proposed to explain the relatively unique morphology of the Wilderness barriers with respect to the southern South African coast. Firstly, the Gouritz River, which possesses the third largest catchment in South Africa (Heydorn, 1989a), debouches only ~75km up-drift (west) of Wilderness. The geometry of the southern Cape coastline is such that the Wilderness embayment falls at the point where the north-easterly trend of the coast from Cape Agulhas first refracts sharply to one slightly south of east, and it thus forms the first major barrier to wind-driven eastward transfer of sediment. Nearshore sediment accumulation around Wilderness is consequently more abundant than anywhere else on the southern African coast (see chapter 3 section 3.4). The correspondingly large size of the Wilderness barriers results in a greater likelihood of their surviving erosional episodes during sea-level highstands than smaller deposits elsewhere, and they may additionally provide protection for any previous generations of barrier located inland.

The second explanation for the uncommon size and morphology of the Wilderness barriers compared to other southern South African coastal aeolianites is the nature of the embayment within which they are located. Globally, spatially separated coastal barriers occur on shallow coastal plains that possess extensive accommodation space. This situation is most common on coasts that have undergone tectonic uplift across the period of barrier formation, e.g. the Coorong Coastal Plain in south-eastern Australia. There, gradual uplift of the coastal plain at ~70 mm ka^{-1} has resulted in the preservation of a series of ten barriers, reaching >100 km inland and dating back to at least 780 ka (Murray-Wallace et al., 2001; Murray-Wallace et al., 2010). Conversely, in the more common scenario where coastal accommodation space is limited, the tendency for Late Quaternary glacio-eustatic sea-level highstands to repeatedly return to the same position has resulted in successive episodes of aeolian deposition either eroding previous deposits, stacking on top of one another, or complex combinations of the two. Composite barrier structures that include material from multiple marine isotope stages are found on tectonically stable or subsiding coasts in south-eastern Australia (Murray-Wallace et al., 2010), Sardinia (Andreucci et al., 2009) and elsewhere on the southern African coast, e.g. KwaZulu-Natal (Wright et al., 2000) and Mozambique (Cooper and Pilkey, 2002; Porat and Botha, 2008).

The crescent-shaped embayment at Wilderness, approximately 40 km long and 6 km deep, provides a volume of accommodation space somewhere intermediate between uplifting coasts and the topographically constrained sites of barrier accumulation found elsewhere in

southern Africa. The embayment was formed by marine incision of easily erodible pre-Cape Kaaimans Group rocks, which form an inlier at Wilderness within the more resistant TMG sandstones that form the majority of the southern Cape coastline. Interestingly, some of the largest transgressive coastal dunefields on the Cape Coast, at False Bay and Duinefonteyn close to Cape Town, also reside in embayments formed by erosion of a pre-Cape geological inlier (the Malmesbury Group, mapped in chapter 3 Figure 3.1). That the False Bay and Duinefonteyn embayments are occupied by transgressive dunes and not barriers, in spite of their broad topographic similarity to Wilderness, confirms the morphology of coastal aeolian deposition is ultimately determined by climatic factors such as wind regime and rainfall seasonality (Roberts et al., 2009). This is supported by the distribution of dune types on the Australian coast, where transgressive dunefields occur only at locations where the coastline is orientated perpendicular to wave and wind fields (Short, 2010).

7.7.3 A generalised model of coastal barrier accumulation

Assuming that wind strength, climate and coastline orientation are conducive to barrier construction in a given location (as opposed to encouraging transgressive dunefield development), and a proximal dissipative sandy beach is also present, the formation and evolution of coastal barrier systems can be defined with reference to a small number of inter-related factors. These are the tectonic stability of the coastline, the volume of accommodation space, and offshore bathymetry. Crustal uplift and the availability of accommodation space controls whether barriers are vertically stacked or spatially separated. In relatively stable tectonic areas, with abundant volumes of sediment available for deflation, and a relatively large plain of subaerially exposed accommodation space, barrier construction through the Mid- to Late-Quaternary will be similar to that found at Wilderness. Unless sediment supply is sufficient to cause shoreline progradation, palaeo-records at such localities are constrained by the degree to which successive sea-level highstands have eroded previous generations of barrier. On tectonically stable coastlines where accommodation space around the contemporary sea-level highstand position is limited, and/or offshore gradients are steeper, erosion of previous deposits is compounded and vertical stacking takes place, resulting in a smaller number of discrete barriers. On tectonically stable coastlines, even relatively small variations in nearshore shelf gradient, such as those caused by incised river valleys, can have a significant influence on the duration of barrier construction at a given point via their modulation of coastline position. Conversely, on coasts subject to tectonic uplift, accommodation space expands over time. In such localities barriers will be spatially separated,

protected from erosion by subsequent sea-level highstands, and provide continuous palaeo-records. The difference in barriers formed on tectonically stable vs. uplifting coastlines is illustrated in Figure 7.9.

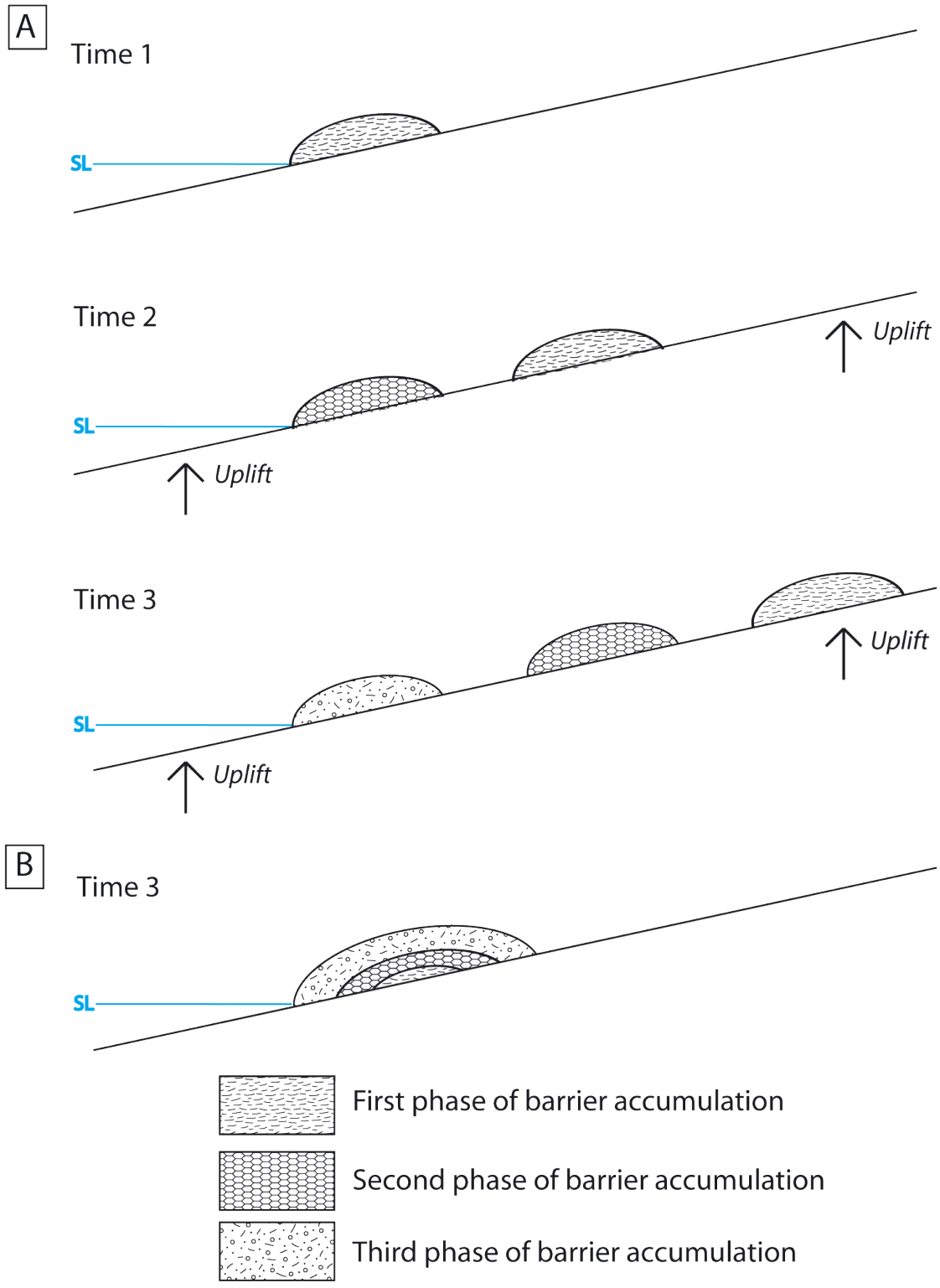

7.9 Models of coastal barrier formation: (a) on an uplifting coastline. Barriers are spatially separated, protected from erosion by subsequent sea-level highstands, and provide continuous palaeo-records; and (b) on a tectonically stable coast. Barriers are vertically stacked and experience erosion as well as deposition in association with sea-level highstands.

In arid regions, palaeo-records of coastal barrier evolution may combine aeolianites dating to both sea-level high- and lowstands. This may be interpreted as reflecting deflation of carbonate sediment from exposed and un-vegetated continental shelves, forming dunes which migrate inland until their progress is halted by preserved highstand deposits or other topographic features. In the more common situation where exposed continental shelves are colonised by vegetation and barrier construction closely tracks sea-level position, the preserved record incorporates only those deposits that have not been submerged and/or eroded. Consequently, current high sea levels bias such records towards Holocene and MIS 5 deposits in most settings.

Rather than viewing coastal barriers as forming during discrete episodes during either sea-level high- or lowstands (e.g. Brooke, 2001; Frébourg et al., 2008), it may be useful to acknowledge that in settings where continental shelves are extensive and sediment is sourced predominantly from the beach, barrier formation is temporally continuous. Dune building tracks the coast as it shifts in response to sea-level change. This is evidenced at Wilderness by the close association of barrier construction with shoreline position, and by the evidence for barrier accumulation during periods of lower sea level provided by the currently submerged aeolianite ridges on the continental shelf (Birch et al., 1978). The largest barriers form at points where sea level repeatedly returns to the same location. If barrier formation is considered in this manner, the three main barrier types described by Roy et al. (1994) (transgressive, regressive and still-stand: chapter 2 section 2.2.3) can be conceptualised as being parts of a single evolutionary system, rather than discrete landforms. At the same time, the vertical stacking of material from subsequent episodes of deposition at Wilderness, and within numerous other barriers (e.g. Cann et al., 1999; Wright et al., 2000; Cooper and Pilkey, 2002), highlights the importance of previous generations of lithified aeolianite in predetermining the exact position of subsequent episodes of deposition.

7.8 Chapter summary

The chapter has brought together the chronological and sediment provenancing results discussed in chapter 6 to present a detailed reconstruction of the Mid- to Late-Quaternary evolution of the Wilderness barrier dunes. The palaeo-record provided by the Wilderness barriers has been compared to other southern Cape aeolianites and to barrier systems globally, and considered with respect to current understanding of coastal barrier formation. Key points can be summarised as follows:

- The three subaerially exposed barriers present at Wilderness have all been constructed within the last three glacial/interglacial cycles. A propensity for vertical stacking is apparent, with the middle barrier containing material deposited in MIS 7, MIS 6, the MIS 5/6 transition and MIS 5e, and the seaward barrier containing material deposited in MIS 6, the MIS 5/6 transition, MIS 5 and the Holocene.
- Barrier construction at Wilderness tracks coastline position as it shifts in response to sea-level change, with the tendency for Mid- to Late-Quaternary sea-level highstands to return to approximately the same position resulting in the preserved terrestrial record reflecting only accumulation following sea-level maxima.
- The chronology of barrier construction at Wilderness provides evidence in support of a regional sea-level transgression prior to MIS 5 that is absent from the global eustatic record, as previously postulated by Marean et al. (2007) and Fisher et al. (2010). In light of this, a reinterpretation of several pre MIS-5 aeolianite ages obtained from coastal deposits elsewhere in southern Africa may be required.
- The source of the Wilderness barrier sands has remained constant throughout their formation from MIS 7 to the Holocene, and comprises a mixture of marine carbonate and terrigenous sediment, with the latter predominantly derived from TMG sandstone. The major source of the terrigenous fraction has most likely been the Gouritz River located ~75 km to the west, with its load transported to the beaches of the Wilderness embayment via longshore drift. Contributions to the terrigenous fraction of the barrier sands have also been sourced locally from the Woodville granite pluton, probably delivered to the nearshore zone by local rivers, and through recycling of material from previous generations of barrier.
- On tectonically stable coastlines, variations in nearshore gradient caused by continental shelf geometry and river valley incision can have a significant influence on the duration of coastal barrier construction at a given locality, though their modulation of coastline position. The importance of previous generations of aeolianite in fixing the exact position of subsequent episodes of deposition in such settings is also highlighted.
- The palaeo-record provided by coastal barriers located on tectonically stable coastlines is a reflection of the degree to which successive sea-level highstands have eroded previous generations of barrier. Where barrier accumulation is particularly significant, such as at Wilderness, records will be more complete due to the protection provided for previous generations of deposition.

8 Conclusion

This chapter summarises the key findings of this thesis, by addressing in turn each of the research objectives originally set out in chapter 1 section 1.4. Conclusions are also drawn regarding the more novel methodologies employed, and possible directions for future work on the themes of this study are considered.

8.1 Meeting the research objectives

8.1.1 Barrier chronology

The first objective focussed on expanding the OSL chronology of barrier construction at Wilderness beyond the single-site studies previously published, all of which were limited to the seaward barrier only (Bateman et al., 2004; Carr et al., 2007; Carr et al., 2010a). The intention was to provide a high-resolution chronological framework for the formation of all three barriers along the full width of the embayment.

Impetus for producing such a chronology was provided by the partial disagreement between the complex record of seaward barrier construction hinted at in the aforementioned studies (which indicate its accumulation took place during both high and low sea levels), and the widely cited model for barrier construction at Wilderness presented by Illenberger (1996). Illenberger (1996) extrapolated a presumed Holocene accumulation rate for the Wilderness barriers to conclude that each barrier formed in two successive sea-level highstands, attributing the seaward barrier to the Holocene and last interglacial (MIS 1 and 5: <10 ka and ~120 ka), the middle barrier to the second- and third-last interglacials (MIS 7 and 9: ~200 and ~320 ka), and the landward barrier to MIS 11 and 13 (~410 and ~500 ka). Prior to the undertaking of this research, Illenberger's model represented the most recent published estimations of middle and landward barrier age.

A total of 36 new OSL age determinations from ten sites within the Wilderness barriers were produced, comprising 24 ages from the seaward barrier, eight from the middle barrier and four from the landward barrier. In combination with a compilation of previously published OSL dates from the literature (Bateman et al., 2004; Carr et al., 2007; Bateman et al., 2008; Carr et al., 2010a; Bateman et al., 2011), results reveal a propensity for vertical stacking of material from separate depositional episodes within both the seaward and middle barriers, in accordance with Illenberger's (1996) model. However, contrary to the timings predicted by Illenberger, the middle barrier contains material deposited in MIS 7, MIS 6, the MIS 5/6

transition and MIS 5e, and the seaward barrier material deposited in MIS 6, the MIS 5/6 transition, MIS 5 and the Holocene. Due to limited access and a small number of visible aeolianite exposures, the landward barrier chronology is less detailed, comprising four ages from two sites, all at similar elevations. The landward barrier ages all broadly relate to MIS 7, though if the middle and seaward barriers are appropriate analogues, material of MIS 9 age is probably present at its core. Even if this is the case, landward barrier formation clearly does not fit the MIS 11-13 time span proposed by Illenberger (1996). Also contrary to Illenberger's model is the overlap in phases of construction across all three barriers. Considering the chronology of barrier accumulation at Wilderness in its entirety, notable phases of accumulation were identified between 245-217 ka, 155-143 ka, 128-121 ka, 91-86 ka and post 6 ka.

At a smaller spatial scale, it was intended that the chronology produced in this research should be detailed enough to reveal any lateral or vertical spatial trends in age within the Wilderness barriers. Paired samples, bracketing bounding surfaces within the aeolianite bedding, were obtained from three localities around the Gerickes Point seaward barrier site. Each pair of samples yielded ages within errors of one another, indicating no discernable pauses in sedimentation (within the limits of the OSL dating technique) between the vertical stacking of parabolic dunes as the barrier coalesced. Similarly rapid accumulation was also observed over larger scales, with ages from exposures at East Elandsvlei (seaward barrier) and East and West Swartvlei (middle barrier) indicating up to ~55 m of vertical accumulation inside single depositional episodes.

Whether any lateral trends in age exist was investigated most thoroughly within the seaward barrier, by comparing OSL ages from sample sites adjacent to the current coastline to their distance from the western edge of the embayment. Results reveal that accumulation of the seaward barrier associated with the penultimate interglacial, MIS 5, continued to the very end of the stage (sub-stage 5a at c. 80 ka) in the eastern half of the embayment, whereas it ceased ~10 ka earlier in the west. Comparison with a DEM of nearshore bathymetry, produced by Bateman et al. (2011), demonstrates the difference is concurrent with a shallower shelf slope to the west, which would have caused earlier sea-level regression (and thus, withdrawal of sediment supply) there. Whether the point at which barrier accumulation associated with the MIS 5 sea-level highstand commenced also varied across the east and west sides of the embayment is less clear, highlighting the tendency for transgressing sea levels to erode and recycle previous generations of coastal deposits, and for coastal barriers (and aeolian deposits in general) to preserve only the latter phases of accumulation at a site.

8.1.2 Relationship between sea level and barrier construction

Objective two was to use the chronological data to firmly constrain the relationship between sea level and the timing of barrier formation at Wilderness. Closely related to this is part of objective four, which was to determine whether the relative importance of terrestrial vs. marine sediment input to the barriers has changed with time.

Early researchers assumed coastal dunes on the southern Cape formed during glacial sea-level lowstands (e.g. Dingle and Rogers, 1972; Tankard and Schweitzer, 1974), but this hypothesis was subsequently discounted as others argued vegetation would have rapidly covered the continental shelf during glacial sea-level lowstands, preventing significant aeolian transportation of sediment inland (Barwis and Tankard, 1983; Illenberger, 1996). The relationship between dune building and sea-level position on the southern Cape coast was again brought into question by Carr et al. (2007), who reported OSL ages from coastal aeolianites falling not only within the MIS 5 sea-level highstand, but also during the preceding MIS 6 glacial period between 142-159 ka. Bateman et al. (2004) hypothesised that increased input of terrestrial sediment may have been more important for barrier construction at Wilderness under low sea levels, citing the low carbonate content of several samples dating to such periods relative to MIS 5 and Holocene material as evidence.

The OSL results presented here confirm the occurrence of significant pre-MIS 5 accumulation at Wilderness, with OSL ages from 140-160 ka obtained from various locations in both the seaward and middle barriers. However, geochemical analyses indicate the source of the seaward barrier sediments has remained constant throughout their accumulation from the Holocene to MIS 6. Additionally, the similarity of particle size distributions amongst samples from all three barriers (which were demonstrated to be largely indistinguishable) suggest there have been no significant changes in transport regime for an even longer period. The presence of significant amounts of carbonate (c. 20 %) in all unweathered barrier samples, and glauconite (an authigenic marine mineral) in seaward barrier material, demonstrates that the transport pathway of sediment to the barriers must involve the nearshore zone.

The importance of a proximal coastline in controlling the position of barrier construction is further demonstrated by a range of findings, namely: (i) the close association observed between the timing of Holocene dune accumulation and sea level resuming a highstand position; (ii) the absence of barrier ages corresponding with low sea levels in MIS 2-4; (iii) the difference in timing of MIS 5 seaward barrier accumulation between the east and west sides of the embayment, caused by modulation of sea-level position by offshore bathymetry (as discussed in the previous section); (iii) the currently submerged aeolianite ridges south of

the embayment surveyed by Birch et al. (1978); and (iv) the barrier-like feature associated with the LGM sea-level position revealed in the offshore DEM produced by Bateman et al. (2011). The hiatus in barrier accumulation during MIS 2-4 could potentially be explained by subsequent reactivation of those deposits in the Holocene or internally driven stochastic noise within continuous low-level activity (as per Telfer et al., 2010), but the high preservation potential of coastal carbonate sands and the spatially extensive sampling scheme employed reduces the likelihood of these possibilities. The Wilderness barrier ages dating to c. 140-160 ka are thus interpreted as indicating a regional pre-MIS 5 sea-level transgression, absent from the global eustatic record, rather than a shift from marine to terrestrial sediment supply. Evidence for a pre-MIS 5 transgressive event in the southern Cape region has also been presented by Marean et al. (2007) and Fisher et al. (2010), and in the northern hemisphere by Siddall et al. (2006). The termination of the last glacial was similarly marked by an episode of rapid sea-level rise followed by an abrupt, but brief return to glacial conditions, inferred from far-field sea-level records and interpreted as reflecting a large meltwater pulse from the Laurentide ice sheet and subsequent disruption of the thermohaline conveyor (Weaver et al., 2003).

8.1.3 Barriers and the inland coversand deposits

Objective three was to clarify the relationship between the Wilderness barriers and the coversand deposits inland of the embayment, which it was hypothesised could have provided a possible source for the barrier sands. OSL dating of samples from the coversand typesite at Makhulu Quarry, conducted by Holmes et al. (2007), demonstrated the coversands to be at least Mid Quaternary in age. Re-dating one of these samples using ITL dating has pushed back the minimum age of the deposit to >1.6 Ma. Three new coversand samples yielded much younger ages, from the LGM, MIS 4 and MIS 10.

Remobilisation of the coversands into estuaries and onto floodplain terraces has been observed during recent rainfall events (Marker, 2003), and the Mid- and Late-Quaternary coversand ages reported in this study potentially indicate such episodes have not been limited to contemporary conditions. It is possible that sediment released from erosion of the coversands could have been transported to the nearshore zone, and consequently recycled to form the barriers. However, analysis of barrier and coversand heavy mineralogy revealed that whilst the coversands are dominated by the ultrastable mineral species zircon, tourmaline and rutile, samples of seaward barrier sands contain a much more diverse range of mineral species.

Findings demonstrate the coversands are thus unable to have made a significant contribution to the barrier sands.

8.1.4 Provenance of the Wilderness barrier dune sands

The fourth objective, partly discussed in section 8.1.2 above, was to establish: (i) whether the relative importance of terrestrial vs. marine sediment input to the Wilderness barriers has changed with time; and (ii) whether or not sediment from local terrestrial sources has been significant in their formation. Trace element geochemistry, particle size data and sample carbonate contents all combine to demonstrate the provenance and transport pathway of the Wilderness barrier sands has remained constant throughout their formation, and involves the marine zone.

The barrier sands were found to possess REE characteristics in line with typical quartz-rich sediments, consistent with a siliciclastic, terrigenous source for their non-carbonate/non-glauconite fraction. To address part (ii) of the objective, whether this material was sourced locally, it was necessary to compare the characteristics of the various local geological formations to those of the barriers. The geology present in the vicinity of the Wilderness embayment includes: the sandstones and metasedimentary rocks of the Table Mountain Group (TMG); the older Neoproterozoic metasedimentary Kaaimans Group; and the Woodville granite pluton. On the basis of combined evidence from various geochemical provenance indicators, it is possible to rule out the Kaaimans Group as having made a significant contribution to the barrier sands. Conversely, similar analyses demonstrate samples of TMG bedrock are geochemically indistinguishable from the barrier sands, strongly suggesting the TMG represents their dominant parent material. TMG bedrock is exposed in a 30-60- km-broad belt along much of the southern Cape coast, so it was not possible to determine whether or not the barrier sands were derived from outcrops local to Wilderness. However, the Gouritz River, ~75 km to the west, traverses TMG rocks and is a much greater contributor of material to the nearshore zone off Wilderness than the small river catchments within the embayment itself (Martin and Flemming, 1986), suggesting it probably represents the dominant source of the barrier sands.

Contrary to the above, the heavy mineral biotite is a dominant constituent of the HM assemblages of the barriers, despite it not being reported as present in the TMG (Potgieter, 1950). Biotite is, however, a major component of both Kaaimans Group rocks and the Woodville Granite pluton. The relative geochemical similarity of certain Woodville Granite

samples to the barrier sands suggests it, rather than the Kaaimans Group, is responsible for contributing this mineral to them. Sediment derived from the Woodville Granite would most likely have been transported to the nearshore zone off Wilderness by local rivers, where it was mixed with marine material and that derived from the TMG before being deflated from the beach for barrier construction.

8.1.5 Reconstructing Mid- to Late-Quaternary barrier evolution at Wilderness and comparisons to similar systems elsewhere

The two final objectives were to combine the dating and provenance data to inform a detailed reconstruction of the emplacement and geomorphological evolution of the Wilderness barrier dunes, and to compare the findings of this research to studies of Quaternary coastal barrier dune systems elsewhere. In reconstructing the emplacement and evolution of the Wilderness barriers, it became clear that the spatial distribution of their OSL ages reveals a complex history of erosion, as well as deposition, within the embayment. The preserved record also emphasises the importance of previous generations of aeolianite in fixing the position of subsequent depositional episodes. The proposed reconstruction of barrier emplacement and evolution at Wilderness demonstrates the utility of incorporating offshore bathymetric data in interpreting chronologies of coastal evolution. It also highlights the limitations of deriving palaeo-records from such deposits, in that the tendency for Late Quaternary interglacial sea-level maxima to repeatedly return to approximately the same position will result in the erosion or submergence of much of the deposition at a site.

Comparing the Wilderness barriers to coastal aeolianite deposits elsewhere on the southern Cape shows the importance of coastal geometry in concentrating sediment supply, and thus the magnitude of deposition, at specific locations. The role of accommodation space in determining the manner of barrier accumulation at a site is also made evident, whereby the vertical stacking of successive deposits (and a resulting smaller number of spatially separated barriers) is encouraged by steeper underlying topography at the point of accumulation. Conversely, the presence of transgressive dunefields, rather than barrier systems, in embayments on the western Cape that are similarly proportioned and situated to Wilderness further supports the assertion made by Roberts et al. (2009), that climatic, rather than topographic, factors are fundamental in controlling whether coastal deposition takes the form of barriers or transgressive dunefields.

A generalised conceptual model of barrier construction over multiple glacial-interglacial cycles was also presented, contrasting the formation of such features on tectonically stable coastlines (such as the southern Cape) to those found on uplifting coastlines. On tectonically stable coastlines, erosion of previous deposits is compounded and vertical stacking takes place, resulting in a smaller number of discrete barriers. Conversely, on coasts subject to tectonic uplift, accommodation space expands over time. In such localities barriers will be spatially separated, protected from erosion by subsequent sea-level highstands, and provide continuous palaeo-records.

8.2 Methodological conclusions and possibilities for future research

Various methods for extending the time limit over which OSL dating of quartz grains can be applied are currently being explored, including thermally transferred OSL (Wang et al., 2006a; Tsukamoto et al., 2008), violet light stimulation OSL (Jain, 2009), and red thermoluminescence (Fattahi and Stokes, 2000; Ganzawa and Ike, 2011). This research presents one of the first practical applications of the isothermal thermoluminescence (ITL) dating technique, with the production of a >1.6 Ma minimum age for the Knysna coversands that is more than triple the previous estimate obtained using standard SAR OSL (Holmes et al., 2007). Other researchers have had mixed success with ITL: Buylaert et al. (2006) and Huot et al. (2006) both reported the occurrence of irreversible sensitivity changes in the first measurement, preventing viable dates being obtained, whereas Choi et al. (2006) experienced no such problems. Vandenberghe et al. (2009) consequently suggested the suitability of ITL might be site-specific.

Age estimations based on palaeoecological analyses for the lignite deposits into which the Knysna coversands grade provides tentative support the ITL age of >1.6 Ma produced in this study is representative of true burial age (Carr et al., 2010b), but further independent tests, such as dating material either side of the Brunhes/Matuyama magnetic horizon are required. If ITL was confirmed appropriate for dating quartz found on the southern Cape, it could be used to re-evaluate the minimum OSL age obtained from one of the landward barrier samples in this study, and further extend the chronology of landward barrier formation with additional sampling. This would facilitate a more reliable assessment of whether the deposit accumulated in the same manner as the seaward and middle barriers, and provide a minimum age for the embayment itself. Many important archaeological and palaeontological sites within quartzitic aeolian sediments understood to be of the Cenozoic age on South Africa's west coast are also

beyond the limits of conventional OSL dating (e.g. Roberts and Brink, 2002; Klein et al., 2007), providing further possibilities for ITL dating in the region.

In order to complete the chronology of barrier formation at Wilderness between MIS 5 and the Holocene, it would be necessary to determine the age of the remnants of aeolianite that remain offshore. Dating the 14 presently submerged ridges inside ~20 km south of the present coastline that are revealed in the side-scan sonar survey of Martin and Flemming (1986) would presumably result in a chronology of MIS 4, MIS 3 and/or MIS 2 activity. Beyond completing the reconstruction of barrier emplacement and evolution at Wilderness, this data would help to address a significant gap remaining in the understanding of coastal barrier systems, that is, their accumulation outside of sea-level highstands. Given current conditions, contemporary observations of these processes are obviously not possible. Roy et al. (1994) suggest barriers on tectonically uplifting coasts provide some manner of analogue for accumulation during sea-level regressions, but the rate of relative sea-level change is orders of magnitude slower in such situations. Dates from the submerged features off Wilderness would reveal whether barriers are most likely to be preserved under falling or rising sea levels, and would also provide information on either the rate of MIS 3/4 sea-level decline or Transgression I sea-level rise on the southern Cape coast respectively.

The provenancing aspect of this study established that Table Mountain Group (TMG) rocks are the dominant source of the Wilderness barrier sands, and that the sands also contain a contribution of locally derived material from the Woodville granite pluton. More broadly, principal component analysis (PCA) was found to be a useful means of interpreting multiple immobile trace element ratios, though it is clear that consideration of the individual element ratios remains necessary in order to understand the significance of the results. The study also demonstrated that bulk trace element data generated for OSL dosimetry can be utilised for provenancing purposes. However, geochemical analyses of the sediment carried by rivers local to the Wilderness embayment produced similar results for several river courses, despite their traversing different geological formations. Non-provenance related factors, such as particle size differences or hydraulic sorting, were consequently interpreted as dominating their trace element signatures, and comparisons with the barrier sands were deemed invalid. Analysing a narrower size fraction of the river sediments would potentially enable viable comparisons to be made, though as previously stated the TMG outcrops along ~1300 km of the southern Cape coast, and it would likely remain impossible to determine whether or not the barrier sands were derived from outcrops local to Wilderness. The utility of establishing this information would also be limited, given that this study has demonstrated barrier construction at Wilderness is closely associated with sea-level position (and associated sediment supply from

the beach), and was not sustained at certain times by a shift from marine to terrestrial sediment sources, as suggested by Bateman et al. (2004).

An interesting aspect of the heavy mineralogy results was the indication that the Holocene dune sands represent material recycled from the seaward barrier aeolianites. In order to further establish the degree to which this has been the case, quartz surface textures could be analysed using scanning electron microscopy (SEM). SEM has proven useful in determining the degree of recycling and transport history of quartz sands from various settings (e.g. Cardona et al., 1997; Abu-Zeid et al., 2001).

8.3 Concluding remarks

This thesis has presented a detailed chronology for the emplacement and evolution of the Wilderness barrier dunes and explained their unique morphology with respect to other southern Cape coastal aeolianite systems. The importance of establishing sediment supply in interpreting chronologies of coastal aeolian activity has been demonstrated, as has the potential for lateral variability and complexity in barrier accumulation to be introduced by local variations in nearshore bathymetry. Results also highlight how the palaeo-records provided by coastal barriers located on tectonically stable coastlines ultimately reflect the degree to which successive sea-level highstands have eroded previous generations of barrier. Consideration of these factors is essential in deriving palaeoenvironmental data from barrier systems and/or correlating them with aeolian activity elsewhere.

9 References

Aagaard, T., Orford, J., and Murray, A. S. (2007). Environmental controls on coastal dune formation; Skallingen Spit, Denmark. *Geomorphology* **83,** 29-47.

Abegg, F. E., Loope, D., and Harris, P. M. (2001). Carbonate eolianites: depostional models and diagenesis. *In* "Modern and ancient carbonate eolianites: sedimentology, sequence stratigraphy, and diagenesis. SEPM Special Publication 71." (F. E. Abegg, P. M. Harris, and D. Loope, Eds.), pp. 17-30.

Abu-Zeid, M. M., Baghdady, A. R., and El-Etr, H. A. (2001). Textural attributes, mineralogy and provenance of sand dune fields in the greater Al Ain area, United Arab Emirates. *Journal of Arid Environments* **48,** 475-499.

Adamiec, G., and Aitken, M. (1998). Dose-rate conversion factors: update. *Ancient TL* **16,** 37-50.

Adger, W. N., Hughes, T. P., Folke, C., Carpenter, S. R., and Rockstrom, J. (2005). Social-Ecological Resilience to Coastal Disasters. *Science* **309,** 1036-1039.

Agrawal, Y. C., McCave, I. N., and Riley, J. B. (1991). Laser diffraction size analysis. *In* "Principles, methods, and application of particle size analysis." (J. P. M. Syvitski, Ed.), pp. 119-128. CUP, Cambridge.

Aitchison, J. (1982). The Statistical-Analysis of Compositional Data. *Journal of the Royal Statistical Society Series B-Methodological* **44,** 139-177.

Aitken, M. J. (1974). "Physics and archaeology." Clarendon Press, Oxford.

Aitken, M. J. (1985). "Thermoluminescence dating." Academic Press, London.

Aitken, M. J. (1998). "An introduction to optical dating: the dating of Quaternary sediments by the use of photon-stimulated luminescence." Oxford University Press, Oxford.

Andreucci, S., Pascucci, V., Murray, A. S., and Clemmensen, L. B. (2009). Late Pleistocene coastal evolution of San Giovanni di Sinis, west Sardinia (Western Mediterranean). *Sedimentary Geology* **216,** 104-116.

Anthony, E. J., Oyédé, L. M., and Lang, J. (2002). Sedimentation in a fluvially infilling, barrier-bound estuary on a wave-dominated, microtidal coast: the Ouémé River estuary, Benin, west Africa. *Sedimentology* **49,** 1095-1112.

Armitage, S. J., Botha, G. A., Duller, G. A. T., Wintle, A. G., Rebelo, L. P., and Momade, F. J. (2006). The formation and evolution of the barrier islands of Inhaca and Bazaruto, Mozambique. *Geomorphology* **82,** 295-308.

Avery, D. M. (1982). Micromammals as palaeoenvironmental indicators and an interpretation of the Late Quaternary in the southern Cape Province, South Africa. *Annals of the South African Museum* **85,** 183-374.

Bagnold, R. A., and Barndorffnielsen, O. (1980). The Pattern of Natural Size Distributions. *Sedimentology* **27,** 199-207.

Bailey, G. W., and Rogers, J. (1997). Chemical oceanography and marine geoscience off southern Africa: Past discoveries in the post-Gilchrist era, and future prospects. *Transactions of the Royal Society of South Africa* **52,** 51-79.

Bailey, R. M., Smith, B. W., and Rhodes, E. J. (1997). Partial bleaching and the decay form characteristics of quartz OSL. *Radiation Measurements* **27,** 123-136.

Ballarini, M., Wallinga, J., Murray, A. S., van Heteren, S., Oost, A. P., Bos, A. J. J., and van Eijk, C. W. E. (2003). Optical dating of young coastal dunes on a decadal time scale. *Quaternary Science Reviews* **22,** 1011-1017.

Banerjee, D., Hildebrand, A. N., Murray-Wallace, C. V., Bourman, R. P., Brooke, B. P., and Blair, M. (2003). New quartz SAR-OSL ages from the stranded beach dune sequence in south-east South Australia. *Quaternary Science Reviews* **22,** 1019-1025.

Bar-Matthews, M., Marean, C. W., Jacobs, Z., Karkanas, P., Fisher, E. C., Herries, A. I. R., Brown, K., Williams, H. M., Bernatchez, J., Ayalon, A., and Nilssen, P. J. (2010). A high resolution and continuous isotopic speleothem record of paleoclimate and

paleoenvironment from 90 to 53 ka from Pinnacle Point on the south coast of South Africa. *Quaternary Science Reviews* **29,** 2131-2145.

Barwis, J. H., and Tankard, A. J. (1983). Pleistocene Shoreline Deposition and Sea-Level History at Swartklip, South-Africa. *Journal of Sedimentary Petrology* **53,** 1281-1294.

Bateman, M., Carr, A. S., Murray-Wallace, C., Roberts, D., and Holmes, P. J. (2008). A dating intercomparison study on Late Stone Age coastal midden deposits, South Africa. *Geoarchaeology* **23,** 715-741.

Bateman, M. D., Boulter, C. H., Carr, A. S., Frederick, C. D., Peter, D., and Wilder, M. (2007). Preserving the palaeoenvironmental record in Drylands: Bioturbation and its significance for luminescence-derived chronologies. *Sedimentary Geology* **195,** 5-19.

Bateman, M. D., Carr, A. S., Dunajko, A. C., Holmes, P. J., Roberts, D. L., McClaren, S. J., Bryant, R. G., Marker, M. E., and Murray-Wallace, C. V. (2011). The evolution of coastal barrier systems: a case study of the Middle-Late Pleistocene Wilderness barriers, South Africa. *Quaternary Science Reviews* **30,** 63-81.

Bateman, M. D., and Catt, J. A. (1996). An absolute chronology for the raised beach and associated deposits at Sewerby, East Yorkshire, England. *Journal of Quaternary Science* **11,** 389-395.

Bateman, M. D., Frederick, C. D., Jaiswal, M. K., and Singhvi, A. K. (2003a). Investigations into the potential effects of pedoturbation on luminescence dating. *Quaternary Science Reviews* **22,** 1169-1176.

Bateman, M. D., Holmes, P. J., Carr, A. S., Horton, B. P., and Jaiswal, M. K. (2004). Aeolianite and barrier dune construction spanning the last two glacial-interglacial cycles from the southern Cape coast, South Africa. *Quaternary Science Reviews* **23,** 1681-1698.

Bateman, M. D., Thomas, D. S. G., and Singhvi, A. K. (2003b). Extending the aridity record of the Southwest Kalahari: current problems and future perspectives. *Quaternary International* **111,** 37-49.

Bauer, B. O., and Davidson-Arnott, R. G. D. (2003). A general framework for modeling sediment supply to coastal dunes including wind angle, beach geometry, and fetch effects. *Geomorphology* **49,** 89-108.

Bauer, B. O., and Sherman, D. J. (1999). Coastal Dune Dynamics: Problems and Prospects. *In* "Aeolian Environments, Sediments and Landforms." (A. S. Goudie, I. Livingstone, and S. Stokes, Eds.), pp. 71-104. Wiley, Chichester.

Beets, D. J., van der Valk, L., and Stive, M. J. F. (1992). Holocene evolution of the coast of Holland. *Marine Geology* **103,** 423-443.

Belknap, D. F., and Mart, Y. (1999). Sea-level lowstand in the eastern Mediterranean: Late Pleistocene coastal terraces offshore northern Israel. *Journal of Coastal Research* **15,** 399-412.

Bennett, M. R., Cassidy, N. J., and Pile, J. (2009). Internal structure of a barrier beach as revealed by ground penetrating radar (GPR): Chesil beach, UK. *Geomorphology* **104,** 218-229.

Beuselinck, L., Govers, G., Poesen, J., and Degraer, G. (1998). Grain-size analysis by laser diffractometry: comparison with the sieve-pipette method. *Catena* **32,** 193-208.

Bhatia, M. R., and Crook, K. A. W. (1986). Trace-Element Characteristics of Graywackes and Tectonic Setting Discrimination of Sedimentary Basins. *Contributions to Mineralogy and Petrology* **92,** 181-193.

Birch, G. F. (1979). Nature and Origin of Mixed Apatite-Glauconite Pellets from the Continental-Shelf Off South-Africa. *Marine Geology* **29,** 313-334.

Birch, G. F. (1980). "Nearshore quaternary sedimentation off the south coast of South Africa (Cape Town to Port Elizabeth)." Govt. Printer, Pretoria.

Birch, G. F., De Plessis, A., and Willis, J. P. (1978). Off shore and on land geological and geophysical investigations of the Wilderness Lakes region. *Transactions of the Geological Society of South Africa* **81,** 339-352.

Blott, S. J., and Pye, K. (2001). GRADISTAT: A grain size distribution and statistics package for the analysis of unconsolidated sediments. *Earth Surface Processes and Landforms* **26,** 1237-1248.

Blott, S. J., and Pye, K. (2006). Particle size distribution analysis of sand-sized particles by laser diffraction: an experimental investigation of instrument sensitivity and the effects of particle shape. *Sedimentology* **53,** 671-685.

Boswell, P. G. H. (1933). "On the mineralogy of sedimentary rocks. A series of essays and a bibliography." T. Murby & Co, London.

Bøtter-Jensen, L., and Duller, G. A. T. (1992). A new system for measuring optically stimulated luminescence from quartz samples. *Nuclear Tracks and Radiation Measurements* **20,** 549-553.

Bøtter-Jensen, L., Mejdahl, V., and Murray, A. S. (1999). New light on OSL. *Quaternary Science Reviews* **18,** 303-309.

Boulter, C. H. (2007). "Reconstructing the palaeenvironmental dynamics of East Central Texas since the Last Glacial Maximum." Unpublished Ph.D. thesis, University of Sheffield.

Bradley, R. S. (2000). Past global changes and their significance for the future. *Quaternary Science Reviews* **19,** 391-402.

Brooke, B. (2001). The distribution of carbonate eolianite. *Earth-Science Reviews* **55,** 135-164.

Brooke, B., Lee, R., Cox, M., Olley, J., and PietscW, T. (2008). Rates of shoreline progradation during the last 1700 years at Beachmere, Southeastern Queensland, Australia, based on optically stimulated luminescence dating of beach ridges. *Journal of Coastal Research* **24,** 640-648.

Brown, R. W., Gallagher, A. J., Gleadlow, A. J. W., and Summerfield, M. A. (2000). Morphotectonic evolution of the South Atlantic margins of Africa and South America. *In* "Geomorphology and global tectonics." (M. A. Summerfield, Ed.), pp. 255-280. Wiley, Chichester.

Bulur, E., Botter-Jensen, L., and Murray, A. S. (2000). Optically stimulated luminescence from quartz measured using the linear modulation technique. *Radiation Measurements* **32,** 407-411.

Burrough, S. L., Thomas, D. S. G., Shaw, P. A., and Bailey, R. M. (2007). Multiphase Quaternary highstands at Lake Ngami, Kalahari, northern Botswana. *Palaeogeography, Palaeoclimatology, Palaeoecology* **253,** 280-299.

Butzer, K. W. (2004). Coastal eolian sands, paleosols, and Pleistocene geoarchaeology of the Southwestern Cape, South Africa. *Journal of Archaeological Science* **31,** 1743-1781.

Buurman, P., Pape, T., and Muggler, C. C. (1997). Laser grain-size determination in soil genetic studies .1. Practical problems. *Soil Science* **162,** 211-218.

Buylaert, J. P., Murray, A. S., Huot, S., Vriend, M. G. A., Vandenberghe, D., De Corte, F., and Van den haute, P. (2006). A comparison of quartz OSL and isothermal TL measurements on Chinese loess. *Radiation Protection Dosimetry* **119,** 474-478.

Cann, J. H., Murray-Wallace, C. V., Belperio, A. P., and Brenchley, A. J. (1999). Evolution of Holocene coastal environments near Robe, southeastern South Australia. *Quaternary International* **56,** 81-97.

Cardona, J. P. M., Gutiérrez Mas, J. M., Bellón, A. S., López-Aguayo, F., and Caballero, M. A. (1997). Provenance of multicycle quartz arenites of Pliocene age at Arcos, southwestern Spain. *Sedimentary Geology* **112,** 251-261.

Carew, J. L., and Mylroie, J. E. (2001). Quaternary carbonate eolianites of the Bahamas: useful analogues for the interpretation of ancient rocks? *In* "Modern and ancient carbonate eolianites: sedimentology, sequence stratigraphy, and diagenesis. SEPM Special Publication 71." (F. E. Abegg, P. M. Harris, and D. Loope, Eds.), pp. 33-45.

Carr, A. S., Bateman, M. D., and Holmes, P. J. (2007). Developing a 150 ka luminescence chronology for the barrier dunes of the southern Cape, South Africa. *Quaternary Geochronology* **2,** 110-116.

Carr, A. S., Bateman, M. D., Roberts, D. L., Murray-Wallace, C. V., Jacobs, Z., and Holmes, P. J. (2010a). The last interglacial sea-level high stand on the southern Cape coastline of South Africa. *Quaternary Research* **73,** 351-363.

Carr, A. S., Boom, A., Dunajko, A. C., Bateman, M. D., Holmes, P. J., and Berrio, J.-C. (2010b). New evidence for the age and palaeoecology of the Knysna Formation, South Africa. *South African Journal of Geology* **113,** 241-256.

Carr, A. S., Thomas, D. S. G., and Bateman, M. D. (2006a). Climatic and sea level controls on Late Quaternary eolian activity on the Agulhas Plain, South Africa. *Quaternary Research* **65,** 252-263.

Carr, A. S., Thomas, D. S. G., Bateman, M. D., Meadows, M. E., and Chase, B. (2006b). Late Quaternary palaeoenvironments of the winter-rainfall zone of southern Africa: Palynological and sedimentological evidence from the Agulhas Plain. *Palaeogeography Palaeoclimatology Palaeoecology* **239,** 147-165.

Carter, R. W. G., Nordstrom, K. F., and Psuty, N. P. (1990). The study of coastal dunes. *In* "Coastal dunes: form and process." (K. F. Nordstrom, N. P. Psuty, and B. Carter, Eds.), pp. 1-16. Wiley, Chichester.

Chase, B. M., and Meadows, M. E. (2007). Late Quaternary dynamics of southern Africa's winter rainfall zone. *Earth-Science Reviews* **84,** 103-138.

Chase, B. M., and Thomas, D. S. G. (2006). Late Quaternary dune accumulation along the western margin of South Africa: distinguishing forcing mechanisms through the analysis of migratory dune forms. *Earth and Planetary Science Letters* **251,** 318-333.

Chen, J. H., Curran, H. A., White, B., and Wasserburg, G. J. (1991). Precise Chronology of the Last Interglacial Period - U-234-Th-230 Data from Fossil Coral Reefs in the Bahamas. *Geological Society of America Bulletin* **103,** 82-97.

Choi, J. H., Murray, A. S., Cheong, C. S., Hong, D. G., and Chang, H. W. (2006). Estimation of equivalent dose using quartz isothermal TL and the SAR procedure. *Quaternary Geochronology* **1,** 101-108.

Clemmensen, L. B., Andreasen, F., Nielsen, S. T., and Sten, E. (1996). The late Holocene coastal dunefield at Vejers, Denmark: Characteristics, sand budget and depositional dynamics. *Geomorphology* **17,** 79-98.

Clemmensen, L. B., Lisborg, T., Fornos, J. J., and Bromley, R. G. (2001). Cliff-front aeolian and colluvial deposits, Mallorca, Western Mediterranean: a record of climatic and environmental change during the last glacial period. *Bulletin of the Geological Society of Denmark* **48,** 217-232.

Clemmensen, L. B., Murray, A., Heinemeier, J., and de Jong, R. (2009). The evolution of Holocene coastal dunefields, Jutland, Denmark: A record of climate change over the past 5000 years. *Geomorphology* **105,** 303-313.

Cockcroft, M. J., Wilkinson, M. J., and Tyson, P. D. (1987). The Application of a Present-Day Climatic Model to the Late Quaternary in Southern-Africa. *Climatic Change* **10,** 161-181.

Compton, J. S. (2001). Holocene sea-level fluctuations inferred from the evolution of depositional environments of the southern Langebaan Lagoon salt marsh, South Africa. *Holocene* **11,** 395-405.

Compton, J. S. (2006). The mid-Holocene sea-level highstand at Bogenfels Pan on the southwest coast of Namibia. *Quaternary Research* **66,** 303-310.

Compton, J. S. (2011). Pleistocene sea-level fluctuations and human evolution on the southern coastal plain of South Africa. *Quaternary Science Reviews*.

Compton, J. S., and Franceschini, G. (2005). Holocene geoarchaeology of the sixteen mile beach barrier dunes in the western cape, South Africa. *Quaternary Research* **63,** 99-107.

Compton, J. S., White, R. A., and Smith, M. (2003). Rare earth element behavior in soils and salt pan sediments of a semi-arid granitic terrain in the Western Cape, South Africa. *Chemical Geology* **201,** 239-255.

Condie, K. C., Dengate, J., and Cullers, R. L. (1995). Behavior of rare earth elements in a paleoweathering profile on granodiorite in the Front Range, Colorado, USA. *Geochimica et Cosmochimica Acta* **59,** 279-294.

Cooper, J. A. G. (2001). Geomorphological variability among microtidal estuaries from the wave-dominated South African coast. *Geomorphology* **40,** 99-122.

Cooper, J. A. G., and Pilkey, O. H. (2002). The barrier islands of southern Mozambique. *Journal of Coastal Research Special Issue* **36,** 164-172.

Cooper, W. S. (1958). "Coastal sand dunes of Oregon and Washington." The Geological Society of America, New York.

Daniels, F., Boyd, C. A., and Saunders, D. F. (1949). Thermoluminescence as a Research Tool. *Science* **109,** 440-440.

Darwin, C. (1851). "Geological observations on coral reefs, volcanic islands and on South America: being the geology of the voyage of the *Beagle*, under the command of Captain Fitzroy, R.N., during the years 1832 to 1836." Stewart & Murray, London.

Davis, R. A., and FitzGerald, D. M. (2004). "Beaches and coasts." Blackwell, Oxford.

Davis, R. A., Yale, K. E., Pekala, J. M., and Hamilton, M. V. (2003). Barrier island stratigraphy and Holocene history of west-central Florida. *Marine Geology* **200,** 103-123.

Deacon, H. J., Jury, M. R., and Ellis, F. (1992). Selective regime and time. *In* "The ecology of fynbos: nutrients, fire and diversity." (R. M. Cowling, Ed.), pp. 7-22. OUP, Cape Town.

Dillenburg, S. R., Esteves, L. S., and Tomazelli, L. J. (2004). A critical evaluation of coastal erosion in Rio Grande do Sul, Southern Brazil. *Annals of the Brazilian Academy of Sciences* **76,** 611-623.

Dillenburg, S. r. R., Roy, P. S., Cowell, P. J., and Tomazelli, L. J. (2000). Influence of Antecedent Topography on Coastal Evolution as Tested by the Shoreface Translation-Barrier Model (STM). *Journal of Coastal Research* **16,** 71-81.

Dingle, R. V., Birch, G. F., Bremner, J. M., DeDecker, R. H., Du Plessis, A., Engelbrecht, J. C., Fincham, M. J., Fitton, B. W., Flemming, B. W., Gentle, R. I., Goodland, S. W., Martin, A. K., Mills, E. G., Moir, G. J., Parker, R. J., Robson, S. H., Rogers, J., Salmon, D. A., Siesser, W. G., Simpson, S. W., Summerhayes, C. P., Westall, F., Winter, A., and Woodborne, M. W. (1987). Deep-sea sedimentary environments around southern Africa (South-East Atlantic and South-West Indian Oceans). *Annals of the South African Museum* **98,** 1-27.

Dingle, R. V., and Rogers, J. (1972). Effects of sea-level changes on the Pleistocene palaeoecology of the Agulhas Bank. *Palaeoecology of Africa* **6,** 55-58.

Dougherty, A. J., FitzGerald, D. M., and Buynevich, I. V. (2004). Evidence for storm-dominated early progradation of Castle Neck barrier, Massachusetts, USA. *Marine Geology* **210,** 123-134.

Dravis, J. J. (1996). Rapidity of freshwater calcite cementation -- implications for carbonate diagenesis and sequence stratigraphy. *Sedimentary Geology* **107,** 1-10.

Duller, G. A. T. (1991). Equivalent Dose Determination Using Single Aliquots. *Nuclear Tracks and Radiation Measurements* **18,** 371-378.

Duller, G. A. T. (2003). Distinguishing quartz and feldspar in single grain luminescence measurements. *Radiation Measurements* **37,** 161-165.

Duller, G. A. T. (2008). Single-grain optical dating of Quaternary sediments: why aliquot size matters in luminescence dating. *Boreas* **37,** 589-612.

Dunajko, A. C., and Bateman, M. D. (2010). Sediment provenance of the Wilderness barrier dunes, southern Cape coast, South Africa. *Terra Nova* **22,** 417-423.

Emiliani, C. (1955). Pleistocene Temperatures. *Journal of Geology* **63,** 538-578.

Erlandson, J. M. (2001). The archaeology of aquatic adaptations: paradigms for a new millenium. *Journal of Archaeological Research* **9,** 287-350.

Fattahi, M., and Stokes, S. (2000). Extending the time range of luminescence dating using red TL (RTL) from volcanic quartz. *Radiation Measurements* **32,** 479-485.

Feathers, J. K. (2003). Single-grain OSL dating of sediments from the Southern High Plains, USA. *Quaternary Science Reviews* **22,** 1035-1042.

Felix, C., and Singhvi, A. K. (1997). Study of non-linear luminescence-dose growth curves for the estimation of paleodose in luminescence dating: Results of Monte Carlo simulations. *Radiation Measurements* **27,** 599-609.

Ferré, E. C., and Améglio, L. (2000). Preserved magnetic fabrics vs. annealed microstructures in the syntectonic recrystallised George granite, South Africa. *Journal of Structural Geology* **22,** 1199-1219.

Finlayson, C., Pacheco, F. G., Rodriguez-Vidal, J., Fa, D. A., Lopez, J. M. G., Perez, A. S., Finlayson, G., Allue, E., Preysler, J. B., Caceres, I., Carrion, J. S., Jalvo, Y. F., Gleed-Owen, C. P., Espejo, F. J. J., Lopez, P., Saez, J. A. L., Cantal, J. A. R., Marco, A. S., Guzman, F. G., Brown, K., Fuentes, N., Valarino, C. A., Villalpando, A., Stringer, C. B., Ruiz, F. M., and Sakamoto, T. (2006). Late survival of Neanderthals at the southernmost extreme of Europe. *Nature* **443,** 850-853.

Fisher, E. C., Bar-Matthews, M., Jerardino, A., and Marean, C. W. (2010). Middle and Late Pleistocene paleoscape modeling along the southern coast of South Africa. *Quaternary Science Reviews* **29,** 1382-1398.

Fitzsimmons, K. E., Magee, J. W., and Amos, K. J. (2009). Characterisation of aeolian sediments from the Strzelecki and Tirari Deserts, Australia: Implications for reconstructing palaeoenvironmental conditions. *Sedimentary Geology* **218,** 61-73.

Fleming, S. J. (1979). "Thermoluminescene techniques in Archaeology." Clarendon Press, Oxford.

Flemming, B. W. (1978). Underwater Sand Dunes Along Southeast African Continental-Margin - Observations and Implications. *Marine Geology* **26,** 177-198.

Flemming, B. W. (1980). Sand Transport and Bedform Patterns on the Continental-Shelf between Durban and Port Elizabeth (Southeast African Continental-Margin). *Sedimentary Geology* **26,** 179-205.

Flenley, J. R. (1981). Introduction. *In* "The Quaternary in Britain: essays, reviews and original work on the Quaternary published in honour of Lewis Penny on his retirement." (J. W. Neale, and J. R. Flenley, Eds.), pp. ix-xi. Pergamon, Oxford.

Flint, R. F. (1957). "Glacial and Pleistocene Geology." John Wiley & Sons, New York.

Flügel, E. (2004). "Microfacies of carbonate rocks: analysis, interpretation and application." Springer, Berlin.

Folk, R. L., and Ward, W. C. (1957). Brazons River bar: a study in the significance of grain size parameters. *Journal of Sedimentary Petrology* **27,** 3-26.

Fornos, J. J., Clemmensen, L. B., Gomez-Pujol, L., and Murray, A. S. (2009). Late Pleistocene carbonate aeolianites on Mallorca, Western Mediterranean: a luminescence chronology. *Quaternary Science Reviews* **28,** 2697-2709.

Fourie, P. H., Zimmermann, U., Beukes, N. J., Naidoo, T., Kobayashi, K., Kosler, J., Nakamura, E., Tait, J., and Theron, J. N. (2011). Provenance and reconnaissance study of detrital zircons of the Palaeozoic Cape Supergroup in South Africa: revealing the interaction of the Kalahari and Rio de la Plata cratons. *International Journal of Earth Sciences* **100,** 527-541.

Franceschini, G., Compton, J. S., and Wigley, R. A. (2003). Sand transport along the Western Cape coast: gone with the wind? *South African Journal of Science* **99,** 317-318.

Frébourg, G., Hasler, C. A., Le Guern, P., and Davaud, E. (2008). Facies characteristics and diversity in carbonate eolianites. *Facies* **54,** 175-191.

Frechen, M., Neber, A., Tsatskin, A., Boenigk, W., and Ronen, A. (2004). Chronology of Pleistocene sedimentary cycles in the carmel Coastal Plain of Israel. *Quaternary International* **121,** 41-52.

Friedman, G. M. (1998). Rapidity of marine carbonate cementation -- implications for carbonate diagenesis and sequence stratigraphy: perspective. *Sedimentary Geology* **119,** 1-4.

Frimmel, H. E., Folling, P. G., and Diamond, R. (2001). Metamorphism of the Permo-Triassic Cape Fold Belt and its basement, South Africa. *Mineralogy and Petrology* **73,** 325-346.

Frimmel, H. E., and Vanachterbergh, E. (1995). Metamorphism of Calc-Silicate and Associated Rocks in the Pan-African Kaaimans Group, Saldania Belt, South-Africa. *Mineralogy and Petrology* **53,** 75-102.

Fryberger, S. G., Schenk, C. J., and Krystinik, L. F. (1988). Stokes surfaces and the effects of near-surface groundwater-table on Aeolian deposition. *Sedimentology* **35,** 21-41.

Galbraith, R. F., and Green, P. F. (1990). Estimating the Component Ages in a Finite Mixture. *Nuclear Tracks and Radiation Measurements* **17,** 197-206.

Galbraith, R. F., Roberts, R. G., Laslett, G. M., Yoshida, H., and Olley, J. M. (1999). Optical dating of single and multiple grains of quartz from jinmium rock shelter, northern Australia, part 1, Experimental design and statistical models. *Archaeometry* **41,** 339-364.

Galbraith, R. F., Roberts, R. G., and Yoshida, H. (2005). Error variation in OSL palaeodose estimates from single aliquots of quartz: a factorial experiment. *Radiation Measurements* **39,** 289-307.

Gale, S. J., and Hoare, P. G. (1991). "Quaternary sediments." Belhaven.

Ganzawa, Y., and Ike, M. (2011). SAR-RTL dating of single grains of volcanic quartz from the late Pleistocene Toya Caldera. *Quaternary Geochronology* **6,** 42-49.

Gardner, D. E. (1955). Beach sand heavy mineral deposits of eastern Australia. *Bureau of Mineral Research, Geology and Geophysics Bulletin* **28**.

Garzanti, E., and Andò, S. (2007). Heavy mineral concentration in modern sands: implications for provenance interpretation. *In* "Heavy minerals in use." (M. A. Mange, and D. T. Wright, Eds.), pp. 517-546. Developments in Sedimentology. Elsevier, Amsterdam.

Goedhart, M. L., and Booth, P. W. K. (2009). Early Holocene extensional tectonics in the South-Eastern Cape Fold Belt, South Africa. *In* "11th SAGA Biennial Technical Metting and Exhibition ", Swaziland.

Goldblatt, P., and Manning, J. C. (2002). Plant diversity of the Cape Region of southern Africa. *Annals of the Missouri Botanical Garden* **89,** 281-302.

Goldsmith, V. (1978). Coastal dunes. *In* "Coastal sedimentary environments." (R. A. J. Davis, Ed.), pp. 171-236. Springer, New York.

Good, R. (1947). "The geography of the flowering plants." Longmans, London.

Gradstein, F. M., Ogg, J. G., and Smith, A. G. (2004). "A geologic time scale 2004." Cambridge University Press, Cambridge ; New York.

Gresse, P. G. (1983). Lithostratigraphy and structure of the Kaaimans Group. *Geological Society of South Africa Special Publication* **12,** 7-19.

Grindley, J. R. (1985). Report No. 30: Knysna (CMS 13). *In* "Estuaries of the Cape Part II: Synopses of available information on individual systems CSIR Research Report 429." (A. E. F. Heydorn, and J. R. Grindley, Eds.), pp. 1-82. CSIR, Stellenbosch.

Gurnis, M., Mitrovica, J. X., Ritsema, J., and van Heijst, H.-J. (2000). Constraining mantle density structure using geological evidence of surface uplift rates: The case of the African Superplume. *Geochem. Geophys. Geosyst.* **1,** 1-31.

Hanson, P. R., Arbogast, A. F., Johnson, W. C., Joeckel, R. M., and Young, A. R. (2010). Megadroughts and late Holocene dune activation at the eastern margin of the Great Plains, north-central Kansas, USA. *Aeolian Research* **1,** 101-110.

Harris, C., Faure, K., Diamond, R. E., and Scheepers, R. (1997). Oxygen and hydrogen isotope geochemistry of S- and I-type granitoids: the Cape Granite suite, South Africa. *Chemical Geology* **143,** 95-114.

Hartmann, D., and Christiansen, C. (1992). The Hyperbolic Shape Triangle as a Tool for Discriminating Populations of Sediment Samples of Closely Connected Origin. *Sedimentology* **39,** 697-708.

Havholm, K. G., Ames, D. V., Whittecar, G. R., Wenell, B. A., Riggs, S. R., Jol, H. M., Berger, G. W., and Holmes, M. A. (2004). Stratigraphy of back-barrier coastal dunes, northern North Carolina and Southern Virginia. *Journal of Coastal Research* **20,** 980-999.

Hayes, M. O. (1979). Barrier island morphology as a function of tidal and wave regime. *In* "Barrier islands: from the Gulf of St Lawrence to the Gulf of Mexico." (S. P. Leatherman, Ed.), pp. 1-27. Academic Press, New York.

Hearty, P. J., Hollin, J. T., Neumann, A. C., O'Leary, M. J., and McCulloch, M. (2007). Global sea-level fluctuations during the Last Interglaciation (MIS 5e). *Quaternary Science Reviews* **26,** 2090-2112.

Hearty, P. J., and Kindler, P. (1995). Sea-Level Highstand Chronology from Stable Carbonate Platforms (Bermuda and the Bahamas). *Journal of Coastal Research* **11,** 675-689.

Helgren, D. M., and Butzer, K. W. (1977). Paleosols of Southern Cape Coast, South-Africa - Implications for Laterite Definition, Genesis, and Age. *Geographical Review* **67,** 430-445.

Henderson, P. (1984). General geochemical properties and abundances of the rare earth elements. *In* "Rare earth element geochemistry." (P. Henderson, Ed.), pp. 1-32. Elsevier Scientific, Amsterdam.

Henshilwood, C. S., Sealy, J. C., Yates, R., Cruz-Uribe, K., Goldberg, P., Grine, F. E., Klein, R. G., Poggenpoel, C., Van Niekerk, K., and Watts, I. (2001). Blombos Cave, Southern Cape, South Africa: Preliminary report on the 1992-1999 excavations of the Middle Stone Age Levels. *Journal of Archaeological Science* **28,** 421-448.

Hesp, P. (2002). Foredunes and blowouts: initiation, geomorphology and dynamics. *Geomorphology* **48,** 245-268.

Hessler, A. M., and Lowe, D. R. (2006). Weathering and sediment generation in the Archean: An integrated study of the evolution of siliciclastic sedimentary rocks of the 3.2 Ga Moodies Group, Barberton Greenstone Belt, South Africa. *Precambrian Research* **151,** 185-210.

Heydorn, A. E. F., and Tinley, K. L. (1980). Synopsis of the Cape coast - natural features, dynamics and utilization. Part 1. Estuaries of the Cape Series. CSIR Research Report No. 380, pp. 97.

Heydorn, H. J. (1989a). Report No. 38 Gourits (CS 25). *In* "Estuaries of the Cape Part II: Synopses of available information on individual systems CSIR Research Report 437." (A. E. F. Heydorn, and P. D. Morant, Eds.), pp. 1-52. CSIR, Stellenbosch.

Heydorn, H. J. (1989b). Report No. 38 Gourits (CSW 25). *In* "Estuaries of the Cape Part II: Synopses of available information on individual systems CSIR Research Report 437." (A. E. F. Heydorn, and P. D. Morant, Eds.), pp. 1-52. CSIR, Stellenbosch.

Heyvaert, V. M. A., and Baeteman, C. (2007). Holocene sedimentary evolution and palaeocoastlines of the Lower Khuzestan plain (southwest Iran). *Marine Geology* **242,** 83-108.

Hoare, P. G., Gale, S. J., Robinson, R. A. J., Connell, E. R., and Larkin, N. R. (2009). Marine Isotope Stage 7-6 transition age for beach sediments at Morston, north Norfolk, UK: implications for Pleistocene chronology, stratigraphy and tectonics. *Journal of Quaternary Science* **24,** 311-316.

Hoffmann, G., Lampe, R., and Barnasch, J. (2005). Postglacial evolution of coastal barriers along the West Pomeranian coast, NE Germany. *Quaternary International* **133-134,** 47-59.

Holmes, P. J., Bateman, M. D., Carr, A. S., and Marker, M. E. (2007). The place of aeolian coversands in the geomorphic evolution of the southern Cape coast, South Africa. *South African Journal of Geology* **110,** 125-136.

Hota, R., and Maejima, W. (2009). Heavy minerals of the Barakar Formation, Talchir Gondwana Basin, Orissa. *Journal of the Geological Society of India* **74,** 375-384.

Hoyt, J. H. (1973). Barrier island formation. *In* "Barrier islands." (M. L. Schwartz, Ed.), pp. 249-259. Dowden, Hutchinson and Ross, Stroudsburg.

Hubert, J. F. (1962). A zircon-tourmaline-rutile maturity index and the interdependence of the composition of heavy mineral assemblages with the gross composition and texture of sandstones. *Journal of Sedimentary Petrology* **32,** 440-450.

Huntley, D. J. (1985). On the Zeroing of the Thermo-Luminescence of Sediments. *Physics and Chemistry of Minerals* **12,** 122-127.

Huntley, D. J., Godfreysmith, D. I., and Thewalt, M. L. W. (1985). Optical Dating of Sediments. *Nature* **313,** 105-107.

Huntsman-Mapila, P., Kampunzu, A. B., Vink, B., and Ringrose, S. (2005). Cryptic indicators of provenance from the geochemistry of the Okavango Delta sediments, Botswana. *Sedimentary Geology* **174,** 123-148.

Huot, S., Buylaert, J. P., and Murray, A. S. (2006). Isothermal thermoluminescence signals from quartz. *Radiation Measurements* **41,** 796-802.

Hutton, J. (1788). Theory of the Earth. *Transactions of the Royal Society of Edinburgh* **1,** 209-304.

Illenberger, W. K. (1993). Variations of Sediment Dynamics in Algoa Bay During the Holocene. *South African Journal of Science* **89,** 187-196.

Illenberger, W. K. (1996). The geomorphologic evolution of the Wilderness dune cordons, South Africa. *Quaternary International* **33,** 11-20.

Illenberger, W. K., and Rust, I. C. (1988). A Sand Budget for the Alexandria Coastal Dunefield, South-Africa. *Sedimentology* **35,** 513-521.

IPCC. (2007). Summary for Policymakers. *In* "Climate Change 2007: Impacts, Adaptation and Vulnerability. Contribution of Working Group II to the Fourth Assessment Report of the Intergovernmental Panel on Climate Change." (M. L. Parry, O. F. Canziani, J. P. Palutikof, P. J. van der Linden, and C. E. Hanson, Eds.). Cambridge University Press, Cambridge.

Irving, S. J., and Meadows, M. E. (1997). Radiocarbon chronology and organic matter accumulation at Vankervelsvlei, near Knysna, South Africa. *South African Geographic Journal* **79,** 101-105.

Irving, S. J. E. (1998). Late Quaternary palaeoenvironments at Vankervelsvlei, near Knysna, South Africa. Unpublished MSc thesis. University of Cape Town, Cape Town.

Jacobs, Z. (2008). Luminescence chronologies for coastal and marine sediments. *Boreas* **37,** 508-535.

Jacobs, Z., Duller, G. A. T., and Wintle, A. G. (2003a). Optical dating of dune sand from Blombos Cave, South Africa: II - single grain data. *Journal of Human Evolution* **44,** 613-625.

Jacobs, Z., Duller, G. A. T., and Wintle, A. G. (2006a). Interpretation of single grain D-e distributions and calculation of D-e. *Radiation Measurements* **41,** 264-277.

Jacobs, Z., Duller, G. A. T., Wintle, A. G., and Henshilwood, C. S. (2006b). Extending the chronology of deposits at Blombos Cave, South Africa, back to 140 ka using optical dating of single and multiple grains of quartz. *Journal of Human Evolution* **51,** 255-273.

Jacobs, Z., Roberts, R. G., Galbraith, R. F., Deacon, H. J., Grun, R., Mackay, A., Mitchell, P., Vogelsang, R., and Wadley, L. (2008). Ages for the Middle Stone Age of Southern Africa: Implications for Human Behavior and Dispersal. *Science* **322,** 733-735.

Jacobs, Z., Wintle, A. G., and Duller, G. A. T. (2003b). Optical dating of dune sand from Blombos Cave, South Africa: I - multiple grain data. *Journal of Human Evolution* **44,** 599-612.

Jain, M. (2009). Extending the dose range: Probing deep traps in quartz with 3.06 eV photons. *Radiation Measurements* **44,** 445-452.

Jain, M., Botter-Jensen, L., Murray, A. S., Denby, P. M., Tsukamoto, S., and Gibling, M. R. (2005). Revisiting TL: dose measurement beyond the OSL range using SAR. *Ancient TL* **23,** 9-24.

Jain, M., Bøtter-Jensen, L., Murray, A. S., and Essery, R. (2007a). A peak structure in isothermal luminescence signals in quartz: Origin and implications. *Journal of Luminescence* **127,** 678-688.

Jain, M., Duller, G. A. T., and Wintle, A. G. (2007b). Dose response, thermal stability and optical bleaching of the 310 °C isothermal TL signal in quartz. *Radiation Measurements* **42,** 1285-1293.

James, N. P. (1997). The cool-water carbonate depositonal realm. *In* "Cool-water carbonates." (N. P. James, and J. A. D. Clarke, Eds.), pp. 1-22.

Jennings, J. N. (1967). Cliff-top dunes. *Australian Geographical Studies* **5,** 40-49.

Jones, G. A., and Kaiteris, P. (1983). A Vacuum-Gasometric Technique for Rapid and Precise Analysis of Calcium-Carbonate in Sediments and Soils. *Journal of Sedimentary Petrology* **53,** 655-660.

Kasper-Zubillaga, J. J., and Carranza-Edwards, A. (2005). Grain size discrimination between sands of desert and coastal dunes from northwestern Mexico. *Revista Mexicana De Ciencias Geologicas* **22,** 383-390.

Kasper-Zubillaga, J. J., and Zolezzi-Ruiz, H. (2007). Grain size, mineralogical and geochemical studies of coastal and inland dune sands from El Vizcaino Desert, Baja California Peninsula, Mexico. *Revista Mexicana De Ciencias Geologicas* **24,** 423-438.

Kasper-Zubillaga, J. J., Zolezzi-Ruiz, H., Carranza-Edwards, A., Giron-Garcia, P., Ortiz-Zamora, G., and Palma, M. (2007). Sedimentological, modal analysis and geochemical studies of desert and coastal dunes, Altar Desert, NW Mexico. *Earth Surface Processes and Landforms* **32,** 489-508.

Klein, R. G. (1978). A Preliminary Report on the Larger Mammals from the Boomplaas Stone Age Cave Site, Cango Valley, Oudtshoorn District, South Africa. *The South African Archaeological Bulletin* **33,** 66-75.

Klein, R. G., Avery, G., Cruz-Uribe, K., and Steele, T. E. (2007). The mammalian fauna associated with an archaic hominin skullcap and later Acheulean artifacts at Elandsfontein, Western Cape Province, South Africa. *Journal of Human Evolution* **52,** 164-186.

Kocurek, G. (1991). Interpretation of Ancient Eolian Sand Dunes. *Annual Review of Earth and Planetary Sciences* **19,** 43-75.

Kocurek, G. (1999). The aeolian rock record (yes, Virginia, it exists, but it really is rather special to create one). *In* "Aeolian environments, sediments, and landforms." (A. Goudie, I. Livingstone, and S. Stokes, Eds.), pp. 239-259. Wiley, Chichester.

Kocurek, G., and Havholm, K. G. (1993). Eolian sequence stratigraphy - a conceptual framework. *In* "Siliciclastic sequence stratigraphy." (P. Weimer, and H. W. Posamentier, Eds.), pp. 393-409. American Association of Petroleum Geologists, Tulsa, Okla.

Komar, P. D. (2007). The entrainment, transport and sorting of heavy minerals by wavs and currents. *In* "Heavy minerals in use." (M. A. Mange, and D. T. Wright, Eds.), pp. 3-48. Elsevier, Amsterdam.

Komar, P. D., and Chi, W. (1984). Processes of selective grain transport and the formation of placers on beaches. *Journal of Geology* **92,** 637-655.

Komar, P. D., Clemens, K. E., Li, Z. L., and Shih, S. M. (1989). The Effects of Selective Sorting on Factor-Analyses of Heavy-Mineral Assemblages. *Journal of Sedimentary Petrology* **59,** 590-596.

Kraft, J. C., Chrzastowski, M. J., Belknap, D. F., Toscano, M. A., and Fletcher, C. H. (1987). The transgressive barrier-lagoon coast of Delaware: morphostratigraphy, sedimentary sequences and responses to relative rise in sea level. *In* "Sea-level fluctuation and coastal evolution." (D. Nummedal, O. H. Pilkey, and J. D. Howard, Eds.), pp. 129-143. SEPM, Oklahoma.

Krynauw, J. R. (1983). Granite intrusion and metamorphism in the Kaaimans Group. *Geological Society of South Africa Special Publication* **12,** 21-32.

Krzanowski, W. J., and Marriott, F. H. C. (1994). "Multivariate analysis part 1: Distributions, ordination and inference " Edward Arnold, London.

Lancaster, N. (1982). Dunes on the Skeleton Coast, Namibia (South West-Africa) - Geomorphology and Grain-Size Relationships. *Earth Surface Processes and Landforms* **7,** 575-587.

Lindesay, J. (1998). Present Climates of Southern Africa. *In* "Climates of the southern continents : present, past and future." (J. E. Hobbs, J. Lindesay, and H. A. Bridgman, Eds.), pp. 5-62. John Wiley & Sons, Chichester.

Lomax, J., Hilgers, A., Wopfner, H., Grün, R., Twidale, C. R., and Radtke, U. (2003). The onset of dune formation in the Strzelecki Desert, South Australia. *Quaternary Science Reviews* **22,** 1067-1076.

Lutjeharms, J. R. E., Monteiro, P. M. S., Tyson, P. D., and Obura, D. (2001). The oceans around southern Africa and regional effects of global change. *South African Journal of Science* **97,** 119-130.

Lyell, C. (1830). "Principles of geology: being an attempt to explain the former changes of the Earth's surface, by reference to causes now in operation." John Murray, London.

Madsen, A. T., Murray, A. S., Andersen, T. J., and Pejrup, M. (2010). Luminescence dating of Holocene sedimentary deposits on Romo, a barrier island in the Wadden Sea, Denmark. *Holocene* **20,** 1247-1256.

Malan, J. A. (1990). "The stratigraphy and sedimentology of the Bredasdorp Group, southern Cape Province." Unpublished MSc thesis, University of Cape Town.

Mange, M. A., and Maurer, H. F. W. (1992). "Heavy minerals in colour." Chapman & Hall.

Mange, M. A., and Wright, D. T. (2007a). Introduction and overview. *In* "Heavy minerals in use." (M. A. Mange, and D. T. Wright, Eds.), pp. xxvii-xliv. Elsevier, Amsterdam.

Mange, M. A., and Wright, D. T. (2007b). Preface. *In* "Heavy minerals in use." (M. A. Mange, and D. T. Wright, Eds.), pp. xxi-xxiii. Elsevier, Amsterdam.

Marean, C. W., Bar-Matthews, M., Bernatchez, J., Fisher, E., Goldberg, P., Herries, A. I. R., Jacobs, Z., Jerardino, A., Karkanas, P., Minichillo, T., Nilssen, P. J., Thompson, E., Watts, I., and Williams, H. M. (2007). Early human use of marine resources and pigment in South Africa during the Middle Pleistocene. *Nature* **449,** 905-908.

Marker, M. E. (2003). The Knysna Basin, South Africa: geomorphology, landscape sensitivity and sustainability. *The Geographical Journal* **169,** 32-42.

Marker, M. E., and Holmes, P. J. (2002). The distribution and environmental implications of coversand deposits in the Southern Cape, South Africa. *South African Journal of Geology* **105,** 135-146.

Marker, M. E., and Holmes, P. J. (2005). Landscape evolution and landscape sensitivity: the case of the southern Cape. *South African Journal of Science* **101,** 53-60.

Marsh, R. E., Prestwich, W. V., Rink, W. J., and Brennan, B. J. (2002). Monte Carlo determinations of the beta dose rate to tooth enamel. *Radiation Measurements* **35,** 609-616.

Martin-Fernandez, J. A., Barcelo-Vidal, C., and Pawlowsky-Glahn, V. (2003). Dealing with zeros and missing values in compositional data sets using nonparametric imputation. *Mathematical Geology* **35,** 253-278.

Martin, A. K. (1987). Comparison of sedimentation rates in the Natal Valley, south-west Indian Ocean with modern sediment yields in east coast rivers of Southern Africa. *South African Journal of Science* **83,** 716-724.

Martin, A. K., and Flemming, B. W. (1983). Nearshore Holocene sedimentation between Mossel Bay and Natures Valley *In* "5th National Oceanography Symposium." Abstract H6, Grahamstown, South Africa.

Martin, A. K., and Flemming, B. W. (1986). The Holocene sediment wedge off the south and east coast of South Africa. *Canadian Society of Petroleum Geologists Memoir* **2,** 27-44.

Martin, A. R. H. (1962). Evidence relating to the Quaternary Histoy of the Wilderness Lakes. *Transactions of the Geological Society of South Africa* **64,** 19-42.

Maud, R. R., and Botha, G. A. (2000). Deposits of the south eastern and southern coasts. *In* "The Cenozoic of southern Africa." (T. C. Partridge, and R. R. Maud, Eds.), pp. 19-32. Oxford University Press, Oxford.

Mauz, B., Baeteman, C., Bungenstock, F., and Plater, A. J. (2010). Optical dating of tidal sediments: Potentials and limits inferred from the North Sea coast. *Quaternary Geochronology* **5,** 667-678.

McKee, E. D., and Ward, W. C. (1983). Eolian environment. *In* "Carbonate depositional environments." (P. A. Scholle, D. G. Bebout, and C. H. Moore, Eds.), pp. 131-170. American Association of Petroleum Geologists, Tulsa.

McLennan, S. M., Hemming, S., McDaniel, D. K., and Hanson, G. N. (1993). Geochemical approaches to sedimentation, provenance, and tectonics. *In* "Processes controlling the

composition of clastic sediments." (M. J. Johnsson, and A. Basu, Eds.), pp. 21-40. Geological Society of America, Boulder, Colorado.
McRae, S. G. (1972). Glauconite. *Earth-Science Reviews* **8,** 397-440.
Meadows, M. E., and Baxter, A. J. (1999). Late Quaternary Palaeoenvironments of the southwestern Cape, South Africa: a regional synthesis. *Quaternary International* **57-8,** 193-206.
Meisel, T., Schöner, N., Paliulionyte, V., and Kahr, E. (2002). Determination of Rare Earth Elements, Y, Th, Zr, Hf, Nb and Ta in Geological Reference Materials G-2, G-3, SCo-1 and WGB-1 by Sodium Peroxide Sintering and Inductively Coupled Plasma-Mass Spectrometry. *Geostandards Newsletter* **26,** 53-61.
Monroe, J. S., and Wicander, R. (2009). "The changing earth: exploring geology and evolution." Brooks/Cole, Belmont.
Moreno, T., Querol, X., Castillo, S., Alastuey, A., Cuevas, E., Herrmann, L., Mounkaila, M., Elvira, J., and Gibbons, W. (2006). Geochemical variations in aeolian mineral particles from the Sahara-Sahel Dust Corridor. *Chemosphere* **65,** 261-270.
Morton, A. C., and Hallsworth, C. (1994). Identifying Provenance-Specific Features of Detrital Heavy Mineral Assemblages in Sandstones. *Sedimentary Geology* **90,** 241-256.
Morton, A. C., and Hallsworth, C. R. (1999). Processes controlling the composition of heavy mineral assemblages in sandstones. *Sedimentary Geology* **124,** 3-29.
Morton, A. C., and Hallsworth, C. R. (2007). Stability of detrital heavy minerals during burial diagenesis. *In* "Heavy minerals in use." (M. A. Mange, and D. T. Wright, Eds.), pp. 215-246. Elsevier, Amsterdam.
Morton, A. C., and Smale, D. (1991). The effects of transport and weathering on heavy minerals from the Cascade River, New Zealand. *Sedimentary Geology* **68,** 117-123.
Muhs, D. R. (2004). Mineralogical maturity in dunefields of North America, Africa and Australia. *Geomorphology* **59,** 247-269.
Muhs, D. R., Bettis, E. A., Aleinikoff, J. N., McGeehin, J. P., Beann, J., Skipp, G., Marshall, B. D., Roberts, H. M., Johnson, W. C., and Benton, R. (2008). Origin and paleoclimatic significance of late Quaternary loess in Nebraska: Evidence from stratigraphy, chronology, sedimentology, and geochemistry. *Geological Society of America Bulletin* **120,** 1378-1407.
Muhs, D. R., Budahn, J., Reheis, M., Beann, J., Skipp, G., and Fisher, E. (2007a). Airborne dust transport to the eastern Pacific Ocean off southern California: Evidence from San Clemente Island. *Journal of Geophysical Research-Atmospheres* **112,** 17.
Muhs, D. R., and Budahn, J. R. (2006). Geochemical evidence for the origin of late Quaternary loess in central Alaska. *Canadian Journal of Earth Sciences* **43,** 323-337.
Muhs, D. R., and Budahn, J. R. (2009). Geochemical evidence for African dust and volcanic ash inputs to terra rossa soils on carbonate reef terraces, northern Jamaica, West Indies. *Quaternary International* **196,** 13-35.
Muhs, D. R., Budahn, J. R., Prospero, J. M., and Carey, S. N. (2007b). Geochemical evidence for African dust inputs to soils of western Atlantic islands: Barbados, the Bahamas, and Florida. *Journal of Geophysical Research-Earth Surface* **112,** 26.
Muhs, D. R., and Holliday, V. T. (2001). Origin of late quaternary dune fields on the Southern High Plains of Texas and New Mexico. *Geological Society of America Bulletin* **113,** 75-87.
Muhs, D. R., Reynolds, R. L., Been, J., and Skipp, G. (2003). Eolian sand transport pathways in the southwestern United States: importance of the Colorado River and local sources. *Quaternary International* **104,** 3-18.
Muhs, D. R., Stafford, T. W., Cowherd, S. D., Mahan, S. A., Kihl, R., Maat, P. B., Bush, C. A., and Nehring, J. (1996). Origin of the late Quaternary dune fields of northeastern Colorado. *Geomorphology* **17,** 129-149.
Murray-Wallace, C. V. (2002). Pleistocene coastal stratigraphy, sea-level highstands and neotectonism of the southern Australian passive continental margin - a review. *Journal of Quaternary Science* **17,** 469-489.

Murray-Wallace, C. V., Bourman, R. P., Prescott, J. R., Williams, F., Price, D. M., and Belperio, A. P. (2010). Aminostratigraphy and thermoluminescence dating of coastal aeolianites and the later Quaternary history of a failed delta: The River Murray mouth region, South Australia. *Quaternary Geochronology* **5,** 28-49.

Murray-Wallace, C. V., Brooke, B. P., Cann, J. H., Belperio, A. P., and Bourman, R. P. (2001). Whole-rock aminostratigraphy of the Coorong Coastal Plain, South Australia: towards a 1 million year record of sea-level highstands. *Journal of the Geological Society* **158,** 111-124.

Murray, A. S., and Funder, S. (2003). Optically stimulated luminescence dating of a Danish Eemian coastal marine deposit: a test of accuracy. *Quaternary Science Reviews* **22,** 1177-1183.

Murray, A. S., and Mohanti, M. (2006). Luminescence dating of the barrier spit at Chilika lake, Orissa, India. *Radiation Protection Dosimetry* **119,** 442-445.

Murray, A. S., and Olley, J. M. (2002). Precision and accuracy in the optically stimulated luminescence dating of sedimentary quartz: a status review. *Geochronometria* **21,** 1-16.

Murray, A. S., and Roberts, R. G. (1998). Measurement of the equivalent dose in quartz using a regenerative-dose single-aliquot protocol. *Radiation Measurements* **29,** 503-515.

Murray, A. S., Roberts, R. G., and Wintle, A. G. (1997). Equivalent dose measurement using a single aliquot of quartz. *Radiation Measurements* **27,** 171-184.

Murray, A. S., and Wintle, A. G. (2000). Luminescence dating of quartz using an improved single-aliquot regenerative-dose protocol. *Radiation Measurements* **32,** 57-73.

Murray, A. S., and Wintle, A. G. (2003). The single aliquot regenerative dose protocol: potential for improvements in reliability. *Radiation Measurements* **37,** 377-381.

Murray, A. S., Wintle, A. G., and Wallinga, J. (2002). Dose estimation using quartz OSL in the non-linear region of the growth curve. *Radiation Protection Dosimetry* **101,** 371-374.

Murray, M. R. (2002). Is laser particle size determination possible for carbonate-rich lake sediments ? *Journal of Paleolimnology* **27,** 173-183.

Nanson, G. C., Chen, X. Y., and Price, D. M. (1992). Lateral migration, thermoluminescence chronology and colour variation of longitudinal dunes near Birdsville in the Simpson Desert, central Australia. *Earth Surface Processes and Landforms* **17,** 807-819.

Nath, B. N., Kunzendorf, H., and Pluger, W. L. (2000). Influence of provenance, weathering, and sedimentary processes on the elemental ratios of the fine-grained fraction of the bedload sediments from the Vembanad Lake and the adjoining continental shelf, southwest coast of India. *Journal of Sedimentary Research* **70,** 1081-1094.

Nield, J. M., and Baas, A. C. W. (2008). The influence of different environmental and climatic conditions on vegetated aeolian dune landscape development and response. *Global and Planetary Change* **64,** 76-92.

Nishimori, H., and Tanaka, H. (2001). A simple model for the formation of vegetated dunes. *Earth Surface Processes and Landforms* **26,** 1143-1150.

Noda, A. (2005). Texture and petrology of modern river, beach and shelf sands in a volcanic back-arc setting, northeastern Japan. *Island Arc* **14,** 687-707.

Nothdurft, L. D., Webb, G. E., and Kamber, B. S. (2004). Rare earth element geochemistry of Late Devonian reefal carbonates, Canning Basin, Western Australia: confirmation of a seawater REE proxy in ancient limestones. *Geochimica et Cosmochimica Acta* **68,** 263-283.

Oldfield, F. (2004). Some personal perspectives on the role of Quaternary science in global change studies. *Global and Planetary Change* **40,** 3-9.

Olivier, M. J., and Garland, G. G. (2003). Short-term monitoring of foredune formation on the east coast of South Africa. *Earth Surface Processes and Landforms* **28,** 1143-1155.

Olley, J., Caitcheon, G., and Murray, A. (1998). The distribution of apparent dose as determined by optically stimulated luminescence in small aliquots of fluvial quartz: Implications for dating young sediments. *Quaternary Science Reviews* **17,** 1033-1040.

Olley, J. M., De Deckker, P., Roberts, R. G., Fifield, L. K., Yoshida, H., and Hancock, G. (2004). Optical dating of deep-sea sediments using single grains of quartz: a comparison with radiocarbon. *Sedimentary Geology* **169,** 175-189.

Olley, J. M., Murray, A., and Roberts, R. G. (1996). The effects of disequilibria in the uranium and thorium decay chains on burial dose rates in fluvial sediments. *Quaternary Science Reviews* **15,** 751-760.

Olley, J. M., Roberts, R. G., and Murray, A. S. (1997). Disequilibria in the uranium decay series in sedimentary deposits at Allen's Cave, Nullarbor Plain, Australia: Implications for dose rate determinations. *Radiation Measurements* **27,** 433-443.

Ollier, C. D. (1985). Morphotectonics of continental margins with great escarpments. *In* "Tectonic geomorphology: proceedings of the 15th annual Binghamton Geomorphology Symposium, September 1984." (M. Morisawa, and J. T. Hack, Eds.), pp. 3-25. Allen & Unwin, Boston.

Olson, S. L., and Hearty, P. J. (2009). A sustained +21 m sea-level highstand during MIS 11 (400 ka): direct fossil and sedimentary evidence from Bermuda. *Quaternary Science Reviews* **28,** 271-285.

Parker, R. J., and Siesser, W. G. (1972). Petrology and origin of some phosphorites from the South African continental margin. *Journal of Sedimentary Petrology* **42,** 434-440.

Parker, R. L., and Fleischer, M. (1968). "Geochemistry of niobium and tantalum: U.S. Geologucal Survey Professional Paper 612."

Partridge, T. C. (1997). Cainozoic environmental change in southern Africa, with special emphasis on the last 200 000 years. *Progress in Physical Geography* **21,** 3-22.

Partridge, T. C., and Maud, R. R. (1987). Geomorphic evolution of southern Africa since the Mesozoic. *South African Journal of Geology* **90,** 179-208.

Partridge, T. C., and Maud, R. R. (2000). Macro-scale geomorphic evolution of southern Africa. *In* "The Cenozoic of southern Africa." (T. C. Partridge, and R. R. Maud, Eds.), pp. 3-18. Oxford University Press, Oxford.

Patterson, R. T., Prokoph, A., Reinhardt, E., and Roe, H. M. (2007). Climate cyclicity in late Holocene anoxic marine sediments from the Seymour-Belize Inlet Complex, British Columbia. *Marine Geology* **242,** 123-140.

Pe-Piper, G., Triantafyllidis, S., and Piper, D. J. W. (2008). Geochemical identification of clastic sediment provenance from known sources of similar geology: The cretaceous Scotian Basin, Canada. *Journal of Sedimentary Research* **78,** 595-607.

Pease, P. P., and Tchakerian, V. P. (2002). Composition and sources of sand in the Wahiba Sand Sea, Sultanate of Oman. *Annals of the Association of American Geographers* **92,** 416-434.

Pease, P. P., and Tchakerian, V. P. (2003). Geochemistry of sediments from Quaternary sand ramps in the southeastern Mojave Desert, California. *Quaternary International* **104,** 19-29.

Peeters, F. J. C., Acheson, R., Brummer, G. J. A., de Ruijter, W. P. M., Schneider, R. R., Ganssen, G. M., Ufkes, E., and Kroon, D. (2004). Vigorous exchange between the Indian and Atlantic oceans at the end of the past five glacial periods. *Nature* **430,** 661-665.

Peterson, C. D., Komar, P. D., and Scheidegger, K. F. (1986). Distribution, geometry, and origin of heavy mineral placer deposits on Oregon beaches (USA). *Journal of Sedimentary Petrology* **56,** 67-77.

Pirkle, F. L., Pirkle, E. C., Pirkle, W. A., Dicks, S. E., Jones, D. S., and Mallard, E. A. (1989). Altama heavy mineral deposits in southeastern Georgia, pp. 425-433.

Porat, N., and Botha, G. (2008). The luminescence chronology of dune development on the Maputaland coastal plain, southeast Africa. *Quaternary Science Reviews* **27,** 1024-1046.

Potgieter, C. T. (1950). The structure and petrology of the George granite plutons and the invaded pre-Cape sedimentary rocks. *Annals of the University of Stellenbosch* **26,** 323-412.

Prescott, J. R., and Hutton, J. T. (1994). Cosmic-Ray Contributions to Dose-Rates for Luminescence and Esr Dating - Large Depths and Long-Term Time Variations. *Radiation Measurements* **23,** 497-500.

Price, D. M., Brooke, B. P., and D. Woodroffe, C. (2001). Thermoluminescence dating of aceolianites from Lord Howe Island and South-West Western Australian. *Quaternary Science Reviews* **20,** 841-846.

Probyn, T. A., Mitchell-Innes, B. A., Brown, P. C., Hutchings, L., and Carter, R. A. (1994). A review of primary production and related processes on the Agulhas Bank. *South African Journal of Science* **90,** 166-173.

Psuty, N. P. (1988). Sediment budget and beach/dune interaction. *Journal of Coastal Research, Special Issue* **3,** 1-4.

Psuty, N. P., and Silveira, T. M. (2010). Global climate change: an opportunity for coastal dunes?? *Journal of Coastal Conservation* **14,** 153-160.

Puchelt, H., and Emmermann, R. (1976). Bearing of rare earth patterns of apatites from igneous and metamorphic rocks. *Earth and Planetary Science Letters* **31,** 279-286.

Pye, K. (1983). Coastal dunes. *Progress in Physical Geography* **7,** 531-557.

Pye, K., and Blott, S. J. (2004). Particle size analysis of sediments, soils and related particulate materials for forensic purposes using laser granulometry. *Forensic Science International* **144,** 19-27.

Pye, K., and Tsoar, H. (1990). "Aeolian sand and sand dunes." Unwin Hyman.

Ramsay, P. J., and Cooper, J. A. G. (2002). Late Quaternary Sea-Level Change in South Africa. *Quaternary Research* **57,** 82-90.

Rao, C. P. (1996). "Modern carbonates, tropical, temperate, polar: Introduction to sedimentology and geochemistry." University of Tasmania, Hobart.

Rau, A. J., Rogers, J., Lutjeharms, J. R. E., Giraudeau, J., Lee-Thorp, J. A., Chen, M. T., and Waelbroeck, C. (2002). A 450-kyr record of hydrological conditions on the western Agulhas Bank Slope, south of Africa. *Marine Geology* **180,** 183-201.

Rick, T. C., Erlandson, J. M., Vellanoweth, R. L., and Braje, T. J. (2005). From Pleistocene mariners to complex hunter-gatherers: The archaeology of the California Channel Islands. *Journal of World Prehistory* **19,** 169-228.

Rieu, R., van Heteren, S., van der Spek, A. J. F., and De Boer, P. L. (2005). Development and Preservation of a Mid-Holocene Tidal-Channel Network Offshore the Western Netherlands, pp. 409-419.

Ringner, M. (2008). What is principal component analysis? *Nat Biotech* **26,** 303-304.

Rink, W. J., and Forrest, B. (2005). Dating Evidence for the Accretion History of Beach Ridges on Cape Canaveral and Merritt Island, Florida, USA. *Journal of Coastal Research* **21,** 1000-1008.

Roberts, D. (2008). Last Interglacial Hominid and Associated Vertebrate Fossil Trackways in Coastal Eolianites, South Africa. *Ichnos-an International Journal for Plant and Animal Traces* **15,** 190-207.

Roberts, D. L., Bateman, M. D., Murray-Wallace, C. V., Carr, A. S., and Holmes, P. J. (2008). Last Interglacial fossil elephant trackways dated by OSL/AAR in coastal aeolianites, Still Bay, South Africa. *Palaeogeography Palaeoclimatology Palaeoecology* **257,** 261-279.

Roberts, D. L., Bateman, M. D., Murray-Wallace, C. V., Carr, A. S., and Holmes, P. J. (2009). West coast dune plumes: Climate driven contrasts in dunefield morphogenesis along the western and southern South African coasts. *Palaeogeography Palaeoclimatology Palaeoecology* **271,** 24-38.

Roberts, D. L., and Brink, J. S. (2002). Dating and correlation of neogene coastal deposits in the Western Cape (South Africa): Implications for neotectonism. *South African Journal of Geology* **105,** 337-352.

Roberts, R. G., Galbraith, R. F., Yoshida, H., Laslett, G. M., and Olley, J. M. (2000). Distinguishing dose populations in sediment mixtures: a test of single-grain optical dating procedures using mixtures of laboratory-dosed quartz. *Radiation Measurements* **32,** 459-465.

Roy, P. S., Cowell, P. J., Ferland, M. A., and Thom, B. G. (1994). Wave-dominated coasts. *In* "Coastal evolution: Late Quaternary shoreline morphodynamics." (R. W. G. Carter, and C. D. Woodroffe, Eds.), pp. 121-186. University Press, Cambridge.

Roy, P. S., Thom, B. G., and Wright, L. D. (1980). Holocene sequences on an embayed high-energy coast: an evolutionary model. *Sedimentary Geology* **26,** 1-19.

Rozendaal, A., Gresse, P. G., Scheepers, R., and Le Roux, J. P. (1999). Neoproterozoic to Early Cambrian Crustal Evolution of the Pan-African Saldania Belt, South Africa. *Precambrian Research* **97,** 303-323.

Rust, I. C. (1977). The evolution of the Paleozoic Cape Basin, southern margin Africa. *In* "The ocean basins and margins. Volume 1, The South Atlantic." (A. E. M. Nairn, and F. G. Stehli, Eds.), pp. 247-276. Plenum Press, New York.

Rust, I. C. (1991). Environmental geology of the coastal zone: a South African perspective. *South African Journal of Marine Science* **10,** 397-405.

Saye, S. E., and Pye, K. (2000). Textural and geochemical evidence for the provenance of aeolian sand deposits on the Aquitane coast, SW France. *In* "Coastal and estuarine environments: sedimentology, geomorphology and geoarchaeology. Geological Society special publication no. 175." (K. Pye, and J. R. L. Allen, Eds.), pp. 173-186. Geological Society, Bath.

Saye, S. E., and Pye, K. (2006). Variations in chemical composition and particle size of dune sediments along the west coast of Jutland, Denmark. *Sedimentary Geology* **183,** 217-242.

Saye, S. E., Pye, K., and Clemmensen, L. B. (2006). Development of a cliff-top dune indicated by particle size and geochemical characteristics: Rubjerg Knude, Denmark. *Sedimentology* **53,** 1-21.

Schlager, W. (2003). Benthic carbonate factories of the Phanerozoic. *International Journal of Earth Sciences* **92,** 445-464.

Schleyer, M. H., Heikoop, J. M., and Risk, M. J. (2006). A benthic survey of Aliwal Shoal and assessment of the effects of a wood pulp effluent on the reef. *Marine Pollution Bulletin* **52,** 503-514.

Schwartz, M. L. (1971). Multiple Causality of Barrier Islands. *Journal of Geology* **79,** 91-&.

Shone, R. W., and Booth, P. W. K. (2005). The Cape Basin, South Africa: A review. *Journal of African Earth Sciences* **43,** 196-210.

Short, A. D. (1984). Beach and Nearshore Facies - Southeast Australia. *Marine Geology* **60,** 261-282.

Short, A. D. (2010). Sediment Transport around Australia-Sources, Mechanisms, Rates, and Barrier Form. *Journal of Coastal Research* **26,** 395-402.

Siddall, M., Bard, E., Rohling, E. J., and Hemleben, C. (2006). Sea-level reversal during Termination II, pp. 817-820.

Siddall, M., Chappell, J., and Potter, E. K. (2007). Eustatic sea level during past interglacials. *In* "The Climate of Past Interglacials." (F. Sirocko, M. Claussen, M. F. Sanchez-Goñi, and T. Litt, Eds.), pp. 75-92. Elsevier.

Siesser, W. G. (1972). Petrology of the Cainozoic coastal limestones of the Cape Province, South Africa. *Transactions of the Geological Society of South Africa* **75,** 177-185.

Singarayer, J. S., Bailey, R. M., and Rhodes, E. J. (2000). Potential of the slow component of quartz OSL for age determination of sedimentary samples. *Radiation Measurements* **32,** 873-880.

Sivan, D., and Porat, N. (2004). Evidence from luminescence for Late Pleistocene formation of calcareous aeolianite (kurkar) and paleosol (hamra) in the Carmel Coast, Israel. *Palaeogeography, Palaeoclimatology, Palaeoecology* **211,** 95-106.

Smith, M. A., Prescott, J. R., and Head, M. J. (1997). Comparison of C-14 and luminescence chronologies at Puritjarra rock shelter, central Australia. *Quaternary Science Reviews* **16,** 299-320.

Spooner, N. A. (1994). The Anomalous Fading of Infrared-Stimulated Luminescence from Feldspars. *Radiation Measurements* **23,** 625-632.

Spooner, N. A., Prescott, J. R., and Hutton, J. T. (1988). The Effect of Illumination Wavelength on the Bleaching of the Thermo-Luminescence (Tl) of Quartz. *Quaternary Science Reviews* **7,** 325-329.

Sprigg, R. C. (1979). Stranded and submerged sea-beach systems of southeast South Australia and the aeolian desert cycle. *Sedimentary Geology* **22,** 53-96.

Stapor, F. W., Mathews, T. D., and Lindfors-Kearns, F. E. (1991). Barrier-Island Progradation and Holocene Sea-Level History in Southwest Florida. *Journal of Coastal Research* **7,** 815-838.

Stauffer, T., and Igushi, T. (1997). Particle size distribution analyzer: Model LA-920. *In* "Readout: Horiba technical reports." pp. 67-74.

Stevens, J. (2002). "Applied multivariate statistics for the social sciences." Lawrence Erlbaum Associates, Mahwah, N.J. ; London.

Stone, A. W., Weaver, A. v. B., and West, W. O. (1998). Climate and weather. *In* "Field guide to the eastern and southern Cape coasts." (R. Lubke, and I. de Moor, Eds.), pp. 41-49. University of Cape Town Press, Rondebosch.

Stuut, J.-B. W., Crosta, X., van der Borg, K., and Schneider, R. R. (2004). Relationship between Antarctic sea ice and southwest African climate during the late Quaternary. *Geology* **32,** 909-912.

Stuut, J.-B. W., Prins, M. A., Schneider, R. R., Weltje, G. J., Jansen, J. H. F., and Postma, G. (2002). A 300-kyr record of aridity and wind strength in southwestern Africa: inferences from grain-size distributions of sediments on Walvis Ridge, SE Atlantic. *Marine Geology* **180,** 221-233.

Takhtajan, A. L., and Cronquist, A. (1986). "Floristic regions of the world." University of California Press, Berkeley.

Tankard, A. J., and Schweitzer, F. R. (1974). The geology of Die Kelders Cave and environs: a palaeoenvironmental study. *South African Journal of Science* **70,** 365-369.

Tauber, F. (1999). Spurious clusters in granulometric data caused by logratio transformation. *Mathematical Geology* **31,** 491-504.

Taylor, S. R., and McLennan, S. M. (1985). "The continental crust: its composition and evolution." Blackwell Scientific, Oxford.

Telfer, M. W. (2006). "Late Quaternary aeolian activity and palaeoenvironments of the southwestern Kalahari: advances from an intensive chronometric investigation at Witpan, South Africa." University of Sheffield.

Telfer, M. W., Bailey, R. M., Burrough, S. L., Stone, A. E. S., Thomas, D. S. G., and Wiggs, G. S. F. (2010). Understanding linear dune chronologies: Insights from a simple accumulation model. *Geomorphology* **120,** 195-208.

Telfer, M. W., and Thomas, D. S. G. (2007). Late Quaternary linear dune accumulation and chronostratigraphy of the southwestern Kalahari: implications for aeolian palaeoclimatic reconstructions and predictions of future dynamics. *Quaternary Science Reviews* **26,** 2617-2630.

Temme, A., Baartman, J. E. M., Botha, G. A., Veldkamp, A., Jongmans, A. G., and Wallinga, J. (2008). Climate controls on late Pleistocene landscape evolution of the Okhombe valley, KwaZulu-Natal, South Africa. *Geomorphology* **99,** 280-295.

Thio-Henestrosa, S., and Martin-Fernandez, J. A. (2005). Dealing with compositional data: The freeware CoDaPack. *Mathematical Geology* **37,** 773-793.

Thom, B. G. (1984). Transgressive and regressive stratigraphies of coastal sand barriers in southeast Australia. *Marine Geology* **56,** 137-158.

Thomas, D. S. G., Bailey, R., Shaw, P. A., Durcan, J. A., and Singarayer, J. S. (2009). Late Quaternary highstands at Lake Chilwa, Malawi: Frequency, timing and possible forcing mechanisms in the last 44 ka. *Quaternary Science Reviews* **28,** 526-539.

Tinker, J., de Wit, M., and Brown, R. (2008a). Linking source and sink: Evaluating the balance between onshore erosion and offshore sediment accumulation since Gondwana break-up, South Africa. *Tectonophysics* **455,** 94-103.

Tinker, J., de Wit, M., and Brown, R. (2008b). Mesozoic exhumation of the southern Cape, South Africa, quantified using apatite fission track thermochronology. *Tectonophysics* **455,** 77-93.

Tinley, K. L. (1985). *Coastal dunes of South Africa*. South African National Scientific Programs Report 109. CSIR, Pretoria.

Toerien, D. K., and Roby, D. J. (1979). 1:250,000 geological series 3322 Oudtshoorn. The Government Printer, Pretoria.

Tomazelli, L. J., and Dillenburg, S. R. (2007). Sedimentary facies and stratigraphy of a last interglacial coastal barrier in south Brazil. *Marine Geology* **244,** 33-45.

Tomazelli, L. J., Villwock, J. A., Dillenburg, S. R., Bachi, F. A., and Dehnhardt, B. A. (1998). Significance of present-day coastal erosion and marine transgression, Rio Grande do Sul, southern Brazil. *Annals of the Brazilian Academy of Sciences* **70,** 221-229.

Tribe, H. M., and Kennedy, D. M. (2010). The geomorphology and evolution of a large barrier spit: Farewell Spit, New Zealand. *Earth Surface Processes and Landforms* **35,** 1751-1762.

Tsoar, H., and Blumberg, D. G. (2002). Formation of parabolic dunes from barchan and transverse dunes along Israel's Mediterranean coast. *Earth Surface Processes and Landforms* **27,** 1147-1161.

Tsukamoto, S., Duller, G. A. T., and Wintle, A. G. (2008). Characteristics of thermally transferred optically stimulated luminescence (TT-OSL) in quartz and its potential for dating sediments. *Radiation Measurements* **43,** 1204-1218.

Tyson, P. D. (1986). "Climatic change and variability in southern Africa." OUP, Cape Town.

Vandenberghe, D. A. G., Jain, M., and Murray, A. S. (2009). Equivalent dose determination using a quartz isothermal TL signal. *Radiation Measurements* **44,** 439-444.

Veevers, J. J. (2004). Gondwanaland from 650-500 Ma assembly through 320 Ma merger in Pangea to 185-100 Ma breakup: supercontinental tectonics via stratigraphy and radiometric dating. *Earth-Science Reviews* **68,** 1-132.

Visser, J. N. J. (1974). The Table Mountain Group: a study in the deposition of quartz arenites on a stable shelf. *Transactions of the Geological Society of South Africa* **77,** 229-237.

Vital, H., and Stattegger, K. (2000). Major and trace elements of stream sediments from the lowermost Amazon River. *Chemical Geology* **168,** 151-168.

Waelbroeck, C., Labeyrie, L., Michel, E., Duplessy, J. C., McManus, J. F., Lambeck, K., Balbon, E., and Labracherie, M. (2002). Sea-level and deep water temperature changes derived from benthic foraminifera isotopic records. *Quaternary Science Reviews* **21,** 295-305.

Wang, X. L., Lu, Y. C., and Wintle, A. G. (2006a). Recuperated OSL dating of fine-grained quartz in Chinese loess. *Quaternary Geochronology* **1,** 89-100.

Wang, X. L., Wintle, A. G., and Lu, Y. C. (2006b). Thermally transferred luminescence in fine-grained quartz from Chinese loess: Basic observations. *Radiation Measurements* **41,** 649-658.

Wang, X. L., Wintle, A. G., and Lu, Y. C. (2007). Testing a single-aliquot protocol for recuperated OSL dating. *Radiation Measurements* **42,** 380-391.

Weaver, A. J., Saenko, O. A., Clark, P. U., and Mitrovica, J. X. (2003). Meltwater Pulse 1A from Antarctica as a Trigger of the BÃ¸lling-AllerÃ¸d Warm Interval, pp. 1709-1713.

Weltje, G. J., and von Eynatten, H. (2004). Quantitative provenance analysis of sediments: review and outlook. *Sedimentary Geology* **171,** 1-11.

Whitmore, G. P., Crook, K. A. W., and Johnson, D. P. (2004). Grain size control of mineralogy and geochemistry in modem river sediment, New Guinea collision, Papua New Guinea. *Sedimentary Geology* **171,** 129-157.

Wigley, R., and Compton, J. S. (2007). Oligocene to Holocene glauconite-phosphorite grains from the Head of the Cape Canyon on the western margin of South Africa. *Deep Sea Research Part II: Topical Studies in Oceanography* **54,** 1375-1395.

Williams, A. H., and Walkden, G. M. (2001). Carbonate eolianites from a eustatically influenced ramp-like setting: the Quaternary of the southern Arabian Gulf. *In* "Modern and ancient carbonate eolianites: sedimentology, sequence stratigraphy, and diagenesis. SEPM Special Publication 71." (F. E. Abegg, P. M. Harris, and D. Loope, Eds.), pp. 77-92.

Wilson, P., Orford, J. D., Knight, J., Braley, S. M., and Wintle, A. G. (2001). Late-Holocene (post-4000 years BP) coastal dune development in Northumberland, northeast England. *Holocene* **11,** 215-229.

Winter, A., and Martin, K. (1990). Late Quaternary history of the Agulhas Current. *Palaeooceanography* **5,** 479-486.

Wintle, A. G. (1973). Anomalous Fading of Thermoluminescence in Mineral Samples. *Nature* **245,** 143-144.

Wintle, A. G. (1997). Luminescence dating: Laboratory procedures and protocols. *Radiation Measurements* **27,** 769-817.

Wintle, A. G. (2008). Fifty years of luminescence dating. *Archaeometry* **50,** 276-312.

Wintle, A. G., and Murray, A. S. (2006). A review of quartz optically stimulated luminescence characteristics and their relevance in single-aliquot regeneration dating protocols. *Radiation Measurements* **41,** 369-391.

Wolfe, S. A., Muhs, D. R., David, P. P., and McGeehin, J. P. (2000). Chronology and geochemistry of late Holocene eolian deposits in the Brandon Sand Hills: Manitoba, Canada. *Quaternary International* **67,** 61-74.

Woodroffe, S. A., and Horton, B. P. (2005). Holocene sea-level changes in the Indo-Pacific. *Journal of Asian Earth Sciences* **25,** 29-43.

Wright, C. I., Miller, W. R., and Cooper, J. A. G. (2000). The late Cenozoic evolution of coastal water bodies in Northern Kwazulu-Natal, South Africa. *Marine Geology* **167,** 207-229.

Wright, L. D., Chappell, J., Thom, B. G., Bradshaw, M. P., and Cowell, P. (1979). Morphodynamics of Reflective and Dissipative Beach and Inshore Systems - Southeastern Australia. *Marine Geology* **32,** 105-140.

Xing, B. S., and Dudas, M. J. (1992). Pedogenic Properties of White Clay Soils of the 3 River Plain, Heilongjiang Province, Pr China. *Geoderma* **54,** 189-211.

Xitao, Z., and Goldsmith, V. (1989). Surficial and Internal Geometry of Carbonate Eolianite in Fujian, China: Climatic and Tectonic Implications. *Journal of Coastal Research* **5,** 765-776.

Yang, X. P., Zhu, B. Q., and White, P. D. (2007). Provenance of aeolian sediment in the Taklamakan Desert of western China, inferred from REE and major-elemental data. *Quaternary International* **175,** 71-85.

Young, G. M., Minter, W. E. L., and Theron, J. N. (2004). Geochemistry and palaeogeography of upper Ordovician glaciogenic sedimentary rocks in the Table Mountain Group, South Africa. *Palaeogeography, Palaeoclimatology, Palaeoecology* **214,** 323-345.

Zhou, D., Chen, H. Z., and Lou, Y. L. (1991). The Logratio Approach to the Classification of Modern Sediments and Sedimentary Environments in Northern South China Sea. *Mathematical Geology* **23,** 157-165.

Zhou, L. P., Williams, M. A. J., and Peterson, J. A. (1994). Late Quaternary Aeolianites, Paleosols and Depositional-Environments on the Nepean Peninsula, Victoria, Australia. *Quaternary Science Reviews* **13,** 225-239.

Appendix 1: Sample carbonate contents

Table 1 Calcium carbonate contents of samples from the Wilderness barrier dunes. Includes samples from this study, KT section originally collected by Carr et al. (2007), and Holocene dune samples originally collected by Carr et al. (2010) (Shfd05040) and Bateman et al. (2011) (Shfd04279-04283). KT section carbonate contents provided by A. Carr (*Pers. comm.*).

Sample	Carbonate content (%)	Sample	Carbonate content (%)	Sample	Carbonate content (%)
Seaward barrier (this study)		**Seaward barrier (previous studies)**		**Middle barrier**	
1. Klein Krantz		**I. KT section**		**6. Rondevlei**	
Shfd09072	31.3	KT2-2	14.5	Shfd09078	15.7
Shfd09073	28.5	KT2-3	9.4	Shfd09079	16.3
2a. Elandsvlei Island		KT2-4	8.7	**7. West Swartvlei**	
Shfd09065	19.2	KT2-6	7.1	Shfd09080	14
Shfd09066	19.4	KT2-8	8.6	Shfd09081	0.06
2b. East Elandsvlei		KT2-9	8.1	Shfd09082	19.6
Shfd08184	15.6	KT2-11	4.3	**8. East Swartvlei**	
Shfd09076	22.3	**J. Holocene dunes**		Shfd08182	21.7
Shfd09077	17.4	Shfd05040	22.7	Shfd08181	22.6
3. Gerickes Point		Shfd04279	30.8	Shfd08183	24.6
Shfd08173	30.8	Shfd04280	26.6	**Landward barrier**	
Shfd08174	36.1	Shfd04281	28.5	**9. North Swartvlei**	
Shfd08175	21.5	Shfd04282	25.5	Shfd09074	14.4
Shfd08176	34.5	Shfd04283	27.6	Shfd09075	12.2
Shfd08177	37.3			**10. Goukamma**	
Shfd08178	33.3			Shfd09069	0.52
Shfd08179	22.3			Shfd09070	19
Shfd08180	27				
Shfd09068	20.1				
Shfd09067	29.6				
Shfd09149	30				
4. Groenvlei					
Shfd08186	31.6				
Shfd08187	32.3				
Shfd08189	27.8				
Shfd08188	34.5				
Shfd09071	36.3				
5. Buffels Bay					
Shfd08185	33.2				

Table 2 Calcium carbonate contents of possible barrier sediment source samples.

Sample	Carbonate content (%)	Sample	Carbonate content (%)	Sample	Carbonate content (%)
Coversands		**River sediments**		**Beach sands**	
Karatara Road	0.04	Touw upper	0.11	Wilderness	21.8
Barrington Road	0	Karatara upper	0.03	Sedgefield	25
Makhulu Quarry 1	5	Goukamma	0	**Lagoon sediments**	
Makhulu Quarry 2	-	Touw lower	0.02	Swartvlei 1	11.9
Makhulu Quarry 3	0.23	Duiwe 1	0	Swartvlei 2	-
Blaricum Heights	5.4	Duiwe 2	0.23	Swartvlei 3	-
		Diep	0	Knysna	18.7
		Hoekraal lower 1	0.06		
		Hoekraal lower 2	0.04		
		Karatara lower	0.17		
		Salt	0.05		

Appendix 2: Sample REE concentrations

Table 1 Rare earth element (REE) concentrations of samples from the seaward Wilderness barrier normalised to chondrite values of Taylor and McLennan (1985).

Sample	La	Ce	Pr	Nd	Sm	Eu	Gd (ppm)	Tb	Dy	Ho	Er	Tm	Yb	Lu
Detection limit (ppm)	0.1	0.1	0.05	0.1	0.1	0.05	0.05	0.05	0.05	0.05	0.05	0.05	0.1	0.05
Chondrite	0.37	0.96	0.14	0.71	0.23	0.09	0.31	0.06	0.38	0.09	0.25	0.04	0.25	0.04
Seaward flank														
Shfd05026	36.78	14.11	21.90	18.14	8.23	4.83	6.11	5.17	4.17	4.00	4.42	3.93	4.03	3.41
Shfd05039	15.53	5.96	9.85	7.17	3.46	2.18	2.88	2.24	2.02	1.65	1.53	1.40	1.61	1.31
Shfd09149	17.71	13.48	11.90	8.02	4.76	2.07	3.43	2.59	2.31	2.12	2.41	1.69	2.02	2.10
Shfd05049	31.34	12.02	21.61	15.47	9.52	4.48	5.62	4.14	3.36	3.06	3.05	3.37	2.82	3.15
Swartvlei Estuary	18.26	7.00	10.73	8.16	4.33	2.18	3.01	2.76	2.36	2.00	2.21	1.97	2.02	2.10
KT section														
KT2-2	46.05	17.66	38.98	26.58	17.32	6.44	8.69	5.86	4.96	3.76	4.10	2.81	2.82	2.89
KT2-3	39.24	15.05	23.50	16.74	9.52	4.71	5.98	4.83	4.07	3.41	3.73	3.93	4.03	3.67
KT2-4	28.61	10.97	18.69	12.80	7.36	3.56	4.02	3.45	2.49	2.23	2.69	2.53	2.82	2.62
KT2-6	34.06	13.06	21.46	15.19	9.09	4.71	5.29	4.14	3.33	2.94	2.97	2.81	2.82	2.89
KT2-8	44.14	16.93	32.55	23.49	12.55	5.98	6.96	5.00	3.75	3.17	3.45	3.09	3.23	2.62
KT2-9	32.97	12.64	22.77	16.17	9.52	4.60	5.33	4.31	2.97	2.82	2.89	2.81	3.23	2.62
KT2-11	28.88	11.08	17.23	11.81	6.93	3.45	3.99	3.28	2.41	2.12	2.01	1.97	2.02	2.10
Holocene dunes														
Shfd05040	48.50	18.60	31.68	25.60	12.55	4.48	8.10	6.38	5.14	4.35	5.34	4.78	5.24	5.25
Shfd04279	85.01	32.60	67.66	49.93	29.44	12.53	14.71	11.03	6.51	5.52	5.78	6.74	6.85	7.09
Shfd04280	47.68	18.29	37.52	26.86	16.45	7.24	8.92	6.38	4.51	3.88	4.02	3.93	4.03	3.94
Shfd04281	35.69	13.69	23.80	17.72	10.39	5.40	6.21	5.17	3.91	3.41	3.86	3.65	3.63	3.94
Shfd04282	78.47	30.09	60.66	46.41	28.14	11.72	14.61	9.48	6.35	5.88	6.39	6.46	7.26	7.09
Shfd04283	62.94	24.14	51.75	39.52	23.38	10.57	13.89	8.62	5.80	5.05	5.58	5.62	6.45	5.77

Table 2 Rare earth element (REE) concentrations of possible barrier sediment source samples normalised to chondrite values of Taylor and McLennan (1985).

Sample	La	Ce	Pr	Nd	Sm	Eu (ppm)	Gd	Tb	Dy	Ho	Er	Tm
Detection limit (ppm)	0.1	0.1	0.05	0.1	0.1	0.05	0.05	0.05	0.05	0.05	0.05	0.05
Chondrite	0.37	0.96	0.14	0.71	0.23	0.09	0.31	0.06	0.38	0.09	0.25	0.04
Coversands												
Karatara Road	49.32	18.91	30.36	22.08	13.42	6.32	10.26	9.14	9.13	7.76	9.40	8.99
Barrington Road	50.95	19.54	38.32	28.41	16.88	6.67	9.28	6.72	5.09	4.70	5.30	5.62
Makhulu Quarry 1	13.90	5.33	8.25	5.77	3.46	2.18	2.55	3.28	2.73	2.94	3.09	3.65
Makhulu Quarry 2	8.99	3.45	5.91	4.22	2.60	1.95	1.63	1.55	1.08	0.94	0.96	
Makhulu Quarry 3	44.69	17.14	27.66	20.25	12.55	5.40	8.69	7.24	7.30	6.58	7.55	7.87
Blaricum Heights	34.60	13.27	22.70	14.77	8.23	3.56	4.28	3.28	2.39	2.12	2.25	2.25
River sediments												
Touw upper	13.90	5.33	8.32	5.63	3.90	1.84	2.71	2.24	2.23	1.65	1.89	1.69
Karatara upper	13.08	5.02	8.03	5.34	3.90	1.61	2.97	2.76	2.81	2.47	2.57	2.53
Goukamma	21.53	8.25	13.21	9.28	5.63	2.53	4.28	3.79	3.28	2.82	3.05	3.09
Touw lower	15.80	6.06	9.78	6.75	3.90	1.72	3.43	2.59	2.41	2.00	2.13	2.25
Duiwe 1	17.98	6.90	11.17	7.59	5.19	2.18	3.69	3.45	2.94	2.70	2.85	2.53
Duiwe 2	26.16	10.03	16.28	11.39	8.23	2.30	5.69	4.83	4.25	3.17	3.13	2.81
Diep	31.06	11.91	20.00	14.49	9.09	3.22	5.46	4.14	3.20	2.94	2.73	3.37
Hoekraal lower 1	14.71	5.64	9.05	6.33	3.90	1.61	2.71	2.24	2.39	1.88	2.17	1.97
Hoekraal lower 2	16.62	6.37	11.09	7.88	6.06	2.07	4.58	4.14	3.94	3.53	3.65	3.93
Karatara lower	16.08	6.17	10.36	7.17	4.76	1.72	3.86	3.79	3.86	3.29	3.53	3.37
Salt	19.62	7.52	11.82	8.44	4.76	2.18	3.10	2.41	2.18	1.65	1.69	1.97
Beach sands												
Wilderness	267.30	102.51	200.73	149.09	88.31	37.47	50.00	32.93	24.25	19.86	24.54	25.84
Sedgefield	22.89	8.78	14.01	10.27	6.06	3.10	4.64	3.10	2.86	2.59	2.37	2.53
Lagoon sediments												
Swartvlei 1	34.88	13.38	25.91	19.55	11.26	5.40	7.71	5.17	3.99	3.64	3.78	3.93
Swartvlei 2	26.43	10.14	18.69	12.94	7.79	3.33	5.69	4.14	3.02	2.70	2.73	2.81
Swartvlei 3	13.90	5.33	8.83	5.91	3.46	1.72	2.45	2.07	1.55	1.53	1.61	-
Knysna	22.34	17.35	14.96	10.41	6.49	3.33	4.08	3.45	2.76	2.59	2.73	2.53
Bedrock - TMG												
Peninsula 1	21.25	8.15	13.72	9.70	5.63	2.53	3.95	2.93	2.73	2.12	2.01	2.81
Peninsula 2	28.88	22.88	17.66	12.24	7.79	4.37	4.25	4.31	3.49	3.06	3.21	3.37
Tchando	17.71	6.79	10.66	7.45	5.19	2.07	3.63	3.79	3.23	2.94	3.17	3.09
Bedrock – Woodville granite												
Woodville 1	45.50	17.45	37.23	30.10	29.00	3.45	25.72	25.52	25.51	23.74	25.06	27.53
Woodville 2	55.04	49.74	46.79	35.30	34.20	4.14	28.17	29.14	28.61	26.67	27.39	29.21
Woodville 3	19.07	15.36	12.85	8.86	6.49	2.64	5.03	5.00	5.67	5.41	5.94	5.62
Woodville 4	9.54	4.18	4.16	2.67	2.16	1.03	1.37	1.72	1.26	1.41	1.65	1.69
Bedrock – Kaaimans												
Homtini	80.11	30.72	54.89	40.79	29.00	14.48	25.20	23.45	24.44	21.50	23.01	20.51
Victoria Bay	65.67	25.18	44.67	35.44	29.00	13.79	23.63	21.38	20.42	17.27	17.95	17.13
Soetkraal	64.31	24.66	23.65	16.32	11.26	8.39	8.07	7.93	7.74	7.99	8.88	10.39
Skaapkop	14.44	5.54	11.09	7.59	8.23	1.61	6.54	7.93	7.98	5.52	5.38	5.34